AD_____

Award Number: W81XWH-08-1-0401

TITLE: High-Throughput Screening of Therapeutic Neural Stimulation Targets: Toward Principles of Preventing and Treating Post-Traumatic Stress Disorder

PRINCIPAL INVESTIGATOR: Edward S. Boyden, Ph.D.

CONTRACTING ORGANIZATION: Massachusetts Institute of Technology
Cambridge, MA 02139

REPORT DATE: September 2009

TYPE OF REPORT: Annual Report

PREPARED FOR: U.S. Army Medical Research and Materiel Command
Fort Detrick, Maryland 21702-5012

REPORT DOCUMENTATION PAGE

Form Approved
OMB No. 0704-0188

1. REPORT DATE *(DD-MM-YYYY)*	2. REPORT TYPE	3. DATES COVERED *(From - To)*
01-09-2009	Annual	1 Sep 2008 – 31 Aug 2009

4. TITLE AND SUBTITLE
High-Throughput Screening of Therapeutic Neural Stimulation Targets: Towards Principles of Preventing and Treating Post-Traumatic Stress Disorder

5a. CONTRACT NUMBER

5b. GRANT NUMBER
W81XWH-08-1-0401

5c. PROGRAM ELEMENT NUMBER

6. AUTHOR(S)
Edward S. Boyden

Email: eboyden3@gmail.com

5d. PROJECT NUMBER

5e. TASK NUMBER

5f. WORK UNIT NUMBER

7. PERFORMING ORGANIZATION NAME(S) AND ADDRESS(ES)
Massachusetts Institute of Technology

Cambridge, MA 02139

8. PERFORMING ORGANIZATION REPORT NUMBER

9. SPONSORING / MONITORING AGENCY NAME(S) AND ADDRESS(ES)
U.S. Army Medical Research and Materiel Command
Ft. Detrick, MD 21702-5012

10. SPONSOR/MONITOR'S ACRONYM(S)

11. SPONSOR/MONITOR'S REPORT NUMBER(S)

12. DISTRIBUTION / AVAILABILITY STATEMENT
Approved for public release; distribution unlimited

13. SUPPLEMENTARY NOTES

14. ABSTRACT
During the first year of our funding, we have discovered, using our optical neural activation techniques, that optical activation of neurons of the infralimbic (IL) cortex, in a mouse model of post-traumatic stress disorder (PTSD), during exposure therapy, results in rapid and enduring remission of the symptoms of PTSD. To accomplish this, in the first year we invented and deployed several novel technologies: we developed viruses that sensitize cortical neurons to being driven and inhibited by light, we developed arrays of optical fibers for delivering light into 3-D patterns in the brain, we secured approval for all behavioral experiments in animals, we developed precision fear-conditioning equipment optimized for optical control, we invented injector arrays that facilitate the injection of viruses throughout the brain, and we developed new neural silencers to improve the screening process. We are continuing to refine these techniques, and to screen for other targets in the brain that can modulate fear symptoms, including cortical areas and the amygdala.

15. SUBJECT TERMS
Fear conditioning, optical neural control, channelrhodopsin, optogenetics, neuroscience, neural circuits, brain, amygdala, cortex

16. SECURITY CLASSIFICATION OF:			17. LIMITATION OF ABSTRACT	18. NUMBER OF PAGES	19a. NAME OF RESPONSIBLE PERSON
a. REPORT	b. ABSTRACT	c. THIS PAGE			USAMRMC
U	U	U	UU	131	19b. TELEPHONE NUMBER *(include area code)*

Standard Form 298 (Rev. 8-98)
Prescribed by ANSI Std. Z39.18

Table of Contents

Page

INTRODUCTION

Post-traumatic stress disorder (PTSD) is characterized by extreme and ongoing anxiety and fear, exacerbated by cues and contexts associated with the initial trauma. A treatment for PTSD that could directly correct aberrant neural activity in the affected neural circuits, without altering the functions of unrelated neural circuits, would be enormously valuable. In a handful of case studies, transcranial magnetic stimulation (TMS), which can be used to activate or silence human brain regions in a noninvasive way, has been applied to the cortex of PTSD patients, but without much success. Clearly it would be optimal to identify the neural circuit target that, when activated or silenced, would provide the greatest degree of prevention and/or improvement in PTSD. Accordingly, we proposed to launch a new approach, the identification of novel neural targets whose activation or silencing can prevent or treat PTSD. We hypothesized that activation or silencing of precisely-defined neural circuit targets would prove efficacious in the prevention and/or treatment of PTSD. By pinpointing such targets, we would greatly inform the use of brain stimulation to treat human PTSD, opening up new circuit-specific interventions of great efficacy and precision. We thus (Aim 1) activates and silenced brain regions in the mouse brain to identify neural circuit targets for the treatment of conditioned anxiety and fear. We also (Aim 2) plan to, in the future, identify sites whose activation or silencing is effective for prevention of the induction of conditioned anxiety and fear. We used viruses to express light-activated proteins in neurons throughout the brain, thus making it feasible to turn on and off brain regions for specific lengths of time. Mice were implanted with optical fibers that projected to different candidate sites distributed throughout the brain. Mice were then classically conditioned to experience anxiety and fear. At various times after the induction of fear, a subset of the mice underwent activation or silencing of a brain region.

BODY

During the first year of our funding, we have discovered, using our optical neural activation techniques, that optical activation of neurons of the infralimbic (IL) cortex, in a mouse model of post-traumatic stress disorder (PTSD), during exposure therapy, results in rapid and enduring remission of the symptoms of PTSD (**Fig. 1B**). This is our major finding so far, and suggests a neural target that may be of value for neuromodulation therapy for PTSD.

A **B**

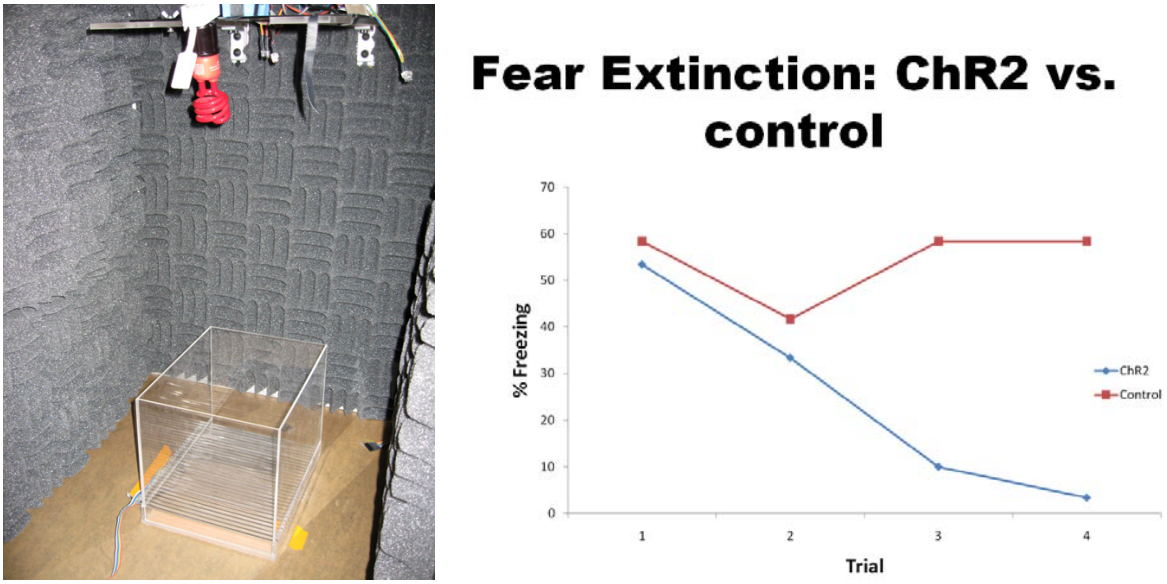

Figure 1. Fear behavior and multi-site optical modulation of fear behavior. A, System for performing fear conditioning in mice, adapted for optical control capability (circuit boards for controlling the system are shown at top). **B,** fear extinction facilitated by optical activation of prefrontal cortex sensitized to light with ChR2 (see **Appendix 7**, ref [2], and **Appendix 8**, ref [3], for conference papers where the data was presented).

Mice were acclimatized to a custom behavior box (**Fig. 1A**), optimized to allow optical control and behavior. As a PTSD model, during training, mice were exposed to a conditioned stimulus (CS) (a 2 kHz tone, 85 dB loudness, 15 seconds long) followed by an unconditioned stimulus (US) (a 1 mA footshock lasting 1 second). This was repeated 6 times. This protocol yielded reliable learning and memory of the association (**Fig. 1B**) and is widely used [4-7]. Extinction/exposure therapy trials consisted of a 2 kHz tone, 85 dB loudness, 15 seconds long, delivered either later the same day, or on a later day. Freezing, a fear response, was then scored as the absence of any movement except for respiration, and position of the mouse within the fear box was scored on an x-y coordinate system. We found that control mice did not recover from the PTSD model (red trace, **Fig. 1B**), whereas optically neuromodulated mice did (blue trace, **Fig. 1B**). In these mice, the infralimbic (IL) cortex was modulated. In humans, this region may therefore be a good target for treating PTSD. Regions like IL are already being explored with neural stimulation for treating depression and obsessive-compulsive disorder (OCD); our work suggests that it might also be useful for PTSD. These results are summarized in two conference papers, [2] in **Appendix 7** and [3] in **Appendix 8**.

Our efforts to make transgenic mice that express optical activators and silencers in specific targets failed (data not shown); accordingly, we innovated two alternative strategies which have

been filed as a patent and also resulted in numerous papers. First, we developed viruses that sensitize cortical neurons to being driven and inhibited by light. These viruses have proven to be extremely powerful for safely and permanently making neurons sensitive to being modulated by light, in our hands [8, 9]. These viruses have even proven safe in non-human primates, safely sensitizing neurons to being activated by light, suggesting that potentially this technology could be used directly as a treatment, as we show in the paper [10] in **Appendix 2**. We also developed parallel injector arrays (**Fig. 2A**), which can make "virtual transgenics" where we deliver viruses to many brain targetes (**Fig. 2B**). In this way we could label regions such as the infralimbic to make them light-sensitive (**Fig. 2F**). A paper describing this patented technology is found in **Appendix 9**, and is accepted to a journal in reference [1]. We also developed arrays of optical fibers for delivering light into 3-D patterns in the brain, so that we could activate or shutdown brain regions (**Fig. 2C, 2D**). These inventions are not yet published – we are writing up the papers right now – but they are patented (**Appendix 4, Appendix 5**).

The optical silencing did not work, which is why the results above focus on optical activation. Accordingly, we developed new neural silencers to improve the screening process. One of these is a fusion gene between multiple older opsins, that when illuminated can result in "informational lesions" (ref. [11], in **Appendix 3**). Another paper, in press at the top journal *Nature* [12], is about a new super-silencer that we discovered, fully described in **Appendix 6**.

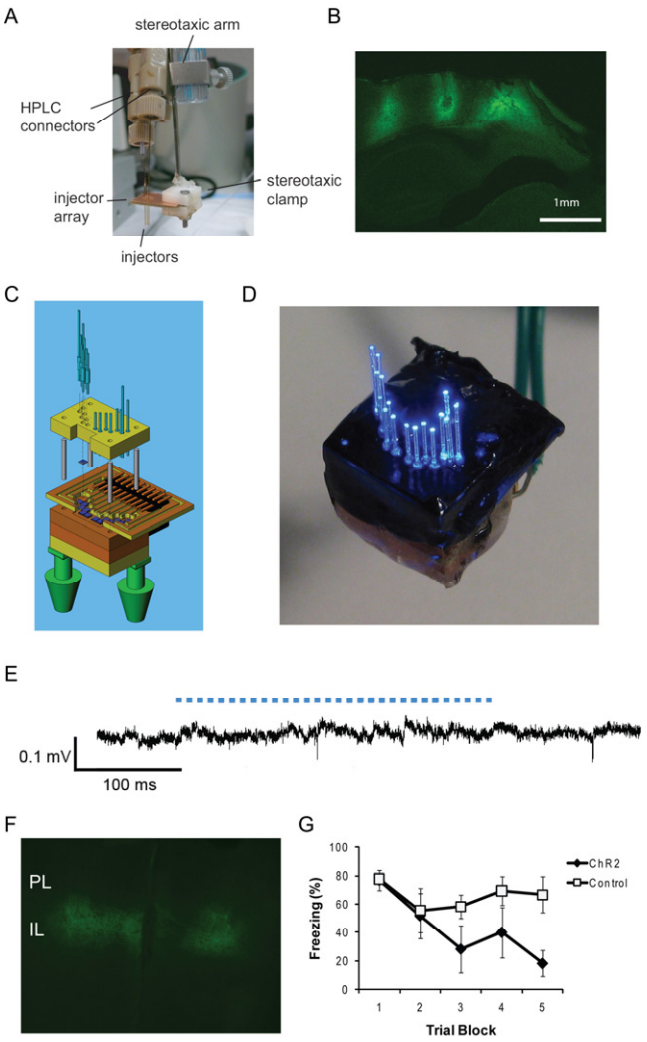

Figure 2. Prototype of an optical fiberarray for independent illumination of dozens of sites within the brain. **A**, photograph of a triple parallel injector array. Adapted from publication in press [1]. **B**, fluorescence image showing ChR2-GFP-labeled cells in three mouse cortical regions, as targeted by the triple injector array shown in **A.** Adapted from publication in press [1]. **C**, Solidworks 3-D exploded schematic of a prototype 16-fiber fiberarray for inactivation of bilateral hippocampal region CA1. **D**, photograph of a realized prototype, volume about 1 cm^3, of the fiberrarray schematized in **C**. **E**, electrodes next to an LED blinking with 0.5 A current (blue dashes) can record spikes (bottom black trace; two spikes visible in the trace) without noise, using a prototype multichannel coaxial power cable. **F**, Low-power fluorescence image of ChR2-GFP expression in IL. **G**, Percent freezing to the tone for ChR2-expressing (filled triangles) and control (open squares) mice. The ChR2 –expressing group showed significantly lower freezing than control by the fifth trial block.

To conclude, we are continuing to refine these techniques, and to screen for other targets in the brain that can modulate fear symptoms, including cortical areas and the amygdala.

KEY RESEARCH ACCOMPLISHMENTS

We:

- discovered, using our optical neural activation techniques, that optical activation of neurons of the infralimbic (IL) cortex, in a mouse model of post-traumatic stress disorder (PTSD), during exposure therapy, results in rapid and enduring remission of the symptoms of PTSD;
- developed viruses that sensitize cortical neurons to being driven and inhibited by light;
- developed arrays of optical fibers for delivering light into 3-D patterns in the brain;
- secured approval for all behavioral experiments in animals;
- developed precision fear-conditioning equipment optimized for optical control;
- invented injector arrays that facilitate the injection of viruses throughout the brain;
- developed new neural silencers to improve the screening process.

We are continuing to refine these techniques, and to screen for other targets in the brain that can modulate fear symptoms, including cortical areas and the amygdala.

REPORTABLE OUTCOMES

Manuscripts (all included in the Appendices):

Han, X., X. Qian, J.G. Bernstein, H.H. Zhou, G.T. Franzesi, P. Stern, R.T. Bronson, A.M. Graybiel, R. Desimone, and E.S. Boyden, Millisecond-timescale optical control of neural dynamics in the nonhuman primate brain. Neuron, 2009. 62(2): p. 191-8.

Chow, B., X. Han, A.S. Dobry, X. Qian, A.S. Chuong, M. Li, M.A. Henninger, P.E. Monahan, and E.S. Boyden, High-Performance Genetically-Targetable Optical Neural Silencing via the Class of Light-Driven Proton Pumps. Nature, 2009. in press.

Han, X., X. Qian, P. Stern, A.S. Chuong, and E.S. Boyden, Informational Lesions: Optical Perturbation of Spike Timing and Neural Synchrony Via Microbial Opsin Gene Fusions. Front. Mol. Neurosci. , 2009. doi:10.3389/neuro.02.012.2009.

Chan, S.C., J.G. Bernstein, and E.S. Boyden, Scalable Fluidic Injector Arrays for Viral Targeting of Intact 3-D Brain Circuits. Journal of Visualized Experiments, 2009. in press.

Abstracts (included in the appendices):

Bernstein, J.G., M.V. Baratta, E.Y. Ko, M.A. Henniger, M. Li, K.A. Goosens, and E.S. Boyden, Modulation of fear behavior via optical fiber arrays targeted to bilateral prefrontal cortex. Society for Neuroscience, 2009.

Boyden, E.S., Optical Neural Control: Engineering Therapeutic Circuit Dynamics: Application to Post-Traumatic Stress Disorder. Military Health Research Forum, Kansas City, MO, 2009. Talk 7-9, Poster P31-11, PTSD Treatment.

Presentations:

Boyden, E. S. (2008) “Optical Neuron Control: Towards Principles of Controlling Neural Circuits.” *Invited speaker*, Integrative Approaches to Brain Complexity Conference, Cold Spring Harbor/Wellcome Trust, Wellcome Trust Conference Center, Hinxton, UK.

Boyden, E. S. (2008) “Optical methods for controlling and correcting neural circuit functions.” *Invited speaker*, "In Vivo Imaging in Recovery After Neural Injury: From Microimaging in Animal Models to Functional Imaging in Man.” Satellite Symposium to the American Congress of Rehabilitation Medicine (ACRM) and the American Society of Neurologic Rehabilitation (ASNR) Joint Educational Conference, Toronto, Canada.

Boyden, E. S. (2008) "High-Precision Genetically-Targeted Optical Control of Normal and Pathological Neural Computations.” *Invited speaker*, HHMI Conference on Genetic Manipulation of Neuronal Activity, Janelia Farm, Ashburn, VA.

Boyden, E. S. (2008) "Optical Brain Control: Analyzing and Engineering Normal and Pathological Neural Circuit Dynamics.” *Invited speaker*, Carolina Biophysics Symposium, Chapel Hill, NC.

Boyden, E. S. (2008) "Optical Brain Control: Analyzing and Engineering Normal and Pathological Neural Circuit Dynamics.” *Invited speaker*, MIT Synthetic Biology Working Group, Cambridge, MA.

Boyden, E. S. (2009) “Novel Tools for Precisely Controlling Brain Functions.” *Invited speaker*, Brain Research Center and Student Biotechnology Network, University of British Columbia, Vancouver, Canada.

Boyden, E. S. (2009) “Optical Brain Control: Analyzing and Engineering Normal and Pathological Neural Circuit Dynamics.” *Invited speaker*, CIMIT Forum, Boston, MA.

Boyden, E. S. (2009) “Optical Brain Control: Analyzing and Engineering Normal and Pathological Neural Circuit Dynamics.” *Invited speaker*, Dept. of Bioengineering, University of Pennsylvania, Philadelphia, PA.

Boyden, E. S. (2009) “Optical Control Of Normal and Pathological Neural Circuit Computations.” *Invited speaker*, McGovern Symposium, Tsinghua University, Beijing, China.

Boyden, E. S. (2009) "Optical Neural Control: Towards Systematic Parsing of the Role of Cell Types in Normal and Abnormal Neural Computation.” Invited talk, MGH-HST Martinos Center Brainmap Series, Cambridge, MA.

Boyden, E. S. (2009) "Optical Brain Control: Towards New Therapies for Brain Disorders.” Invited speaker, Optical Society of America (New England Section Meeting), Cambridge, MA.

Boyden, E. S. (2009) “Optical Neural Control: Analyzing and Engineering Normal and Pathological Neural Circuit Dynamics.” *Invited speaker*, Tufts Neuroscience Symposium, Tufts University, Cambridge, MA.

Boyden, E. S. (2009) “Towards Understanding The Circuits of Cognition: Engineering Tools for Analyzing Primate Brain Dynamics.” *Invited speaker, along with Xue Han,* New England Primate Research Center (NEPRC), Harvard Medical School, Southborough, MA.

Boyden, E. S. (2009) “Optical Activation of Neurons.” *Invited speaker,* Challenges for 21st Century Photonics, CIPS, MIT, Cambridge, MA.

Boyden, E. S. (2009) "Optical Brain Control: Towards New Insights and Therapies.” *Invited speaker,* Psychiatric Genetics and Translational Research Seminar, Masschusetts General Hospital, Boston, MA.

Boyden, E. S. (2009) “Enabling Systematic Neuroscience with Novel Optical Neural Control Strategies.” *Invited speaker,* Cold Spring Harbor Laboratories, NY.

Boyden, E. S. (2009) “Optical Neural Control Prosthetics.” *Invited speaker,* No Barriers Festival, Miami, FL.

Boyden, E. S. (2009) “Optical Cell-Specific Neuromodulation: Towards Engineering the Brain for Therapeutic Purposes.” *Invited speaker,* Medtronic, Minneapolis, MN.

Boyden, E. S. (2009) "Optical control of the brain: Understanding thought, engineering cures.” Invited Speaker, HST Summer Institute Biomedical Optics Lecture Series, Massachusetts General Hospital, Boston, MA.

Boyden, E. S. (2009) “Technologies for controlling neural circuit dynamics.” Sloan-Swartz 2009 Annual Meeting on Computational Neuroscience, Harvard, Cambridge, MA.

Boyden, E. S. (2009) “Enabling Systematic Neuroscience with Novel Optical Neural Control Strategies.” Invited Seminar, Indiana University, Bloomington, IN.

Patents:
“Optical Cell Control Prosthetics,” U.S. Application # 60/917,055.

“Prosthetic Systems for Therapeutic Optical Activation and Silencing of Genetically-Targeted Neurons,” 61/021,612.

“Methods and Compositions of Optical Neural Control in Primate Brain,” U.S. provisional application 61115291.

“Scalable, Patient-Customized, Parallel Gene Therapy Injector Array,” U. S. provisional application 61115167.

Funding based on this work:
NIH RC2 GO Grant, Modulating Cortical and Sub-cortical Brain Circuits in Chronic Facial Pain, 9/30/09-9/29/11.

NIH RC1 Challenge Grant, Optogenetic control of attention through prefrontal synchrony, 9/30/09-9/29/11.

Employment/training supported:
The grant supported the work of one postdoctoral fellow, Michael Baratta, who has been carrying out the work.

CONCLUSION
The efforts so far are promising. They have revealed a major new target for neuromodulation therapy for PTSD, and may help with translational efforts to use deep brain stimulation (DBS) or transcranial magnetic stimulation (TMS) to modulate neural circuits. We anticipate seeking to translate this to the clinic, and are seeking collaborators. Furthermore, our surprising finding that the technologies work great in non-human primates, suggests that perhaps optical neural control could itself be used in human patients. We are excited to continue to refine our findings and to reveal both clinical insights on how TMS and DBS may be used, as well as new optical inventions that may directly enable new treatments for PTSD.

REFERENCES

1. Chan, S.C., J.G. Bernstein, and E.S. Boyden, *Scalable Fluidic Injector Arrays for Viral Targeting of Intact 3-D Brain Circuits.* Journal of Visualized Experiments, 2009. **in press**.
2. Boyden, E.S., *Optical Neural Control: Engineering Therapeutic Circuit Dynamics: Application to Post-Traumatic Stress Disorder.* Military Health Research Forum, Kansas City, MO, 2009. **Talk 7-9, Poster P31-11, PTSD Treatment**.
3. Bernstein, J.G., M.V. Baratta, E.Y. Ko, M.A. Henniger, M. Li, K.A. Goosens, and E.S. Boyden, *Modulation of fear behavior via optical fiber arrays targeted to bilateral prefrontal cortex.* Society for Neuroscience, 2009.
4. Han, C.J., C.M. O'Tuathaigh, L. van Trigt, J.J. Quinn, M.S. Fanselow, R. Mongeau, C. Koch, and D.J. Anderson, *Trace but not delay fear conditioning requires attention and the anterior cingulate cortex.* Proc Natl Acad Sci U S A, 2003. **100**(22): p. 13087-92.
5. Tseng, W., R. Guan, J.F. Disterhoft, and C. Weiss, *Trace eyeblink conditioning is hippocampally dependent in mice.* Hippocampus, 2004. **14**(1): p. 58-65.
6. Crestani, F., R. Keist, J.M. Fritschy, D. Benke, K. Vogt, L. Prut, H. Bluthmann, H. Mohler, and U. Rudolph, *Trace fear conditioning involves hippocampal alpha5 GABA(A) receptors.* Proc Natl Acad Sci U S A, 2002. **99**(13): p. 8980-5.
7. Zhao, M.G., H. Toyoda, S.W. Ko, H.K. Ding, L.J. Wu, and M. Zhuo, *Deficits in trace fear memory and long-term potentiation in a mouse model for fragile X syndrome.* J Neurosci, 2005. **25**(32): p. 7385-92.
8. Han, X. and E.S. Boyden, *Multiple-color optical activation, silencing, and desynchronization of neural activity, with single-spike temporal resolution.* PLoS ONE, 2007. **2**(3): p. e299.
9. Boyden, E.S., F. Zhang, E. Bamberg, G. Nagel, and K. Deisseroth, *Millisecond-timescale, genetically targeted optical control of neural activity.* Nat Neurosci, 2005. **8**(9): p. 1263-8.
10. Han, X., X. Qian, J. Bernstein, H.-H. Zhou, G. Talei Franzesi, S. P., R.T. Bronson, A. Graybiel, R. Desimone, and E.S. Boyden, *Millisecond-timescale optical control of neural dynamics in the nonhuman primate brain.* in press, Neuron, 2009.
11. Han, X., X. Qian, P. Stern, A.S. Chuong, and E.S. Boyden, *Informational Lesions: Optical Perturbation of Spike Timing and Neural Synchrony Via Microbial Opsin Gene Fusions.* Front. Mol. Neurosci. , 2009. **doi:10.3389/neuro.02.012.2009**.
12. Chow, B., X. Han, A.S. Dobry, X. Qian, A.S. Chuong, M. Li, M.A. Henninger, P.E. Monahan, and E.S. Boyden, *High-Performance Genetically-Targetable Optical Neural Silencing via the Class of Light-Driven Proton Pumps.* Nature, 2009. **in press**.
13. Han, X., X. Qian, J.G. Bernstein, H.H. Zhou, G.T. Franzesi, P. Stern, R.T. Bronson, A.M. Graybiel, R. Desimone, and E.S. Boyden, *Millisecond-timescale optical control of neural dynamics in the nonhuman primate brain.* Neuron, 2009. **62**(2): p. 191-8.

APPENDIX 1

CV of Ed Boyden

Edward S. Boyden, Ph. D.

email esb@media.mit.edu - *web* http://www.media.mit.edu/~esb/
cell - (650) 468-5625 - *phone* (617) 324-3085 - *fax* (617) 253-7035
office MIT Media Lab, E15-430, 20 Ames St., Cambridge, MA 02139

Vision

To engineer intelligent, targeted control interfaces for neural circuits, in order to repair pathology, augment cognition, and reveal new insights into the human condition.

Research and work activities

Massachusetts Institute of Technology, Cambridge, MA (2007-present)
Assistant Professor, MIT Media Lab (Benesse Career Development Professor)
Joint Professor, MIT Department of Biological Engineering
Joint Professor, MIT Department of Brain and Cognitive Sciences
Leader, Synthetic Neurobiology Group
Developing tools for systematic analysis and engineering of the brain.

Massachusetts Institute of Technology, Cambridge, MA (2006-2007)
Visiting Scientist, MIT Media Lab; Leader, Neuroengineering and Neuromedia Group
Developing tools for systematic analysis and engineering of the brain.

Stanford University, Stanford, CA (2005-2006)
Helen Hay Whitney fellow, Depts. of Bioengineering, Applied Physics, Biological Sciences
Inventing optical methods for accelerating neuroscience progress.

Boyden Innovations, Cambridge, MA (2005-present)
Sole proprietor, Independent inventor
Developing novel medical devices and applications of physics to systematic bioengineering.

Stanford University, Stanford, CA (1999-2004)
Hertz predoctoral fellow, Program in Neurosciences, Depts. of Molecular and Cellular Physiology and Neurobiology, with Drs. Jennifer Raymond and Richard Tsien.
Studied how neural circuits selectively engage plasticity to store specific memories.
Developed optical methods for controlling neural activity.

Bell Labs, Lucent Technologies, Murray Hill, NJ (1998-99)
Research assistant, with Drs. Sebastian Seung and Michale Fee.
Created an elementary phase-resetting model of birdsong stochasticity.
Helped implement active electrode stabilizer for neural recordings in awake animals.

Massachusetts Institute of Technology, MIT Media Lab, Cambridge, MA (1998-99)
Graduate research, with Dr. Neil Gershenfeld.
Design and fabrication of prototype nuclear magnetic resonance (NMR) quantum computer.
Engineered control software for the MIT ORCA-1 autonomous submarine.
Designed hardware for a MEMS accelerometer using electron-tunneling.

Massachusetts Institute of Technology, MIT Media Lab, Cambridge, MA (1996-98)
Research assistant, with Dr. Neil Gershenfeld.
Programmed machine-learning tools for reconstructing dynamics of a digital violin.
Created 3D, non-contact interactive design program based on electric field imaging of hands.

Activision, Inc., Santa Monica, CA (1997)
Research programmer
Designed real-time, physics-based animation engine for video games.

University of North Texas Chemistry Department, Denton, TX (1994-95)
Research assistant, with Dr. Paul Braterman
Research on the origins of life; synthesized and analyzed layered double hydroxides with intercalated anions.

Education

Stanford University, Stanford, CA (1999-2005)
GPA: 4.1/4.0
PhD candidate, Neurosciences
Thesis title: *Task-specific neural mechanisms of memory encoding*

Massachusetts Institute of Technology, Cambridge, MA (1995-99)
GPA: 5.0/5.0
M.Eng. Electrical Engineering and Computer Science
B.S. Electrical Engineering and Computer Science
B.S. Physics
Thesis title: *Quantum Computation: Theory and Implementation*

Texas Academy of Mathematics and Science, University of North Texas, Denton, TX (1993-95)
GPA: 4.0/4.0

Major awards

2008, Discover Magazine, 20 Best Scientists Under Age 40
2008, NSF Emerging Frontiers in Research and Innovation Grant (Cognitive Optimization and Prediction: From Neural Systems to Neurotechnology)
2008, NSF SGER (Small Grant for Exploratory Research)
2008, MIT McGovern Institute for Brain Research Neurotechnology (MINT) Award
2008, Congressionally-Directed Medical Research Program (CDMRP) Post-Traumatic Stress Disorder Concept Award
2008, MIT Alumni Class Funds Award for Excellence in Educational Innovation
2008, NARSAD Young Investigator Award
2008-2010, Alfred P. Sloan Research Fellowship
2007, Discovery Science Channel, Top 5 'Best Science Moments 2007'
2007, Society for Neuroscience (SFN) Research Award for Innovation in Neuroscience (RAIN)
2007, NIH Director's New Innovator Award
2007, MIT, Benesse Career Development Professor Chair
2007, Wallace H. Coulter Foundation Early Career Translational Research Award in Biomedical Engineering
2007, MIT McGovern Institute for Brain Research Neurotechnology (MINT) Award
2006, Technology Review TR35, World's Top 35 Innovators under Age 35
2006, Fannie and John Hertz Foundation, Top Ph.D. Thesis Prize
2005-07, McKnight Endowment Fund for Neuroscience, Technological Innovations in Neuroscience Award, Investigator
2005-2006, Helen Hay Whitney Fellowship
2004, Dan David Prize Scholarship (Future Dimension, Brain Sciences)
2004, NIH Ruth L. Kirschstein National Research Service Award
1999-2004, Fannie and John Hertz Fellowship
1999, MIT Microelectromechanical Systems design competition, 1st place
1998, International Autonomous Underwater Vehicle Competition, 1st place
1995-1996, MIT Electrical Engineering and Computer Science, letters of commendation (top 2% at MIT), in 3 of the 4 core courses
1995, International Chemistry Olympiad, selected to U.S. team
1995, USA Mathematical Talent Search, Winner
1995, National Merit Finalist
1995, Tandy Technology Scholar
1994, Robert A. Welch Foundation Research Scholarship
1994, University of North Texas, outstanding chemistry student
1993-95, University of North Texas, Dean's List
1993, Texas State Science and Engineering Fair, SEMATECH Mathematics Prize
1993, Texas State Science and Engineering Fair, 1st place, Mathematics division

Classes Taught

Biological Instrumentation and Measurement, 20.309, MIT (Spring 2009)
Sensing and measurement aimed at quantitative molecular/cell/tissue analysis in terms of genetic, biochemical, and biophysical properties. Methods include light and fluorescence microscopies, and electro-mechanical probes (atomic force microscopy, optical traps, MEMS devices). Application of statistics, probability, signal and noise analysis, and Fourier techniques to experimental data. Preferences given to juniors and seniors.

Applications of Neuroengineering, MAS.882/9.433, MIT (Spring 2008, Spring 2009)

Project-focused course in which students take top-down approach to developing technologies that address critical clinical and basic-science problems of human brain function. Focus is on application of engineering principles to development of systematically powerful tools. Problem domains include neurological/psychiatric disorders, consciousness, and human cognitive augmentation. Students work in teams to apply cross-disciplinary (e.g., molecular, physical, nanotechnological) building blocks to design new tools for the analysis and engineering of the brain.

Principles of Neuroengineering, MAS.881/20.452/9.422, MIT (Fall 2007, Fall 2008)
Covers principles underlying current and future technologies for brain analysis and engineering, for neurology, psychiatry, and neuroscience. Focuses on using biophysical, biochemical, and anatomical models to understand technology design constraints governing ability to observe and alter brain function. Topics include functional magnetic resonance imaging, electromagnetic recording/stimulation, neuropharmacology, optical cellular imaging, and gene/stem-cell therapy. Design projects by student teams.

Neurotechnology Ventures, (MAS.961/9.912J/HST.588 in Spring 2007; MAS.883/9.455/20.454/15.128/HST.588 thereafter), MIT (Spring 2007, Fall 2008)
A special seminar focused on the challenges of envisioning, planning and building startups; commercializing innovations from neuroscience; and the blossoming domain of neuroengineering. (Primary instructor; taught in collaboration with J. Bonsen and R. Ellis-Behnke. Simulcast to Hong Kong and Taiwan.)

Social and professional activities

Professional, conferences/meetings/events

2010, Computational and Systems Neuroscience (CoSyNe) Meeting, Reviewer
2009, SPIE BiOS 2009 Meeting, Neurons and Photons Conference, San Jose, CA, Program Committee
2008, National Academies Keck Futures Initiative 2008: Complex Systems, Arnold and Mabel Beckman Center, Irvine, CA, invited participant
2008, NIH Blueprint for Neuroscience Research, Pain Grand Challenges/Transformative R01 Workshop, invited participant
2008, Neuron to Synapse Meeting, Harvard Medical School, Boston, MA, Scientific Committee
2008, Computational and Systems Neuroscience (CoSyNe) Meeting, Workshop Organizer, "How to solve systems neuroscience problems with molecular tools," Snow Bird, Utah
2007, NIH Blueprint for Neuroscience Research, Neuroplasticity Workshop, invited participant
2007, BodyNets 2007 Conference, Florence, Italy, Technical Program Committee member
2000, NINDS Conference on Computational and Theoretical Neuroscience: From Synapse to Circuitry, writer

Professional, other

2009-present, *Technology Review*, columnist
2009-present, SPIE, member
2007-present, *Technology Review*, official blogger/writer
2007-present, Fannie and John Hertz Foundation, Fellowship Interviewer
2003-present, MIT Entrepreneur Center E-Society, member
2000-present, Society for Neuroscience, member

Consulting, non-profit

2009-present, Lifeboat Foundation, Advisory Board
2007-2008, Innerspace Foundation, Scientific Advisory Board
2006, United Kingdom Office of Horizon Scanning, Institute for the Future, Palo Alto, CA, invited workshop participant
2004-present, Fannie and John Hertz Foundation

MIT

2009-present, MIT Interdepartmental Graduate Program in Biophysics, faculty member
2009-present, MIT Molecular and Cellular Neuroscience Track, faculty member

2009-present, MIT Microsystems Technology Laboratories, affiliate member
2008-present, MIT Department of Brain and Cognitive Sciences, Joint Professor
2007-present, MIT Media Lab Center for Human Augmentation, Co-Director
2007-present, MIT McGovern Institute for Brain Research, Associate Member
2007-present, MIT Picower Center for Learning and Memory, Affiliate Professor
2007-present, MIT Department of Biological Engineering, Joint Professor
2007, MIT Department of Biological Engineering, Affiliate Professor
2006-present, MIT Computational and Systems Biology Initiative, Faculty Member

Major Publications

Papers (peer-reviewed)

1. Maguire, Y., Boyden, E. S., Gershenfeld, N. (2000) Toward a table-top quantum computer, *IBM Systems Journal* 39:3&4, p.823.

2. Boyden, E. S., Raymond, J. L. (2003) Active reversal of motor memories reveals rules governing memory encoding, *Neuron* 39(6):1031-42.

3. Boyden, E. S., Katoh, A., Raymond, J. L. (2004) Cerebellum-dependent learning: The role of multiple plasticity mechanisms, *Annual Review of Neuroscience* 27:581-609.

4. Kimpo, R. R.*, Boyden, E. S.*, Katoh, A., Ke, M. C., Raymond, J. L. (2005) Distinct patterns of stimulus generalization of increases and decreases in VOR gain, *Journal of Neurophysiology* 94(5):3092-3100. (* equal co-first authors)

5. Boyden, E. S., Zhang, F., Bamberg, E., Nagel, G., Deisseroth, K. (2005) Millisecond-timescale, genetically-targeted optical control of neural activity, *Nature Neuroscience* 8(9):1263-1268.

6. Boyden, E. S., Katoh, A., Pyle, J. L., Chatila, T. A., Tsien, R. W., Raymond, J. L. (2006) Selective engagement of plasticity mechanisms for motor memory storage, *Neuron* 51(6):823-834.

7. Zhang, F., Wang, L.-P., Boyden, E. S., Deisseroth, K. (2006) Channelrhodopsin-2 and optical control of excitable cells, *Nature Methods* 3(10):785-92.

8. Han, X. and Boyden, E. S. (2007) Multiple-color optical activation, silencing, and desynchronization of neural activity, with single-spike temporal resolution, *PLoS ONE* 2(3): p. e299.

9. Wang, H., Peca, J., Matsusaki, M., Matsusaki, K., Noguchi, J., Qiu, L., Wang, D., Zhang, F., Boyden, E. S., Deisseroth, K., Kasai, H., Hall, W. C., Feng, G., Augustine, G. J. (2007) High-speed mapping of synaptic connectivity using photostimulation in channelrhodopsin-2 transgenic mice, *Proceedings of the National Academy of Sciences* 104(19):8143-848.

10. Liao, Y. J., Safa, P., Chen, Y.-R., Sobel, R. A., Boyden, E. S., Tsien, R. W. (2008) Anti-Ca^{2+} channel antibody attenuates Ca^{2+} currents and mimics cerebellar ataxia *in vivo*, *Proceedings of the National Academy of Sciences* 105(7):2705-2710.

11. Han, X., Qian, X., Bernstein, J.G., Zhou, H.-H., Talei Franzesi, G., Stern, P., Bronson, R.T., Graybiel, A.M., Desimone, R., and Boyden, E.S. (2009) Millisecond-Timescale Optical Control of Neural Dynamics in the Nonhuman Primate Brain, *Neuron* 62(2): 191-198.

12. Han X, Qian X, Stern P, Chuong A and Boyden ES (2009) Informational Lesions: Optical Perturbation of Spike Timing and Neural Synchrony Via Microbial Opsin Gene Fusions. *Frontiers in Molecular Neuroscience*, 2:12. doi:10.3389/neuro.02.012.2009

13. Chan, S. C., Bernstein, J. G., Boyden, E. 13. Chow, B.Y., Han, X., Qian, X., Li, M., Monahan, P.E., Chuong, A.S., Boyden, E.S. (2009) High-Performance Neural Activity Silencing by Light-Driven Proton Pumping, in press, Nature.

14. Chan, S. C., Bernstein, J. G., Boyden, E. S. (2009) Scalable Fluidic Injector Arrays for Viral Targeting of Intact 3-D Brain Circuits. in press, Journal of Visualized Experiments.

Conference Papers and Talks (Refereed)

1. Schoner, B., Cooper, C., Douglas, C. L., Boyden, E. S., Gershenfeld, N. A. (1999) Data-driven modeling of acoustical instruments, *Journal of the Acoustic Society of America* 105(2):1328.

2. Fletcher, R., Omojola, O., Boyden, E. S., Gershenfeld, N. (1999) Reconfigurable Agile Tag Reader Technologies for Combined EAS and RFID capability, *Proceedings of the Second IEEE Workshop on Automatic Identification Advanced Technologies*, Summit, New Jersey.

3. Boyden, E. S., Tsien, R. W., Chatila, T. A., Raymond, J. L. (2003) Is oppositely directed motor learning implemented with inverse plasticity mechanisms?, Proceedings of the Annual Symposium on Advances in Computational Motor Control, Volume 2, Emanuel Todorov and Reza Shadmehr, editors, New Orleans, Louisiana.

4. Boyden, E. S., Chatila, T. A., Raymond, J. L. (2004) "The contribution of inverse plasticity mechanisms to cerebellum-dependent learning." *Talk*, at *Computational and Systems Neuroscience (CoSyNe)*, Cold Spring Harbor, NY, March 24-28, 2004.

5. Han, X., and Boyden, E. S. (2007) Two-color, bi-directional optical voltage control of genetically-targeted neurons, *Spotlight Presentation*, at *Computational and Systems Neuroscience (CoSyNe)*, Salt Lake City, UT, Feb 22-25, 2007.

6. Bernstein, J. G., Han, X., Henninger, M. A., Ko, E. Y., Qian, X., Franzesi, G. T., McConnell, J. P., Stern, P., Desimone, R., and Boyden, E. S. (2008) Prosthetic systems for therapeutic optical activation and silencing of genetically-targeted neurons. Proc Soc Photo Opt Instrum Eng, 6854:68540H.

7. Chow B, Han X, Qian X and Boyden E (2009). High-performance halorhodopsin variants for improved genetically-targetable optical neural silencing. Frontiers in Systems Neuroscience. Conference Abstract: Computational and systems neuroscience. doi: 10.3389/conf.neuro.10.2009.03.347

8. Boyden E, Franzesi G T, Qian X, Li M, Han X, Borgers C, Kopell N J, Le Beau F and Whittington M A (2009). Probing mechanisms of gamma rhythmogenesis with cell type-specific optical neural control. Frontiers in Systems Neuroscience. Conference Abstract: Computational and systems neuroscience. doi: 10.3389/conf.neuro.10.2009.03.299

Patents and Patent Applications (Total: 140 patents or patents pending)

1. “Light-activated cation channel and uses thereof,” U.S. Application # 11/459,636.
2. “Light-activated cation channel and uses thereof,” U.S. Application # 11/459,637.
3. “Light-activated cation channel and uses thereof,” U.S. Application # 11/459,638.
10. “Genetically-Targetable Optical Inactivation of Excitable Cells,” serial number unknown.
11. “Genetically-Targetable Optical Inactivation of Excitable Cells,” U.S. Application # 60/903,248.
15. “Software Engine, Platform, and System for Customizable, Adaptive Hypnosis,” U.S. Application # 60/916,880.
16. “Integrated Device for Transcranial Current Stimulation and Electroencephalography and Uses Thereof,” U.S. Application # 60/916,953.
17. “Wearable, Portable, Modular Transcranial Magnetic Stimulation device,” U.S. Application # 60/916,989.
18. “Optical Cell Control Prosthetics,” U.S. Application # 60/917,055.
103. “Prosthetic Systems for Therapeutic Optical Activation and Silencing of Genetically-Targeted Neurons,” 61/021,612.
116. “Methods and Compositions of Optical Neural Control in Primate Brain,” U.S. provisional application 61115291.
117. “Scalable, Patient-Customized, Parallel Gene Therapy Injector Array,” U. S. provisional application 61115167.

GENBANK Contributions

Nucleotide

1. EF537649, Synthetic construct mammalian codon-optimized halorhodopsin gene, complete cds, 876 bases. Submitted April 4, 2007.
2. EU714030, Synthetic construct channel rhodopsin-2-GFP (ChR2-GFP) gene, complete cds. Submitted May 11, 2008.

Protein

1. ABQ08589, Mammalian codon-optimized halorhodopsin [synthetic construct], 291 amino acids. Submitted April 4, 2007.
2. ACD89032, channel rhodopsin-2-GFP [synthetic construct], 554 amino acids. Submitted May 11, 2008.

Theses

1. Boyden, E. S. (1999) Quantum Computing: Theory and Implementation, *Master's Thesis in Electrical Engineering and Computer Science, Bachelor's Thesis in Physics*, Massachusetts Institute of Technology.

2. Boyden, E. S. (2005) Task-selective neural mechanisms of memory encoding, *Ph. D. Thesis in Neurosciences*, Stanford University.

Synthetic Neurobiology Memos

1. Synthetic Neurobiology Memo #1 (2006) Optical Fiber/Laser System for In Vivo (Multicolor) Light Delivery for Brain Neuromodulation. Online.

2. Synthetic Neurobiology Memo #2 (2009) Lentivirus production for high-titer, cell-specific, in vivo neural labeling. Online.

Byline Articles

1. Boyden, E. S. (2000) Computational and Theoretical Neuroscience: From Synapse to Circuitry. *National Institutes of Health/National Institute of Neurological Disorders and Stroke*, Technical Report for Workshop of April 28, 2000.

2. Boyden, E. S. (2007) Engineering the Brain ('Notebooks' column), *Technology Review*, March/April 2007 issue, p. 34-35. *Featured on MIT homepage.*

3. Boyden, E. S. In Pursuit of Human Augmentation. Ed Boyden's Blog. Technology Review. 9/17/07. (http://www.technologyreview.com/blog/boyden/21839/).

4. Boyden, E. S. Open Philanthropy. Ed Boyden's Blog. Technology Review. 9/24/07. (http://www.technologyreview.com/blog/boyden/21850/).

5. Boyden, E. S. Synthetic Neurobiology. Ed Boyden's Blog. Technology Review. 10/9/07. (http://www.technologyreview.com/blog/boyden/21871/).

6. Boyden, E. S. How to Think. Ed Boyden's Blog. Technology Review. 11/13/07. (http://www.technologyreview.com/blog/boyden/21925/). *Featured on MIT homepage.*

7. Boyden, E. S. Training a Generation of Neuroengineers. Ed Boyden's Blog, Technology Review. 4/22/08. (http://www.technologyreview.com/blog/boyden/22055/).

8. Boyden, E. S. Inverting the Core. Ed Boyden's Blog. Technology Review. 7/14/08. (http://www.technologyreview.com/blog/boyden/22096/). *Featured on MIT homepage.*

9. Boyden, E. S. Research as a Community-Building Activity Ed Boyden's Blog. Technology Review. 7/28/08. (http://www.technologyreview.com/blog/boyden/22102/).

10. Boyden, E. S. Averting Disasters, Preventing Problems. Ed Boyden's Blog. *Technology*

Review. 9/2/08. (http://www.technologyreview.com/blog/boyden/22122/).

11. Boyden, E. S. Civilization as Experiment. Ed Boyden's Blog. *Technology Review*. 1/19/09. (http://www.technologyreview.com/blog/boyden/22512/).

12. Boyden, E. S. The Singularity and the Fixed Point. Column, *Technology Review.* 9/4/2009. (http://www.technologyreview.com/biomedicine/23354/).

Other writings

1. Boyden, E. S. (1996) “The Practical Physicist's OpenGL tutorial.” Online.

2. Boyden, E. S. (1997) “Tree-based Cluster Weighted Modeling: Towards A Massively Parallel Real-Time Digital Stradivarius.” Online.

3. Boyden, E. S. (1997) “A physics-based animation engine.” Online.

4. Altshuler, R. C., Boyden, E. S., Chase, C. C., Davis, B. M., Delatorre, F. J., Edelson, J., Elgart, J. D., Gates, H. G., Hancher, M. D., Hasan, L. M., Huang, A. S., Knaian, A. N., Lee, F., Newburg, S. O., Polito, B. F., Reynolds, M. S., Smith, E. D., Warmann, E. C. (1998) “The ORCA-1: An Autonomous Underwater Vehicle.” Online.

5. Boyden, E. S., El Rifai, O., Hubert, B., Karpman, M., Roberts, D. (1999) “A High-Performance Tunneling Accelerometer.” Online.

Invited talks

1. Boyden, E. S. (2003) “How multiple plasticity mechanisms contribute to versatile motor learning.” *Invited talk,* Stanford Neurosciences Program 2003 Retreat, Monterey, CA.

2.. Boyden, E. S. (2005) “Causal roles of neurons and neural circuits in learning and behavior.” *Invited talk,* Hertz Foundation Scholars 2005 Retreat, Pt. Reyes, CA.

3. Boyden, E. S. (2006) “Solving the brain systematically: tools for the analysis and engineering of neural circuits.” *Invited talk*, Google Tech Talk series, Google, Mountain View, CA.

4. Boyden, E. S. (2006) “Cutting-edge technologies for the systematic analysis of neural circuit dynamics.” *Invited talk*, UCSF, Program in Bioengineering Seminar Series, San Francisco, CA.

5. Boyden, E. S. (2006) “Resolving the computational role of specific neural circuit elements.” *Invited talk*, McGovern Institute, MIT, Cambridge, MA.

6. Boyden, E. S. (2006) “Towards the analysis of cortical computation via optical control of neural activity.” *Invited talk*, Computation and Neural Systems, Caltech, Pasadena, CA.

7. Boyden, E. S. (2006) “Enabling technologies for controlling neural circuit functions.” *Invited talk*, Brain Science Program, Brown University, Providence, RI.

8. Boyden, E. S. (2006) “Technologies for the systematic analysis of neural circuit function.” *Invited talk*, Center for Brain Science, Harvard University, Cambridge, MA.

9. Boyden, E. S. (2006) “Neural Circuit Technology: Towards New Brain Interfaces and Biological Tools.” *Invited talk*, MIT Media Laboratory, MIT, Cambridge, MA.

10. Boyden, E. S. (2006) “Engineering tools for engineering the brain.” *Invited talk*, Division of Engineering, Brown University, Providence, RI.

11. Boyden, E. S. (2006) “Ultraprecise biological interfaces: Controlling life with light.” *Opening night talk*, Science Foo Camp, Google, Mountain View, CA.

12. Boyden, E. S. (2006) “Launching the Open Brain Stimulator Project.” *Session leader,* Foo Camp, O’Reilly Media, Sebastopol, CA.

13. Boyden, E. S. (2006) “The future of neural devices.” *Invited talk*, Stanford Biodesign Program, Stanford, CA.

14. Boyden, E. S. (2006) “Systematic approaches for understanding neural circuit function.” *Invited talk*, Center for Basic Neuroscience, UT Southwestern Medical School, Dallas, TX.

15. Boyden, E. S. (2007), “Technologies for the Precise Control of Neural Circuits.” *Invited talk*, Sloan-Swartz Seminars on Theoretical Neurobiology, Salk Institute for Biological Studies, San Diego, CA.

16. Boyden, E. S. (2007) “New Technologies for Repairing Neural Computations.” *Invited talk,* The Stanley Center for Psychiatric Research, MIT, Cambridge, MA.

17. Boyden, E. S. (2007) “Technologies for engineering neural circuit function.” *Invited talk,* Department of Biological Engineering, MIT, Cambridge, MA.

18. Boyden, E. S. (2007) “Engineering the Brain: Towards Systematic Cures for Neural Disorders.” *Featured speaker*, MIT Media Lab H2.0 (Human 2.0) Symposium, MIT, Cambridge, MA. http://h20.media.mit.edu/pdfs/esb2007-0509.pdf

19. Boyden, E. S. (2007) “Engineering the Brain.” *Invited talk*, Department of Psychiatry, Harvard/MGH, Boston, MA.

20. Boyden, E. S. (2007) “Towards enabling ultraprecise optical prosthetics.” *Invited talk*, Massachusetts Eye and Ear Infirmary, Boston, MA.

21. Boyden, E. S. (2007) "What Do We Need to Know, to do Practical Cognitive Augmentation?" *Invited session leader*, with Vaughan Bell, Science Foo Camp, Google, Mountain View, CA.

22. Boyden, E. S. (2007) “Brain-Engineering Technologies: Towards Making us Smarter and Happier.” *Invited talk*, AARP National Event and Expo, Boston, MA.

23. Boyden, E. S. (2007) “Engineering the Brain.” *Featured speaker*, Emerging Technologies (aka TR ETC, EmTech) Conference at MIT, Sept. 25-27, 2007

24. Boyden, E. S. (2007) “Towards ultraprecise optical prosthetics for treating pain: enabling technologies and testing.” *Invited speaker*, MGH-Charlestown, Boston, MA.

25. Boyden, E. S. (2007) “Controlling neural circuits: towards synthetic neurobiology.” *Invited speaker*, Harvard University Division of Applied Sciences, Cambridge, MA.

26. Boyden, E. S. (2007) “Principles of controlling neural circuit functions: towards synthetic neurobiology.” *Invited speaker*, Intel Corporation, Santa Clara, CA.

27. Boyden, E. S. (2007) “Neural Control Technologies and Uses Thereof.” *Invited speaker*, Innerspace Foundation, Boston, MA.

28. Boyden, E. S. (2008) “Towards a New Generation of Intelligent Brain Interfaces.” *Invited speaker*, Canon.

29. Boyden, E. S. (2008) “Engineering the brain.” *Invited speaker*, Honda.

30. Boyden, E. S. (2008) “Talking to the Mind: New Approaches to Engineering the Brain.” *Invited speaker,* The International House of Japan.

31. Boyden, E. S. (2008) “New Ideas on how to Get Information Into and Out of the Brain.” *Invited speaker*, NEC.

32. Boyden, E. S. (2008) “New Ideas on how to Get Information Into and Out of the Brain.” *Invited speaker*, Hitachi.

33. Boyden, E. S. (2008) “Optical Neuron Control: Understanding and Engineering Normal and Pathological Neural Dynamics.” *Invited speaker*, Boston University.

34. Boyden, E. S. (2008) “Genetically-Targeted Optical Neuromodulation: Towards

Circuitwide Control of Normal and Pathological Neural Computation." *Speaker (and workshop organizer/session chair)*, Computational and Systems Neuroscience (CoSyNe) Workshop, Snowbird, UT.

35. Boyden, E. S. (2008) "Synthetic Neurobiology: Towards Engineering Brain Circuits for Health and Human Augmentation." *Featured speaker,* O'Reilly ETech (Emerging Technology) Conference, San Diego, CA.

36. Boyden, E. S. (2008) "Optical Neural Control: Understanding Normal and Pathological Neuronal Circuit Dynamics." *Invited speaker,* MIT Modern Optics and Spectroscopy Seminar Series, Cambridge, MA.

37. Boyden, E. S. (2008) "Optical Neural Control: Analyzing and Engineering Normal and Pathological Neuronal Circuit Dynamics." *Invited speaker,* Psychiatry Department, Yale University, New Haven, CT.

38. Boyden, E. S. (2008) "Optical Neural Control: Analyzing and Engineering Normal and Pathological Neuronal Circuit Dynamics." *Invited speaker,* Brain and Cognitive Sciences Department, MIT, Cambridge, MA.

39. Boyden, E. S. (2008) "Prosthetic Systems for Therapeutic Optical Activation and Silencing of Genetically-Targeted Neurons." *Invited speaker,* MEMS for Implantable Medical Devices Symposium, MIT, Cambridge, MA.

40. Boyden, E. S. (2008) "Optical Neural Control: Analyzing and Engineering Normal and Pathological Neuronal Circuit Dynamics." *Invited speaker*, 2008 Neuroscience Spring Symposium, University of Michigan.

41. Boyden, E. S. (2008) "Prosthetic Optical Fiber Systems for Therapeutic Neural Activation and Silencing." *Invited speaker*, Corning, Inc., Corning, NY.

42. Boyden, E. S. (2008) "Controlling neural circuit elements to understand and engineer their roles in cognition." *Invited speaker,* NYU, New York City, NY.

43. Boyden, E. S. (2008) "Optical Neural Control: Analyzing and Engineering Normal and Pathological Neuronal Circuit Dynamics." *Invited speaker,* Neuron to Synapse Meeting (sponsored by GeneExpression Systems), Harvard Medical School, Boston, MA.

44. Boyden, E. S. (2008) "Repairing Neural Circuits: Principles for Thinking About Epilepsy, Depression, and Schizophrenia." *Invited speaker*, Kavli Science Journalism Workshop 'Frontiers of Brain Science,' Knight Science Journalism Fellowships Program, MIT, Cambridge, MA.

45. Boyden, E. S. (2008) "Optical Neural Control: Analyzing and Engineering Normal and Pathological Neuronal Circuit Dynamics." *Invited speaker*, Neuroimaging Groups presentation, Marine Biology Laboratory, Woods Hole, MA.

46. Boyden, E. S. (2008) "What should we really be doing, to understand neural systems?." *Invited speaker*, Grass Lab Tuesday night talk, Marine Biology Laboratory, Woods Hole, MA.

47. Boyden, E. S. (2008) "Optical Brain Control: Analyzing and Engineering Normal and Pathological Neural Circuit Dynamics." *Invited speaker*, Integrative Brain Reseach Symposium, Sapporo, Japan.

48. Boyden, E. S. (2008) "Optical Brain Control: Analyzing and Engineering Normal and Pathological Neural Circuit Dynamics." *Invited speaker*, NIMH Intramural Retreat, Gettysburg, PA.

49. Boyden, E. S. (2008) "Optical Neuron Control: Towards Principles of Controlling Neural Circuits." *Invited speaker*, Integrative Approaches to Brain Complexity Conference, Cold Spring Harbor/Wellcome Trust, Wellcome Trust Conference Center, Hinxton, UK.

50. Boyden, E. S. (2008) "Optical methods for controlling and correcting neural circuit

functions." *Invited speaker*, "In Vivo Imaging in Recovery After Neural Injury: From Microimaging in Animal Models to Functional Imaging in Man." Satellite Symposium to the American Congress of Rehabilitation Medicine (ACRM) and the American Society of Neurologic Rehabilitation (ASNR) Joint Educational Conference, Toronto, Canada.

51. Barry, B., Boyden, E., Lang, E. (2008) "Software Technologies in the Delivery of Intelligent Language Hypnosis Engines." Procedural Hypnosis: From Bench Top to Bedside (Symposium), 59th Annual Scientific Program, October 24-26, 2008 Hypnosis 2008: Foundations & Frontiers, Society for Clinical and Experimental Hypnosis.

52. Boyden, E. S. (2008) "High-Precision Genetically-Targeted Optical Control of Normal and Pathological Neural Computations." *Invited speaker*, HHMI Conference on Genetic Manipulation of Neuronal Activity, Janelia Farm, Ashburn, VA.

53. Boyden, E. S. (2008) "Optical Brain Control: Analyzing and Engineering Normal and Pathological Neural Circuit Dynamics." *Invited speaker*, Carolina Biophysics Symposium, Chapel Hill, NC.

54. Boyden, E. S. (2008) "Optical Brain Control: Analyzing and Engineering Normal and Pathological Neural Circuit Dynamics." *Invited speaker*, MIT Synthetic Biology Working Group, Cambridge, MA.

55. Boyden, E. S. (2009) "Novel Tools for Precisely Controlling Brain Functions." *Invited speaker*, Brain Research Center and Student Biotechnology Network, University of British Columbia, Vancouver, Canada.

56. Boyden, E. S. (2009) "Optical Brain Control: Analyzing and Engineering Normal and Pathological Neural Circuit Dynamics." *Invited speaker*, CIMIT Forum, Boston, MA.

57. Boyden, E. S. (2009) "Optical Brain Control: Analyzing and Engineering Normal and Pathological Neural Circuit Dynamics." *Invited speaker*, Dept. of Bioengineering, University of Pennsylvania, Philadelphia, PA.

58. Boyden, E. S. (2009) "Optical Control Of Normal and Pathological Neural Circuit Computations." *Invited speaker*, McGovern Symposium, Tsinghua University, Beijing, China.

59. Boyden, E. S. (2009) "Optical Neural Control: Towards Systematic Parsing of the Role of Cell Types in Normal and Abnormal Neural Computation." Invited talk, MGH-HST Martinos Center Brainmap Series, Cambridge, MA.

60. Boyden, E. S. (2009) "Optical Brain Control: Towards New Therapies for Brain Disorders." Invited speaker, Optical Society of America (New England Section Meeting), Cambridge, MA.

61. Boyden, E. S. (2009) "Optical Neural Control: Analyzing and Engineering Normal and Pathological Neural Circuit Dynamics." *Invited speaker*, Tufts Neuroscience Symposium, Tufts University, Cambridge, MA.

62. Boyden, E. S. (2009) "Towards Understanding The Circuits of Cognition: Engineering Tools for Analyzing Primate Brain Dynamics." *Invited speaker, along with Xue Han,* New England Primate Research Center (NEPRC), Harvard Medical School, Southborough, MA.

63. Boyden, E. S. (2009) "Optical Activation of Neurons." *Invited speaker,* Challenges for 21st Century Photonics, CIPS, MIT, Cambridge, MA.

64. Boyden, E. S. (2009) "Optical Brain Control: Towards New Insights and Therapies." *Invited speaker,* Psychiatric Genetics and Translational Research Seminar, Masschusetts General Hospital, Boston, MA.

65. Boyden, E. S. (2009) “Enabling Systematic Neuroscience with Novel Optical Neural Control Strategies.” *Invited speaker,* Cold Spring Harbor Laboratories, NY.

66. Boyden, E. S. (2009) “Optical Neural Control Prosthetics.” *Invited speaker,* No Barriers Festival, Miami, FL.

67. Boyden, E. S. (2009) “Optical Cell-Specific Neuromodulation: Towards Engineering the Brain for Therapeutic Purposes.” *Invited speaker,* Medtronic, Minneapolis, MN.

68. Boyden, E. S. (2009) "Optical control of the brain: Understanding thought, engineering cures.” Invited Speaker, HST Summer Institute Biomedical Optics Lecture Series, Massachusetts General Hospital, Boston, MA.

69. Boyden, E. S. (2009) “Technologies for controlling neural circuit dynamics.” Sloan-Swartz 2009 Annual Meeting on Computational Neuroscience, Harvard, Cambridge, MA.

70. Boyden, E. S. (2009) “Enabling Systematic Neuroscience with Novel Optical Neural Control Strategies.” Invited Seminar, Indiana University, Bloomington, IN.

Other non-peer-reviewed talks and conference papers

1. Schoner, B., Cooper, C., Douglas, C., Boyden, E. S., Gershenfeld, N. (1998) “Cluster Weighted Modeling for Time Series (How to Build a Digital Strad).” *Workshop on Nonlinear Dynamics and Statistics*, Issac Newton Institute, Cambridge.

2. Chen, G., Foletti, D. L., Boyden, E. S., Holz, R. W., Scheller, R. H., Tsien, R. W. (2000) "Differential functions of Rab3A in regulating excitatory and inhibitory transmission in hippocampal neurons.” *Society for Neuroscience*, Online.

3. Boyden, E. S., Raymond, J. L. (2002) "Induction, timecourse, and persistence of mouse vestibulo-ocular reflex adaptation.” *Society for Neuroscience*, Online.

4. Boyden, E. S., Chatila, T. A., Raymond, J. L. (2003) "Motor memories in the vestibulo-ocular reflex of CaMKIV knockout mice.” *Society for Neuroscience*, Online.

5. Mong, C., Cao, Y. Q., Boyden, E. S., Abbott, L. C., Tsien, R. W. (2003) "Properties of cortical spreading depression across visual cortex in mice with spontaneous mutations in P/Q-type Ca+2 channels.” *Society for Neuroscience*, Online.

6. Liao, Y. J., Boyden, E. S., Tsien, R. W. (2003) "Anti-calcium channel antibody affects cerebellar synaptic transmission in a model of acquired channelopathy.” *Society for Neuroscience,* Online.

7. Liao, Y. J., Safa, P., Boyden, E. S., Tsien, R. W. (2004) "Antibody-mediated altered cerebellar transmission.” *Channels, Receptors, and Synapses Meeting*, Cold Spring Harbor, NY, April 2004.

8. Kimpo, R. R., Katoh, A., Boyden, E. S., Raymond, J. L. (2004) "Patterns of generalization constrain encoding of learned opposite changes in the vestibulo-ocular reflex.” *Society for Neuroscience*, Online.

9. Liao, Y. J., Safa, P., Boyden, E. S., Tsien R. W. (2004) "Antibody-mediated channelopathy in a model of paraneoplastic cerebellar ataxia.” *Society for Neuroscience*, Online.

10. Boyden, E. S., “Content-selective neural mechanisms of memory encoding.” (2005) *Catalyzing the Future*, Fannie and John Hertz Foundation Symposium.

11. Boyden, E. S., Zhang, F., Bamberg, E., Nagel, G., and Deisseroth, K. (2005) "Millisecond-timescale optical control of neural computation via channelrhodopsin-2.” Talk, at *Society For Neuroscience*, Online.

12. Zhang, F., Boyden, E. S., Deisseroth, K. (2005) "Genetic and optical strategies for using channelrhodopsin-2 to control diverse neural functions." *Society for Neuroscience*, Online.

13. Boyden, E. S., Safa, P., Pyle, J. L., Neogi, M., Raymond, J. L., Tsien, R. W. (2005) "Gene expression patterns in the medial vestibular nucleus indicate the direction of motor learning in the vestibulo-ocular reflex." Talk, at *Society for Neuroscience*, Online.

14. Wang H., Peca J., Qiu L., Wang D., Zhang F., Boyden E. S., Deisseroth K., Feng G., Augustine G. J., Hall W. C. (2006) "Circuit analysis using optical stimulation in ChR2 transgenic mice." *Society for Neuroscience*, Online.

15. Peca, J., Wang, H., Arenkiel, B. R., Matsusaki, M., Davison, I. G., Matsusaki, K., Noguchi, J., Qiu, L., Wang, D., Zhang, F., Zhao, S., Berglund, K., Feliciano, C., Boyden, E. S., Kasai, H., Hall, W. C., Deisseroth, K., Ehlers, M. D., Augustin, G. J., Feng, G. (2007) A transgenic tool for controlling neuronal activity with light, Society for Neuroscience, Online.

16. Han, X., and Boyden, E. S. (2007) "Two-Color, Bi-Directional Optical Voltage Control of Genetically-Targeted Neurons." *Computational and Systems Neuroscience (CoSyNe)*, Salt Lake City, UT, Feb 22-25, 2007.

17. (Henninger, M. A.), Bernstein, J., Ko, E., Strelzoff, A., Chan, S. C. Y., Gidwaney, V., Stickgold, E., Tentori, A. M., McConnell, J., Rodriguez, A., Monahan, P., Talei Franzesi, G., Han, X., Qian, X., Boyden, E. S. (2008) "A scalable toolbox for systematic, cell-specific optical control of entire 3-D neural circuits in the intact mammalian brain." *Society for Neuroscience*, Online. (M. A. Henninger sponsored the abstract submission, but J. Bernstein performed the key work.)

18. Han, X., Qian, X., Bernstein, J., Zhou, H., Graybiel, A., Desimone, R., Boyden, E. S. (2008) "Millisecond-timescale optical control of specific genetically-targeted neurons and neural circuits in primate cerebral cortex." *Society for Neuroscience*, Online.

19. Han, X., Qian, X., Talei Franzesi G., Stern, P., Boyden, E. S. (2008) "Molecular toolboxes for quantitatively precise, genetically-targeted optical control of normal and pathological neural network dynamics." *Society for Neuroscience*, Online.

20. Horsager, A., Liu, J.-W., Boyden, E. S., Arman, A. C., Matteo, B. C.,, Sampath, A. P., Hauswirth, W.W. (2009) "Restoring visual function in adult rd1 mice using virally-delivered channelrhodopsin." *Association for Research in Vision and Opthalmology*, Online.

21. Liu, J.-W., Horsager, A., Ding, M., Mani, S., Chiodo, V.A., Boyden, E.S., Hauswirth, W.W. (2009) "AAV-mediated ON Bipolar Cell Targeting In The rd1 Mouse Lacking Photoreceptors." *Association for Research in Vision and Opthalmology*, Online.

22. Tsien, R. W., Barrett, C. F., Safa, P., Chen, Y.-R., Boyden, E. S., Liao, Y. J. (2008) "Genetic and Acquired Neural Diseases Involving Voltage-gated Calcium Channels." Abstract, Sixty-Second Annual Meeting of the Society of General Physiologists, Woods Hole, MA.

23. Boyden, E. (2009) "Optical neural control: towards treating neurological and psychiatric disorders." Talk at Photons and Neurons, Conference 7180, BiOS 2009, Photonics West 2009, SPIE, January 2009.

24. Han, X., Qian, X., Bernstein, J., Zhou, H., Graybiel, A., Desimone, R., Boyden, E.S. (2009) "Safety and efficacy of genetically-targeted optical neuromodulation in non-human primates." Talk at Photons and Neurons, Conference 7180, BiOS 2009, Photonics West 2009, SPIE, January 2009.

25. Han, X., Qian, X., Bernstein, J., Zhou, H., Graybiel, A., Desimone, R., Boyden, E.S. (2009) "Excitatory-inhibitory network interactions during cell-specific optical cortical control."

Talk at Photons and Neurons, Conference 7180, BiOS 2009, Photonics West 2009, SPIE, January 2009.

26. Lang, E. V., Diamond, S. G., Flory, N., Barry, B., (Boyden, E. S.) (2008) “Hypnosis and Empathic Communication in Medical Practice -- A Report.” American Psychological Association Convention, Session 1264.

27. Bernstein, J. G., Baratta, M. V., Ko, E. Y., Henninger, M. A. Li, M., Goosens, K., Boyden, E. S. (2009) “Modulation of fear behavior via optical fiber arrays targeted to bilateral prefrontal cortex.” *Society for Neuroscience*, Online.

28. Talei Franzesi, G., Borgers, C., Qian, X., Li, M., Han, X., Kopell, N., LeBeau, F., Whittington, M., Boyden, E. S. (2009) “Dynamical properties of gamma-frequency cell assemblies in the hippocampus probed with optical neural control and computational modeling.” *Society for Neuroscience*, Online.

29. McCarthy, M., Han, X., Boyden, E. S., Kopell, N. (2009) “Striatum as a possible source of exaggerated beta oscillations in Parkinson’s Disease: insights from computational models.” *Society for Neuroscience*, Online.

30. Zorzos, A. N., Bernstein, J. G., Boyden, E.S., Fonstad, C. G. (2009) “Integrated microstructure lightguides for ultradense optical neural control of 3-dimensional neural circuits.” *Society for Neuroscience*, Online.

31. Zorzos, A. N., Dietrich, A., Talei Franzesi, G., Chow, B., Han, X., Fonstad, C. G., Boyden, E.S. (2009) “Light-proof neural recording electrodes.” *Society for Neuroscience*, Online.

32. Desai, M., Bernstein, J., Atallah, H., Kahn, I., Moore, C. I., Kopell, N., Graybiel, A., Boyden, E. S. (2009) “Integration of optical neural control and high-field fMRI: Towards systematic exploration of functional neural dynamics with ‘Opto-fMRI’.” *Society for Neuroscience*, Online.

33. Horsager, A., Liu, J.-W., Boyden, E.S., Arman, A.C., Matteo, B.C., Sampath, A.P., Hauswirth, W.W. (2009) “Circuit-specific expression of channelrhodopsin restores visual function in blind rd1, rd16, and rho -/- mice.” *Society for Neuroscience*, Online.

34. Shin, S.-L., Boyden, E. S., Katoh, A., Zhao, G. Q., Raymond, J.L. (2009) “Adaptive timing is impaired in mice deficient in presynaptic LTP.” *Society for Neuroscience*, Online.

35. Chow, B.Y., Han, X., Qian, X., Li, M., Chuong, A. S., Monahan, P.E., Dobry, A.S., Boyden, E.S. (2009) “High-efficacy, temporally-precise, in vivo neural silencing via light-driven proton pumping.” *Society for Neuroscience*, Online.

36. Chow, B.Y., Han, X., Qian, X., Li, M., Chuong, A. S., Monahan, P.E., Dobry, A.S., Boyden, E.S. (2009) “Multiple-color optical silencing of distinct neural populations using novel classes of light-driven ion pumps.” *Society for Neuroscience*, Online.

37. Cao, R., Cardin, J., Higashikobo, B., Knoblich, U., Brumberg, J. C., Boyden, E. S., Moore, C. I. (2009) “Testing the hemoneural hypothesis: Specific control of blood flow and functional two photon imaging.” *Society for Neuroscience*, Online.

38. Boyden, E. S. (2009) Optical Neural Control: Engineering Therapeutic Circuit Dynamics: Application to Post-Traumatic Stress Disorder, Talk 7-9, Poster P31-11, PTSD Treatment, Military Health Research Forum, Kansas City, MO.

39. Boyden, E. S. (2009) “Systematic Optical Control of Neural Circuits.” Fifth Annual NIH Director’s Pioneer Award Symposium, National Institutes of Health, Bethesda, MD.

Book chapters

1. Task Group Summary 6 (The Brain), The National Academies Keck Futures Initiative: Complex Systems: Task Group Summaries, 2009, ISBN 0-309-13725-X, National Academies Keck Future Initiative, National Academies Press, Washington DC.

2. Boyden, E. S., Han, X., Talei Franzesi, G., Chan, S., Bernstein, J., Qian, X., Li, M. (2009) "New Techniques for Investigating Brain Rhythms: Optical Neural Control and Multielectrode Recording," In: Rhythms of the Neocortex: Where Do They Come From and What Are They Good For? (Kopell N., ed.) pp. 65-75. Washington, DC: Society for Neuroscience.

APPENDIX 2

Han, X., Qian, X., Bernstein, J.G., Zhou, H.-H., Talei Franzesi, G., Stern, P., Bronson, R.T., Graybiel, A.M., Desimone, R., and Boyden, E.S. (2009) Millisecond-Timescale Optical Control of Neural Dynamics in the Nonhuman Primate Brain, *Neuron* 62(2): 191-198.

Neuron
Report

Millisecond-Timescale Optical Control of Neural Dynamics in the Nonhuman Primate Brain

Xue Han,[1,*] Xiaofeng Qian,[1] Jacob G. Bernstein,[1] Hui-hui Zhou,[2] Giovanni Talei Franzesi,[1] Patrick Stern,[3] Roderick T. Bronson,[3] Ann M. Graybiel,[2] Robert Desimone,[2] and Edward S. Boyden[1,2,4,*]
[1]Media Lab, Synthetic Neurobiology Group
[2]McGovern Institute, Department of Brain and Cognitive Sciences
[3]Koch Center for Cancer Research
[4]Department of Biological Engineering
Massachusetts Institute of Technology, 77 Massachusetts Avenue, Cambridge, MA 02139, USA
*Correspondence: xuehan1@gmail.com (X.H.), esb@media.mit.edu (E.S.B.)
DOI 10.1016/j.neuron.2009.03.011

SUMMARY

To understand how brain states and behaviors are generated by neural circuits, it would be useful to be able to perturb precisely the activity of specific cell types and pathways in the nonhuman primate nervous system. We used lentivirus to target the light-activated cation channel channelrhodopsin-2 (ChR2) specifically to excitatory neurons of the macaque frontal cortex. Using a laser-coupled optical fiber in conjunction with a recording microelectrode, we showed that activation of excitatory neurons resulted in well-timed excitatory and suppressive influences on neocortical neural networks. ChR2 was safely expressed, and could mediate optical neuromodulation, in primate neocortex over many months. These findings highlight a methodology for investigating the causal role of specific cell types in nonhuman primate neural computation, cognition, and behavior, and open up the possibility of a new generation of ultraprecise neurological and psychiatric therapeutics via cell-type-specific optical neural control prosthetics.

INTRODUCTION

The rhesus macaque is an important model species for understanding neural computation, cognition, and behavior, as well as for probing the circuit-level basis of human neurological and psychiatric disorders. To resolve how complex functions emerge from the activity of diverse cell types, ideally one would be able to perturb the activity of genetically specified cell types and neural pathways in the primate brain, in a temporally precise fashion. In one recent study, adeno-associated virus (AAV) was used to deliver the *Drosophila* allatostatin receptor to neurons in the primate thalamus (Tan et al., 2006), enabling neural silencing via intracranial delivery of the small molecule allatostatin. In general, however, the adaptation of neural control tools to the primate brain has been slow in comparison to the rapid adaptation of such tools for characterizing circuit functions in worms, flies, and mice (reviewed in Luo et al., 2008). Indeed, although molecular techniques have been used to deliver genetic payloads to the primate brain (e.g., Kordower et al., 2000; Liu et al., 2004; Stettler et al., 2006), as well as to make transgenic primates (Chan et al., 2001; Yang et al., 2008), no attempts have been made to target genes to genetically specified neuron types. Here we used channelrhodopsin-2 (ChR2), a genetically encoded molecular sensitizer that enables activation of neurons in response to pulses of blue light (Boyden et al., 2005; Han and Boyden, 2007; Ishizuka et al., 2006; Li et al., 2005; Nagel et al., 2003; Zhang et al., 2007), to assess the impact of selective activation of cortical excitatory neurons on primate cortical dynamics. We used optical fibers in conjunction with microelectrodes to perform simultaneous in vivo optical stimulation and electrical recording in the awake primate. Selectively activating ChR2-positive excitatory neurons resulted in well-timed excitatory and suppressive influences on neural activity, reflecting neural dynamics downstream of excitatory neuron activation. ChR2 was safely expressed and could mediate temporally precise optical neural stimulation of significant volumes of cortical tissue for months after viral injection, opening up the possibility for such technologies to support precise, cell-specific optical control prosthetics for patients with severe neurological and psychiatric disorders.

RESULTS

We targeted ChR2-GFP to neurons in the frontal cortex in two monkeys (denoted N and A), by injecting VSVg-pseudotyped lentivirus carrying the ChR2-GFP gene behind the 1.3 kb α-CaMKII promoter (Figure 1A; details in Supplemental Experimental Procedures, available online), as used before in mice to target excitatory neurons (Dittgen et al., 2004). To insure repeatable targeting of viruses, optical fibers, and electrodes to the same sites over extended periods of time (Figure 1B), we designed and used a grid to coordinate stereotactic virus injections, photostimulation, and recording (Figure 1C). Histology showed that 1 μl viral injections labeled roughly spherical regions of cortex 1.4 ± 0.5 mm in diameter (mean ± standard deviation [SD]; exemplar in Figure 1D; details in Figure S4, available online). We did not observe GFP-positive cells in thalamic regions that project to injected regions, indicating a lack of retrograde labeling using lentivirus prepared as described. ChR2-GFP appeared to be

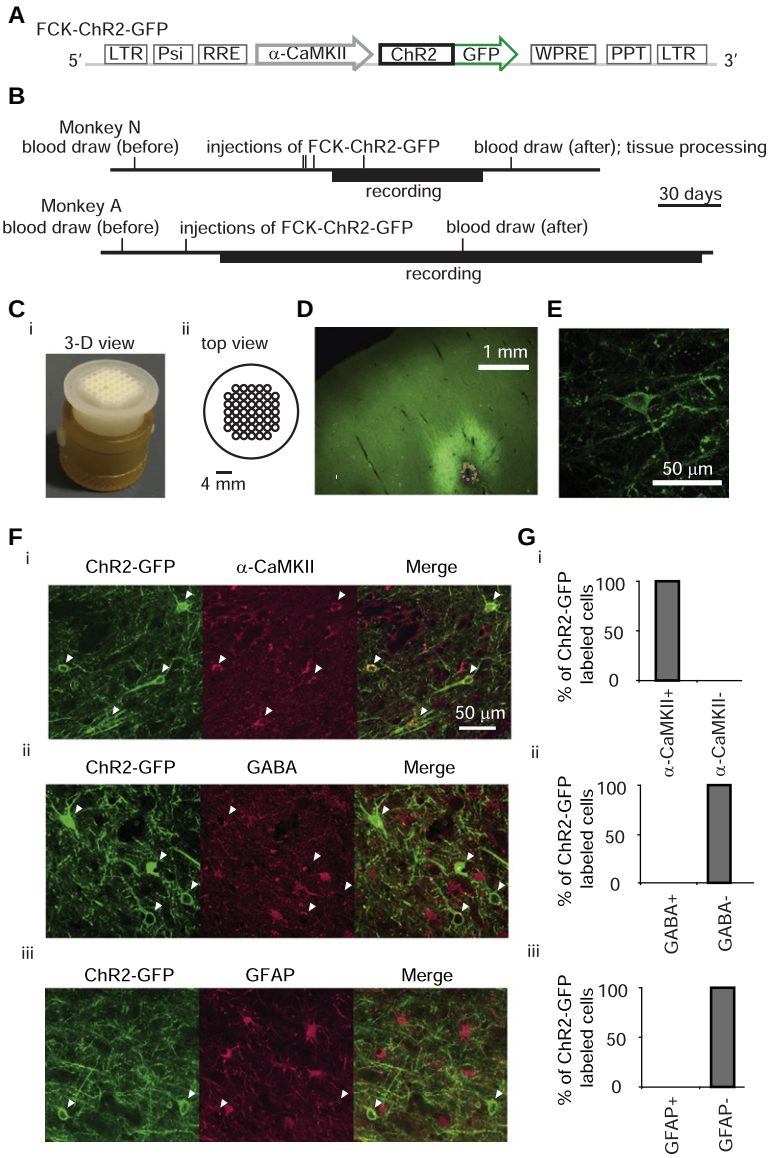

Figure 1. Expression of ChR2-GFP in Excitatory Neurons in Frontal Cortex of Primate Brain

(A) Schematic of lentiviral cassette. (B) Timeline of experiments for monkey N (top) and monkey A (bottom). (C) 3D printed targeting grid, inserted into a recording chamber (Ci) and in a top-view schematic (Cii). (D) Fluorescence image showing ChR2-GFP expression in deep layers of cortex (coronal slice; dotted magenta circle indicates diameter of virus injection cannula). (E) Representative cortical neuron expressing ChR2-GFP. (F) Images of anti-GFP fluorescence (left) as well as immunofluorescence of three cell-type markers: α-CaMKII (Fi), GABA (Fii), and GFAP (Fiii) (middle; right, overlay of the two left images). Arrowheads indicate ChR2-GFP-positive cell bodies. (G) Percent of ChR2-GFP-positive cells coexpressing each of the three markers in (F).

well localized to the plasma membrane at the cell body and throughout neuronal processes (Figure 1E). To assess the cell-type specificity of ChR2-GFP gene expression driven by the α-CaMKII promoter, we immunostained primate cortical slices with antibodies against the excitatory neuron-specific marker α-CaMKII (Jones et al., 1994; Tighilet et al., 1998), the inhibitory neuron-specific neurotransmitter GABA (Hendry et al., 1989; Houser et al., 1983), and the astrocyte-specific marker glial fibrillary acidic protein (GFAP) (Cahoy et al., 2008; McLendon and Bigner, 1994). Neurons expressing ChR2-GFP were positive for α-CaMKII (Figure 1Fi), but not GABA (Figure 1Fii) or GFAP (Figure 1Fiii). Of the ChR2-GFP-positive neurons examined, all coexpressed α-CaMKII (127/127 cells; Figure 1Gi), but none coexpressed GABA (Figure 1Gii, 0/78 cells) or GFAP (Figure 1Giii, 0/84 cells). In order to gauge the efficiency of viral labeling, we counted the fraction of α-CaMKII-positive cells that expressed ChR2-GFP. Near centers of injection sites, where ChR2-GFP expression peaked, 78% ± 8% of the α-CaMKII-positive cells expressed ChR2-GFP (mean ± SD; n = 3 fields of view; 42 ChR2-GFP neurons counted). Thus, lentivirus expressing ChR2-GFP under the α-CaMKII promoter enables cell-specific targeting and efficient expression of ChR2-GFP in excitatory neurons of the monkey frontal cortex.

Given the extended duration of nonhuman primate experiments, and the prospect of using cell-specific optical neuroprosthetics for therapy, we assessed the safety of ChR2-GFP expression in primate brain. After months of ChR2-GFP expression, during which time we repeatedly illuminated neurons with blue light and successfully made recordings, we saw widespread expression of ChR2-GFP in healthy-looking neurons, with no histological abnormalities in neurons or glia, and no immune reaction at the cellular or antibody level (Figure 2; see detailed text in Supplemental Data). These multiple lines of evidence together support the safety of ChR2-GFP expression in the brain of the nonhuman primate, and if supported by further and longer-term analyses, may provide the basis for cell-specific neuromodulation therapy in humans.

To assess the effect of optical activation of ChR2-expressing excitatory neurons on frontal cortical neural circuits in awake monkey, we developed a system appropriate for in vivo monkey use, coupling a fiber to a blue 473 nm laser (Bernstein et al., 2008) and assembling multiple electrodes into independently controlled drives (Figures 3Ai and 3Aii), which were then inserted into a single hole within the 3D printed grid (Figure 1C). This setup allowed us to record from neurons while exposing local cortex to pulses of blue light. In regions of cortex that were not virus labeled, we never observed light modulation of neural activity (n = 32 such sites). In regions that were virus labeled, many neurons increased their firing rate during cortical exposure to blue light (Figures 3B and 3C). We called these neurons "excited" units. In addition to these excited units, many neurons decreased their firing rate during cortical exposure to blue light (Figures 3D and 3E). We called these neurons "suppressed" units, because they did not increase firing rate during blue light exposure, but instead

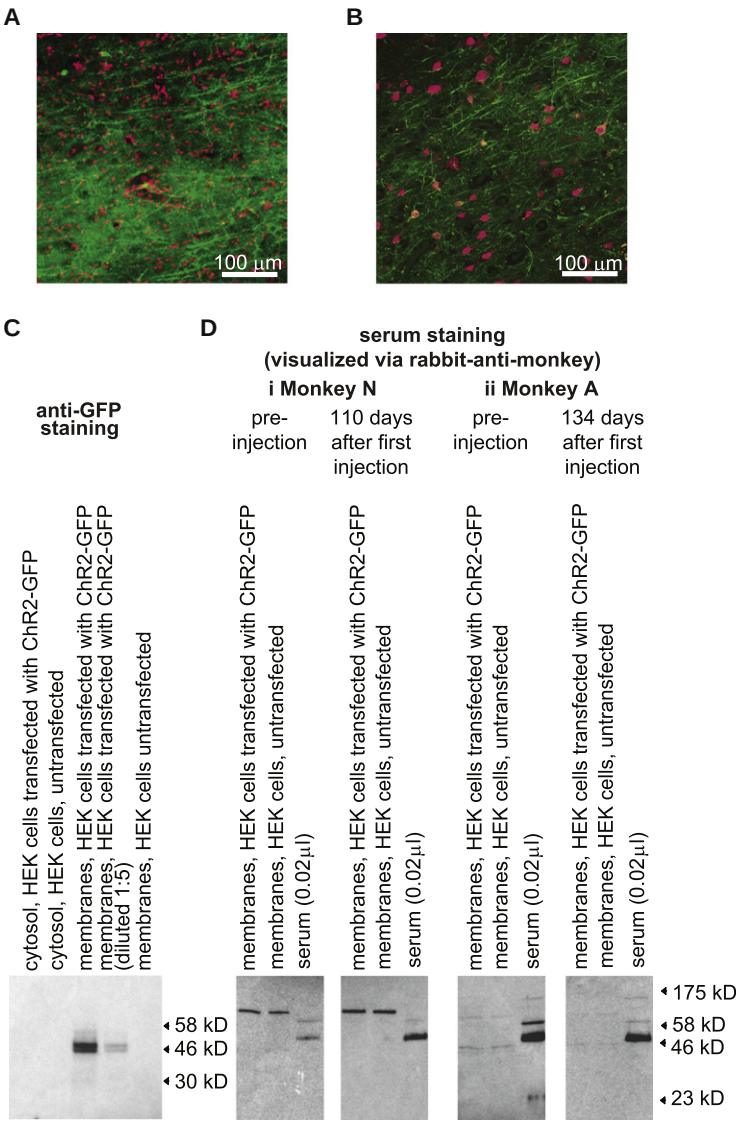

Figure 2. Analyses of Potential Immune Responses against ChR2-GFP-Expressing Neurons in Primate Cortex

(A) Nuclear DNA staining (red; To-Pro-3 stain) of slices of monkey cortex containing ChR2-GFP-expressing neurons (green). (B) Neuronal staining (red; NeuN antibody) of slices of monkey cortex containing ChR2-GFP-expressing neurons (green). (C) Validation of ChR2-GFP expression in HEK cells via western blotting, using anti-GFP antibody. From left to right, lanes show, immunostained with anti-GFP: cytosolic fraction of HEK cells transfected with ChR2-GFP plasmid, cytosolic fraction of untransfected HEK cells, membrane fraction of HEK cells transfected with ChR2-GFP plasmid, membrane fraction (diluted 1:5) of HEK cells transfected with ChR2-GFP plasmid, and membrane fractions of untransfected HEK cells. (D) Assessment of monkey serum reaction to ChR2-GFP, for monkey N (Di) and monkey A (Dii), via western blotting, comparing preinjection (left) to postinjection (right). Membrane fractions of HEK cells transfected with ChR2-GFP (left lane), membrane fractions of untransfected HEK cells (middle lane), and monkey serum samples (right lane) were incubated with monkey serum (1:50 dilution), followed by rabbit-anti-monkey secondary antibody for visualization.

decreased firing rate during light delivery, even after brief illumination (i.e., a single light pulse). We hypothesized that since suppressed units decreased their firing rates without having undergone prior increases in spiking, the observed suppression was due to neural network activity, i.e., recruitment of inhibitory neurons downstream of the driven excitatory neurons. For both the excited and suppressed units, action potential waveforms elicited during light exposure were not different from waveforms observed in the dark ($p > 0.1$ for each of $n = 15$ excited single units; Kolmogorov-Smirnov test comparing waveform shapes in light versus dark; exemplars in Figures 3F and 3G). In regions where excited or suppressed units were found, few light-nonmodulated units were observed (Figure S5). These excited and suppressed units were also observed in the cortex of mice, when excitatory neurons expressing ChR2-GFP were activated by light (Figure S3). Light did, however, result in a low-frequency electrical artifact on our tungsten electrodes in the brain, presumably due to the photoelectric effect; this artifact was removed from our data by high-pass filtering (see Figure S1). Light (80 mW/mm^2 radiant flux out the tip of the fiber) modulated neurons at distances over 1.2 mm away from the fiber (Figure S2).

In the monkey cortex, we recorded 50 excited and 20 suppressed units during illumination with 200 ms blue light pulses. Out of these 70 units, 31 were single units (15 excited, 16 suppressed) and 39 were multiunits (35 excited, 4 suppressed). We pooled multiunits and single units for analysis unless otherwise indicated. Excited and suppressed units had similar baseline firing rates ($p > 0.2$, t test; only single units compared) and similar waveform shapes (see Supplemental Experimental Procedures). For excited units, firing rates increased rapidly at light onset, and then settled to a lower steady-state firing level (Figure 3H). For suppressed units, firing rates fell sharply after a short delay, and remained low for the duration of the light pulse (Figure 3J). For both excited and suppressed units, after light cessation the firing rates often dipped below baseline levels for ~100 ms. We quantified the magnitude of these changes in firing rate during three distinct periods: the first 20 ms of light exposure ("beginning of light"), the period between 20 ms after light onset and 20 ms after light cessation ("steady state"), and during the 20 ms period starting 20 ms after light cessation ("after light"). Excited units fired at 750%, 370%, and 46% of baseline firing rate during these three periods, respectively, in each case significantly different from baseline ($p < 0.0001$ for each, paired t test; Figure 3I). For single units, which yield absolute values of firing rate, excited neurons fired at 37 ± 7 Hz, 16 ± 4 Hz, and 1.3 ± 1 Hz during these three periods (mean ± standard error [SE]; $n = 15$ single units); baseline their firing rates was 6.5 ± 1.3 Hz. In contrast to the excited units, suppressed units did not change their firing rates relative to baseline during the beginning of light period ($p > 0.5$, paired t test; Figure 3K), but reduced their firing rates by 76% and 75%, respectively, during the steady state and after light periods

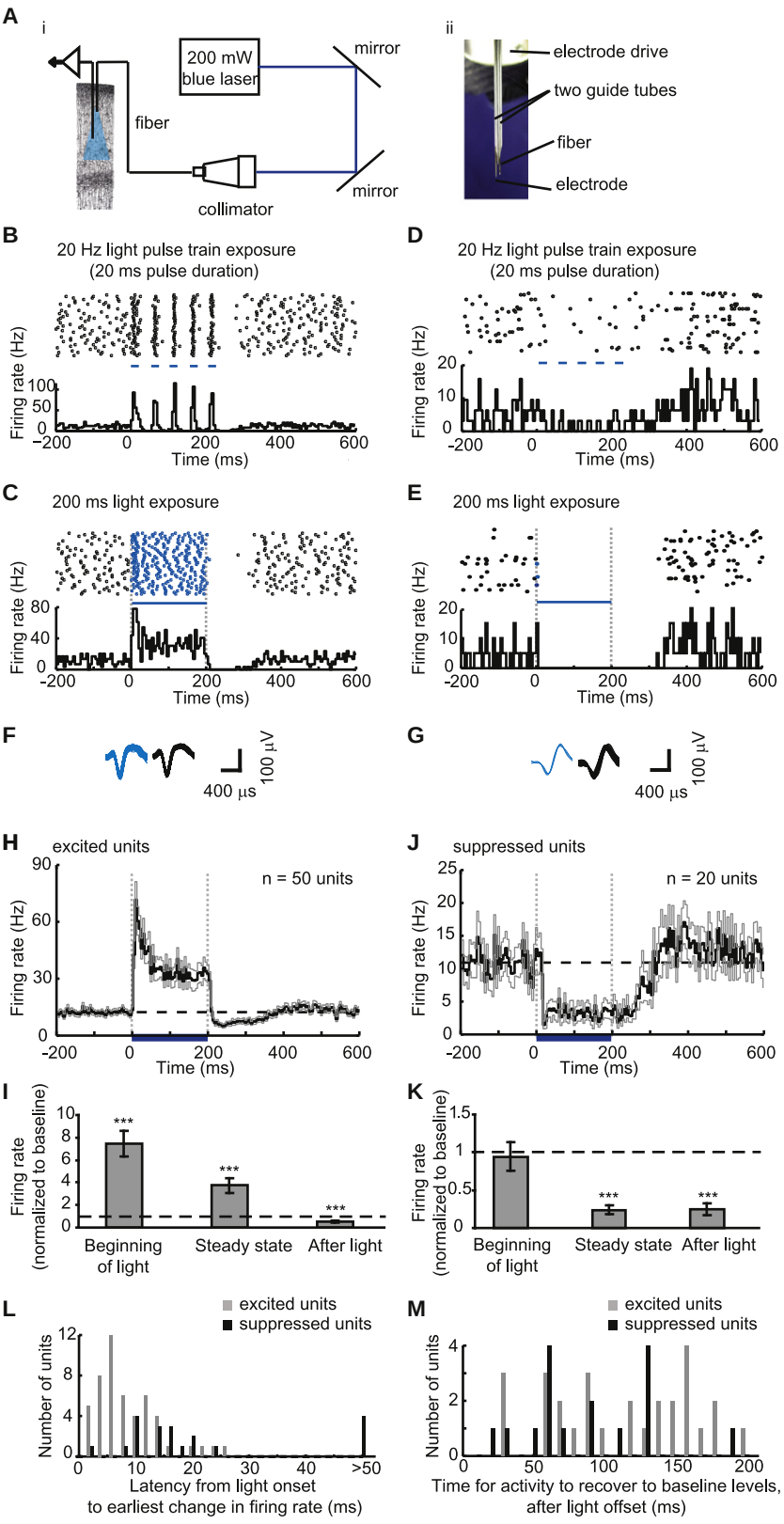

Figure 3. Increases and Decreases in Neural Activity Resulting from Optical Stimulation of Excitatory Neurons

(A) Apparatus for optical activation and electrical recording. (Ai) Schematic. (Aii) Photograph, showing optical fiber (200 μm diameter) and electrode (200 μm shank diameter) in guide tubes. (B and C) Increases in spiking activity in one neuron during blue light illumination (five pulses, 20 ms duration each [B], and 1 pulse, 200 ms duration [C]). In each panel, shown at top is a spike raster plot displaying each spike as a black dot; 40 trials are shown in horizontal rows (in this and subsequent raster plots); shown at bottom is a histogram of instantaneous firing rate, averaged across all trials; bin size, 5 ms (in this and subsequent histogram plots). Periods of blue light illumination are indicated by horizontal blue dashes, in this and subsequent panels. (D and E) Decreases in spiking activity in one neuron during blue light illumination (five pulses, 20 ms duration (D), and one pulse, 200 ms duration [E]). As with (B) and (C), shown at top are spike raster plots and shown at bottom are histograms of instantaneous firing rate. (F and G) Action potential waveforms elicited during light (shown in blue, left) or occurring spontaneously in darkness (shown in black, right), for the neurons plotted in (C) and (E), respectively. (H) Instantaneous firing rate, averaged across all excited units recorded upon 200 ms blue light exposure (black line, mean; gray lines, mean ± SE; n = 50 units). (I) Relative firing rate (i.e., firing rate during the indicated period, divided by baseline firing rate) during the first 20 ms after light onset ("beginning of light"), during the period between 20 ms after light onset and 20 ms after light cessation ("steady state"), and during the 20 ms period starting 20 ms after light cessation ("after light"), for the n = 50 units shown in (H). (***), significantly different ($p < 0.0001$; paired t test) from baseline rate (shown as dotted line); plotted is mean ± SE. (J) Instantaneous firing rate averaged across all suppressed units upon 200 ms blue light exposure (black line, mean; gray lines, mean ± SE; n = 20 units). (K) Relative firing rate, during the beginning of light, steady state, and after light periods, for the n = 20 units shown in (J). (L) Histogram of latencies between light onset and the earliest change in firing rate, for excited units (gray bars, n = 50 units) and suppressed units (black bars, n = 20 units); latencies longer than 50 ms were plotted in a bin labeled ">50." (M) Histogram of time elapsed until activity recovery to baseline after light cessation, for excited (gray bars, n = 28 units) and suppressed (black bars, n = 16 units) units that had lower-than-baseline firing rates during the after light period.

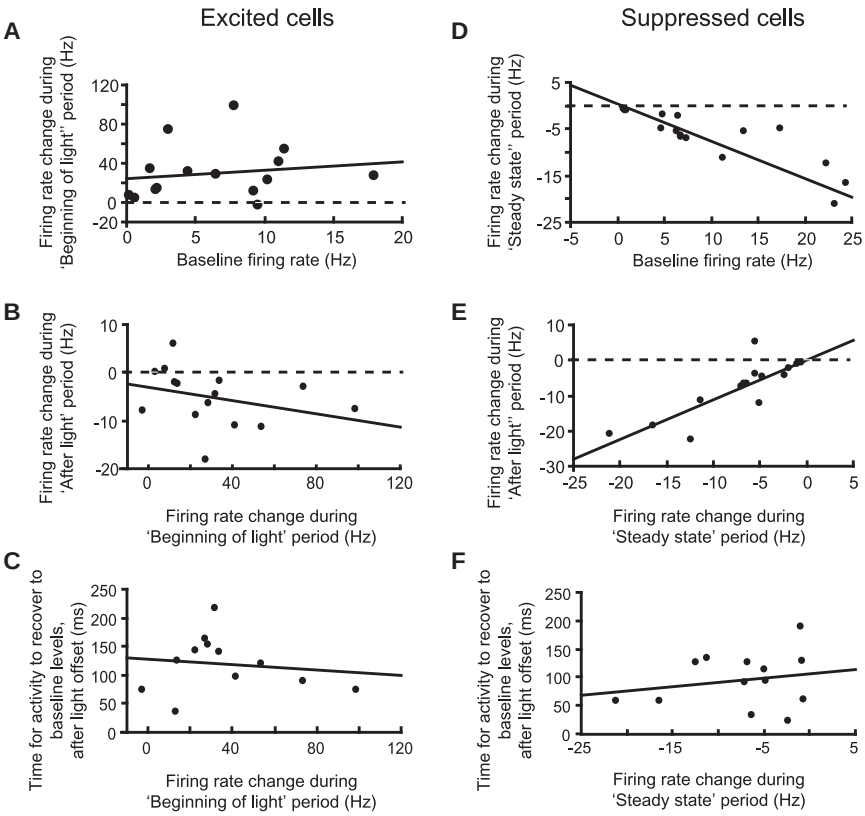

Figure 4. Comparison of Neural Activity Levels within Excited and Suppressed Single Units, before, during, and after Light Exposure

(A) Firing rate change during the beginning of light period (i.e., firing rate during beginning of light minus baseline firing rate) versus baseline firing rate, for excited cells (n = 15 excited single units). (B) Firing rate change during the after light period versus during the beginning of light period, for excited single units. (C) Time elapsed until activity recovery to baseline level after light cessation, versus firing rate change during the beginning of light period, for excited single units. (D) Firing rate change during the steady state period, versus baseline firing rate, for suppressed cells (n = 16 suppressed single units). (E) Firing rate change during the after light period versus during the steady state period, for suppressed single units. (F) Time elapsed until activity recovery to baseline level after light cessation, versus firing rate change during the steady state period, for suppressed single units.

(significantly lower than that during baseline [$p < 0.0001$, paired t test], but not different from each other; $p > 0.8$). Suppressed single units fired at 7.4 ± 1.7 Hz, 3.1 ± 1.0 Hz, and 2.5 ± 1.2 Hz during these three periods, respectively (mean ± SE; n = 16 single units); baseline firing rate was 9.9 ± 2.0 Hz.

We compared the latencies to changes in firing rate between excited versus suppressed units, and found two different, but overlapping, distributions. Excited units rapidly responded to light with latencies of 8.8 ± 0.8 ms (mean ± SE; Figure 3L). This short latency was not different from the first-spike latency of ChR2-positive cultured pyramidal neurons responding to pulses of blue light ($p > 0.6$, unpaired t test; compared to published data in Boyden et al., 2005), consistent with the idea, but not proving, that excited units were ChR2-positive pyramidal cells. In contrast to the short latencies of excited units, suppressed units began decreasing their firing rates 30.8 ± 8.0 ms after light onset (mean ± SE), a latency significantly longer than the latency for the increases in firing rates of excited units ($p < 0.0001$, unpaired t test). This difference is consistent with our hypothesis that suppressed units decreased their firing rates through neural network mechanisms involving inhibitory neuron recruitment, whereas excited units were directly activated by light. After light cessation (after light period), the majority of excited and suppressed units exhibited firing rates below baseline levels (28 out of 50 excited units; 16 out of 20 suppressed units). The time for this reduced firing rate to recover to baseline was similar for excited and suppressed units (Figure 3M, $p > 0.1$, unpaired t test), consistent with the idea that suppressive influences downstream of excitatory neuron activation are mediated by a neural-network-scale phenomenon such as inhibitory neuron recruitment.

To probe the nature of neural suppression further, we examined the activity of single units before, during, and after light exposure. For excited cells, we found that increases in firing rate during optical stimulation were independent of baseline firing rate ($R^2 = 0.025$, $p > 0.5$; Figure 4A; n = 15 excited single units). In addition, decreases in firing rate after light cessation were independent of the light-induced increases in firing rate ($R^2 = 0.096$, $p > 0.2$; Figure 4B). Finally, the time for firing rate to recover to baseline levels after light cessation was independent of prior increases in firing rate ($R^2 = 0.016$, $p > 0.7$; Figure 4C; n = 12 excited single units that decreased activity during the after light period). Thus, excited cells fired before, during, and after light exposure, in independent fashions. In contrast to excited units, for suppressed units decreases in firing rate during light exposure were highly correlated with baseline firing rate ($R^2 = 0.749$, $p < 0.0001$; Figure 4D; n = 16 suppressed single units): for each additional Hz of baseline firing rate, light exposure decreased firing by an additional ~0.6 Hz. In addition, the decrease in firing rate of suppressed neurons after light cessation was correlated with the decrease in firing rate during light exposure ($R^2 = 0.673$, $p < 0.0001$; Figure 4E). However, as for excited cells, the time for the firing rate to recover to baseline level was independent of prior reductions in activity levels for suppressed cells (e.g., during the steady state period; $R^2 = 0.045$, $p > 0.4$; Figure 4F; n = 13 suppressed single units that had significant decreases in activity during the after light period). Thus, for suppressed cells, but not for excited cells, light-induced changes in activity were correlated with baseline activity, as though the magnitudes of spontaneous and light-suppressed activity were both functions of a common neural network state. We further probed the response of excited cells with trains of light pulses at 10, 20,

and 50 Hz (Figure S6), finding that while spike probability fell during long, high-frequency trains, spike timing remained reliable, and therefore ChR2 may subserve the ability to use light to control cortical synchrony.

DISCUSSION

We have demonstrated millisecond-timescale optical activation of excitatory neurons in the frontal cortex of nonhuman primates, using lentivirally delivered ChR2, and have characterized the impact of such optical control on cortical circuits. This work demonstrates the feasibility of applying optogenetic methods to primate neural circuits, and points the way toward the potential use of optical control in a new generation of therapies for the improvement of human health. Immediately, this technology makes it possible to activate a region containing a set of excitatory neurons while avoiding the modulation of fibers of passage, or of neurons projecting into the region. Light stimulation did result in a slow electrical artifact on the metal electrode, which was easily filtered out from our spike recordings. Single viral injections labeled on the order of 1 mm^3 of brain tissue, comparable to the volume illuminated by single optical fibers, suggesting that arrays of viral injectors and optical fibers may enhance the ability to systematically modulate cell and circuit activities during behavior.

We found that whereas many neurons were excited during light activation of excitatory neurons, others were profoundly suppressed during light exposure. In addition, many excited and suppressed cells exhibited a period of reduced neural activity after cessation of light activation. These excited and suppressed effects were also observed in mouse cortical neurons under similar optical stimulation conditions. These effects may be due to biophysical properties of the neurons recorded, for example hyperpolarization after depolarization-induced opening of BK and SK potassium channels (Bekkers, 2000; Sah and Davies, 2000; Storm, 1987; Vogalis et al., 2003). But several independent lines of reasoning support the hypothesis that suppression emerges from recruitment of networks of inhibitory cells downstream of activated ChR2-positive excitatory cells. First, suppressed neurons underwent reductions in spike firing without having undergone prior increases in spike firing, which implies that cell-autonomous mechanisms such as postdepolarization hyperpolarization cannot be the sole mechanism mediating the observed suppression. Second, the latency to the decrease in firing after light onset was significantly longer for suppressed cells than the latency to the increase in firing was for excited cells, consistent with suppressed cells being downstream of light-activated cells. Third, suppressed neurons decreased activity during light exposure in proportion to their basal firing rate, whereas light-driven excitation was independent of basal firing rate, consistent with suppression being mediated through a mechanism related to the one that sustains baseline firing, i.e., network activity. Finally, postillumination reductions in neural activity were similar in duration across excited and suppressed neurons, again suggesting that these effects may be more due to emergent properties of the neural network that a given neuron is embedded in, rather than that cell's autonomous history of activity. Future studies will explore which inhibitory neurons are recruited by excitatory neurons to create activity patterns like those found here; one possibility is that somatostatin-positive interneurons that can be activated by stimulation of single excitatory neurons (Kapfer et al., 2007) could potentially mediate excitation-induced suppression. It will also be interesting to see if such dynamics can subserve oscillatory activity: in Figures 3H and 3J, the rebound depolarization after the end of activity suppression is suggestive of a possible natural timescale of activity fluctuation in the delta-theta range.

Electrical microstimulation is an important tool for both basic neuroscience and for therapeutic neuromodulation, but how it impacts neural circuit dynamics remains unclear. In microstimulation experiments where recording was also performed, some neurons dramatically decreased activity in response to electrical microstimulation (e.g., Butovas et al., 2006; Butovas and Schwarz, 2003; Seidemann et al., 2002). These electrical stimulation-induced decreases possessed some of the same attributes of the suppressions here observed; for example, the duration of the inhibition was largely independent of the amount of activation induced (Butovas and Schwarz, 2003). This inhibition was pharmacologically associated with GABAergic neuron recruitment (Butovas et al., 2006), but it remained unknown whether electrical microstimulation must directly recruit GABAergic neurons, or whether activation of excitatory neurons would be sufficient to create such inhibition. Here we prove that driving excitatory neurons alone is sufficient to result in periods of activity suppression in a significant population of cortical neurons. We found similar responses in mouse neocortex, which suggests that such neural dynamics might be a general property of neocortical circuits under neuromodulation. Thus, even when just one cell type is manipulated, its impact on the brain must be evaluated in the context of the neural network in which it is embedded. Principles must be derived for how to control a circuit, even given a delimited set of cell types to be controlled, in order to achieve a desired physiological, behavioral, or clinical outcome.

Optically activating excitatory neurons is just one step along the path of implementing cell-type-specific optical control in primates. Future viral, promoter, injection, and illumination innovations will need to be developed to match the manipulations possible in mice and other classical genetic model systems. Optical neural silencing strategies for primates will also be critical, perhaps involving light-activated chloride pumps such as halorhodopsins (Halo/NpHR) (Han and Boyden, 2007; Zhang et al., 2007). Especially for questions involving higher-order activity patterns such as neural synchrony, the ability to use ChR2 and Halo in concert to create "informational lesions," in which precise neural patterns are disrupted, may prove especially useful (Han and Boyden, 2007).

Launching the verification of the safety and efficacy of ChR2 function in rhesus macaques is a critical step toward any potential clinical translational path for cell-type-specific optical neural control prosthetics. Given that in many disorders, the functions of specific cell types are compromised, it is possible that the ability to optically remedy aberrant activity in specific cell types will spur precise, side-effect-free treatments for neural disorders. As a first step toward this synthetic neurobiology goal, here we have shown that ChR2 performs efficaciously and without immune attack in the macaque brain, and appears to

be safe over many months despite repeated viral injections and repeated illumination sessions.

EXPERIMENTAL PROCEDURES

Detailed descriptions are provided in the Supplemental Data. All procedures were in accordance with the NIH Guide for Laboratory Animals and approved by the MIT Animal Care and Use and Biosafety Committees. Two rhesus monkeys, 7–11 years of age, weighing 8–15 kg, were equipped for awake headfixed physiology. High-titer replication-incompetent lentivirus encoding for ChR2-GFP was produced and injected into premotor cortex/frontal eye fields, via custom hardware. Optical stimulation proceeded via a 200 μm diameter optical fiber coupled to a 200 mW blue laser. Electrophysiological recording was performed using tungsten electrodes guided parallel to the optical fiber, using independent microdrives. Signal conditioning and acquisition were performed with a Plexon data acquisition system and analyzed with Matlab. The brain of one of the two monkeys was fixed and examined with immunostaining and confocal microscopy.

SUPPLEMENTAL DATA

The supplemental data for this article include Results, Experimental Procedures, and six Figures and can be found at http://www.neuron.org/supplemental/S0896-6273(09)00210-4.

ACKNOWLEDGMENTS

We thank the MIT Division of Comparative Medicine for help with serum collection, and H. Hall and P. Harlen for help with preparing cortical slices. We thank members of the Boyden and Desimone labs, and E. Tehovnik, for their suggestions on the manuscript. This work was supported by NIH-EY002621-31; a HHWF fellowship to X.H.; a McGovern Institute Neurotechnology Award to E.S.B., R.D., and X.H.; grant NIH-EY12848 to A.G.; and grants NIH-EY017292 and EY017921 to R.D. E.S.B. acknowledges support from the NIH Director's New Innovator Award (DP2 OD002002-01), NSF, Department of Defense, NARSAD, Alfred P. Sloan Foundation, Jerry Burnett Foundation, SFN Research Award for Innovation in Neuroscience, MIT Media Lab, MIT McGovern Institute, Benesse Foundation, MIT Neurotechnology Fund, and Wallace H. Coulter Foundation.

Accepted: March 9, 2009
Published: April 29, 2009

REFERENCES

Bekkers, J.M. (2000). Distribution of slow AHP channels on hippocampal CA1 pyramidal neurons. J. Neurophysiol. *83*, 1756–1759.

Bernstein, J.G., Han, X., Henninger, M.A., Ko, E.Y., Qian, X., Franzesi, G.T., McConnell, J.P., Stern, P., Desimone, R., and Boyden, E.S. (2008). Prosthetic systems for therapeutic optical activation and silencing of genetically-targeted neurons. Proc Soc Photo Opt Instrum Eng *6854*, 68540H.

Boyden, E.S., Zhang, F., Bamberg, E., Nagel, G., and Deisseroth, K. (2005). Millisecond-timescale, genetically targeted optical control of neural activity. Nat. Neurosci. *8*, 1263–1268.

Butovas, S., and Schwarz, C. (2003). Spatiotemporal effects of microstimulation in rat neocortex: a parametric study using multielectrode recordings. J. Neurophysiol. *90*, 3024–3039.

Butovas, S., Hormuzdi, S.G., Monyer, H., and Schwarz, C. (2006). Effects of electrically coupled inhibitory networks on local neuronal responses to intracortical microstimulation. J. Neurophysiol. *96*, 1227–1236.

Cahoy, J.D., Emery, B., Kaushal, A., Foo, L.C., Zamanian, J.L., Christopherson, K.S., Xing, Y., Lubischer, J.L., Krieg, P.A., Krupenko, S.A., et al. (2008). A transcriptome database for astrocytes, neurons, and oligodendrocytes: a new resource for understanding brain development and function. J. Neurosci. *28*, 264–278.

Chan, A.W., Chong, K.Y., Martinovich, C., Simerly, C., and Schatten, G. (2001). Transgenic monkeys produced by retroviral gene transfer into mature oocytes. Science *291*, 309–312.

Dittgen, T., Nimmerjahn, A., Komai, S., Licznerski, P., Waters, J., Margrie, T.W., Helmchen, F., Denk, W., Brecht, M., and Osten, P. (2004). Lentivirus-based genetic manipulations of cortical neurons and their optical and electrophysiological monitoring in vivo. Proc. Natl. Acad. Sci. USA *101*, 18206–18211.

Han, X., and Boyden, E.S. (2007). Multiple-color optical activation, silencing, and desynchronization of neural activity, with single-spike temporal resolution. PLoS ONE *2*, e299.

Hendry, S.H., Jones, E.G., Emson, P.C., Lawson, D.E., Heizmann, C.W., and Streit, P. (1989). Two classes of cortical GABA neurons defined by differential calcium binding protein immunoreactivities. Exp. Brain Res. *76*, 467–472.

Houser, C.R., Hendry, S.H., Jones, E.G., and Vaughn, J.E. (1983). Morphological diversity of immunocytochemically identified GABA neurons in the monkey sensory-motor cortex. J. Neurocytol. *12*, 617–638.

Ishizuka, T., Kakuda, M., Araki, R., and Yawo, H. (2006). Kinetic evaluation of photosensitivity in genetically engineered neurons expressing green algae light-gated channels. Neurosci. Res. *54*, 85–94.

Jones, E.G., Huntley, G.W., and Benson, D.L. (1994). Alpha calcium/calmodulin-dependent protein kinase II selectively expressed in a subpopulation of excitatory neurons in monkey sensory-motor cortex: comparison with GAD-67 expression. J. Neurosci. *14*, 611–629.

Kapfer, C., Glickfeld, L.L., Atallah, B.V., and Scanziani, M. (2007). Supralinear increase of recurrent inhibition during sparse activity in the somatosensory cortex. Nat. Neurosci. *10*, 743–753.

Kordower, J.H., Emborg, M.E., Bloch, J., Ma, S.Y., Chu, Y., Leventhal, L., McBride, J., Chen, E.Y., Palfi, S., Roitberg, B.Z., et al. (2000). Neurodegeneration prevented by lentiviral vector delivery of GDNF in primate models of Parkinson's disease. Science *290*, 767–773.

Li, X., Gutierrez, D.V., Hanson, M.G., Han, J., Mark, M.D., Chiel, H., Hegemann, P., Landmesser, L.T., and Herlitze, S. (2005). Fast noninvasive activation and inhibition of neural and network activity by vertebrate rhodopsin and green algae channelrhodopsin. Proc. Natl. Acad. Sci. USA *102*, 17816–17821.

Liu, Z., Richmond, B.J., Murray, E.A., Saunders, R.C., Steenrod, S., Stubblefield, B.K., Montague, D.M., and Ginns, E.I. (2004). DNA targeting of rhinal cortex D2 receptor protein reversibly blocks learning of cues that predict reward. Proc. Natl. Acad. Sci. USA *101*, 12336–12341.

Luo, L., Callaway, E.M., and Svoboda, K. (2008). Genetic dissection of neural circuits. Neuron *57*, 634–660.

McLendon, R.E., and Bigner, D.D. (1994). Immunohistochemistry of the glial fibrillary acidic protein: basic and applied considerations. Brain Pathol. *4*, 221–228.

Nagel, G., Szellas, T., Huhn, W., Kateriya, S., Adeishvili, N., Berthold, P., Ollig, D., Hegemann, P., and Bamberg, E. (2003). Channelrhodopsin-2, a directly light-gated cation-selective membrane channel. Proc. Natl. Acad. Sci. USA *100*, 13940–13945.

Sah, P., and Davies, P. (2000). Calcium-activated potassium currents in mammalian neurons. Clin. Exp. Pharmacol. Physiol. *27*, 657–663.

Seidemann, E., Arieli, A., Grinvald, A., and Slovin, H. (2002). Dynamics of depolarization and hyperpolarization in the frontal cortex and saccade goal. Science *295*, 862–865.

Stettler, D.D., Yamahachi, H., Li, W., Denk, W., and Gilbert, C.D. (2006). Axons and synaptic boutons are highly dynamic in adult visual cortex. Neuron *49*, 877–887.

Storm, J.F. (1987). Action potential repolarization and a fast after-hyperpolarization in rat hippocampal pyramidal cells. J. Physiol. *385*, 733–759.

Tan, E.M., Yamaguchi, Y., Horwitz, G.D., Gosgnach, S., Lein, E.S., Goulding, M., Albright, T.D., and Callaway, E.M. (2006). Selective and quickly reversible

inactivation of mammalian neurons in vivo using the Drosophila allatostatin receptor. Neuron *51*, 157–170.

Tighilet, B., Hashikawa, T., and Jones, E.G. (1998). Cell- and lamina-specific expression and activity-dependent regulation of type II calcium/calmodulin-dependent protein kinase isoforms in monkey visual cortex. J. Neurosci. *18*, 2129–2146.

Vogalis, F., Storm, J.F., and Lancaster, B. (2003). SK channels and the varieties of slow after-hyperpolarizations in neurons. Eur. J. Neurosci. *18*, 3155–3166.

Yang, S.H., Cheng, P.H., Banta, H., Piotrowska-Nitsche, K., Yang, J.J., Cheng, E.C., Snyder, B., Larkin, K., Liu, J., Orkin, J., et al. (2008). Towards a transgenic model of Huntington's disease in a non-human primate. Nature *453*, 921–924.

Zhang, F., Wang, L.P., Brauner, M., Liewald, J.F., Kay, K., Watzke, N., Wood, P.G., Bamberg, E., Nagel, G., Gottschalk, A., and Deisseroth, K. (2007). Multimodal fast optical interrogation of neural circuitry. Nature *446*, 633–639.

Neuron, volume *61*

Supplemental Data

Millisecond-Timescale Optical Control of Neural Dynamics in the Nonhuman Primate Brain

Xue Han, Xiaofeng Qian, Jacob G. Bernstein, Hui-hui Zhou, Giovanni Talei Franzesi, Patrick Stern, Roderick T. Bronson, Ann M. Graybiel, Robert Desimone, and Edward S. Boyden

SUPPLEMENTAL RESULTS

Safety assessments. There are no defined immunostimulatory activities known to date to be associated with these light-activated channels. However, the membrane protein ChR2 (and the soluble protein GFP) are exogenously derived from non-primate organisms, raising the possibility that expression of such molecules in specific cells could, in theory, provoke an immune attack on those cells. Thus, we performed a series of different analyses to explore this possibility, focusing on brain regions with high densities of ChR2-GFP positive cells that were not immediately abutting the scar left by the cannula used for viral infusion. First, in the histological analysis of monkey N, performed 110 days after the first viral injection (and 81 days after the last viral injection), we saw ChR2-GFP expression in many excitatory cells (up to ~80%, near the center of injection sites). The widespread persistence of expression of these exogenous proteins in healthy-looking cells, several months after viral gene delivery**,** implies a lack of cytotoxic immune response against cells expressing ChR2-GFP (e.g., compare to (Aktas et al., 2005; Bien et al., 2002; Murphy et al., 2007)). Second, the recordings of neural activity modulated by light (**Figs. 3-4**) indicated functional expression of ChR2 in neurons throughout the period of the experiment (over 8 months for monkey A), even after many sessions of repeated blue-light illumination of the same set of cells. Third, to assess cellular architecture at the site of ChR2-GFP expression, we stained either the nuclei of all cells with the nucleic acid stain To-Pro-3 (**Fig. 2A**), or just the nuclei of neuronal cells with antibody to the neuron-specific nuclear marker NeuN (**Fig. 2B**). We did not detect disruptions of cellular architecture, even in regions with a high density of ChR2-GFP-expressing cells. Fourth, we measured the density of reactive astrocytes, using GFAP staining (Ridet et al., 1997). The density of GFAP-positive cells was identical in regions with a high density of ChR2-GFP expressing cells (13.5 ± 1.5 GFAP-positive cells per $2.5*10^6$ μm^3, mean ± SE) and in regions with no ChR2-GFP expressing cells, far away from the cannula (14.4 ± 1.5 GFAP positive cells per volume) ($p > 0.5$, unpaired t-test; n = 13 fields of view each), confirming that ChR2-GFP expression did not evoke gliosis. This lack of disorganization and immune cell infiltration was consistent with the excellent appearance of the ChR2-GFP-positive neurons (see also **Fig. 1**), as well as the physiological health of the neurons (**Fig. 3-4)**, even after many months of viral expression, and strongly suggests that a functional immune response did not occur.

Finally, we took a step towards assessing the presence of antibodies against ChR2-GFP in the serum of the two monkeys by Western blotting samples of their serum against purified membranes of HEK cells transfected with ChR2-GFP plasmids. Control western blotting with a rabbit polyclonal antibody against whole GFP consistently labeled two bands around 46 kD (approximately 75% of the molecular weight of the entire ChR2-GFP fusion protein, suggesting that we were consistently isolating two sizable fragments of the entire protein). These bands were detected only in the membrane fraction of HEK cells transfected with ChR2-GFP plasmid, and not in the cytosolic fraction of HEK cells transfected with ChR2-GFP plasmid, implying that we are indeed isolating a membrane-localized protein (**Fig. 2C**). These bands were not detected in membranes of untransfected HEK cells, confirming specificity of the antibody staining. Western blotting with monkey serum (1:50), obtained before vs. after viral injections, detected in neither case any specific reactivity to membranes of HEK cells transfected with ChR2-GFP, when compared to membranes of untransfected HEK cells (**Fig. 2D**). In greater detail: for both monkeys, there was nonspecific binding of serum to membranes of HEK cells, but there was no difference in binding of serum to membranes of ChR2-GFP transfected vs. untransfected HEK cells. Furthermore, there was no difference in the binding of serum to a given membrane extract, when we compared before vs. after virus injection. (The observed bands in the blotting of monkey serum against untransfected HEK cells do, however, suggest that our Western blot is capable of detecting some immune response in monkey serum, to a molecule found in untransfected cultured HEK cells.) Finally, we assessed the presence of antibodies in the monkey serum, by running the serum itself in a lane (**Fig. 2D**), and using a secondary antibody against monkey antibodies for visualization; this procedure revealed bands appropriate for antibodies in the serum (given that the heavy chain weighs ~50 kD). Taken together, these lines of evidence support a lack of productive immune response following neuron-specific expression of ChR2-GFP in primate brain.

Optical artifact at low frequencies on metal electrode tips in saline. When electrodes made of tungsten (as used in the in vivo recordings in monkey cortex reported in this paper) were immersed in saline, we observed a voltage deflection that occurred when the electrode tip was illuminated with light. Shown in **Supplemental Fig. 1A** are traces recorded on a tungsten electrode in saline being illuminated by a pulsed laser beam (120 mW). This voltage deflection was qualitatively proportional, in amplitude, to the magnitude of the incident light; the artifact was still visible when incident light power was reduced to 1% of the value that elicited the artifact in **Supplemental Fig. 1A**. The voltage slowly evolved over many tens of milliseconds, and accordingly was only recorded when the electrode voltage was measured on the low-frequency channel of the Plexon amplifier ("field potential channel," 0.7-170 Hz; **Supplemental Fig. 1Ai, ii,** *top traces*). This voltage deflection was not recorded when the electrode voltage was recorded on the high-frequency channel of the Plexon amplifier ("spike channel," 250-8000 Hz; **Supplemental Fig. 1Ai, ii,** *bottom traces*).

When light illuminated parts of the electrode other than the tip, no artifact was recorded; only illumination of the tip-saline interface resulted in the voltage transient. This phenomenon is consistent with a classical photoelectrochemical finding, the Becquerel

effect, in which illumination of an electrode placed in saline can produce a voltage on the electrode (Gratzel, 2001; Honda, 2004). Consistent with the generality of the Becquerel effect as a property of electrode-electrolyte interfaces, we observed this artifact even when the electrode material was switched to an alternative material, such as stainless steel, platinum-iridium, silver/silver chloride, gold, nichrome, or copper (data not shown). For a given positioning of electrode and light beam, and a given light power intensity, artifacts were observed to be stable in amplitude and timecourse, throughout the delivery of repeated light pulses. The artifact has been reported by another group using channelrhodopsin-2 as well, using silver electrodes for recording cortical responses (Ayling et al., 2009).

Similar slowly-evolving voltage deflections were observed when tungsten electrodes were used to record neural activity in the brain within a few millimeters of the fiber tip, during optical stimulation (**Supplemental Fig. 1Bi, ii,** *top traces*) with a radiant flux of 80 mW/mm^2 out the tip of the optical fiber (sufficient to activate neurons within about a cubic millimeter of brain, **Supplemental Figs. 2** and **5**). It is possible that part of this voltage deflection is due to the local field potential (LFP), but it is not possible in these data to resolve the LFP from the artifact. At a distance 1 millimeter away from the optical fiber tip, a distance at which optical neural activation was greatly reduced (**Supplemental Fig. 2**), the amplitude of the voltage deflection was reduced, but nonzero. Because the voltage deflection was slowly-evolving over many tens of milliseconds, spike waveforms were detected without corruption by the artifact, in the high-frequency channel of the Plexon amplifier (**Supplemental Fig. 1Bi, ii,** *bottom traces*). However, local field potentials and field oscillations, which reflect coherent neural dynamics in the range of Hz to tens of Hz, may be difficult to isolate from this Becquerel artifact using the electrodes here tested. We have not seen the artifact with pulled glass micropipettes (such as previously used in Boyden et al., 2005 and Han and Boyden, 2007, or in the mouse recordings described below). Thus, for recordings of local field potentials and other slow signals of importance for neuroscience, hollow glass electrodes may prove useful.

Dependence of light modulation of ChR2-expressing neurons upon light power and fiber position. We investigated the dependence of optical neural excitation on light amplitude by systematically decreasing the light intensity while recording from excited cells. We found, consistent with earlier reports in cultured neurons and in transgenic mice (e.g., (Boyden et al., 2005; Wang et al., 2007)), that light power intensity on the order of several mW/mm^2 were optimal for driving neural activity (n = 11; **Supplemental Fig. 2Ai-iii**). To explore the geometry of this situation for the primate brain, we recorded excited units, holding laser power intensity constant at 80 mW/mm^2, and retracted the optical fiber from its most efficacious position, in 200 micron increments. As expected, light-driven spiking decreased as the fiber was retracted (n = 7; **Supplemental Fig. 2Bi-iii**). Excited units lost their optical modulation fully when the optical fiber was retracted by an average of 1.2 ± 0.4 mm (mean ± SD), suggesting that a volume of about a cubic millimeter could be addressed in primate cortex, by a single fiber, at this power level. Interestingly, there was a noticeable trend for the after-light suppression of activity to vanish at lower light power intensities than did the beginning-of-light excitation of activity (e.g., compare the curves in **Supplemental Fig. 2Ai vs. Aiii**, or the curves in

Supplemental Fig. 2Bi vs. Biii). This observation is consistent with the idea that the suppression is mediated by distributed neural networks (presumably part of which is illuminated, even when the neuron being recorded is not being illuminated), whereas excitation requires immediate light delivery to the neuron being recorded (or perhaps to neurons very close by).

Excited and suppressed neural responses in mouse frontal cortex. To test whether the excited vs. suppressed responses observed (**Fig. 3**) were primate-specific, we repeated the experiment in rodent cortex. We injected FCK-ChR2-GFP lentivirus into the mouse frontal cortex (0.62 mm anterior, 0.5 mm lateral, and 0.5 mm deep, relative to bregma), so that ChR2-GFP was selectively expressed in excitatory neurons (37 of 37 GFP-positive neurons counted were α-CaMKII positive, whereas 0 of 32 GFP-positive neurons counted were GABA-positive). 4 weeks to 8 months after virus injection, we performed extracellular recordings on awake, head-fixed mice. 200 ms-duration blue light pulse illumination of ChR2-GFP-expressing excitatory neurons evoked both excited and suppressed responses in frontal cortical neurons (**Supplemental Fig. 3**). Thus, the heterogeneous responses observed in different neurons in the frontal cortex are not unique to the primate, but are also present in rodents, suggesting that simultaneous excited and suppressed responses may be a general property of cortical neural networks upon excitatory cell activation.

Spatial properties of viral labeling in primate frontal cortex. To assess the spatial extent of cells labeled by a single 1 μL virus injection in primate frontal cortex, we identified 6 well-isolated injection sites with clear borders and clear central cannula scars (such as the one shown in **Fig. 1D**). To estimate the diameter of the sphere containing ChR2-GFP expressing cells, we measured the fluorescence magnitudes along lines through the centers of virus injection sites (avoiding the cannula scar), as assessed in coronal slices (**Supplemental Fig. 4)**. Each injection of ~ 1 μl virus labeled a spherical region of ~1.4 mm in diameter (1.4 ± 0.5 mm, mean ± standard deviation (SD); n = 6 spheres of cells); the center cannula scar had an average diameter of 0.29 ± 0.07 mm (mean ± standard deviation; n = 6), similar to the actual diameter of the cannulas here used, of 0.25 mm.

Distribution of response types along individual electrode tracks. To probe the spatial distribution of excited and suppressed units, as well as of non-responsive units, we recorded neural responses in an unbiased fashion by advancing the electrode in 300 μm steps along a track, while keeping the fiber immobilized. The electrode position was, at each location, adjusted (± 40 microns) in the dark to optimize neural recording quality, and then illumination was performed to assess whether the recorded units fell into one of three response categories: excited, suppressed, or no response. Above or below certain depths along the track, presumably defined by the virus injection ball diameter (see above), chiefly unresponsive units were found. Between the farthest-separated depths along a track where units responded to light (e.g., either with excitation or suppression), practically all units recorded between these two depths were either excited or suppressed during light exposure (**Supplemental Fig. 5**), with only one non-responsive unit found in between responsive units during the five experiments shown. The distance between the

highest and lowest units recorded that were modulated by light ranged from 0.9-1.5 mm, consistent with the measurements of viral labeling (**Supplemental Fig. 4**) and the measurements of light delivery volume (**Supplemental Fig. 2**). Note that since units may have been multiunits, this experiment puts a lower bound on the fraction of non-responsive neurons in the observed regions (since if multiple neurons are recorded together and classified as one multiunit, then if any of the neurons are light-modulated, the entire multiunit will likely be classified as light-modulated). However, the fact that almost all cells recorded were modulated by light is consistent with the idea that the observed modulations were largely mediated by neural network-propagated activity, as the fraction of cells virally infected was significantly lower than 100%.

Rhythmic network activity mediated by ChR2 drive of excitatory cells in vivo. Rhythmic and oscillatory activity in the brain have been associated with many cognitive, emotional, sensory, and motor functions, raising the possibility that the ability to optically alter brain rhythms could lead to a better understanding of the causal role of such network dynamics in normal and pathological behavior. Accordingly, we probed the temporal precision of ChR2-driven network activity in primate cortex by exposing excited units to extended 10, 20, and 50 Hz trains of blue light pulses (pulse durations 20, 20, and 10 ms respectively) (**Supplemental Fig. 6**). Spike rates (measured during the 20 ms after the onset of each light pulse) elicited by each pulse declined somewhat during the course of each train, as evidenced by lower steady-state firing rates (mean response to the last 5 light pulses) than maximum firing rates (resulting from the first light pulse of the train) (10 Hz: $p < 0.005$, paired t-test, $n = 8$ units; 20 Hz: $p < 0.005$, $n = 14$ units; 50 Hz: $p < 0.05$, $n = 9$ units). In the steady state, light pulses resulted in spike rates that were 70%, 48% and 55% of those elicited by the first light pulses for 10 Hz, 20 Hz and 50 Hz trains, respectively (**Supplemental Fig. 6Aii, Bii, Cii**). Thus, while spiking could still be reliably elicited by pulse train protocols over an extended time, the probability of firing decreased somewhat throughout such trains, especially at pulse rates 20 Hz and higher. Even so, the trial-to-trial jitter of the spikes was ~4 ms, averaged across units (**Supplemental Fig. 6Aiii, Biii, Ciii)**, and did not change throughout the trains ($p > 0.1$ for all frequencies, paired t-test). Thus, spike timing remained reliable across a wide range of frequencies, despite a reduction in firing probability throughout long, high-frequency pulse trains, suggesting that ChR2-mediated drive of excitatory cells may enable the probing of the role of neural synchrony in cortical computation.

SUPPLEMENTAL FIGURE LEGENDS

Supplemental Figure 1. Voltage deflections observed on tungsten electrodes immersed in saline (**A**) or brain (**B**), upon tip exposure to 200 ms blue light pulses (**i**) or trains of 10 ms blue light pulses delivered at 50 Hz (**ii**). Light pulses are indicated by blue dashes. Electrode data was hardware filtered using two data acquisition channels operating in parallel, yielding a low-frequency component ("field potential channel") and a high-frequency component ("spike channel"). For the "spike channel" traces taken in brain (**B**), spikes were grouped into 100 ms bins, and then the binned spikes were displayed beneath corresponding parts of the simultaneously acquired "field potential channel"

signal (59 and 53 repeated light exposures for **Bi** and **Bii** respectively). (Shown are the spikes in 8 such bins – the 2 bins before light onset, the 2 bins during the light delivery period, and the 4 bins after light cessation.) For all other signals shown, 10 overlaid traces are plotted.

Supplemental Figure 2. Light intensity dependence of neural activity driven by ChR2-mediated activation of excitatory neurons. **A**, neural activity during 'Beginning of light' (**i**), 'Steady state' (**ii**), and 'After light' (**iii**) time periods, upon illumination with different light power intensities (plotted is mean ± SE; n = 11 excited units). **B**, neural activity during 'Beginning of light' (**i**), 'Steady state' (**ii**), and 'After light' (**iii**) periods, when optical fibers were retracted, holding the electrode still (plotted is mean ± SE; n = 7 excited units).

Supplemental Figure 3. Increases and decreases in firing rates of neurons in mouse frontal cortex, during optical stimulation of excitatory neurons. **A**, increases in spiking activity in one neuron during blue light illumination (200 ms duration). *Top,* spike raster plot displaying each spike as a black dot; 25 trials are shown in horizontal rows, in this and subsequent raster plots; *bottom*, histogram of instantaneous firing rate (averaged across all trials; bin size, 5 ms, in this and subsequent histogram plots). **B**, decreases in spiking activity in one neuron during blue light illumination (200 ms duration). *Top,* spike raster plot; *bottom*, histogram of instantaneous firing rate.

Supplemental Figure 4. Fluorescence magnitudes measured along lines taken through the centers of spheres of virally-labeled neurons, each created by one injection of 1 microliter of ChR2-GFP lentivirus. Shown are the mean (black lines) and the mean $\pm$ SD (gray lines) for n = 6 well-isolated spheres of virally-labeled cells.

Supplemental Figure 5. Quantitation of the number of light-responsive and light-unresponsive units detected along five individual electrode tracks, each sampled every 300 microns. The farthest-separated depths where units responded to light were first identified, and each unit recorded between those two depths was then classified according to its activity profile – excitation, suppression, or nonresponsive – during light illumination.

Supplemental Figure 6. Driving oscillatory cortical activity by activating ChR2 expressing excitatory neurons with rhythmic blue light pulse trains, at 10 Hz (**A**), 20 Hz (**B**), and 50 Hz (**C**). For each of these three pulse rates, plotted in subpanel **i** is the histogram of instantaneous firing rate (bin size, 5 ms) averaged across all excited units tested (black lines, mean; gray lines, mean ± SE; n = 8 units for 10 Hz, n = 14 units for 20 Hz, and n = 9 units for 50 Hz). Plotted in subpanel **ii** is the firing rate divided by baseline firing rate, during the 20 ms following the onset of each light pulse, and averaged across all excited units tested (mean ± SE)). Plotted in subpanel **iii** is the jitter of spike times elicited by each pulse, calculated as the across-trial standard deviation of the time of the first spike elicited within 20 ms of each light pulse onset and averaged across all excited units tested (mean ± SE).

SUPPLEMENTAL EXPERIMENTAL PROCEDURES

Virus design and production. Replication-incompetent VSVg-pseudotyped lentivirus was produced via triple transfection of FCK-ChR2-GFP lentiviral plasmid (available at http://www.addgene.org/pgvec1?f=c&cmd=findpl&identifier=15814), the viral helper plasmid (pΔ8.74, information at http://www.addgene.org/pgvec1?vectorid=5682&f=v&cmd=showvecinfo), and the pseudotyping plasmid pMD2.G, encoding for the VSVg coat protein (http://www.addgene.org/pgvec1?f=c&cmd=findpl&identifier=12259). VSVg was used because it enables viral infection of a wide range of cell types, including neurons *in vivo* (Naldini et al., 1996). HEK293FT cells (Invitrogen) were plated onto four T175 flasks in D10 medium (DMEM + 10% FBS + 1% penicillin-streptomycin + 1% sodium pyruvate). At near 100% confluence, cells were transfected with DNA (per flask: 22 μg FCK-ChR2-GFP, 15 μg pΔ8.74, 7 μg pMD2.G, 132 μL Fugene 6, brought up to 4.5 mL with DMEM, mixed according to the Fugene instructions, and then added to 16 mL of D10). 24 hours later, the cells were given 20 mL of virus production media (Ultraculture (Lonza) + 1% penicillin-streptomycin + 1% sodium pyruvate +1% sodium butyrate). 48 hours later, the supernatant was spun down at 2000 rpm in a Beckman benchtop Allegra centrifuge for 5 min, filtered through a 0.45 micron filter, and then ultracentrifuged at 22000 rpm in a SW-28 rotor, through a 20% sucrose + phosphate buffered saline (PBS) cushion, for 2 hours at 4°C. The pellets were then slowly resuspended in 30-100 microliters of PBS, and aliquotted in single-use aliquots for storage at −80°C. This protocol enabled production of clean, non-toxic, high-titer (roughly estimated at ~10^9 infectious units/mL) lentivirus for injection into the brain.

General surgical procedures. Two rhesus monkeys (*Macaca mulatta*), 7-11 years of age, weighing 8-15 kg, were used. All procedures were in accordance with the National Institutes of Health Guide for the care and use of Laboratory Animals and approved by the Massachusetts Institute of Technology Animal Care and Use Committee. Under isoflurane anesthesia, a titanium headpost and recording chambers were surgically affixed to the skull, and a craniotomy opened up in one or more of the chambers, according to MRI-determined coordinates for the periarcuate regions (premotor/FEF areas) of the frontal cortex.

Virus injection. The virus was injected through a 31-gauge stainless steel cannula held in a microdrive (Plexon NAN Drive) attached to the recording chamber while the monkey was seated in a primate chair. The cannula was connected via polyethylene tubing to a Hamilton syringe, placed in a syringe pump (Harvard Apparatus), and the syringe, tubing, and cannula filled with silicone oil (Sigma). To insure the ability to both target virus to the desired area, and to return to the same site later for reliable electrophysiology and optical control, we designed a custom 3-D targeting grid using Solidworks (Solidworks Corp.), and printed it out of acrylic (VisiJet SR 200 Plastic Material acrylic) with a 3-D printer with ~50-micron resolution (3D Systems, Inc.). This grid is analogous to commercially available grids from Crist Instrument Co., but tuned for the specific geometries of interest for this joint electrical-optical experiment. One microliter of virus

was injected over a 10 minute period. We then waited an extra 10 minutes for the virus to diffuse away from the site of injection before withdrawing the cannula at a slow rate of 0.12-0.3 mm/min.

The injection strategy was designed to target cortical tissue on each side (posterior and anterior) of the arcuate sulcus (i.e., premotor cortex and FEF, respectively). Thus, to hit the deepest targets of the sulcus, a deeper termination point was required (i.e., we stopped the injector 7 mm below the dura) than to hit targets more anterior or more posterior to the sulcus (i.e., we stopped the injector 5 mm below the dura). The angle of the injection was approximately vertical, and ultimately governed by the placement of the chamber on the skull. Viral injection was accomplished by lowering a 31-gauge steel cannula (250 microns in diameter) into a given site in the grid, targeting the depth as described above, and then injecting 1 μL of FCK-ChR2-GFP virus at that depth. Then, we repeatedly (4-6 times, as appropriate) retracted the injector in 1 mm steps, injecting an additional 1 μL each time, until the cannula was fully retracted. In this way, we attempted to label large regions on both sides of the arcuate sulcus.

Optical stimulation hardware. A 200 mW blue laser (A-L473-200, Aixiz) was coupled to a 200 micron-diameter optical fiber (FIBER-200-UV, Ocean Optics, although sometimes we also used 100 micron fibers) through a homebuilt collimator setup (AC254-040-A1-ML lens, mounted on a modified SM1L20 lens tube, and attached to a SM1SMA fiber adapter, the assembly of which was mounted on a KM100T mirror mount, all from Thorlabs). To prepare the fiber to connect to our homebuilt collimator assembly, we used an SMA connector terminator kit (TERM-KIT, Ocean Optics). The laser, collimator, and mirrors (BB1-E02, mounted on KM100 mirror mounts, Thorlabs), were mounted on a standard optics breadboard (MB1824, Thorlabs), as outlined in (Bernstein et al., 2008). Laser light power was measured with an 818-SL photodetector (Newport Co.)

The fiber was then placed into a stainless steel cannula slightly larger than the optical fiber, and then guided into the brain, using the same electrode drive described above. The laser was controlled via TTL pulses driven by a pulse generator (DS8000, WPI Inc.), with the timing controlled by a computer through the software package, Cortex (http://www.cortex.salk.edu/).

Electrophysiological recording and optical stimulation. Standard tungsten electrodes of 1-2 MΩ resistance (FHC, Inc.) were guided into the brain along a track parallel to the fiber (separated by 0-600 μm), via a second drive. The guide tubes holding the electrode and holding the fiber were often glued parallel to one another, so that fibers and electrodes would remain laterally spaced within 0.6 mm of one another throughout the experiment (recording more lateral to the fiber reduced the probability of obtaining optically modulated cells, although we did not quantitate this in detail). Fibers and electrodes were lowered separately through their respective guide tubes at a slow rate of ~1.5 μm/s to minimize any potential deformation of the cortical surface. Guide tubes did not enter the brain, but instead rested outside the dura; only the fibers and electrodes entered, lowered through the guide tubes.

Data amplification, filtering and acquisition were performed with a Multichannel Acquisition Processor (MAP) system (Plexon, Inc.), which contains multiple data acquisition channels. Each data acquisition channel is split into two parallel channels and filtered with two different bandpass filters to reveal content at different frequencies. The "spike channel" used throughout this paper is defined by Plexon as 250 Hz – 8 kHz and sampled at 40 kHz. The other channel, the "field potential channel," is defined by Plexon as 0.7 Hz -170 Hz. Spikes recorded on the spike channel were semi-automatically detected using an interactively-set threshold, and the spike waveforms were offline sorted to distinguish putative single vs. putative multiple units using principal component analysis (PCA) (Offline Sorter, Plexon, Inc.). Most of the neurons recorded had broad spike waveforms with trough-to-peak duration >250 μs (3 out of 31 single neurons had trough-to-peak waveform durations of 100-200 μs, and the rest had trough-to-peak waveform durations of 250-425 μs), indicating that most of the recorded neurons were putative excitatory neurons (Mitchell et al., 2007). Spike timing was defined as the moment of threshold crossing. Light resulted in a slow artifact on the electrode (**Supplemental Fig. 1**), which was easily separable from the spike trains through high-pass filtering.

During the experiment, one fiber and one or more electrodes were lowered into the brain of an awake headfixed monkey, and optical stimulation was performed while units were recorded. During the recording period, the monkeys were awake and freely viewing, in a dimly lit room. Our targets in arcuate sulcus contain premotor areas; we did not observe overt eye or limb movements during experiments with the stimuli used. Occasional juice rewards were delivered to insure alertness, but no tasks nor reward contingencies were scheduled in the described recording sessions. Our recording strategy was to position the electrode near the fiber by searching for the slow light-induced artifact, and then optimizing the electrode position to record neurons. Subregions of the targeted areas could be found in which no units were modulated by light, and subregions were also found in which almost 100% of the units were modulated by light (**Supplemental Fig. 5**).

Artifact characterization in saline. Electrodes were positioned in saline and targeted by the laser beam. Voltage deflections were amplified, filtered and acquired with a Multichannel Acquisition Processor (MAP) system (Plexon, Inc.). Specifically, the "field potential channel" is defined by Plexon as 0.7-170 Hz and sampled at 1 kHz or 20 kHz. The "spike channel" is defined by Plexon as 250 Hz – 8 kHz and sampled at 20 kHz or 40 kHz.

Electrophysiology data analysis. Electrophysiological data analysis was performed using MATLAB (Mathworks, Inc.). Light-modulated neurons were identified and classified by performing a paired t-test, for each neuron, between the firing rate during the 200 ms period before light onset ('baseline firing rate') vs. during the period of light exposure, across all trials for that neuron, and thresholded at the $p < 0.05$ significance level. Units that showed significant increases in firing rate during any of three time periods – the first 20 ms of light exposure ('Beginning of light'), the period between 20 ms after light onset and 20ms after light cessation ('Steady state'), and during the 20 ms

period starting 20 ms after light cessation ('After light') – were defined as excited units. Units that showed no increase in firing rate during any of these three periods, but showed reduction in firing rate during any of the periods, were defined as suppressed units. To determine the latency between light onset and the neural response (or, for **Fig. 3M**, the time for after-light suppression to recover back to baseline), we swept a 6 ms-long sliding window through the electrophysiology data and looked for the earliest 6 ms period that deviated from baseline firing rate, as assessed by performing a paired t-test for the firing rate during each window vs. during the baseline period, across all trials for each neuron. Latency was defined as the time from light onset to the time at which firing rate was significantly different from baseline for the following 12 ms. Normalizing firing rate at a given timepoint to baseline was performed by taking the ratio of firing rate at that timepoint, to the baseline firing rate. Firing rate change during a given period was defined as the firing rate during that period, minus the baseline firing rate. Jitter was defined as the standard deviation, across repeated trials, of the timing of the first spike that occurred after the onset of a light pulse.

Mouse optical activation and recording. Adult Swiss Webster or C57 mice were used. All procedures were in accordance with the National Institutes of Health Guide for the care and use of Laboratory Animals and approved by the Massachusetts Institute of Technology Animal Care and Use Committee. Under isoflurane anesthesia, 1 μL lentivirus made with FCK-ChR2-GFP was injected through a craniotomy to the premotor area (0.62 mm anterior, 0.5 mm lateral, and 0.5 mm deep, relative to bregma). A custom-fabricated plastic headpost was affixed to the skull, and the craniotomy was protected with agar and covered with a plastic plate. Recordings (cell-attached or extracellular recordings) were made on headfixed, awake mice up to 8 months after virus injection, using glass microelectrodes of ~5MΩ filled with PBS, containing silver/silver-chloride wire electrodes. Signals were amplified with a Multiclamp 700B amplifier, digitized with a Digidata 1440 and acquired with pClamp 10 (Molecular Devices). Data analysis was with Matlab.

Histology and immunofluorescence. One of the two monkeys, Monkey N, weight 8.6 kg, was deeply anesthetized with an overdose of pentobarbital (>70 mg/kg, i.v.), and then the borders of the 3-D targeting grid were marked in the brain by insertion of 18-gauge cannulas into grid holes near the corners. Then the animal was immediately perfused through the left ventricle, first with phosphate buffered saline (PBS; pH 7.3) (2 liters), then with 4% paraformaldehyde in PBS (4 liters), followed by 2 liters of PBS. The cannulas were then removed, and the brain was blocked and cryoprotected in PBS with 20% glycerol + 0.1% sodium azide (>2 days). Brains were then cut into 60 μm coronal sections on a sliding microtome, and stored in PBS + 0.1% sodium azide.

Brain slices were washed and permeabilized 3 times for 30 minutes each in a solution containing PBS, 100 mM glycine, and 0.5% triton X-100 (PTG solution), and then blocked for 2 hours in PTG + 2% normal goat serum from Jackson Immunochemicals (PTB solution). Slices were then incubated with primary antibody in PTB solution overnight at 4^{o}C on a shaker, then washed 4 times for 30 minutes each with PTG solution, and then incubated in the secondary antibody in PTB solution for 2 hours at

room temperature. Finally, the slices were washed 3 times for 30 minutes each with PTG solution, and for 30 minutes in PBS + 100 mM glycine. Antibodies and stains used were rabbit anti-α-CaMKII (1:50, Santa Cruz Biotechnology), rabbit anti-GABA (1:500, Sigma), rabbit anti-GFAP (1:1000, Upstate), mouse anti-NeuN (1:1000, Chemicon), To-Pro–3 iodide (1:2000, Invitrogen), chicken anti-GFP (1:500, Chemicon), Alexa 488 goat anti-chicken (1:500), and Alexa 568 goat anti-rabbit (1:500) (Invitrogen). Slices were mounted with Vectashield solution (Vector Labs), and visualized with a Zeiss LSM Pascal confocal microscope.

Confocal data analysis of immunostaining and cell counting was performed by taking 3-D z-stacks with a 63x oil lens (Zeiss), each 202 x 202 x 60 microns in volume. To maximize accuracy of overlap determination and cell counting, cells were first identified on the green (ChR2-GFP) and red (cell-type marker) channels separately, then overlap was assessed.

For measuring the diameters of the spheres of virally-labeled cells, images containing well-isolated spheres of GFP fluorescence (n = 6 such sites) were taken using an Olympus fluorescence microscope (using 4x or 10x objective lenses). We measured the diameter of each virus sphere as follows, using ImageJ (NIH): first, we visually estimated the center of each virus sphere by examining each section through the virus sphere, and drew a randomly-oriented line through this center. (In choosing this line we did, however, avoid the cannula injection hole.) Then, we extracted the magnitudes of the fluorescence values for each pixel along this line, after performing a flat-field correction. The diameter of the spheres of GFP fluorescence was then determined as the distance between the two points at which the fluorescence fell to 20% of the peak, defined as the median of the 50 highest fluorescence values along the line. To facilitate comparison of different images for statistical purposes, we normalized each set of magnitudes to the peak, and identified the midpoint as halfway between the two points at which the fluorescence fell to 20% of the peak. For the population data (**Supplemental Fig. 4**), the normalized curves were aligned at their midpoints, and mean and standard deviation were calculated.

Western blotting. Non-human primate blood samples were collected in a Sarstedt Serum Monovette tube, and centrifuged in a Hettich Rotofix 32 Centrifuge at 2,000 RPM for 10 minutes. The serum was then transferred into a Sarstedt screw cap storage tube and then stored at -80 °C until ready for analysis. HEK cell membranes containing ChR2-GFP were prepared by transfecting 10-cm plates of HEK cells with ChR2-GFP under the CAG promoter. 3 days later, the cells from one such plate, as well as one control plate, were resuspended in PBS and centrifuged for 10 min at 2000 rpm in a benchtop centrifuge at 4^{o}C. Cell pellets were resuspended in 1 ml PBS with proteinase inhibitors (Roche), lysed in a cup sonicator for 15 seconds and centrifuged for 2 minutes at 13,000 rpm at 4^{o}C. The pelleted membranes were then resuspended in 0.5 ml Laemmli sample buffer containing SDS (Bio-Rad Inc.). For Western blotting, wells of 12% polyacrylamide gels (Bio-Rad Inc.) were loaded with 15 μl of this solution, or of a 1:5 dilution thereof. Additionally, some wells were loaded with 0.02 μL of monkey serum (a total of 15 μL, containing 1:750 diluted monkey serum), in order to assay the antibody content. After electrophoresis, proteins were transferred from the gel to a PVDF membrane (Bio-Rad

Inc.), which was then washed for 10 mins in TBS (20 mM Tris/HCl and 150 mM NaCl, pH, 7.4), blocked with 3% BSA in TBS for 2 hours, then washed and incubated with rabbit-anti-GFP antibody (1:1000, Invitrogen) or monkey serum for 2 hours at 4^{o}C while shaking. The PVDF membrane was then washed 3 times for 10 mins each, with 0.5% Tween 20 in TBS, followed with washing in TBS once, and then incubated with horseradish peroxidase (HRP)-conjugated goat-anti-rabbit or rabbit-anti-monkey secondary antibody (1:80,000, Sigma) for 2 hours. The PVDF membrane was then washed again, as described above. HRP was then imaged by adding Western Lightning Chemiluminescence Reagent Plus substrate (PerkinElmer).

REFERENCES

Aktas, O., Smorodchenko, A., Brocke, S., Infante-Duarte, C., Schulze Topphoff, U., Vogt, J., Prozorovski, T., Meier, S., Osmanova, V., Pohl, E.*, et al.* (2005). Neuronal damage in autoimmune neuroinflammation mediated by the death ligand TRAIL. Neuron *46*, 421-432.

Ayling, O.G., Harrison, T.C., Boyd, J.D., Goroshkov, A., and Murphy, T.H. (2009). Automated light-based mapping of motor cortex by photoactivation of channelrhodopsin-2 transgenic mice. Nat Methods.

Bernstein, J.G., Han, X., Henninger, M.A., Ko, E.Y., Qian, X., Franzesi, G.T., McConnell, J.P., Stern, P., Desimone, R., and Boyden, E.S. (2008). Prosthetic systems for therapeutic optical activation and silencing of genetically-targeted neurons. Proceedings - Society of Photo-Optical Instrumentation Engineers *6854*, 68540H.

Bien, C.G., Bauer, J., Deckwerth, T.L., Wiendl, H., Deckert, M., Wiestler, O.D., Schramm, J., Elger, C.E., and Lassmann, H. (2002). Destruction of neurons by cytotoxic T cells: a new pathogenic mechanism in Rasmussen's encephalitis. Ann Neurol *51*, 311-318.

Boyden, E.S., Zhang, F., Bamberg, E., Nagel, G., and Deisseroth, K. (2005). Millisecond-timescale, genetically targeted optical control of neural activity. Nat Neurosci *8*, 1263-1268.

Gratzel, M. (2001). Photoelectrochemical cells. Nature *414*, 338-344.

Honda, K. (2004). Dawn of the evolution of photoelectrochemistry. Journal of Photochemistry and Photobiology A: Chemistry *166*, 63-68.

Mitchell, J.F., Sundberg, K.A., and Reynolds, J.H. (2007). Differential attention-dependent response modulation across cell classes in macaque visual area V4. Neuron *55*, 131-141.

Murphy, K.M., Travers, P., and Walport, M. (2007). Janeway's Immunobiology, 7th edn.

Naldini, L., Blomer, U., Gallay, P., Ory, D., Mulligan, R., Gage, F.H., Verma, I.M., and Trono, D. (1996). In vivo gene delivery and stable transduction of nondividing cells by a lentiviral vector. Science *272*, 263-267.

Ridet, J.L., Malhotra, S.K., Privat, A., and Gage, F.H. (1997). Reactive astrocytes: cellular and molecular cues to biological function. Trends Neurosci *20*, 570-577.

Wang, H., Peca, J., Matsuzaki, M., Matsuzaki, K., Noguchi, J., Qiu, L., Wang, D., Zhang, F., Boyden, E., Deisseroth, K.*, et al.* (2007). High-speed mapping of synaptic connectivity using photostimulation in Channelrhodopsin-2 transgenic mice. Proc Natl Acad Sci U S A *104*, 8143-8148.

Han et al., Supplementary Figure 1

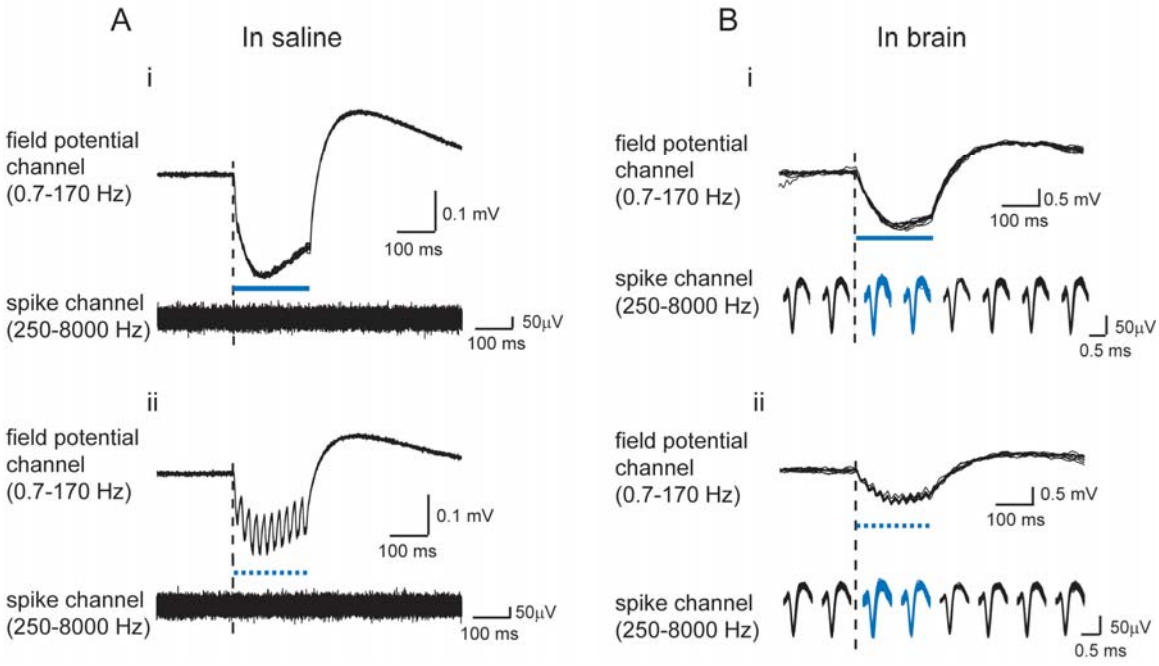

Han et al., Supplementary Figure 2

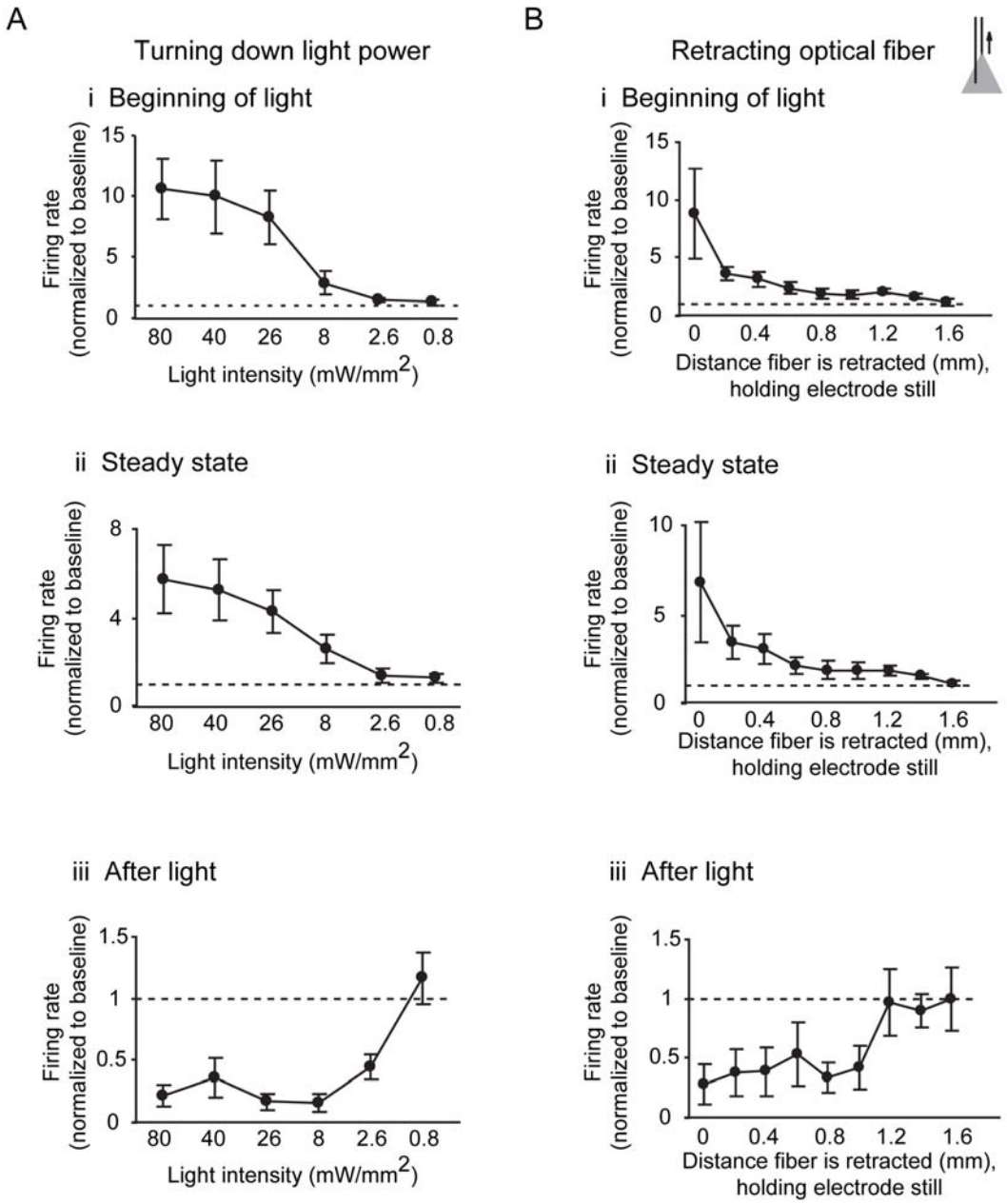

Han et al., Supplementary Figure 3

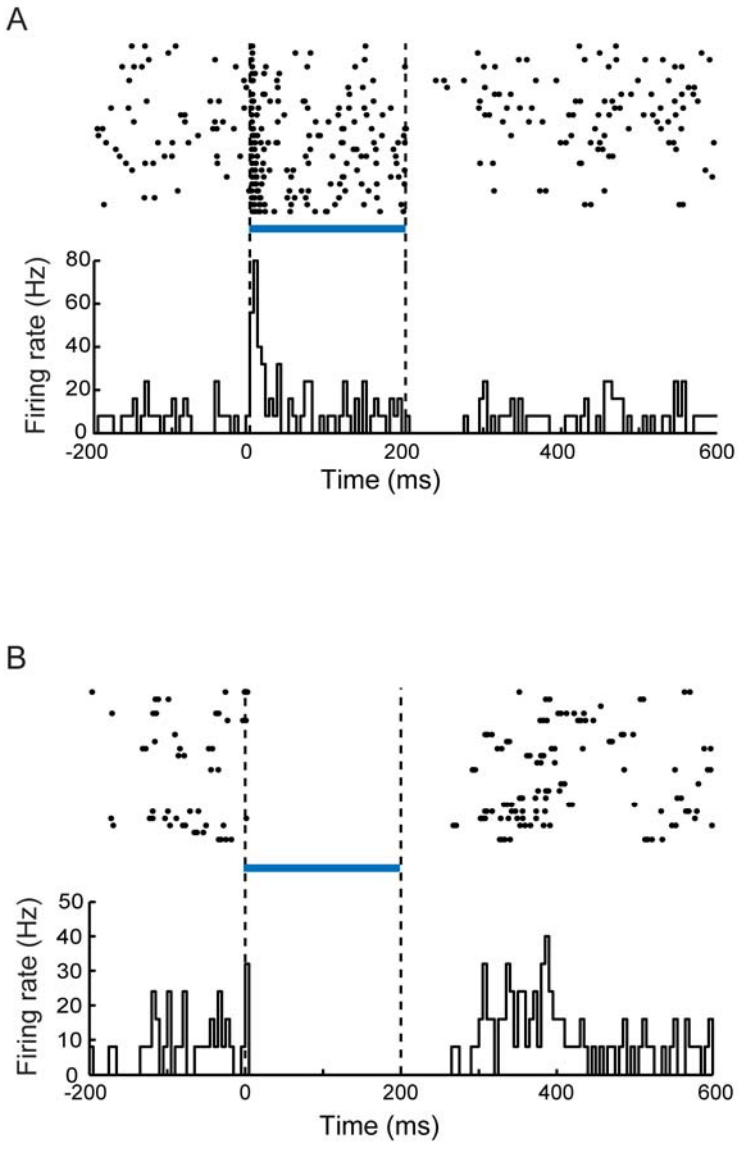

Han et al., Supplementary Figure 4

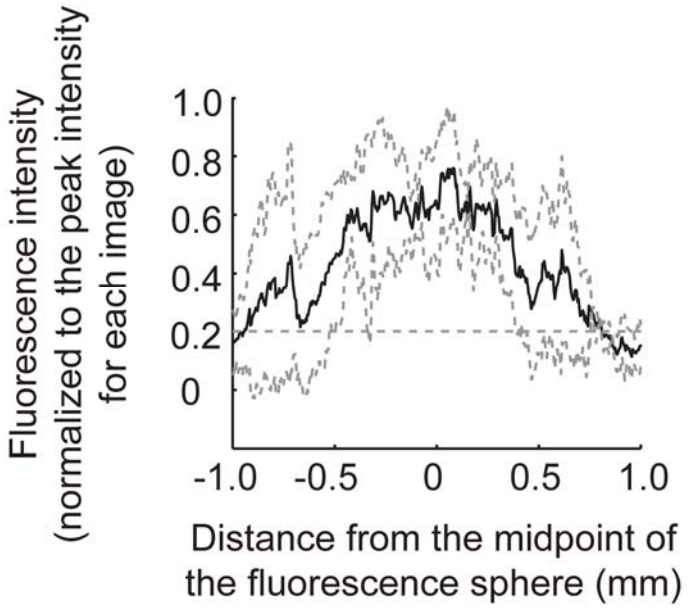

Han et al., Supplementary Figure 5

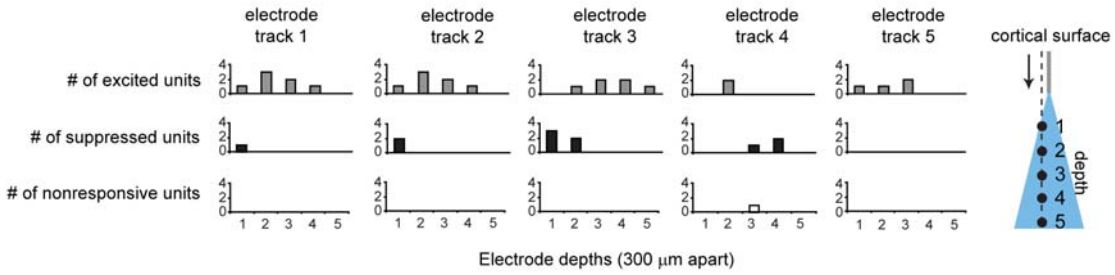

Han et al., Supplementary Figure 6

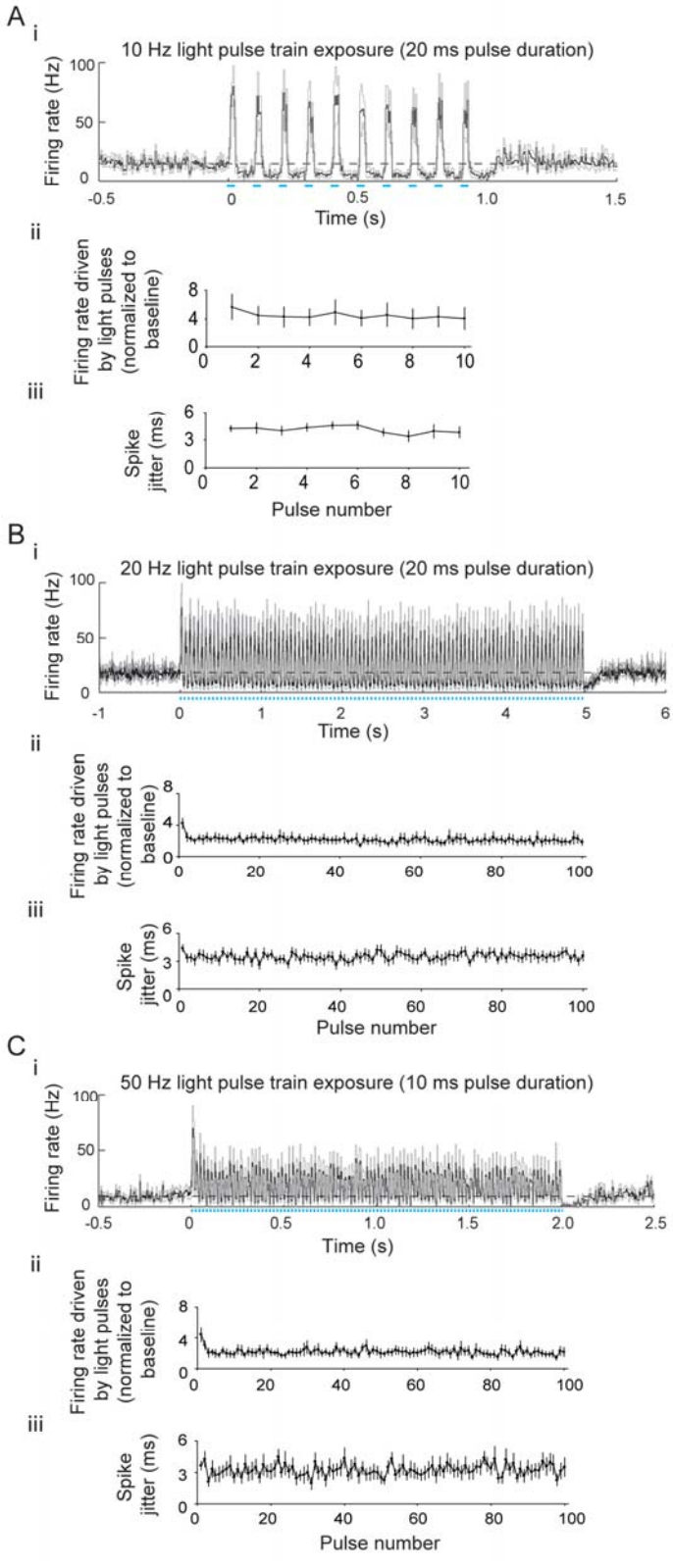

APPENDIX 3

Han X, Qian X, Stern P, Chuong A and Boyden ES (2009) Informational Lesions: Optical Perturbation of Spike Timing and Neural Synchrony Via Microbial Opsin Gene Fusions. ***Frontiers in Molecular Neuroscience,*** **2:12. doi:10.3389/neuro.02.012.2009**

frontiers in
MOLECULAR NEUROSCIENCE

ORIGINAL RESEARCH ARTICLE
published: 27 August 2009
doi: 10.3389/neuro.02.012.2009

Informational lesions: optical perturbation of spike timing and neural synchrony via microbial opsin gene fusions

Xue Han[1,2,3], Xiaofeng Qian[1,3], Patrick Stern[4], Amy S. Chuong[1] and Edward S. Boyden[1,2,3,5]*

[1] *MIT Media Lab, Massachusetts Institute of Technology, Cambridge, MA, USA*
[2] *Brain and Cognitive Sciences, Massachusetts Institute of Technology, Cambridge, MA, USA*
[3] *McGovern Institute, Massachusetts Institute of Technology, Cambridge, MA, USA*
[4] *Koch Center for Cancer Research, Massachusetts Institute of Technology, Cambridge, MA, USA*
[5] *Biological Engineering, Massachusetts Institute of Technology, Cambridge, MA, USA*

Edited by:
Jochen C. Meier, Max Delbrück Center for Molecular Medicine, Germany

Reviewed by:
Miles A. Whittington, Newcastle University, UK
Antoine Adamantidis, Stanford University School of Medicine, USA

***Correspondence:**
Edward S. Boyden, MIT Media Lab, E15-430, 20 Ames St., Cambridge, MA 02139, USA.
e-mail: edboyden@mit.edu

Synchronous neural activity occurs throughout the brain in association with normal and pathological brain functions. Despite theoretical work exploring how such neural coordination might facilitate neural computation and be corrupted in disease states, it has proven difficult to test experimentally the causal role of synchrony in such phenomena. Attempts to manipulate neural synchrony often alter other features of neural activity such as firing rate. Here we evaluate a single gene which encodes for the blue-light gated cation channel channelrhodopsin-2 and the yellow-light driven chloride pump halorhodopsin from *Natronobacterium pharaonis*, linked by a 'self-cleaving' 2A peptide. This fusion enables proportional expression of both opsins, sensitizing neurons to being bi-directionally controlled with blue and yellow light, facilitating proportional optical spike insertion and deletion upon delivery of trains of precisely-timed blue and yellow light pulses. Such approaches may enable more detailed explorations of the causal role of specific features of the neural code.

Keywords: optogenetics, channelrhodopsin-2, halorhodopsin, fusion protein, synchrony

INTRODUCTION

It has long been debated to what extent synchronous or precisely-timed neural activity contributes to neural computation and behavior. Synchronous neural activity within or between brain regions has been observed during, or associated with, many brain functions including timing-dependent plasticity, global stimulus feature processing, visuomotor integration, emotion, working memory, motor planning, and attention (e.g., Gray et al., 1989; Roelfsema et al., 1997; Brivanlou et al., 1998; Donoghue et al., 1998; Steinmetz et al., 2000; Fries et al., 2001; Tallon-Baudry et al., 2001; Froemke and Dan, 2002; Perez-Orive et al., 2002; Seidenbecher et al., 2003; Courtemanche and Lamarre, 2004; Buschman and Miller, 2007), as measured with multielectrode recording, electroencephalography (EEG), magnetoencephalography (MEG), and local field potential (LFP) analysis. Furthermore, abnormal patterns of neural synchrony have been associated with a variety of neurological and psychiatric disorders such as Parkinson's disease, epilepsy, autism, and schizophrenia (e.g., Bragin et al., 2002; Uhlhaas and Singer, 2006; Berendse and Stam, 2007; Brown, 2007; Huguenard and McCormick, 2007; Orekhova et al., 2007; Gonzalez-Burgos and Lewis, 2008; Roopun et al., 2009). Computationally, synchrony has been implicated in multiple processes, including grouping neurons into 'cell assemblies' that can more effectively represent information to downstream neural networks, acting as a clock for gating or multiplexing information, coordinating information flow within small neural networks, selecting stimuli for attention, and performing pattern recognition (e.g., Hopfield and Brody, 2001; Friedrich et al., 2004; Tiesinga and Sejnowski, 2004; Borgers et al., 2005, 2008; Sohal et al., 2009). However, determining the causal role of neural synchrony to neural computation and behavior has remained elusive, in part because selective perturbation of spike timing is difficult. In some specific systems, in which pharmacological or genetic strategies for selectively disrupting synchrony happened to be compatible with local cellular and network properties, pioneering attempts have been made to perturb spike timing without altering other aspects of neural coding such as spike rate (MacLeod and Laurent, 1996; Bao et al., 2002; Robbe et al., 2006), but no generalized method for doing so exists.

Recently we and others have developed strategies for optically sensitizing neurons to being activated and silenced with different colors of light, by delivering the gene encoding for the blue light-gated cation channel channelrhodopsin-2 (ChR2) or the gene for the yellow-light driven chloride pump halorhodopsin from *N. pharaonis* (Halo/NpHR) to neurons, and illuminating them with pulses of light (Boyden et al., 2005; Han and Boyden, 2007; Zhang et al., 2007). New neural activators and silencers continue to be developed, and these molecules have already begun to be applied to the study of neural dynamics, as investigators optically drive the activity of excitatory and inhibitory neurons and electrophysiologically characterize the resultant patterns (e.g., Boyden et al., 2009; Cardin et al., 2009; Han et al., 2009; Sohal et al., 2009; Talei Franzesi et al., 2009). However, none of these experiments have attempted to isolate the distinct properties of synchrony and spike rate, both of which are modulated when neurons are activated or silenced by using either ChR2 or Halo by itself. Previously, we presented a strategy for perturbing spike timing without altering spike rate (Han and Boyden, 2007), taking advantage of the fact that the spectral peaks for ChR2 activation

and Halo activation are separated by over 100 nm (**Figure 1A**), making it possible to express both molecules in the same neuron (**Figure 1B**), thus conferring bi-directional control of the voltage of that neuron by blue and yellow light (**Figures 1C,D**) (Han and Boyden, 2007). As a consequence of this two-color bidirectional voltage control, precisely-timed blue and yellow light pulse trains, delivered to a neuron expressing both ChR2 and Halo, can be used to insert spikes into, and delete spikes from, the ongoing activity experienced by that neuron (**Figure 1E**), resulting in precise perturbations of spike timing without changing overall spike rate (**Figures 1F,G**). However, the delivery of two separate genes to precisely the same cell population can be a daunting proposition. Furthermore, it is important that ChR2 and Halo be expressed in a predictable proportion to one another, so that the insertion and deletion of spikes can be balanced; separate delivery of the two genes, or independent expression of the two genes, would not accomplish this. Recently we and others have presented gene fusions between ChR2 and Halo that enable them to be expressed in the same expression cassette, bridging ChR2 and Halo with an optimized form of the 'self-cleaving' 2A peptide sequence from foot-and-mouth disease virus or other picornaviruses (Han et al., 2008; Tang et al., 2009). The 2A sequence encourages a ribosomal skip between a glycine and proline within the 2A sequence, resulting in separate proteins being formed from the sequences on either side (Ryan et al., 1991; Ryan and Drew, 1994). In the Tang et al. paper, the first peer-reviewed presentation of opsin fusions using a 2A peptide bridge, the authors showed functional expression of both opsins in the same cell, *in vivo*, after delivery via AAV. We here quantitate the proportional expression of ChR2 and Halo in the same cell when they are expressed separated by a 2A bridge, and discuss the consequences for the specific difficult experimental goal of perturbing synchrony and precise spike timing. Such proteins will also be useful for exploring a large set of systems neuroscience experiments in which bi-directional control of the activity of a given neuron population is desired.

MATERIALS AND METHODS

CELL CULTURE

All procedures involving animals were conducted in accordance with the National Institutes of Health Guide for the care and use of laboratory animals and approved by the Massachusetts Institute of Technology Animal Care and Use Committee. Hippocampal regions CA3-CA1 of postnatal day 0 Swiss Webster or C57 mice from Taconic or Jackson Labs were isolated and treated with trypsin (1 mg/ml) for ~12 min. Digestion was stopped by Hanks solution supplemented with 20% fetal bovine serum and trypsin inhibitor (Sigma). Tissue was dissociated with Pasteur pipettes and centrifuged at 1000 rpm at 4°C for 10 min. Dissociated neurons were plated on glass coverslips pre-coated with Matrigel (BD Biosciences) at a rough density of approximately two to four hippocampi per 20 coverslips. Neurons were transfected using a commercially available calcium phosphate transfection kit (Invitrogen), at 3–5 days *in vitro*. GFP fluorescence was used to identify successfully-transfected neurons, indicating a net transfection efficiency of 1–10%. All images and electrophysiological recordings were made on 9–15 day-*in-vitro* neurons (approximately 6–10 days after transfection).

MOLECULAR BIOLOGY

The ChR2GFP-2A-HaloYFP-N1 plasmid ('ChR2-2A-Halo') was constructed by first inserting the extended N-terminus 2A sequence (DNA sequence AAGAAACAGAAAATTGTGGCACC AGTGAAACAGACTTTGAATTTTGACCTTCTCAAGTTGGCG GGAGACGTCGAGTCCAACCCTGGGCCC, translated peptide sequence KKQKIVAPVKQTLNFDLLKLAGDVESNPGP) into the BsrGI and NotI sites in the pEGFP-N1 vector, followed by inserting ChR2-GFP without stop codon into the KpNI and BsrGI sites in front of the 2A sequence, and then by inserting Halo-YFP without start codon into the XbaI and EcoRI sites downstream of the 2A sequence. The pEGFP-N1 vector drives gene expression from the CMV promoter.

ELECTROPHYSIOLOGY

Whole cell patch clamp recording was made on 9–15 day-*in-vitro* neurons using a Multiclamp 700B amplifier, connected to a Digidata 1440 digitizer (Molecular Devices) attached to a PC running pClamp 10. During recording, neurons were bathed in Tyrode's solution containing (in mM) 150 NaCl, 2.4 KCl, 2 CaCl, 2 MgCl, 10 HEPES, 10 Glucose, 10 μM NBQX, 10 μM gabazine and 50 μM D-APV. Borosilicate glass (Warner) pipettes were filled with a solution containing (in mM) 130 K-Gluconate, 7 KCl, 2 NaCl, 1 MgCl2, 0.4 EGTA, 10 HEPES, 2 ATP-Mg, 0.3 GTP-Tris and 20 sucrose. Pipette resistance was ~5 MΩ and the access resistance was 10–25 MΩ, which was monitored throughout the voltage-clamp recording.

Light-induced membrane photocurrents were induced by brief light pulses separated by periods in the dark, in neurons current-clamped or voltage-clamped, respectively. Light pulse trains were either input directly into pClamp software (Molecular Devices) or synthesized by custom scripts written in MATLAB (Mathworks), then played back through a Sutter DG-4 light source via a Digidata 1440 (Molecular Devices). Light was reflected into the sample off of a 700DCXRU (Chroma) dichroic in a Leica DMI6000B inverted microscope. In the DG-4, a yellow filter (Chroma, bandpass 575 ± 25 nm) was used to deliver light to activate Halo, and a GFP excitation filter (bandpass 470 ± 20 nm) was used to activate ChR2. Powers out the 40× objective were approximately 10 mW/mm^2 in irradiance.

DATA ANALYSIS

Amplitude and timing data were analyzed using Clampfit 10 (Molecular Devices) and custom analysis scripts written in MATLAB.

RESULTS

We recently presented a demonstration of how one could use co-expression of separate ChR2 and Halo genes to support optical disruption of the timing of spikes, without significant alteration of spike rate (**Figure 1**, adapted from Han and Boyden, 2007). In review of this previously-published work (see Han and Boyden, 2007 for detailed results and methods): we cultured hippocampal neurons and then caused them to fire precisely-timed spike trains by patch clamping them in current-clamp mode, and repeatedly delivering to each neuron the same filtered Gaussian white noise current trace (see **Figure 1Ei**, top, for a fragment thereof). Such noisy currents had been previously found to induce reliable spike

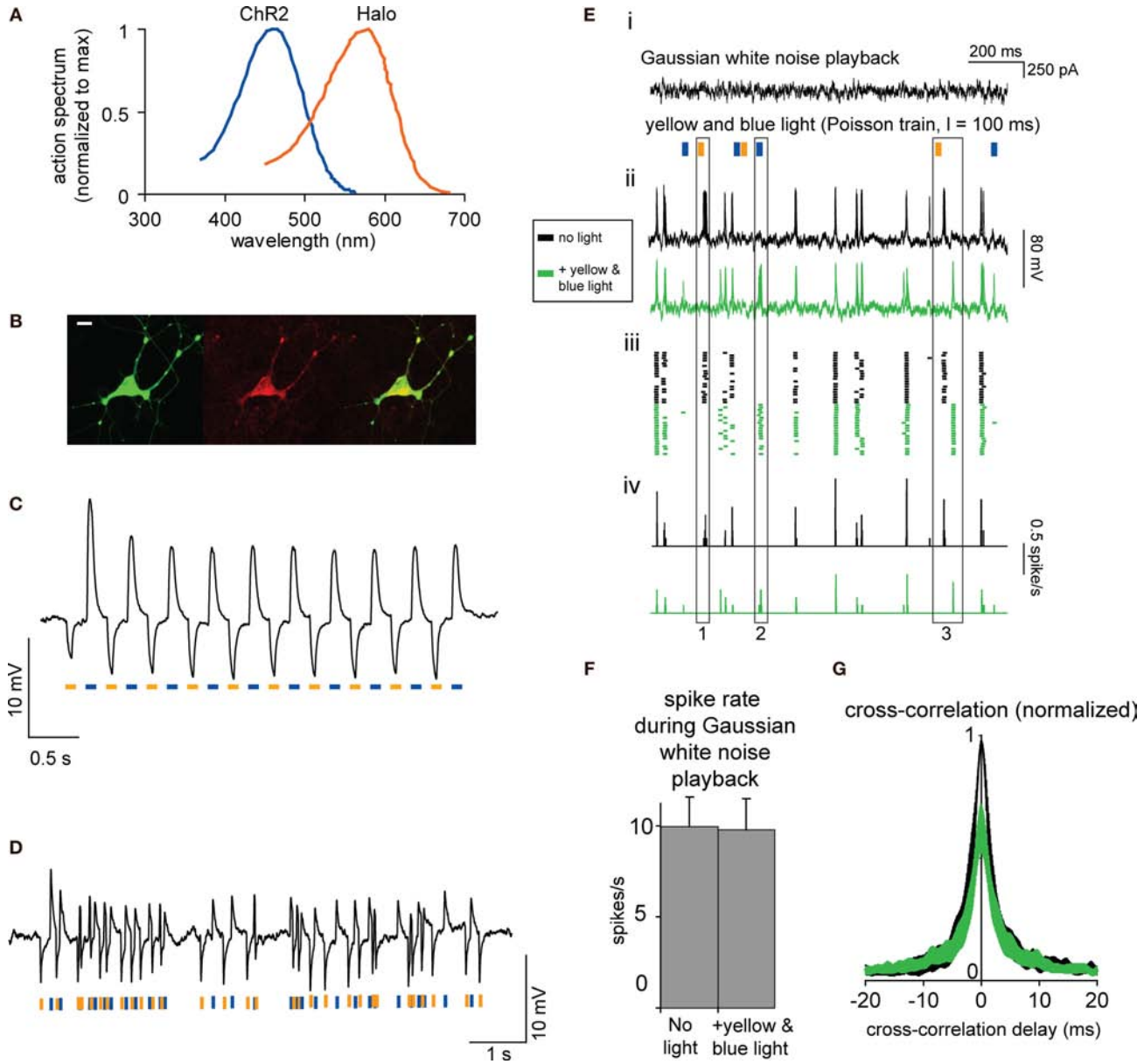

FIGURE 1 | Schema for how to alter neural spike timing, using two-color illumination of neurons co-transfected with both ChR2 and Halo in a 1:1 ratio. Adapted from (Han and Boyden, 2007). **(A)** Action spectrum for ChR2 (blue, adapted from Nagel et al., 2003), overlaid with absorption spectrum for Halo (orange, adapted from Duschl et al., 1990). Each spectrum is normalized to its own peak, for ease of comparison. **(B)** Co-expression of Halo-GFP (*left*) and ChR2-mCherry (*middle*) in a single neuron expressing both (*right*, overlay). Scale bar, 20 μm. **(C)** Hyperpolarization and depolarization events elicited in a single representative neuron, by two interleaved 2.5 Hz trains of yellow and blue light pulses (50 ms duration each), denoted by bars of respective coloration below the trace. **(D)** Hyperpolarization and depolarization events induced in a representative neuron by a Poisson train (mean inter-pulse interval λ = 100 ms) of alternating pulses of yellow and blue light (10 ms duration), denoted by bars of respective coloration below the trace. **(E)** Optical disruption of spike timing, without alteration of spike rate, for a representative current-clamped hippocampal neuron transfected simultaneously with ChR2 and Halo *in vitro*. Vertical boxes (labeled at bottom 1, 2, 3) highlight features referred to in the text of the Results. **(i)** Stimulus trace showing a subsegment of the somatically injected filtered Gaussian white noise current used in all these experiments (top), as well as of the Poisson train (mean inter-pulse interval λ = 100 ms) of alternating yellow and blue light pulses (bottom). **(ii)** 20-trace overlays of voltage responses to the somatically injected white noise current, either with no light (top, black traces) or with delivery of a Poisson train of yellow and blue light pulses (bottom, green traces). **(iii)** Spike raster plots for the traces shown in **(Eii)**. **(iv)** Spike-timing histograms (bin size: 500 μs) for the rasters shown in **(Eiii)**. **(F)** Spike rates of current-clamped hippocampal neurons transfected simultaneously with ChR2 and Halo *in vitro* (n = 7), injected with filtered Gaussian white noise current, either with no light (left) or with concurrent delivery of a Poisson train of yellow and blue light pulses (right). Plotted is mean ± standard error. **(G)** Cross-correlation between spike trains elicited by the same filtered Gaussian white noise current injection, played twice, when either both current injections were performed in the dark (black curve), or when one of the current injections was performed with concurrent delivery of a Poisson train of yellow and blue light pulses (green trace). Data is plotted as mean ± standard error (averaged across n = 7 neurons).

trains in current-clamped neurons in acute cortical brain slices (Mainen and Sejnowski, 1995). On some trials, we also illuminated the neuron with the Poisson train of alternating yellow and blue light pulses shown in **Figure 1D** (see **Figure 1Ei**, bottom). We found that when delivered alone, the filtered Gaussian white noise current trace indeed induced reliably-timed spike trains, across repeated trials (see **Figure 1Eii**, top, for 20 overlaid traces, and **Figure 1Eiii**, top, for corresponding spike rasters). When an optically-sensitized neuron was additionally driven by the Poisson train of yellow and blue light pulses, the neuron fired spikes with different timings than occurred in darkness, but the resultant spikes were nevertheless still similar across repeated trials of current injection + light illumination (see **Figure 1Eii**, bottom, and **Figure 1Eiii**, bottom, for overlaid traces and spike rasters respectively, for 20 trials; **Figure 1Eiv** shows spike histograms). Inspection of this data shows that relative to the spike train elicited by current injection alone, the Poisson train of light pulses could sometimes abolish spikes that were previously reliable (vertical box 1 spanning **Figures 1Ei–iv**), create new spikes which were not previously present (vertical box 2 spanning **Figures 1Ei–iv**), or advance or delay the timing of specific spikes relative to their original timing in the dark (vertical box 3 spanning **Figures 1Ei–iv**). We compared mean spike rates for neurons receiving the filtered Gaussian white noise current injection alone vs. with the additional Poisson light pulse train, and found no difference in spike rates for these two conditions ($p > 0.90$, *t*-test; $n = 7$ neurons; **Figure 1F**), indicating that our optical intervention preserved spike rate. However, precise spike timing was altered significantly: cross-correlations of the spike trains elicited from the filtered Gaussian white noise current injection alone vs. with the additional Poisson light pulse train resulted in zero-lag cross-correlations that were on average 37% smaller than cross-correlations of pairs of spike trains elicited from the filtered Gaussian white noise current injection alone ($p < 0.005$, $n = 7$ neurons). This indicates that precise spike timing was indeed disrupted by the activation of Halo and ChR2, even while spike rate was preserved.

The strategy illustrated in **Figure 1** centers around the idea of using blue light to push the voltage of a cell over spike threshold, and using yellow light to push the voltage of a cell under spike threshold. Critical to this strategy is the proportional expression of ChR2 and Halo in a predictable ratio to one another. Ideally, for every spike inserted, another will be deleted. A neuron that expresses high levels of both ChR2 and Halo will have a high probability of generating a spike in response to a blue light pulse, but will also have a high probability of losing a spike in response to a yellow light pulse. On the other hand, a neuron that expresses low levels of both ChR2 and Halo will have a low probability of generating a spike in response to a blue light pulse, but will also have a lower probability of losing a spike in response to a yellow light pulse. Thus to a first approximation, the strategy in **Figure 1** should work to disrupt spike timing but not spike rate, independent of the net expression levels of ChR2 and Halo, as long as their proportion is kept constant. Of course, this approximation will break down if the scenario approaches an extreme: for example, a high-firing rate neuron may not be responsive to blue light pulses because of a ceiling effect on firing rate, but may be greatly affected by yellow pulses; on the other hand, a low-firing rate neuron may respond to blue light pulses with increased spiking, but may have few spikes to lose when yellow light pulses arrive. Thus it will be important to choose light pulse trains that deliver light pulses at appropriate rates given the neural population under investigation; the light pulse rate should scale with the firing rate of the neural population (and in principle, could even be adapted in real time during a physiology or behavior experiment). Two further comments should be made: given that ChR2 and Halo generate intrinsically different scales of currents (ChR2's peak currents are an order of magnitude greater than Halo's), the ratio of blue to yellow light powers may need to be adjusted to balance the current magnitudes against one another. Finally, in the intact brain *in vivo*, light powers will fall off with distance from the light source; however, the difference between blue and yellow light power attenuation in brain tissue is not very large over the short distances (~1 mm) utilized for *in vivo* optical control scenarios, which are significantly less than the absorption length constant of visible light in tissue (Bernstein et al., 2008b). Tiling the brain with arrays of LED- or laser-coupled optical fibers may allow for more even light distribution in the brain, than possible with just one inserted fiber (Bernstein et al., 2008a; Zorzos et al., 2009).

To express both ChR2 and Halo in a stoichiometric ratio, we evaluated a number of candidate strategies. Using two viruses to deliver the two genes could lead to significant variation of the ChR2/Halo ratio across cells. Placing an internal ribosome entry site (IRES) – a long sequence of several hundred base pairs, large compared to the space accorded in many kinds of viral vector – in between two genes often results in much lower expression of the second gene (levels 0–20% those of the first gene) (Mizuguchi et al., 2000; Hennecke et al., 2001; Yu et al., 2003; Osti et al., 2006). We decided upon a methodology using the 'self-cleaving' 2A sequence (**Figure 2A**) from foot-and-mouth disease virus (Ryan et al., 1991; Ryan and Drew, 1994). When an mRNA encoding for ChR2-2A-Halo is being translated, a specific Gly-Pro bond in the 2A sequence would not be enduringly formed by the ribosome (a 'ribosomal skip'), resulting in the separate translation of ChR2 and Halo into separate proteins. We utilized a variant of 2A with additional amino acids appended to the N-terminus which enhances cleavage from 90% to 96–99% (as assessed by an *in vitro* translation assay) (Donnelly et al., 2001a,b) (**Figure 2A**, blue and green colored residues). The use of a different 2A peptide to co-express channelrhodopsin-2 and halorhodopsin within a single gene was recently published, including proof-of-principle electrophysiological data resulting from *in vivo* infection of neurons with the resulting virus (Tang et al., 2009). Here, expression of the ChR2-2A-Halo gene by transfection in cultured hippocampal neurons resulted in excitatory and inhibitory photocurrents in response to blue and yellow light respectively. The photocurrents were smaller than would result from expression of either gene alone (**Figure 2C**), in part because of overlap in the two molecules' action spectra (**Figure 1A**). Blue-light elicited photocurrents, measured in voltage clamp mode, were 157 ± 63 pA ($n = 22$ neurons; mean ± standard deviation), ~30% of the value previously reported for raw ChR2 expression in cultured hippocampal neurons (Boyden et al., 2005), and yellow-light elicited photocurrents were 40 ± 24 pA, ~45% of the value previously reported for raw Halo expression in cultured hippocampal neurons (Han and Boyden, 2007). These currents, nevertheless,

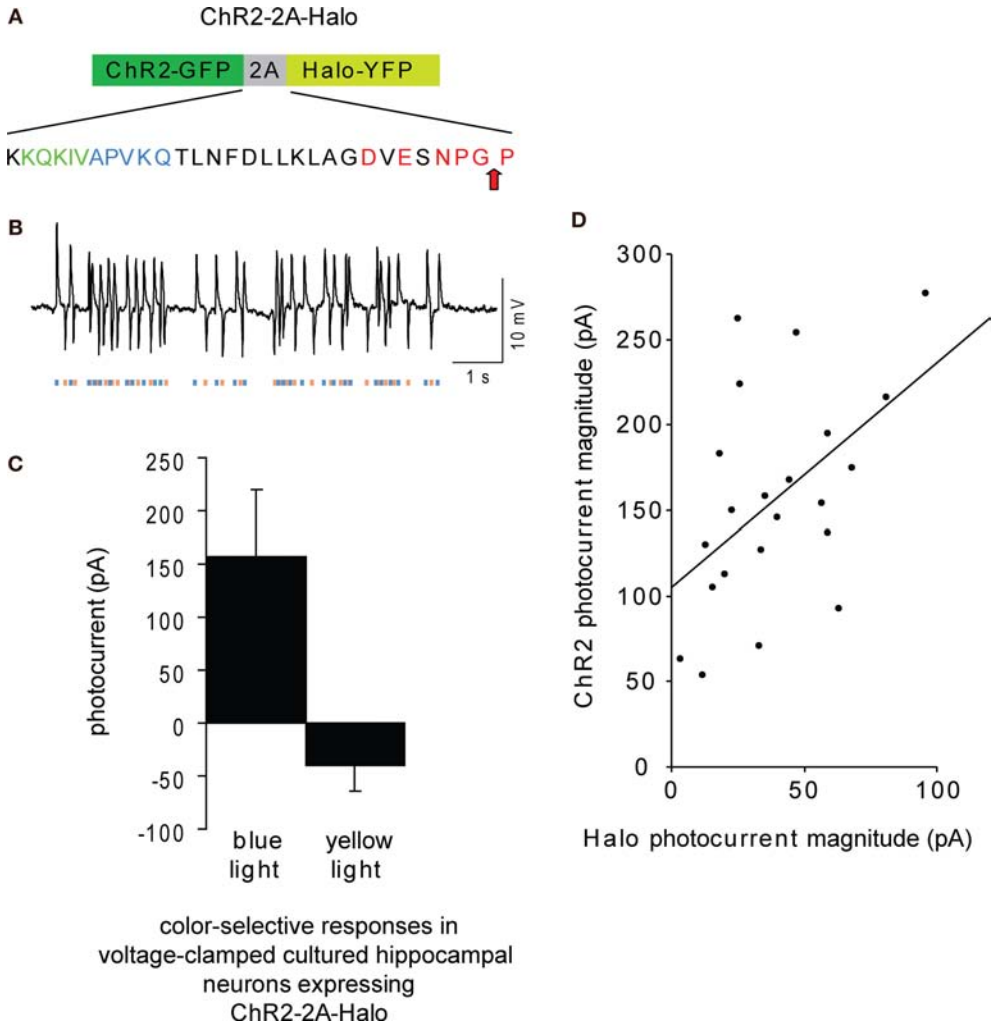

FIGURE 2 | Gene fusion enabling proportional co-expression of ChR2 and Halo under a single promoter. (A) Schematic of the gene fusion ChR2-2A-Halo, highlighting the sequence of the 2A peptide here used. Red letters indicate consensus sequence for 2A-like ribosomal skip sequence (Donnelly et al., 2001a; de Felipe et al., 2006); blue letters indicate amino acids from the 1D peptide sequence that, when appended to the N-terminus of the 2A sequence, increase *in vitro*-translated protein cleavage from 90% to 96%, and green letters are part of a sequence from the 1D peptide sequence that boosts *in vitro*-translated protein cleavage to 99–100% levels (Donnelly et al., 2001a,b). **(B)** Hyperpolarization and depolarization events induced in a representative current-clamped hippocampal neuron *in vitro*, transfected with ChR2-2A-Halo, by a Poisson train (mean inter-pulse interval λ = 100 ms) of alternating pulses of yellow and blue light (10 ms duration), denoted by bars of respective coloration below the trace. **(C)** Peak photocurrents measured in voltage clamped ChR2-2A-Halo-expressing cultured hippocampal neurons under 1-s blue (left) or yellow (right) exposure (n = 22 neurons; bars represent mean ± standard deviation). **(D)** Plot of magnitude of blue light-elicited photocurrents vs. magnitude of yellow light-elicited photocurrents. Line shows linear regression fit to the plotted data.

are sufficient to cause a neuron near the threshold of spiking to fire an action potential or to be momentarily silent, and routinely resulted, in current-clamped neurons, in effective perturbations of membrane voltage by 5–10 mV (**Figure 2B**). Plotting, for each recorded neuron, the blue-light elicited photocurrents vs. the yellow-light elicited photocurrents yielded a significant linear relationship with correlation coefficient $r = 0.51$ ($R^2 = 0.26$, $p < 0.02$; **Figure 2D**). Thus, the 2A expression vector here utilized was able to mediate proportional, functional expression of ChR2 and Halo in the same cell.

What kinds of experiment are enabled by the use of linked microbial opsins for bi-directional control of the voltage of individual neurons? Many 'obvious' but much-desired experiments may be facilitated with use of this reagent. For example, by appending to ChR2 a myosin-binding domain (MBD) that preferentially targets it to cell bodies and dendrites (Lewis et al., 2009), the resultant ChR2-MBD-2A-Halo could enable activation of a population of neurons when their cell bodies are illuminated with blue light, as well as silencing of specific projections when their axonal terminals are illuminated with yellow light. The ability to guarantee that a single population of neurons can be both activated and silenced is itself valuable, enabling testing of necessity and sufficiency of the same population of neurons, to a specific neural computation or behavior. However, it is useful to explore conceptually how this technology might be useful for probing complex questions concerning synchrony. We have, in **Figure 3**,

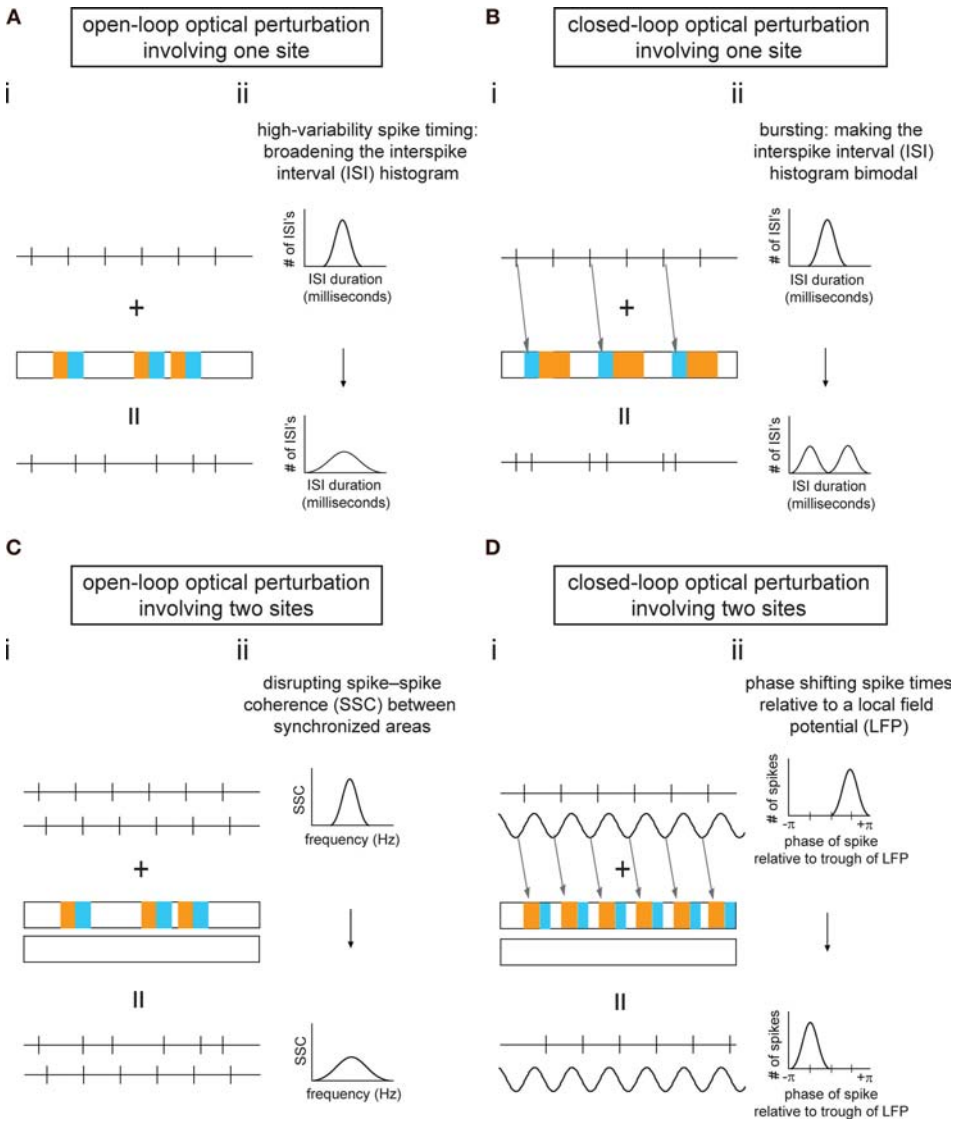

FIGURE 3 | Synchrony- and spike timing-perturbation protocols, enabled by use of ChR2-2A-Halo. Each of the four panels **(A–D)** displays a schematic experimental protocol **(i)** along with the anticipated effect of the protocol on neural circuit dynamics **(ii)**. An example is given for each of four kinds of experiment – **(A)** open-loop/one site, **(B)** closed-loop/one site, **(C)** open-loop/two sites, **(D)** closed-loop/two sites. Detailed descriptions of each panel follow. **(A)** Shows the use of Poisson train light pulse delivery to a site in which rhythmically-firing neurons express ChR2-2A-Halo. This protocol results in the interspike interval (ISI) becoming more variable than in the unilluminated state. **(i)** From top to bottom: spike train trace (for one example neuron) in dark; timeline of when yellow or blue light is delivered; spike train trace (for the example neuron) in light (e.g., the result of combining the original case, shown at top, with the delivery of light, shown in the middle). **(ii)** From top to bottom: ISI histogram in dark; ISI histogram in light. **(B)** Shows the use of optical perturbation in a closed-loop fashion, triggering blue-yellow pairs of light pulses off of particular recorded spikes in order to make the spike train more bursty. **(i)** From top to bottom: spike train trace in dark; timeline of when yellow or blue light is delivered (in this case, each blue-yellow pair is triggered by a spike; each trigger is indicated by an arrow); spike train trace under the closed-loop protocol. **(ii)** From top to bottom: ISI histogram in dark; ISI histogram under the closed-loop protocol. **(C)** Shows the use of optical perturbation in the style of **(Ai)**, with light delivered to one site to disrupt the timing of activity at that site, relative to another site, which is left unilluminated. **(i)** From top to bottom: spike train traces recorded at two sites in the dark; timeline of when yellow or blue light is delivered to one of the sites while the other is kept in the dark; spike train traces in light. **(ii)** From top to bottom: spike-spike coherence (see Fries et al., 2008 for experimental examples of this measure) across the two areas plotted vs. spike frequency, measured in dark; spike-spike coherence across the two areas plotted vs. spike frequency, measured when one site is illuminated. **(D)** Shows the use of optical perturbation in a closed-loop fashion, triggering yellow-blue pairs of light pulses at one site, off of a feature of the local field potential (LFP) recorded at another site, which is left unilluminated. In this case, the trough of the LFP (bandpass filtered to yield a defined set of frequencies) at the second site serves as the trigger for delaying spikes at the first site. **(i)** From top to bottom: spike train trace and local field potential trace recorded at two separate sites; timeline of when yellow or blue light is delivered to the site from which spikes are recorded (in this case, each yellow-blue pair is triggered by the trough of the LFP at the second site; each trigger is indicated by an arrow); spike train trace and local field potential trace under the closed-loop protocol. **(ii)** From top to bottom: phase relationship between spikes recorded at the first site and local field potential troughs recorded at the second site, in the dark (e.g., see Pesaran et al., 2002; Gregoriou et al., 2009) for examples of this kind of data); phase relationship between spikes recorded at the first site and local field potential troughs recorded at the second site, under the closed-loop protocol.

outlined in schematic form four protocols enabling perturbation of spike timing or synchrony, in order to study their contribution to circuit output. In all four cases, appropriately-timed blue and yellow light pulses are used to disrupt the timing of spikes in a region containing neurons sensitized to light with a 2A construct, thus altering the spike statistics. Because light will be delivered to all the neurons within a defined region, one caveat may apply: the optically-sensitized neurons in the region will be exposed to the same temporal pattern of blue and yellow light, and this common input may alter (e.g., increase) the synchrony between optically-sensitized neurons within the illuminated region; this may potentially complicate experiments where altered synchrony within a region is undesired, although again the use of multiple light sources to deliver multiple light patterns to a single region may ameliorate this issue.

One protocol is a direct generalization of the strategy outlined in **Figure 1**, the delivery of a light pulse train to a brain region to increase interspike interval (ISI) variability, turning rhythmic neurons into irregularly-firing ones (**Figure 3A**). This 'informational lesion' might enable the deletion of the information encoded by the precision of spiking of those cells, without eliminating all activity generated by those cells, and thereby causing a gross disruption of connected circuits (as might occur with a conventional lesion of the cells of interest). A slightly more complex version of this idea is illustrated in **Figure 3B**, in which light pulses are precisely triggered, in a closed-loop fashion, upon the occurrence of particular recorded spikes, so that the neuronal firing rate becomes more bursty (but, once again, without changing overall spike rates). The ability to test the role of bursting in spike signaling may help resolve how the temporal integration properties of neural circuit elements contribute to neural computations. The 2A strategy can also be used to disrupt correlations between multiple regions that exhibit synchrony (**Figure 3C**), making spike timing more variable in one region so that its activity correlation with activity in a second region decreases, or making spike timing more variable in one region to see if such activity causally influences the activity within the second region. In this way it might be possible to understand how regions communicate and process information together in a coordinated fashion. As a final example, the multi-site experiment can also be performed in a closed-loop fashion (**Figure 3D**), triggering the delivery of a specific light pulse train to one region, upon a particular phase of the local field potential (LFP) recorded in a second region, and thus phase shifting spike times in the first region with respect to the LFP of the second. Many other possible protocols exist; the key advance enabled by the 2A construct in such protocols is the ability to lesion information or alter information in the brain, without grossly disrupting the spike rate, as happens with traditional lesions, some forms of pharmacology, or normal activation or silencing of neurons.

DISCUSSION

We here discuss the implications of gene fusions of ChR2 and Halo, linked by the 'self-cleaving' 2A peptide, capable of supporting cellular synthesis of both opsins in proportion to one another, towards enabling a set of neurons to be simultaneously sensitized to blue light activation and yellow-light silencing. As an example of computational neuroscience-driven molecular engineering, such reagents may enable novel kinds of perturbation, such as the disruption of spike timing in the absence of altering spike rate. The construct presented here is freely available from the nonprofit service Addgene (reagent 'ChR2-2A-Halo' at http://www.addgene.org/Edward_Boyden) and is ready for use for transfection, gene gunning (Zhang et al., 2008), transgenic implementation (Wang et al., 2007), or electroporation (Petreanu et al., 2007; Lagali et al., 2008). The current construct, ChR2-2A-Halo yielded, when transfected into neurons, blue- and yellow-light elicited currents that were 30–40% of those obtained when ChR2 or Halo were expressed alone, respectively. Another paper that recently also disclosed the use of a 2A bridge to co-express ChR2 and Halo also showed currents that were smaller than those resulting from expression of individual opsins alone (Tang et al., 2009). These are still useful currents, especially if the goal is to dither the activity of a neuron above and below spike threshold in order to add and subtract spikes (as opposed to strongly driving or inhibiting neurons); however, a question for any technology is whether the efficacy can be improved further. One solution would be to use stronger opsins to begin with, such as novel molecules like ChIEF (Lin et al., 2009) and Arch (Chow et al., 2009a,b), which can mediate functionally higher currents than ChR2 and Halo, respectively. Other methods for expressing two genes also exist: for example, bi-directional promoters can lead to higher expression levels than can 2A, but at the expense of significantly more variability in the ratio of the protein levels resulting from each gene (e.g., see Fig. 3A in Amendola et al., 2005), due to the greater chance for noise to creep in downstream of the stoichiometry-determining event.

The prospects for using optical control technologies for ultraprecise neuromodulation therapies in clinical settings are exciting, since precise activation and silencing of specific cell types may increase efficacy and reduce side effects of treatments relative to purely electrical methods. However, it is important to consider not just straightforward optical activation and silencing, but also complex perturbations such as desynchronization as here described, which could enable correction of neural dynamics abnormalities such as those found in neurological and psychiatric disorders like Parkinson's and epilepsy. As pre-clinical studies of the safety and efficacy of optical control technology begin (Han et al., 2009), it will be increasingly important to derive principles of neural control, prototyping novel therapies that take full advantage of the computational power of these new technologies.

ACKNOWLEDGMENTS

ESB acknowledges funding by the NIH Director's New Innovator Award (DP2 OD002002-01), as well as by the NSF (0835878 and 0848804), the McGovern Institute Neurotechnology Award Program, the Department of Defense, NARSAD, the Alfred P. Sloan Foundation, the Jerry Burnett Foundation, the SFN Research Award for Innovation in Neuroscience, the MIT Media Lab, the Benesse Foundation, and the Wallace H. Coulter Foundation. XH acknowledges the Helen Hay Whitney Foundation and NIH 1K99MH085944. Thanks to Jennifer Raymond and Bob Desimone for discussions.

REFERENCES

Amendola, M., Venneri, M. A., Biffi, A., Vigna, E., and Naldini, L. (2005). Coordinate dual-gene transgenesis by lentiviral vectors carrying synthetic bidirectional promoters. *Nat. Biotechnol.* 23, 108–116.

Bao, S., Chen, L., Kim, J. J., and Thompson, R. F. (2002). Cerebellar cortical inhibition and classical eyeblink conditioning. *Proc. Natl. Acad. Sci. U.S.A.* 99, 1592–1597.

Berendse, H. W., and Stam, C. J. (2007). Stage-dependent patterns of disturbed neural synchrony in Parkinson's disease. *Parkinsonism Relat. Disord.* 13(Suppl. 3), S440–S445.

Bernstein, J., Ko, E., Strelzoff, A., Chan, S. C. Y., Gidwaney, V., Stickgold, E., Tentori, A. M., (Henninger, M. A., listed as first author since sponsor of poster), McConnell, J., Rodriguez, A., Monahan, P. A., Talei Franzesi, G., Han, X., Qian, X., and Boyden, E. S. (2008a). A scalable toolbox for systematic, cell-specific optical control of entire 3-D neural circuits in the intact mammalian brain. *Soc. Neurosci.* 493.4, UU25.

Bernstein, J. G., Han, X., Henninger, M. A., Ko, E. Y., Qian, X., Franzesi, G. T., McConnell, J. P., Stern, P., Desimone, R., and Boyden, E. S. (2008b). Prosthetic systems for therapeutic optical activation and silencing of genetically-targeted neurons. *Proc. Soc. Photo Opt. Instrum. Eng.* 6854, 68540H.

Borgers, C., Epstein, S., and Kopell, N. J. (2005). Background gamma rhythmicity and attention in cortical local circuits: a computational study. *Proc. Natl. Acad. Sci. U.S.A.* 102, 7002–7007.

Borgers, C., Epstein, S., and Kopell, N. J. (2008). Gamma oscillations mediate stimulus competition and attentional selection in a cortical network model. *Proc. Natl. Acad. Sci. U.S.A.* 105, 18023–18028.

Boyden, E., Franzesi, G. T., Qian, X., Li, M., Han, X., Borgers, C., Kopell, N. J., Le Beau, F., and Whittington, M. A. (2009). Probing mechanisms of gamma rhythmogenesis with cell type-specific optical neural control. *Front. Syst. Neurosci. Conference Abstract: Computational and Systems Neuroscience.* doi: 10.3389/conf.neuro.3310.2009.3303.3299.

Boyden, E. S., Zhang, F., Bamberg, E., Nagel, G., and Deisseroth, K. (2005). Millisecond-timescale, genetically targeted optical control of neural activity. *Nat. Neurosci.* 8, 1263–1268.

Bragin, A., Wilson, C. L., Staba, R. J., Reddick, M., Fried, I., and Engel, J., Jr. (2002). Interictal high-frequency oscillations (80–500 Hz) in the human epileptic brain: entorhinal cortex. *Ann. Neurol.* 52, 407–415.

Brivanlou, I. H., Warland, D. K., and Meister, M. (1998). Mechanisms of concerted firing among retinal ganglion cells. *Neuron* 20, 527.

Brown, P. (2007). Abnormal oscillatory synchronisation in the motor system leads to impaired movement. *Curr. Opin. Neurobiol.* 17, 656–664.

Buschman, T. J., and Miller, E. K. (2007). Top-down versus bottom-up control of attention in the prefrontal and posterior parietal cortices. *Science* 315, 1860–1862.

Cardin, J. A., Carlen, M., Meletis, K., Knoblich, U., Zhang, F., Deisseroth, K., Tsai, L. H., and Moore, C. I. (2009). Driving fast-spiking cells induces gamma rhythm and controls sensory responses. *Nature,* 459, 663–667.

Chow, B., Han, X., Qian, X., and Boyden, E. S. (2009a). High-performance halorhodopsin variants for improved genetically-targetable optical neural silencing. *Front. Syst. Neurosci. Conference Abstract: Computational and Systems Neuroscience*. doi: 10.3389/conf.neuro.10.2009.03.347.

Chow, B., Han, X., Qian, X., Li, M., Chuong, A. S., Monahan, P. E., Dobry, A. S., and Boyden, E. S. (2009b). High-efficacy, temporally-precise, in vivo neural silencing via light-driven proton pumping. *Soc. Neurosci.* 338.2, GG97.

Courtemanche, R., and Lamarre, Y. (2004). Local field potential oscillations in primate cerebellar cortex: synchronization with cerebral cortex during active and passive expectancy. *J. Neurophysiol.* 93, 2039–2052.

de Felipe, P., Luke, G. A., Hughes, L. E., Gani, D., Halpin, C., and Ryan, M. D. (2006). E unum pluribus: multiple proteins from a self-processing polyprotein. *Trends Biotechnol.* 24, 68–75.

Donnelly, M. L., Hughes, L. E., Luke, G., Mendoza, H., ten Dam, E., Gani, D., and Ryan, M. D. (2001a). The 'cleavage' activities of foot-and-mouth disease virus 2A site-directed mutants and naturally occurring '2A-like' sequences. *J. Gen. Virol.* 82, 1027–1041.

Donnelly, M. L., Luke, G., Mehrotra, A., Li, X., Hughes, L. E., Gani, D., and Ryan, M. D. (2001b). Analysis of the aphthovirus 2A/2B polyprotein 'cleavage' mechanism indicates not a proteolytic reaction, but a novel translational effect: a putative ribosomal 'skip'. *J. Gen. Virol.* 82, 1013–1025.

Donoghue, J. P., Sanes, J. N., Hatsopoulos, N. G., and Gaal, G. (1998). Neural discharge and local field potential oscillations in primate motor cortex during voluntary movements. *J. Neurophysiol.* 79, 159–173.

Duschl, A., Lanyi, J. K., and Zimanyi, L. (1990). Properties and photochemistry of a halorhodopsin from the haloalkalophile, *Natronobacterium pharaonis*. *J. Biol. Chem.* 265, 1261–1267.

Friedrich, R. W., Habermann, C. J., and Laurent, G. (2004). Multiplexing using synchrony in the zebrafish olfactory bulb. *Nat. Neurosci.* 7, 862–871.

Fries, P., Reynolds, J. H., Rorie, A. E., and Desimone, R. (2001). Modulation of oscillatory neuronal synchronization by selective visual attention. *Science* 291, 1560–1563.

Fries, P., Womelsdorf, T., Oostenveld, R., and Desimone, R. (2008). The effects of visual stimulation and selective visual attention on rhythmic neuronal synchronization in macaque area V4. *J. Neurosci.* 28, 4823–4835.

Froemke, R. C., and Dan, Y. (2002). Spike-timing-dependent synaptic modification induced by natural spike trains. *Nature* 416, 433–438.

Gonzalez-Burgos, G., and Lewis, D. A. (2008). GABA neurons and the mechanisms of network oscillations: implications for understanding cortical dysfunction in schizophrenia. *Schizophr. Bull.* 34, 944–961.

Gray, C. M., Konig, P., Engel, A. K., and Singer, W. (1989). Oscillatory responses in cat visual cortex exhibit inter-columnar synchronization which reflects global stimulus properties. *Nature* 338, 334–337.

Gregoriou, G. G., Gotts, S. J., Zhou, H., and Desimone, R. (2009). High-frequency, long-range coupling between prefrontal and visual cortex during attention. *Science* 324, 1207–1210.

Han, X., and Boyden, E. S. (2007). Multiple-color optical activation, silencing, and desynchronization of neural activity, with single-spike temporal resolution. *PLoS ONE* 2, e299. doi: 10.1371/journal.pone.0000299.

Han, X., Qian, X., Bernstein, J. G., Zhou, H. H., Franzesi, G. T., Stern, P., Bronson, R. T., Graybiel, A. M., Desimone, R., and Boyden, E. S. (2009). Millisecond-timescale optical control of neural dynamics in the nonhuman primate brain. *Neuron* 62, 191–198.

Han, X., Qian, X., Talei Franzesi, G., Stern, P., and Boyden, E. (2008). Molecular toolboxes for quantitatively precise, genetically-targeted optical control of normal and pathological neural network dynamics. *Soc. Neurosci.* 493.9, UU30.

Hennecke, M., Kwissa, M., Metzger, K., Oumard, A., Kroger, A., Schirmbeck, R., Reimann, J., and Hauser, H. (2001). Composition and arrangement of genes define the strength of IRES-driven translation in bicistronic mRNAs. *Nucleic Acids Res.* 29, 3327–3334.

Hopfield, J. J., and Brody, C. D. (2001). What is a moment? Transient synchrony as a collective mechanism for spatiotemporal integration. *Proc. Natl. Acad. Sci. U.S.A.* 98, 1282–1287.

Huguenard, J. R., and McCormick, D. A. (2007). Thalamic synchrony and dynamic regulation of global forebrain oscillations. *Trends Neurosci.* 30, 350–356.

Lagali, P. S., Balya, D., Awatramani, G. B., Munch, T. A., Kim, D. S., Busskamp, V., Cepko, C. L., and Roska, B. (2008). Light-activated channels targeted to ON bipolar cells restore visual function in retinal degeneration. *Nat. Neurosci.* 11, 667–675.

Lewis, T. L., Jr., Mao, T., Svoboda, K., and Arnold, D. B. (2009). Myosin-dependent targeting of transmembrane proteins to neuronal dendrites. *Nat. Neurosci.* 12, 568–576.

Lin, J. Y., Lin, M. Z., Steinbach, P., and Tsien, R. Y. (2009). Characterization of engineered channelrhodopsin variants with improved properties and kinetics. *Biophys. J.* 96, 1803–1814.

MacLeod, K., and Laurent, G. (1996). Distinct mechanisms for synchronization and temporal patterning of odor-encoding neural assemblies. *Science* 274, 976–979.

Mainen, Z. F., and Sejnowski, T. J. (1995). Reliability of spike timing in neocortical neurons. *Science* 268, 1503–1506.

Mizuguchi, H., Xu, Z., Ishii-Watabe, A., Uchida, E., and Hayakawa, T. (2000). IRES-dependent second gene expression is significantly lower than cap-dependent first gene expression in a bicistronic vector. *Mol. Ther.* 1, 376–382.

Nagel, G., Szellas, T., Huhn, W., Kateriya, S., Adeishvili, N., Berthold, P., Ollig, D., Hegemann, P., and Bamberg, E. (2003). Channelrhodopsin-2, a directly light-gated cation-selective membrane channel. *Proc. Natl. Acad. Sci. U.S.A.* 100, 13940–13945.

Orekhova, E. V., Stroganova, T. A., Nygren, G., Tsetlin, M. M., Posikera, I. N., Gillberg, C., and Elam, M. (2007). Excess of high frequency electroencephalogram oscillations in boys with autism. *Biol. Psychiatry* 62, 1022–1029.

Osti, D., Marras, E., Ceriani, I., Grassini, G., Rubino, T., Vigano, D., Parolaro, D., and Perletti, G. (2006). Comparative analysis of molecular strategies attenuating positional effects in lentiviral vectors carrying multiple genes. *J. Virol. Methods* 136, 93–101.

Perez-Orive, J., Mazor, O., Turner, G. C., Cassenaer, S., Wilson, R. I., and Laurent, G. (2002). Oscillations and sparsening of odor representations in the mushroom body. *Science* 297, 359–365.

Pesaran, B., Pezaris, J. S., Sahani, M., Mitra, P. P., and Andersen, R. A. (2002). Temporal structure in neuronal activity during working memory in macaque parietal cortex. *Nat. Neurosci.* 5, 805–811.

Petreanu, L., Huber, D., Sobczyk, A., and Svoboda, K. (2007). Channelrhodopsin-2-assisted circuit mapping of long-range callosal projections. *Nat. Neurosci.* 10, 663–668.

Robbe, D., Montgomery, S. M., Thome, A., Rueda-Orozco, P. E., McNaughton, B. L., and Buzsaki, G. (2006). Cannabinoids reveal importance of spike timing coordination in hippocampal function. *Nat. Neurosci.* 9, 1526–1533.

Roelfsema, P. R., Engel, A. K., Konig, P., and Singer, W. (1997). Visuomotor integration is associated with zero time-lag synchronization among cortical areas. *Nature* 385, 157–161.

Roopun, A. K., Traub, R. D., Baldeweg, T., Cunningham, M. O., Whittaker, R. G., Trevelyan, A., Duncan, R., Russell, A. J., and Whittington, M. A. (2009). Detecting seizure origin using basic, multiscale population dynamic measures: preliminary findings. *Epilepsy Behav.* 14(Suppl. 1), 39–46.

Ryan, M. D., and Drew, J. (1994). Foot-and-mouth disease virus 2A oligopeptide mediated cleavage of an artificial polyprotein. *EMBO J.* 13, 928–933.

Ryan, M. D., King, A. M., and Thomas, G. P. (1991). Cleavage of foot-and-mouth disease virus polyprotein is mediated by residues located within a 19 amino acid sequence. *J. Gen. Virol.* 72(Pt 11), 2727–2732.

Seidenbecher, T., Laxmi, T. R., Stork, O., and Pape, H. C. (2003). Amygdalar and hippocampal theta rhythm synchronization during fear memory retrieval. *Science* 301, 846–850.

Sohal, V. S., Zhang, F., Yizhar, O., and Deisseroth, K. (2009). Parvalbumin neurons and gamma rhythms enhance cortical circuit performance. *Nature* 459, 698–702.

Steinmetz, P. N., Roy, A., Fitzgerald, P. J., Hsiao, S. S., Johnson, K. O., and Niebur, E. (2000). Attention modulates synchronized neuronal firing in primate somatosensory cortex. *Nature* 404, 187–190.

Talei Franzesi, G., Borgers, C., Qian, X., Li, M., Han, X., Kopell, N., LeBeau, F., Whittington, M., and Boyden, E. S. (2009). Dynamical properties of gamma-frequency cell assemblies in the hippocampus probed with optical neural control and computational modeling. *Soc. Neurosci.* 321.13, D1.

Tallon-Baudry, C., Bertrand, O., and Fischer, C. (2001). Oscillatory synchrony between human extrastriate areas during visual short-term memory maintenance. *J. Neurosci.* 21, RC177.

Tang, W., Ehrlich, I., Wolff, S. B., Michalski, A. M., Wolfl, S., Hasan, M. T., Luthi, A., and Sprengel, R. (2009). Faithful expression of multiple proteins via 2A-peptide self-processing: a versatile and reliable method for manipulating brain circuits. *J. Neurosci.* 29, 8621–8629.

Tiesinga, P. H., and Sejnowski, T. J. (2004). Rapid temporal modulation of synchrony by competition in cortical interneuron networks. *Neural Comput.* 16, 251–275.

Uhlhaas, P. J., and Singer, W. (2006). Neural synchrony in brain disorders: relevance for cognitive dysfunctions and pathophysiology. *Neuron* 52, 155–168.

Wang, H., Peca, J., Matsuzaki, M., Matsuzaki, K., Noguchi, J., Qiu, L., Wang, D., Zhang, F., Boyden, E., Deisseroth, K., Kasai, H., Hall, W. C., Feng, G., Augustine, G. J. (2007). High-speed mapping of synaptic connectivity using photostimulation in Channelrhodopsin-2 transgenic mice. *Proc. Natl. Acad. Sci. U.S.A.* 104, 8143–8148.

Yu, X., Zhan, X., D'Costa, J., Tanavde, V. M., Ye, Z., Peng, T., Malehorn, M. T., Yang, X., Civin, C. I., and Cheng, L. (2003). Lentiviral vectors with two independent internal promoters transfer high-level expression of multiple transgenes to human hematopoietic stem-progenitor cells. *Mol. Ther.* 7, 827–838.

Zhang, F., Wang, L. P., Brauner, M., Liewald, J. F., Kay, K., Watzke, N., Wood, P. G., Bamberg, E., Nagel, G., Gottschalk, A., and Deisseroth, K. (2007). Multimodal fast optical interrogation of neural circuitry. *Nature* 446, 633–639.

Zhang, Y. P., Holbro, N., and Oertner, T. G. (2008). Optical induction of plasticity at single synapses reveals input-specific accumulation of alphaCaMKII. *Proc. Natl. Acad. Sci. U.S.A.* 105, 12039–12044.

Zorzos, A. N., Bernstein, J. G., Boyden, E S., and Fonstad, C. G. (2009). Integrated microstructure lightguides for ultradense optical neural control of 3-dimensional neural circuits. *Soc. Neurosci.* 388.1, GG96.

Conflict of Interest Statement: The authors declare that the research was conducted in the absence of any commercial or financial relationships that could be construed as a potential conflict of interest.

Received: 07 July 2009; paper pending published: 21 July 2009; accepted: 10 August 2009; published online: 27 August 2009.
*Citation: Han X, Qian X, Stern P, Chuong AS and Boyden ES (2009) Informational lesions: optical perturbation of spike timing and neural synchrony via microbial opsin gene fusions. Front. Mol. Neurosci. **2**:12. doi: 10.3389/neuro.02.012.2009*

APPENDIX 4

“Prosthetic Systems for Therapeutic Optical Activation and Silencing of Genetically-Targeted Neurons,” US Patent Application 61/021,612.

US 20090210039A1

(19) **United States**

(12) **Patent Application Publication**

(10) **Pub. No.: US 2009/0210039 A1**

(43) **Pub. Date: Aug. 20, 2009**

Boyden et al.

(54) **PROSTHETIC SYSTEM FOR THERAPEUTIC OPTICAL ACTIVATION AND SILENCING OF GENETICALLY-TARGETED NEURONS**

(76) Inventors: **Edward S. Boyden**, Cambridge, MA (US); **Jacob G. Bernstein**, Cambridge, MA (US); **Michael Henninger**, Cambridge, MA (US)

Correspondence Address:
NORMA E HENDERSON
HENDERSON PATENT LAW
13 JEFFERSON DR
LONDONDERRY, NH 03053 (US)

(21) Appl. No.: **12/355,745**

(22) Filed: **Jan. 16, 2009**

Related U.S. Application Data

(63) Continuation-in-part of application No. 12/118,673, filed on May 9, 2008.

(60) Provisional application No. 61/021,612, filed on Jan. 16, 2008, provisional application No. 60/917,055, filed on May 9, 2007.

Publication Classification

(51) **Int. Cl.**
A61N 5/067 (2006.01)
A61N 5/06 (2006.01)

(52) **U.S. Cl.** **607/89**; 607/88

(57) **ABSTRACT**

An optical prosthesis that permits control of neural circuits comprises a probe having a set of light sources, drive circuit connections connected to each light source, a housing surrounding the light sources and drive circuit connections, and drive circuitry for driving and controlling the probe. The drive circuit connections and drive circuitry may optionally provide for wireless communication. The light sources may be light-emitting diodes, lasers, or other suitable sources. The device may optionally include sensors for monitoring the target cells. The present invention is also a multi-dimensional array of probes, each probe having a set of light sources, drive circuit connections connected to each light source, a housing surrounding the light sources and the drive circuit connections, drive circuitry for driving and controlling the probes, and supporting hardware that holds the probes in position with respect to each other and the target cells.

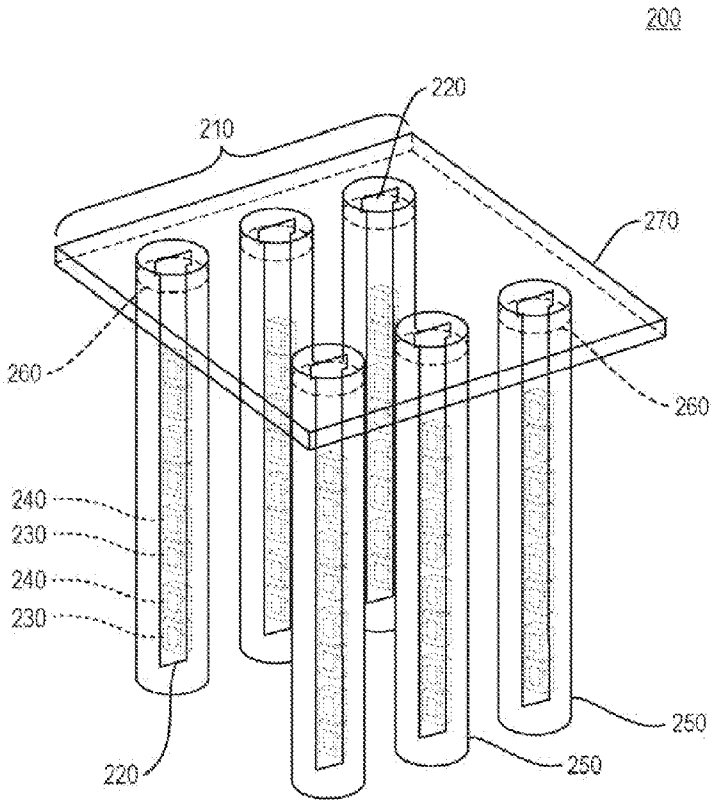

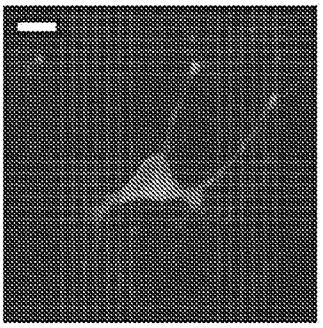

FIG. 1A

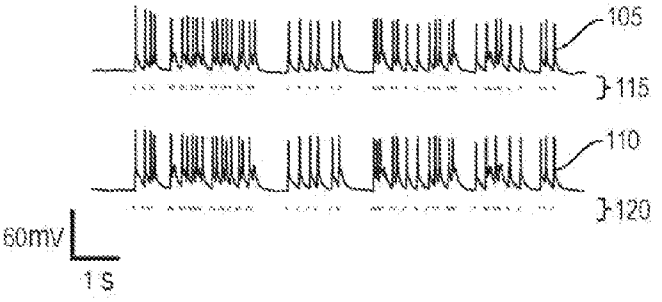

FIG. 1B

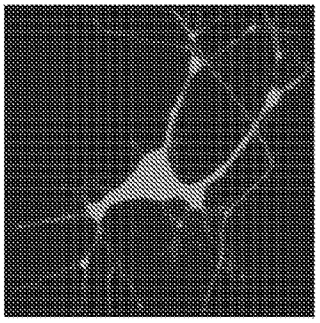

FIG. 1C

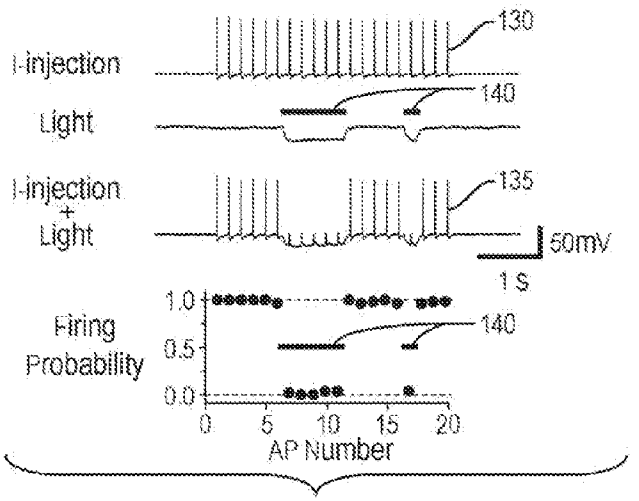

FIG. 1D

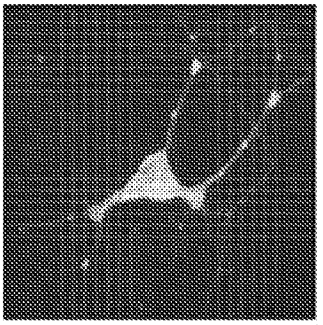

FIG. 1E

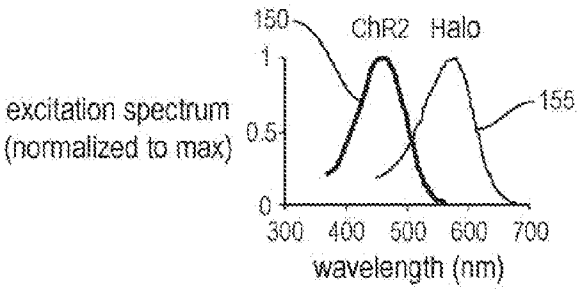

FIG. 1F

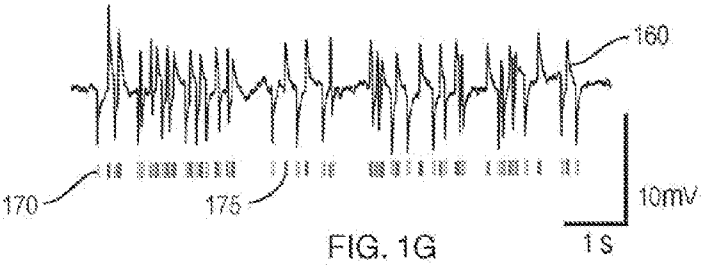

FIG. 1G

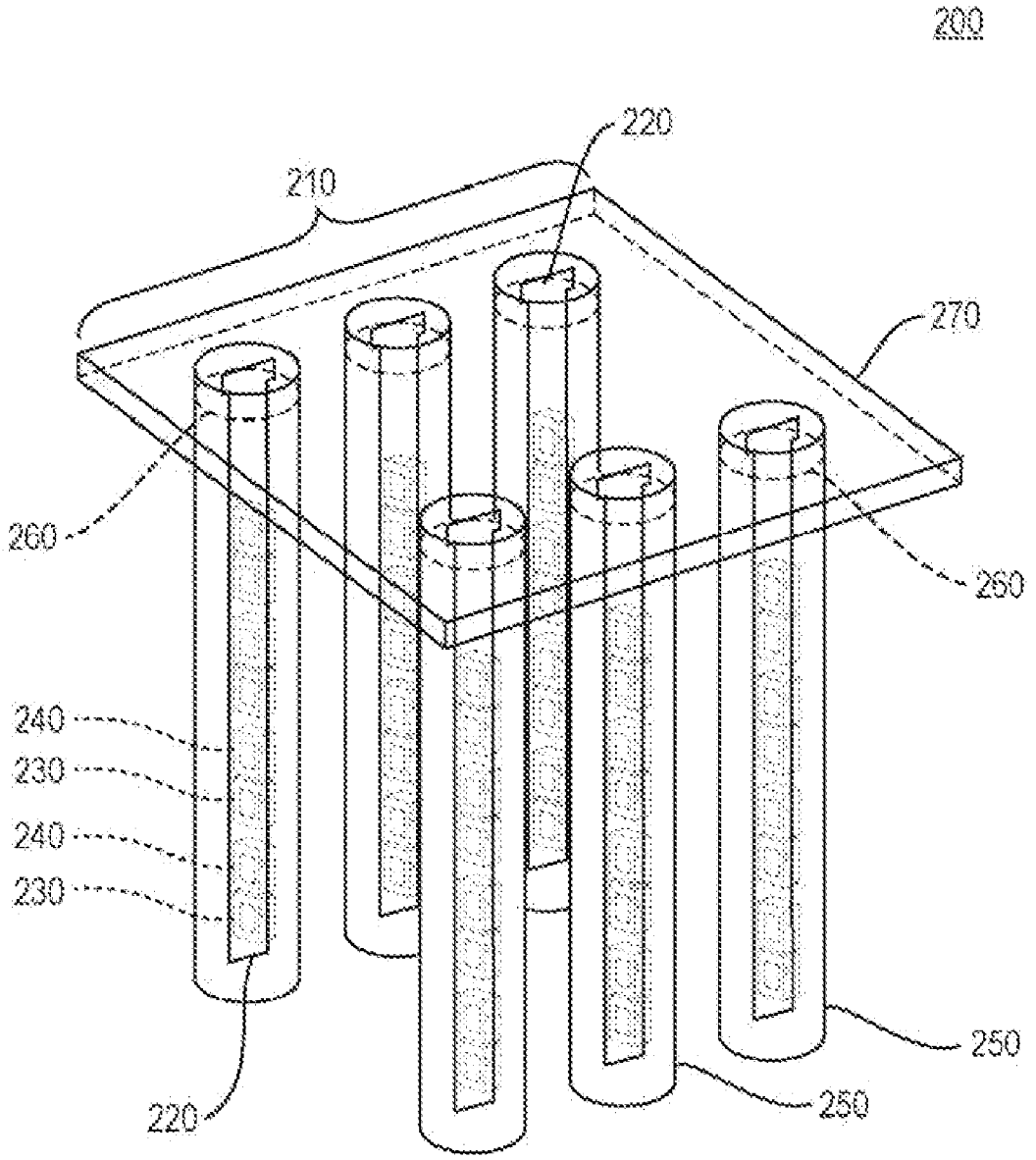

FIG. 2

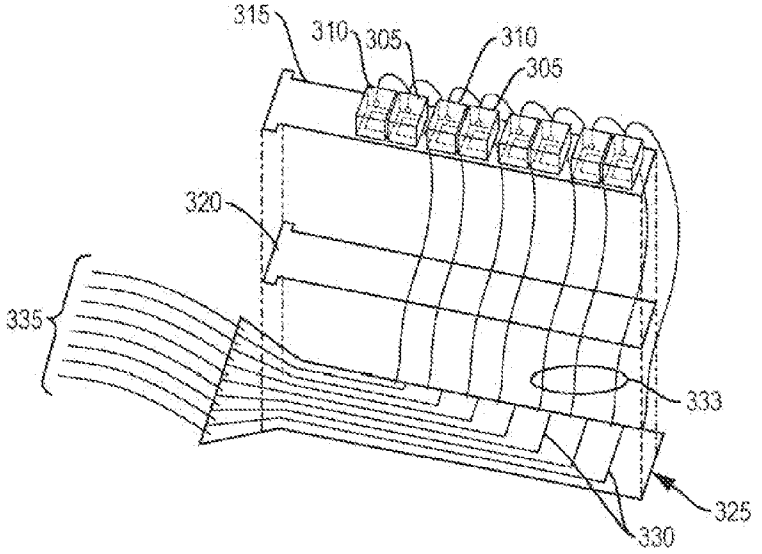
315
310
305
310
305
320
335
333
325
330

FIG. 3A

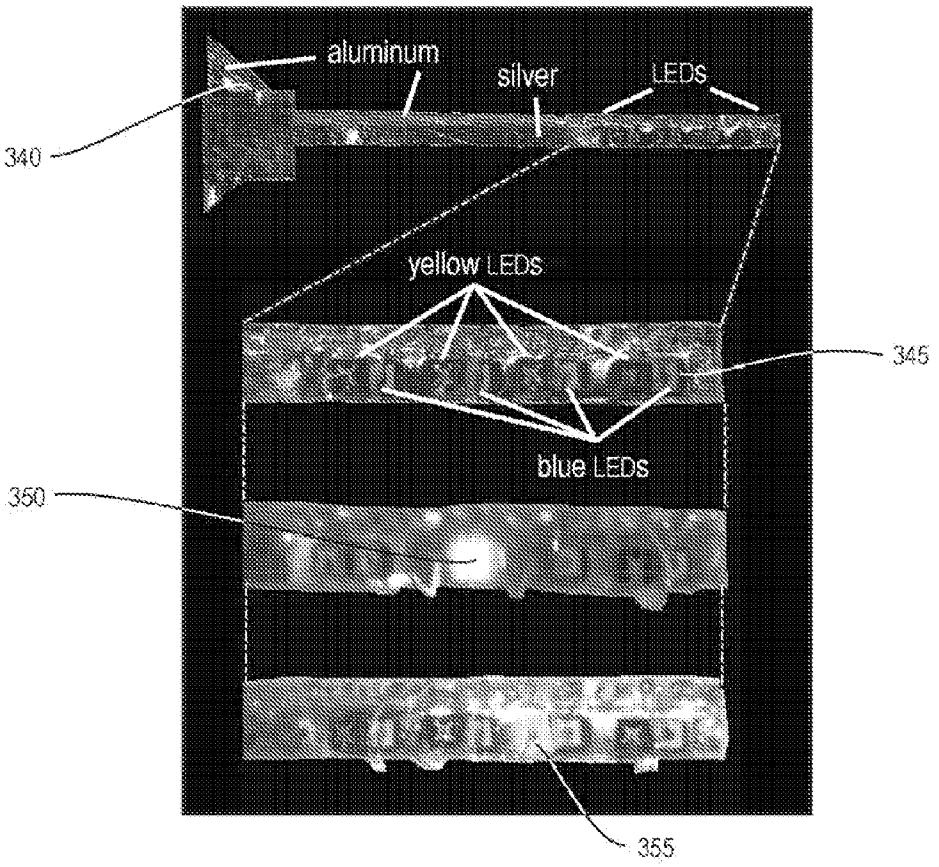
aluminum
silver
LEDs
340
yellow LEDs
345
blue LEDs
350
355

FIG. 3B

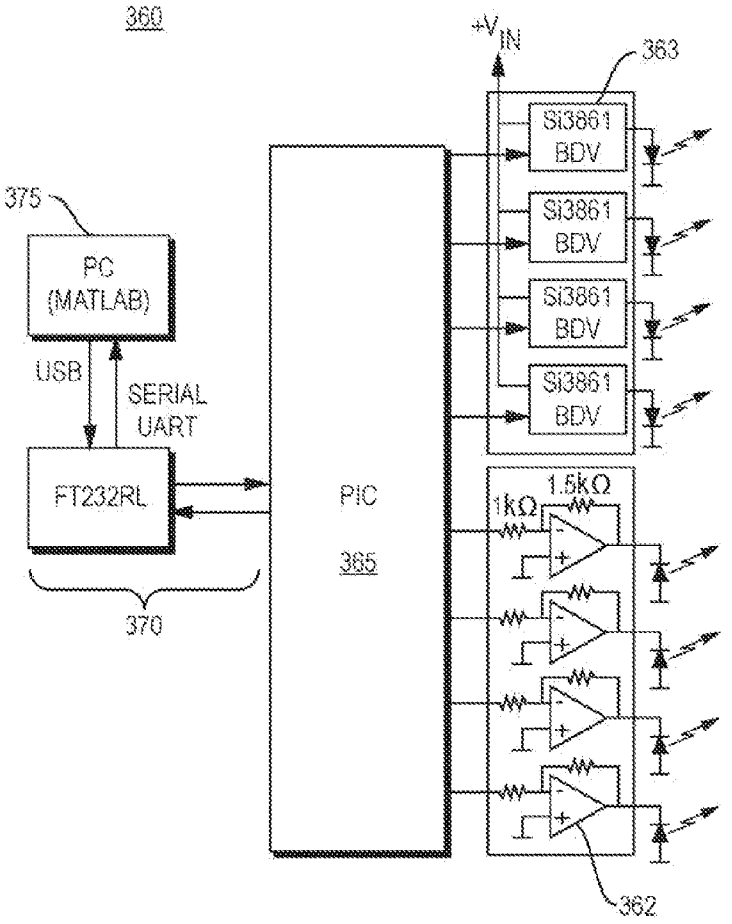
360
+V IN
363
Si3861 BDV
Si3861 BDV
Si3861 BDV
Si3861 BDV
375
PC (MATLAB)
USB
SERIAL UART
FT232RL
370
PIC
365
1.5kΩ
1kΩ
362

FIG. 3C

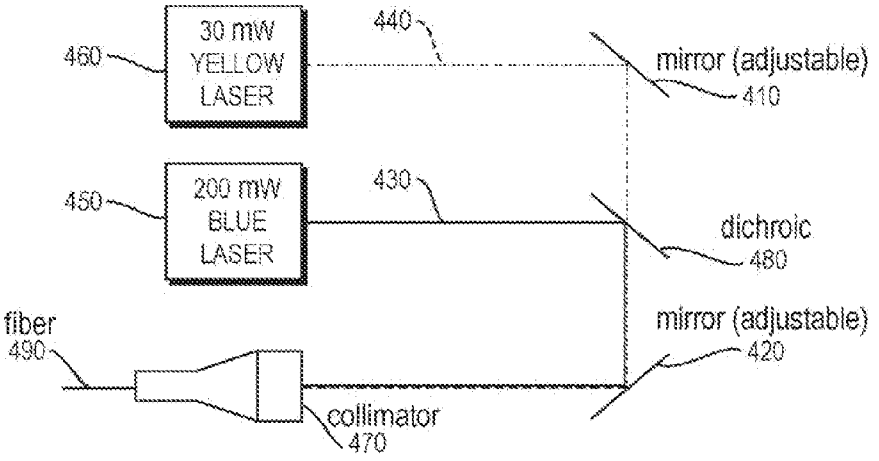
30 mW YELLOW LASER
460
440
mirror (adjustable)
410
200 mW BLUE LASER
450
430
dichroic
480
fiber
490
mirror (adjustable)
420
collimator
470

FIG. 4

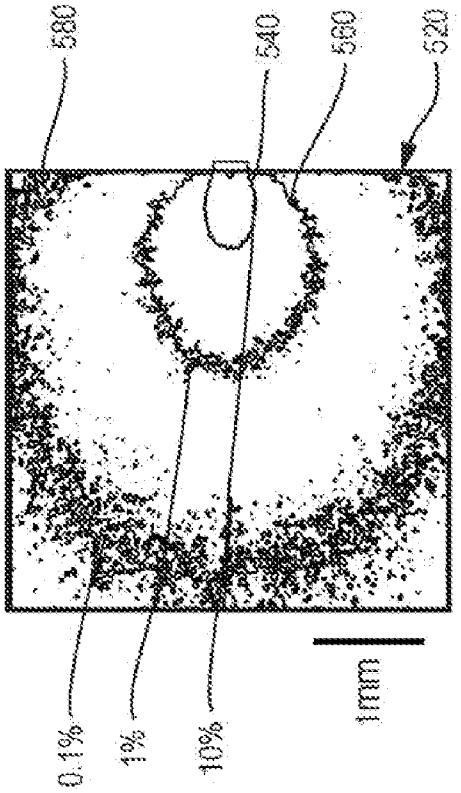

FIG. 5B

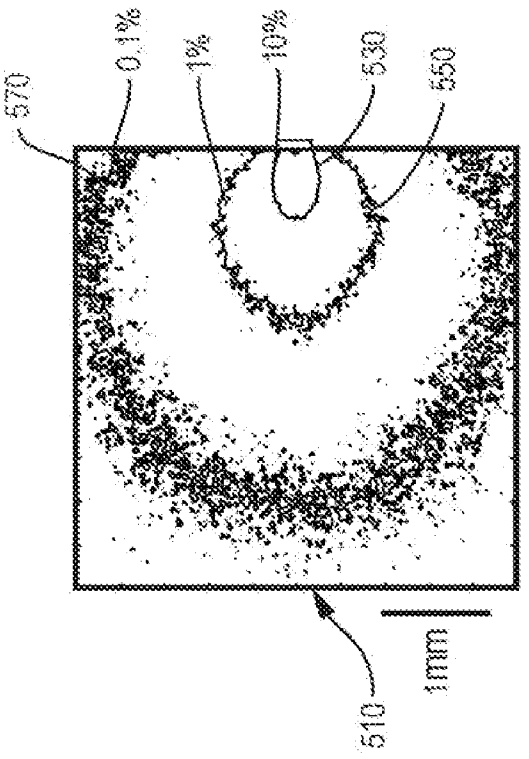

FIG. 5A

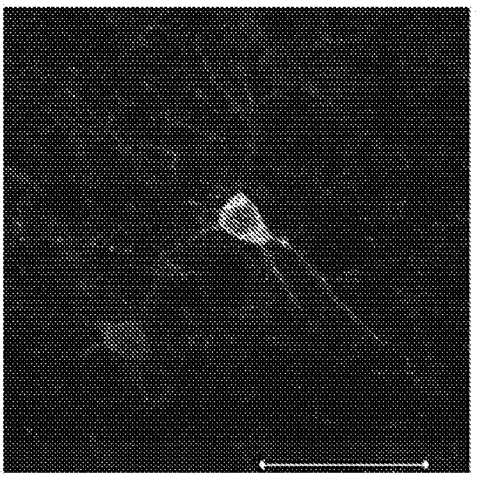

FIG. 6

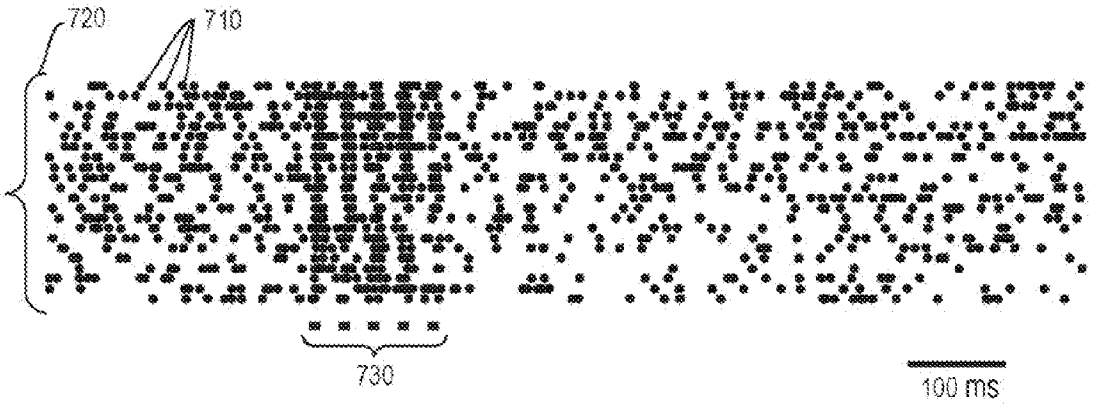

FIG. 7

PROSTHETIC SYSTEM FOR THERAPEUTIC OPTICAL ACTIVATION AND SILENCING OF GENETICALLY-TARGETED NEURONS

RELATED APPLICATIONS

[0001] This application claims the benefit of U.S. Provisional Application Ser. No. 61/021,612, filed Jan. 16, 2008, the entire disclosure of which is herein incorporated by reference.

[0002] This application is also a continuation-in-part of co-pending U.S. patent application Ser. No. 12/118,673, filed May 9, 2008, which claims the benefit of U.S. Provisional Application Ser. No. 60/917,055, filed May 9, 2007, the entire disclosures of which are herein incorporated by reference.

STATEMENT REGARDING FEDERALLY SPONSORED RESEARCH OR DEVELOPMENT

[0003] This invention was made with U.S. government support under Grant Number DP2OD002002, awarded by the National Institutes of Health (NIH). The government has certain rights in this invention.

FIELD OF THE TECHNOLOGY

[0004] The present invention relates to methods and devices for control of cell function and, in particular, to prosthetic devices for optical control of cells.

BACKGROUND

[0005] Many neural disorders are associated with aberrant activity in specific cell types or neural projection pathways embedded within the densely-wired, heterogeneous matter of the brain. Many diseases of the human brain and nervous system are related to the dysfunction of specific neuron types that undergo pathological changes in number, excitability, anatomy, or synaptic connectivity. These changes lead, via altered neural circuit activity, to the perceptual, cognitive, emotional, and motor deficits associated with various neurological and psychiatric illnesses. For example, temporal lobe epilepsy is associated with increased excitability and connectivity of specific excitatory neurons [C. Bernard, A. Anderson, A. Becker et al., *Science* 305 (5683), 532 (2004); E. R. Sanabria, H. Su, and Y. Yaari, *J Physiol* 532 (Pt 1), 205 (2001); L. R. Shao and F. E. Dudek, *J Neurophysiol* 92 (3), 1366 (2004); C. R. Houser, J. E. Miyashiro, B. E. Swartz et al., *J Neurosci* 10 (1), 267 (1990)] and the loss of specific kinds of inhibitory interneurons [P. S. Buckmaster and F. E. Dudek, *J Comp Neurol* 385 (3), 385 (1997)] in the hippocampus, whereas schizophrenia is associated with atrophy of a specific kind of inhibitory neuron in the prefrontal cortex [D. A. Lewis, T. Hashimoto, and D. W. Volk, *Nat Rev Neurosci* 6 (4), 312 (2005)].

[0006] These cell classes, or other cell types within the affected neural circuits, may possibly serve as novel and powerful clinical targets. An ideal therapy would permit correction of activity just in specific target neurons, while leaving other neurons unaltered. By activating and silencing specific cell classes, perhaps even in an adaptive way that depends upon the state of the neural circuit, it may be possible to devise efficacious, side effect-free treatments for a multitude of neurological and psychiatric diseases. For example, a disease in which a specific kind of neuron has become pathologically overexcitable, such as is the case in epilepsy, may be treatable via cell-specific neural silencing, whereas a disease in which a specific neuron has become underactive (as in the case of schizophrenia) may be treatable via cell-specific neural activation. However, until recently, tools precise enough to perform this kind of neural-circuit level activity sculpting have not existed.

[0007] Neurologists and psychiatrists have altered neural activity in the brain via the use of non cell-type specific electromagnetic methods (e.g., deep brain stimulation (DBS) and transcranial magnetic stimulation (TMS)), showing that stimulating a single bulk chunk of neural tissue within the brain can reliably, although often only partially, alleviate symptoms of disorders as diverse as depression [M. S. George, E. M. Wassermann, W. A. Williams et al., *Neuroreport* 6 (14), 1853 (1995); A. Pascual-Leone, B. Rubio, F. Pallardo et al., *Lancet* 348 (9022), 233 (1996); H. S. Mayberg, A. M. Lozano, V. Voon et al., *Neuron* 45 (5), 651 (2005)], epilepsy [D. A. Groves and V. J. Brown, *Neuroscience and biobehavioral reviews* 29 (3), 493 (2005); K. N. Fountas, J. R. Smith, A. M. Murro et al., *Stereotactic and functional neurosurgery* 83 (4), 153 (2005); M. Morrell, *Current opinion in neurology* 19 (2), 164 (2006)], chronic pain [D. Rasche, P. C. Rinaldi, R. F. Young et al., *Neurosurgical focus* 21 (6), E8 (2006); R. R. Tasker and O. Vilela Filho, *Stereotactic and functional neurosurgery* 65 (1-4), 122 (1995)], Parkinson's disease [A. L. Benabid, P. Pollak, A. Louveau et al., *Applied neurophysiology* 50 (1-6), 344 (1987); R. P. Iacono, R. R. Lonser, G. Maeda et al., *Acta neurochirurgica* 137 (1-2), 106 (1995); R. Pahwa, S. Wilkinson, D. Smith et al., *Neurology* 49 (1), 249 (1997); R. Kumar, A. M. Lozano, Y. J. Kim et al., *Neurology* 51 (3), 850 (1998); L. Lopiano, M. Rizzone, B. Bergamasco et al., *Neurology* 56 (4), 552 (2001); A. L. Benabid, P. P. Krack, A. Benazzouz et al., *Neurology* 55 (12 Suppl 6), S40 (2000)], and cluster headache [M. Leone, *Lancet Neurol* 5 (10), 873 (2006)]. These stimulation technologies overcome some of the issues associated with other methods, such as the irreversibility of surgical ablation of brain tissue [W. Penfield and T. Rasmussen, *The Cerebral Cortex of Man: A Clinical Study of Localization of Function*. (Macmillian 1950)] and the widespread side effects associated with many drugs [P. I. Rosebush and M. F. Mazurek, *Neurology* 52 (4), 782 (1999); J. L. Herranz, J. A. Armijo, and R. Arteaga, *Epilepsia* 29 (6), 794 (1988); S. L. McElroy, P. E. Keck, Jr., and L. M. Friedman, *The Journal of clinical psychiatry* 56 Suppl 2, 49 (1995)]. However, systematic principles of how to control aberrant activity in neural circuits have not been described, in part because of the nonspecific nature of electrical and magnetic stimulation. Such fields cannot be focused at a distance due to their fundamental physical properties, and cannot be targeted to specific cell types within a volume of tissue due to the relative nonselectivity of the action of such fields upon neurons.

[0008] The ability to optically activate or inactivate genetically-specified excitable target cells, such as central nervous system neurons, glia, peripheral neurons, skeletal muscle, smooth muscle, cardiac muscle, pancreatic islet cells, thymus cells, immune cells, or other excitable cells, embedded in intact tissue, such as brain, peripheral nervous system, muscle, and skin, would enable radical new treatments for many disorders (e.g., neuropathic pain, Parkinson's disease, epilepsy, diabetes, and other diseases). Ideally, for each disease, which neural cell targets offer the greatest therapeutic potential and what patterns of activity must be imposed in order to optimally correct the pathological state may be identified. In this way, principles of neural control can be identi-

fied that permit optimal resculpting of the aberrant activity in the brain that contributes to illness. It might further be possible to use optical neural control technologies directly as a therapy, sensitizing specific targets in the human brain to light and then activating, silencing, or reshaping their activities as required.

[0009] Molecular genetic methods for making cells, such as neurons, sensitive to being activated (e.g., depolarized) or inactivated (e.g., hyperpolarized) by light have been previously developed. For example, in X. Han and E. S. Boyden, "Multiple-color optical activation, silencing, and desynchronization of neural activity, with single-spike temporal resolution," *PLoS ONE* 2, e299 (2007) and E. S. Boyden, F. Zhang, E. Bamberg et al., *Nat Neurosci* 8 (9), 1263 (2005), tools are described that permits specific genetically-defined excitable cells, such as neurons of different classes, to be activated and silenced with different colors of light. These tools center around a set of naturally-occurring membrane proteins that, when exposed to light of the appropriate wavelength, move ions from one side of the plasma membrane to the other. The naturally-occurring light-activated proteins channelrhodopsin-2 (ChR2) and halorhodopsin (Halo NpHR) can, when genetically expressed in neurons, enable them to be safely, precisely, and reversibly activated and silenced by pulses of blue and yellow light, respectively. FIGS. **1**A-G show that the light-activated cation channel channelrhodopsin-2 (abbreviated ChR2, from the green algae *C. reinhardtii*), when expressed in neurons, makes neurons optically activatable by millisecond-timescale pulses of blue light (FIGS. **1**A, **1**B); the light-activated chloride pump halorhodopsin (abbreviated Halo or NpHR, from the archaebacterium *N. pharaonis*) similarly makes neurons electrically silenceable by pulses of yellow light (FIGS. **1**C, **1**D); and together these molecular tools, when expressed in an appropriate ratio, can enable bi-directional control of neural activity by pulses of blue and yellow light (FIGS. **1**E-G), enabling spike-level neural activity control. These molecules can be targeted to neurons by any of the means available to modern biotechnology, including the use of viruses or transgenic methods.

[0010] As shown in FIGS. **1**A-G, neuron-expressing channelrhodopsin-2 is fused to mCherry (FIG. **1**A; bar, 20 μm) and halorhodopsin is fused to GFP (FIG. **1**C). The overlay is shown in FIG. **1**E. In FIG. **1**B, Poisson trains of spikes **105**, **110** are elicited by pulses of blue light **115**, **120** in two different neurons. In FIG. **1**D, light-driven spike blockade **130** is depicted for a representative hippocampal neuron, and another light-driven spike blockade **135** is shown for a population of neurons (n=7). Neuronal firing was induced by pulsed somatic current injection (300 pA, 4 ms). Hyperpolarization was induced by periods of yellow light **140**. As seen for spike blockade **135**, yellow light **140** drives Halo to block neuron spiking, leaving spikes elicited during periods of darkness intact. In FIG. **1**F, action spectrum **150** for ChR2 overlaid with absorption spectrum **155** for *N. pharaonis halorhodopsin*. FIG. **1**G depicts hyperpolarization and depolarization events **160** induced in a representative neuron by a Poisson train of alternating pulses (10 ms) of yellow **170** and blue **175** light.

[0011] While these molecular genetic methods make cells, such as neurons, sensitive to being activated or inactivated by light, methods are for delivering light to precise locations in intact tissues are still required. In co-pending U.S. patent application Ser. No. 12/118,673, published as U.S. Pat. App. Pub. No. 2008/0306576, several first-generation devices are described for accomplishing this, including sets of light sources (e.g., LEDs, lasers) coupled to optical fibers whose ends deliver light to specified groups of target cells within tissue, sets of light sources in hypodermic cannulas that can deliver light locally to specified groups of target cells within tissue, and sets of light sources attached to nerve cuff holding devices that stably bring the light sources into close proximity to a group of target nerve cells. In conjunction with the sets of light sources, control and power electronics enable battery-powered, wearable, fully implantable, wirelessly-operated, and/or remotely-powered versions of the electronics to drive the light sources, thus enabling the use of the devices as prosthetics. While simple and flexible, the laser setup of this approach can be expensive, bulky, and consume a lot of power. Furthermore, since it requires optical fibers to be inserted into the brain that are simultaneously connected to a heavy, fixed laser, use of such a system constrains the movement of animals and increases the risk of tangling or breakage of optical fibers. These problems worsen if insertion of multiple fibers is desired. In addition, optical fibers emit light only at their end, meaning that an optical fiber damages a significant volume of brain tissue, compared to the amount of brain tissue that is illuminated.

SUMMARY

[0012] The present invention is an optical prosthesis that can be used to directly remedy aberrant activity in corrupted human brain circuits by controlling neural circuits. It is a scalable, fully-implantable optical prosthetic capable of delivering light of appropriate intensity and wavelength to targeted neurons at arbitrary 3-D locations within the brain, enabling activation and silencing of specific neuron types at multiple locations. The device can be implanted in the brains of animals in order to reveal principles of neural control, and also serves as a prototype for optical prosthetics that may be practical for human use.

[0013] In one aspect, the present invention comprises a set of light sources with optional accessory hardware for guiding light, supporting hardware to hold members of the set of light sources with respect to each other, with respect to the target cells, and perhaps with respect to external structures, and control and drive electronics that provide regulated power to the light sources, communicate data, stimulation protocols, and algorithms to and from the outside world, and optionally monitor target cell state.

[0014] In one embodiment, the present invention is a prosthetic device for optical control of target cells, comprising a probe having a set of light sources, drive circuit connections connected to each light source, a housing surrounding the light sources and the drive circuit connections, and drive circuitry for driving and controlling the probe. The drive circuit connections and drive circuitry may optionally provide for wireless communication. The light sources may be light-emitting diodes, lasers, or any other suitable source known in the art. The housing may be a glass capillary tube. The prosthetic device may optionally include sensors for monitoring the target cells.

[0015] In another embodiment, the present invention is a prosthetic device for optical control of target cells, comprising an array of probes, each probe having a set of light sources, drive circuit connections connected to each light source, a housing surrounding the light sources and the drive circuit connections, drive circuitry for driving and controlling

the probes, and supporting hardware that holds the probes in position with respect to each other and the target cells. The array of probes may be two- or three-dimensional.

BRIEF DESCRIPTION OF THE DRAWINGS

[0016] Other aspects, advantages and novel features of the invention will become more apparent from the following detailed description of the invention when considered in conjunction with the accompanying drawings wherein:

[0017] FIG. **1**A is a photograph depicting neurons optically activated through the light-activated cation channel channelrhodopsin-2 by millisecond-timescale pulses of blue light;

[0018] FIG. **1**B depicts Poisson trains of spikes elicited by pulses of blue light in two different neurons;

[0019] FIG. **1**C is a photograph depicting neurons electrically silenced through light-activated chloride pump halorhodopsin by pulses of yellow light;

[0020] FIG. **1**D depicts light-driven spike blockades for a representative hippocampal neuron and for a population of neurons, with hyperpolarization induced by periods of yellow light;

[0021] FIG. **1**E is a photograph depicting bi-directional control of neural activity by pulses of blue and yellow light, enabling spike-level neural activity control;

[0022] FIG. **1**F is a graph depicting an action spectrum for channelrhodopsin-2 overlaid with an absorption spectrum for *N. pharaonis* halorhodopsin;

[0023] FIG. **1**G is depicts hyperpolarization and depolarization events induced in a representative neuron by a Poisson train of alternating pulses of yellow and blue light;

[0024] FIG. **2** is an exemplary embodiment of a 3D LED array for enabling activation and silencing of activity in targeted brain regions, according to one aspect of the present invention;

[0025] FIG. **3**A is an expanded view of an exemplary embodiment of a 1-D probe useful in constructing a 3D array, according to one aspect of the present invention;

[0026] FIG. **3**B a photograph of a prototype implementation of the ID probe of FIG. **3**A, according to one aspect of the present invention;

[0027] FIG. **3**C is an exemplary embodiment of an LED driver circuit useful with a 3D array, according to one aspect of the present invention;

[0028] FIG. **4** is schematic of an exemplary setup for focusing blue and yellow light down a fiber to be implanted inside the head, for bi-directional control of a single kind of neuron at a single site within the brain, according to one aspect of the present invention;

[0029] FIGS. **5**A and **5**B are Monte Carlo simulations of how blue and yellow photons, respectively, travel through the brain from LEDs, according to one aspect of the present invention;

[0030] FIG. **6** is a photograph of neurons in the mouse brain expressing Halo-GFP under the CaMKII promoter, which preferentially labels excitatory neurons; and

[0031] FIG. **7** is an experimentally-produced raster plot indicating occurrences of spikes elicited from an excitatory neuron expressing ChR2 in a monkey cortex in response to a brief train of blue light stimulation.

DETAILED DESCRIPTION

[0032] The present invention comprises several parts: a set of light sources (such as, but not limited to, LEDs or lasers) with optional accessory hardware for guiding light, supporting hardware to hold members of the set of light sources with respect to each other, with respect to the target cells such as, but not limited to, brain, glia, peripheral nerve, skeletal muscle, smooth muscle, cardiac muscle, pancreatic islet cells, thymus cells, or other excitable cells, embedded in the tissue (such as, but not limited to, brain, peripheral nervous system, muscle, skin, pancreas, and heart), and perhaps held firm with respect to external structures (such as, but not limited to, skull, skeleton, muscle, or skin), and control and drive electronics that monitor target cell state, provide regulated power to the light sources, communicate data, stimulation protocols, and algorithms to and from the outside world, and/or may be remotely powered by external electromagnetic fields or other kinds of wireless energy. A set of light sources is needed because, since tissues are highly scattering, in many cases no one light source will be able to illuminate all the target cells in the entire desired target area. Each individual light source must receive electrical power and deliver light locally to its target cells.

[0033] In a preferred embodiment, a 3-D array of LEDs capable of targeting arbitrary brain structures enables activation, silencing, and the resculpting of activity throughout multiple brain regions. This 3D array provides a probe that is inexpensive, compact, power-efficient, self-contained, and capable of exerting optical control over a large region of brain tissue while causing a minimum of brain damage. The present invention employs such 3-D arrays of compact, inexpensive, long-lasting, and bright light-emitting diodes (LEDs), capable of targeting arbitrary brain regions for activation or silencing. Unlike an optical fiber, which can only deliver light to a single point in the brain per penetrating device, a linear array of LEDs inserted into the brain can deliver light to points in the brain up and down the probe. In the preferred embodiment, the device is compact (human DBS electrodes are <1.5 mm wide), is capable of delivering bright light into deep brain structures, and does not heat the brain beyond an acceptable limit (typically, 1° C.). One efficient way to implement a 3-D array of LEDs is to create a 2-D array of 1-D probes.

[0034] FIG. **2** is an exemplary embodiment of a device that enables 3-D arrays of yellow and blue LEDs to activate, silence, and resculpt neural activity in arbitrary 3-D patterns. As shown in FIG. **2**, device **200** is a 2-D array **210** of 1-D LED-bearing probes **220**, each of which has alternating blue **230** and yellow **240** LEDs going down its length. The 1-D probes **220** are placed in glass capillaries **250** to prevent brain heating. The capillaries are then arranged into 2-D array **220** by placing them in form-fitting holes **260** within plastic plate **270**. Each 1-D probe projects vertically down into the brain. Glass capillary **250** electrically and thermally isolates the LEDs from the brain; the heat is instead wicked up the 1-D probe to cool the LEDs. The 2-D array **210** is assembled by placing multiple glass capillaries **250** containing 1-D probes **210** into cylindrical holes **260** in plastic plate **270** and then sealing capillaries **250** to plate **270** using epoxy. Such an array of probes then enables optical control of arbitrary 3-D sets of neurons distributed in multiple regions.

[0035] Arranging 1-D probes into a 2-D array is not difficult: almost any plate with appropriate holes will do to organize the 1-D probes into an array. The 1-D probe itself, though, must fit all of the required components into a small enough glass capillary to avoid causing much damage upon insertion into the brain. FIG. **3**A depicts an expanded view of

an exemplary embodiment of a 1-D probe that is suitable for this purpose and can act as the fundamental building block of the 3-D probe of FIG. **2**. In FIG. **3**A, blue **305** and yellow **310** LEDs are soldered to ground plane **315**. Ground plane **315** attaches, via epoxy layer **320**, to underlying base sheet **325**. Base sheet **25** has control traces **330** for delivering power to each LED **305**, **310** independently via wire bonding **333**. Control wires **335** attach each LED control trace **330** to the control circuitry.

[0036] In a prototype implementation of the probe of FIG. **3**A, 460 nm blue and 590 nm yellow LEDs, 300 microns on a side, were soldered to a 25-micron thick sheet of silver trimmed to be 650 microns wide. The silver sheet acts as the ground plane for the LEDs, and attaches, via a layer of insulating epoxy, to an underlying 25-micron thick aluminum sheet. The aluminum sheet is patterned, using an ultraviolet excimer laser, to have separate control traces for delivering power to each LED independently. Each LED is attached to a unique control trace on the aluminum sheet, via wire bonding.

[0037] The entire device is then placed into a thin (<1 mm diameter) glass capillary tube. The ends of the glass capillary are sealed with a biocompatible epoxy, thus sealing in an insulting layer of air between the LED probe and its glass capillary housing. These glass capillaries can then be inserted into holes in a plastic square, resulting in a 2-D array of the 1-D probes. FIG. **3**B is a photograph of this prototype implementation. Shown in FIG. **3**B, are whole 1-D LED probe **340**, a magnified view of LED part **345** of the probe, a magnified view of the LED part of the probe with one blue LED **350** on, and a magnified view of the LED part of the probe with one yellow LED **355** on.

[0038] Control traces **330** connect to cable **335** that leads out of the glass capillary, to an multi-channel LED driver circuit, for optimally driving the yellow and blue LEDs. FIG. **3**C depicts an exemplary embodiment of LED driver circuit **360** according to this aspect of the present invention. The LED driver circuit **360** comprises typical drive electronics known in the art, such as op-amps **362** and load drivers **363**, and is controlled via PIC microcontroller **365**. PIC microcontroller **365** talks over USB port **370** to PC **375** running MATLAB or other suitable software known in the art, thus allowing pulse sequences to be uploaded to PIC **365** in real time without necessitating complete reprogramming of the chip.

[0039] In a prototype implementation, the fiber arrays were implemented using individual lasers or LEDs, but arrays of vertical cavity surface emitting lasers (VCSELs) or other optical sources may work just as well. If in the future xenon bulbs, halogen lamps, incandescent bulbs, or other light sources become miniaturized enough to fit in, they would also be suitable for use with the present invention (with filters on the bulbs). A particularly appealing way to modulated LED power with a simple circuit is to pulse width modulate (PWM) the LED. A particularly simple wireless method is just to attach an LED to an inductor, which will then be remotely powerable.

[0040] In the description and implementation of the present invention, it will be understood by one of ordinary skill in the art that each of the variations on the component parts of the invention are swappable with any of the other variations. Similarly, when a use of the present invention is described with respect to a particular tissue or body part, it will be understood by one of ordinary skill in the art that the invention can be used in a similar manner for other body parts and tissues. For example, if a use is described is for the "brain," then it may similarly used in any other bodily tissue (e.g., peripheral nerve, pancreas, etc.). As another example, if it is described how to affix something to the skin, it may similarly be used in dealing with muscle and other tissues as well. The terms light source or LED are also used interchangeably, as they all have similar functionality in the context of the present invention. The light produced by the source may be visible light, infrared, spectrally complex, or any other type of light found to be suitable for the particular application. Further, while the use of wireless communications is described herein chiefly in the language of RF transceiving, it will be clear to one of skill in the art that any kind of wireless communication, such as, but not limited to, ultrasound or light may also be advantageously used in the present invention.

[0041] Although for central nervous system applications, the 1-D LED probe shown in FIG. **3**A is utilized as part of a larger 3-D system, such as the embodiment depicted in FIG. **2**, the device shown in FIG. **3**A represents in itself an extraordinarily flexible building block for getting light into the nervous system effectively, safely, and inexpensively. In this embodiment, LEDs are simply placed on thin sheets of metal (which can be curved if desired), and the 1-D probes can be made as long or as short as desired, using the rapid-prototyping tools here described. Accordingly, optical cochlear prostheses, vestibular prostheses, and peripheral nerve prostheses may be rapidly deployed using the device of FIGS. **2** and **3**A-C. Although the above optical probe is as small or smaller than comparable human devices (e.g., DBS electrodes), even smaller versions capable of controlling neurons in animals as small as a juvenile mouse may be constructed.

[0042] In a preferred implementation, an optional dichroic, beamsplitter, or other equivalent optical part known in the art may be attached to a fiber to couple two different light sources (such as, but not limited to, a blue LED and a yellow LED, or a blue laser and a yellow laser) into the fiber, so that the target cells at the end of the fiber can be more easily activated and deactivated by two different colors of light. This may further be generalized to a series of cascaded dichroics, capable of coupling more than two colors of light into the same fiber.

[0043] In order to develop a reliable testbed for activation and silencing of genetically-sensitized neurons with blue and yellow light, a prototype system capable of coupling two strong lasers into a single optical fiber was constructed. Two diode-pumped solid state (DPSS) lasers, a yellow (593 nm) 30 mW laser and a blue (473 nm) 200 mW laser (Aixiz Int'l.) were employed. These lasers can be activated for milliseconds at a time when triggered by TTL pulses. FIG. **4** is schematic of an exemplary setup for focusing blue and yellow light down a fiber to be implanted inside the head, for bi-directional control of a single kind of neuron at a single site within the brain, according to one aspect of the present invention.

[0044] As shown in FIG. **4**, two mirrors **410**, **420** on adjustable gimbals steered beams **430**, **440** from blue **450** and yellow **460** lasers into fiber collimator **470** (Thorlabs F810SMA), with the assistance of dichroic element **480** (Chroma) that reflects blue light and passes yellow light, thus bringing the two laser beams into collinearity. SMA-terminated multimode fiber **490**, 200 microns in diameter and capable of passing light throughout the visible range, was inserted into collimeter **470**. The free end of fiber **490**, highly polished, could then be inserted into the brain of an experimental animal. In the prototype embodiment, the power coming out of the fiber approached 800 mW/mm^2 in the blue,

sufficient to stimulate ChR2, and 110 mW/mm^2 in the yellow, sufficient to stimulate Halo. In a mouse, a thin polyimide tube trimmed to the correct length, and inserted into the brain to stereotactically target the brain region of interest, serves easily as a guide cannula for inserting the fiber; gluing a thin washer onto the fiber helped prevent insertion of the fiber into the brain beyond the desired point.

[0045] In one embodiment, an optional steerable element, such as, but not limited to, a galvanometer, an acousto-optic deflector, a MEMS mirror, or other steering device is employed on one or both ends of the fiber, to direct light in a controlled way, thus enabling locally selective targeting of the light to specific areas of the tissue, preferably with as few moving parts as possible.

[0046] To activate channelrhodopsin-2 and halorhodopsin molecules in mammalian neurons requires light of the appropriate color at a radiant flux of 10 mW/mm^2 or greater, for maximal activation [E. S. Boyden, F. Zhang, E. Bamberg et al., *Nat Neurosci* 8 (9), 1263 (2005); X. Han and E. S. Boyden, *PLoS ONE* 2, e299 (2007); H. Wang, J. Peca, M. Matsuzaki et al., *Proc Natl Acad Sci USA* 104(19), 8143 (2007)]. A radiant flux of 1 mW/mm^2 will activate approximately 50% of the molecules, and a radiant flux of 0.1 mW/mm^2 will activate very few of the molecules [E. S. Boyden, F. Zhang, E. Bamberg et al., *Nat Neurosci* 8 (9), 1263 (2005); X. Han and E. S. Boyden, PLoS ONE 2, e299 (2007); H. Wang, J. Peca, M. Matsuzaki et al., *Proc Natl Acad Sci USA* 104 (19), 8143 (2007)]. Since light is absorbed and scattered as it passes through tissue, this means that relatively bright light sources are needed to activate neurons embedded in tissue; furthermore, it implies that for any given light source, there will be heterogeneity in the power that reaches neurons at various distances from the light source.

[0047] Simulation of LED light penetration into the brain. The efficacy of optical activation varies across 3 log units of power, from almost no stimulation at 0.1 mW/mm^2, to near-maximal stimulation at 10 mW/mm^2. Accordingly, a computational model was implemented that permitted rapidly estimating the power at various distances from blue and yellow LEDs embedded in the brain, aiming for an accuracy level better than a fraction of a log unit. Initially, Monte Carlo simulations of how light emitted from blue and yellow LEDs would be absorbed or scattered in the brain were modeled using 300 μm×300 μm blue (460 nm) and yellow (590 nm) LEDs, placed on the surface of a cube of brain gray matter 4 millimeters on a side. The Monte Carlo simulation was performed by dividing the cube of gray matter into a 200×200×200 grid of voxels, each 20 μm×20 μm×20 μm in dimension. A subset of the models were also tested with 10 μm×10 μm×10 μm voxels, producing identical results and proving that the model resolution was sufficient. Optical modeling and data analysis were done on a PC using MATLAB, and plotted in MATLAB or Excel.

[0048] Data was interpolated data from A. N. Yaroslavsky, P. C. Schulze, I. V. Yaroslavsky et al., *Physics in medicine and biology* 47 (12), 2059 (2002) to obtain scattering coefficients for brain gray matter of 10 mm^{-1} for blue light and 9 mm^{-1} for yellow light, and to obtain absorption coefficients of 0.07 mm^{1} for blue light and 0.027 mm^{-1} for yellow light. Since light propagation close to the LED was the factor of interest, before the orientation of photon trajectories is randomized by multiple scattering events, an anisotropic scattering model based upon the Henyey-Greenstein phase function was used, utilizing anisotropy parameters of 0.88 for blue light and 0.89 for yellow light [A. N. Yaroslavsky, P. C. Schulze, I. V. Yaroslavsky et al., *Physics in medicine and biology* 47 (12), 2059 (2002); T. Binzoni, T. S. Leung, A. H. Gandjbakhche et al., *Physics in medicine and biology* 51 (17), N313 (2006)]. 10^6 packets of photons were launched in a Lambertian radiation pattern from random points on the luminous surface of the LED, and their propagation was modeled based on the algorithm of A. N. Yaroslavsky, P. C. Schulze, I. V. Yaroslavsky et al., *Physics in medicine and biology* 47 (12), 2059 (2002). In essence, whenever a photon packet entered a voxel, the program probabilistically calculated the forecasted traveling distance before the next scattering event. If that traveling distance took the photon packet out of the starting voxel, then the packet was attenuated appropriately for the distance it traveled within the starting voxel, and the process would then restart upon entry of the photon packet into the new voxel. If that traveling distance ended the trip of the photon packet within the starting voxel, then the packet was attenuated appropriately for the distance it traveled within the starting voxel, and a new direction of packet propagation was randomly chosen according to the Henyey-Greenstein function.

[0049] Using this model, FIGS. **5**A and **5**B, which are Monte Carlo simulations of how blue (FIG. **5**A) and yellow (FIG. **5**B) photons travel through the brain from LEDs, were generated, depicting the contours at which the light intensity falls off to 10%, 1%, and 0.1% of the intensity of light at the surface of the LED. In FIGS. **5**A and B, squares **510**, **520** representing 4 mm×4 mm cross-sections taken through the 4 mm×4 mm×4 mm cube are simulated; the cross-sections are taken by slicing the cube through the LED center. Contours represent cross-sections of the surfaces at which the radiant flux drops to 10% 530, 540, 1% 550, 560, and 0.1% 570, 580 of their values on the LED surface.

[0050] To implement the model results, the 280 μm×280 μm blue (460 nm) C460EZ290-S2400 LED from Cree [Cree, CPR3CQ.pdf, (2007)] and the 305 μm×305 μm yellow (590 nm) HWFR-B317 LED from Lumileds [Lumileds, DS42.PDF (2007)], were employed. The blue LED has a 1% contour envelope that resembles an ellipse 1.6 mm long and 1.4 mm wide; at a peak power of 24 mW, the 1% contour equates to ~3 mW/mm^2 radiant flux—an intensity easily sufficient to activate ChR2. Similarly, for the yellow LED, the 1% contour envelope resembles an ellipse 1.7 mm long and 1.5 mm wide, which at its peak power of 86 mW equates to a radiant flux of ~15 mW/mm^2 for yellow light, an intensity sufficient to activate the majority of Halo molecules. Of course, to illuminate smaller volumes, the light power can always be decreased. Thus, the model indicates that standard 300-micron LEDs should be able to illuminate brain volumes across a broad scale, all the way from cubic microns to several cubic millimeters.

[0051] The computational model is designed to estimate the power at various distances away from the LED, with accuracy significantly better than a log unit. The quality of the model was assessed experimentally by taking pictures, on a CCD camera, of the blue and yellow LEDs running at 100 microwatts power, through cortical slices of increasing thickness (150, 350, and 550 microns). Experimental measurements were made of the diameter of the contour circle at which the light intensity falls off to 10% of the intensity of light at the surface of the LED. The ratio of this diameter to the diameter of the contour computed via the Monte Carlo model, in a plane a comparable distance away from the LED and parallel to the LED front surface, came out to 0.74±0.33

(mean±standard deviation; n=4 LED-slice thickness combinations), indicating that the model is accurate to the specifications desired. This comparison was repeated for the 1% contours and the ratio was found to be 0.73±0.06 (n=5 LED-slice thickness combinations). There was a trend for the images to be somewhat dimmer than the model would predict. It is possible that vast uncertainty in tissue parameters, which is a subject of ongoing debate in the literature [A. N. Yaroslavsky, P. C. Schulze, I. V. Yaroslavsky et al., *Physics in medicine and biology* 47 (12), 2059 (2002)], underlies some of this variability. In addition, natural brain heterogeneity may also explain the small differences between the experimentally-obtained data and the simulation model (which assumes purely one kind of gray matter).

[0052] The present invention has been prototyped and experimentally verified using several testing methodologies. The ability to make specific neurons in the brain light-sensitive, using a viral approach and control of neural activity in the cortex of the non-human primate, a key step in the translation of such technology for human clinical use, were demonstrated. In these tests, one experiment assessed intact tissue expression in mouse. Mammalian codon-optimized forms of channelrhodopsn-2 and halorhodopsin, abbreviated as hChR2 and Halo, have been previously developed [X. Han and E. S. Boyden, *PLoS ONE* 2, e299 (2007)]. These genes were inserted into a lentiviral vector that allows cloning in different promoters, or DNA regulatory elements, upstream of the gene of interest. For example, the CaMKII promoter targets predominantly excitatory neurons. FIG. **6** is a photograph of neurons in the mouse brain expressing Halo-GFP under the CaMKII promoter, which preferentially labels excitatory neurons [T. Dittgen, A. Nimmerjahn, S. Komai et al., *Proc Natl Acad Sci USA* 101 (52), 18206 (2004)]. In FIG. **6**, the Scalebar represents 50 μm. A pipeline was developed for obtaining promoters by cloning them out of bacterial artificial chromosomes (BACs) and then inserting them into lentiviral plasmids upstream of hChR2 or Halo. Small virus test batches are then created, and promoter strength and selectivity in the mouse brain are subsequently rapidly screened. By screening promoters in a wholesale fashion, it is possible to identify and validate new candidate promoters for targeting specific cell types.

[0053] For this experiment, replication incompetent lentiviruses were produced via triple transfection of plasmids containing the promoter and gene of interest (e.g., F(CK)-Halo-GFP or F(CK)-ChR2-GFP), the viral helper plasmid (pΔ8.91), and the pseudotyping plasmid (pMD2.G, encoding the coat protein VSV-G). Briefly, HEK293FT cells (Invitrogen) were plated onto four T175 flasks in D10 medium (comprising DMEM+10% FBS+1% pen-strep, 1% sodium pyruvate, and 1% sodium bicarbonate). At 100% confluence, cells were transfected with DNA using Fugene: 22 micrograms of plasmids containing the promoter and gene of interest, 15 micrograms of pΔ8.91, and 5 micrograms of pMD2.G, were mixed with 132 microliters of Fugene 6 and 4.5 mL of MEM, prepared according to the instructions of the manufacturers of Fugene. 24 hours later, the cells were washed with D10 and then given 30 mL of virus production media (comprising Opti-MEM w/GlutaMAX-I+1% pen-strep, 1% sodium pyruvate, and 1% sodium bicarbonate). 48 hours later, the supernatant was harvested, filtered through a 0.45 micron filter flask (pre-wetted with D10), and then the filtrate was ultracentrifuged over a 20% sucrose cushion at 22000 rpm in a SW-28 rotor for 2 hours at 4° C. The pellet was then resuspended in 30 microliters of PBS over a period of several hours, and aliquoted the virus for storage at −80° C.

[0054] Viruses were tested for efficacy in sensitizing specific neuron types to being activated/silenced by light by being injected into the cerebral cortex of mice. Mice were anesthetized with 1.25-2% isoflurane and placed into a custom stereotax. A dental drill was used to make a small craniotomy, through which 1-2 microliters of virus was injected into the cerebral cortex of the mouse brain. The virus was injected through a pulled borosilicate glass pipette (tip ~5 microns wide; shank ~4 mm long), pulled with a Sutter P-97 puller. This glass pipette was connected to a Hamilton syringe (placed in a syringe pump, from Harvard Apparatus) via a thin plastic tube filled with silicone oil. Virus infusion was carried out by actuating the Harvard Apparatus pump to inject slowly (e.g., 0.1 microliters per minute) over a period of 20 minutes. After the viral payload was delivered, 10-20 minutes was allowed to pass in order for the virus to diffuse away from the site of injection before withdrawing the pipette at a slow rate (e.g., 2 mm/min). The scalp of the mouse was then sealed with Vetbond, and the animal administered buprenorphine and returned to its home cage.

[0055] One to four weeks after virus injection, acute slices of brain tissue were cut in order to assess the targeted cells for strength and specificity of gene expression, as described in J. Bischofberger, D. Engel, L. Li et al., *Nature protocols* 1 (4), 2075 (2006). Briefly, mice were anesthetized with isoflurane and decapitated, and the brains were removed to ice cold cutting solution (87 mM NaCl, 25 mM $NaHCO_3$, 25 mM glucose, 75 mM sucrose, 2.5 mM KCl, 1.25 mM NaH_2PO_4, 0.5 mM $CaCl_2$ and 7 mM $MgCl_2$, bubbled with 95% O_2/5% CO_2). Time between death and completion of brain removal was less than 1 minute. Brains were then blocked and glued to a dish for cutting with a vibrating tissue slicer (Leica VT1000S) into sections 240 microns thick. Slices were incubated at 35° C. for 30 minutes, then stored at room temperature. Slices were acutely examined in physiological saline (125 mM NaCl 25 mM $NaHCO_3$, 25 mM glucose, 2.5 mM KCl, 1.25 mM NaH_2PO_4, 2 mM $CaCl_2$, and 1 mM $MgCl_2$). At this time, cells were examined electrophysiologically through whole-cell patch clamp (access resistance, 4-8 megaohms), conducted with a Molecular Devices Multiclamp 700B setup.

[0056] In a second test, optically-elicited spike trains were obtained from a primate cortex. In order to translate the precise optical neural control technology of the present invention to humans, the feasibility and safety must be tested in non-human primates, whose brains and other bodily systems more closely resemble humans than do those of rodents. Accordingly, both for safety and efficacy testing, and for animal model development, the primate may represent a natural preclinical testbed for optical neural control technologies.

[0057] The basic methods employed in the test were as described in T. Womelsdorf, P. Fries, P. P. Mitra et al., *Nature* 439 (7077), 733 (2006). Briefly, a craniotomy and plastic chamber implantation was performed over the frontal eye field (FEF) region of the cortex of a rhesus macaque that had been prepared with a headpost, and trained to fixate upon a point. Recordings were made with tungsten microelectrodes (1-2 megaohm impedance) that were slowly advanced through cortical tissue until single units were isolated, acquiring data via a Multichannel Acquisition Processor from Plexon, Inc. Spike recordings were filtered, and spikes isolated using an interactively-set threshold. To facilitate precise

and repeatable optical stimulation and recording, a recording chamber insert with a grid of evenly-spaced holes was designed and fabricated, in order to facilitate optimal placement of electrodes and optical fibers.

[0058] As a test case, a male rhesus macaque was prepared for cortical recording in the frontal eye field (FEF) area of cortex, as predicted by MRI scans and validated with electrophysiology. Surgically injection of 1-4 μL of virus expressing ChR2-GFP under the CaMKII promoter into a site within FEF was undertaken, using the equipment described previously. After a 2-week waiting period for the virus to express, and a polished, 200 micron-thick optical fiber whose other end was fiber-coupled to a 200 mW blue (473 nm) laser was inserted. After optimizing the recording, the laser was activated to fire brief pulses of blue light by delivering 10 ms-long TTL pulses separated by 20 ms pauses (i.e., 33.3 Hz stimulation), and elicited trains of well-timed spikes.

[0059] FIG. **7** is a raster plot showing the experimentally-obtained occurrences of spikes elicited from an excitatory neuron expressing ChR2 in a monkey cortex in response to a brief train of blue light stimulation. As shown in FIG. **7**, spikes (black dots) **710**, in 22 consecutive spike trains (each row of black dots) **720** were elicited in response to blue light stimulation. Each horizontal row **720** reflects one recording of the response to five blue pulses **730** of light, each lasting 10 ms and separated from the next by 20 ms (i.e., 33.3 Hz stimulation rate). This result demonstrates, for the first time, that both the genetic targeting of neurons, and the use of light to activate them, can work successfully in the macaque cortex, a key translational milestone along the road to human use of the present invention.

[0060] The present invention is advantageously employed for the purpose of activating or silencing circuits in a targeted way. The device is capable of activating and silencing neurons at the scale of microns to millimeters, and is inexpensive, reliable, and easy to use. Effective viral targeting of excitatory neurons in the intact brain has been demonstrated using the present invention. The experimental results have demonstrated for the first time that optical neural control technologies are capable of working in the intact primate brain, a major milestone in the quest to enable novel human therapies. The present invention may be advantageously used to understand how to control neural circuits to compensate for the loss or alteration of specific cell types, as often occur in neurological and psychiatric diseases ranging from obesity, to pain, to Parkinson's, to epilepsy. Neural control technologies such as DBS and TMS are increasing in popularity for the treatment of a great number of diseases, but because their mechanisms of therapeutic action are poorly understood, few generalized strategies or principles have emerged governing the design of treatments that use these technologies. By explicitly seeking out neural targets and activity patterns that enable control of neural circuits, a better understanding may be obtained of the principles governing the correction of deficits at the neural-circuit level.

[0061] While the present invention is applied herein to use light to excite and inhibit electrically excitable cells; it will be clear to one of skill in the art that it may be adapted to deliver light to other realms, such as, but not limited to, to drive the production of cAMP in deep tissue, to simulate the action of a G-protein coupled receptor acting drug, or to change the pH of a cell. There are many therapeutic reasons to desire these abilities. The present invention may be advantageously adapted to enable cell- and circuit-level control in human patients of neurological and psychiatric disorders. Over 600 patients have been treated with genes delivered into their cells via the adeno-associated virus (AAV) vector, in 48 separate trials, without a single serious adverse event resulting from the virus [*Nat Biotechnol* 25 (9), 949 (2007)]. AAV is ubiquitous (perhaps 90% of people have been exposed to it) and causes no symptoms by itself. Accordingly, the field of gene therapy is moving in directions that could make optical prosthetics highly beneficial and practical at some point in the not-so-distant future. Furthermore, the fact that ChR2 and Halo may be useful for controlling many neural circuits throughout the nervous system may simplify the exploration of this gene therapy space: once these molecules have been tested for basic efficacy and safety in a few kinds of neuron, subsequent validation attempts may proceed quite rapidly, for use in novel cell types. Systems for optical targeting of specific neural circuit elements may enable a new generation of high-precision therapies for brain disorders.

[0062] While a preferred embodiment of the present invention is disclosed, many other implementations will occur to one of ordinary skill in the art and are all within the scope of the invention. Each of the various embodiments described above may be combined with other described embodiments in order to provide multiple features. Furthermore, while the foregoing describes a number of separate embodiments of the apparatus and method of the present invention, what has been described herein is merely illustrative of the application of the principles of the present invention. Other arrangements, methods, modifications, and substitutions by one of ordinary skill in the art are therefore also considered to be within the scope of the present invention, which is not to be limited except by the claims that follow.

What is claimed is:

1. A prosthetic device for optical control of target cells, comprising:

a probe, the probe comprising:

a plurality of light sources;

a plurality of drive circuit connections, at least one drive circuit connection being connected to each light source; and

a housing surrounding the plurality of light sources and the drive circuit connections; and

drive circuitry for driving and controlling the probe, the drive circuitry being capable of communicating with the probe through the drive circuit connections.

2. The device of claim **1**, the drive circuit connections and drive circuitry further comprising circuitry for wireless communication.

3. The device of claim **1**, wherein the light sources are light-emitting diodes.

4. The device of claim **3**, wherein the light-emitting diodes are blue and yellow.

5. The device of claim **1**, wherein the light sources are lasers.

6. The device of claim **1**, wherein the housing is a glass capillary tube.

7. The device of claim **6**, wherein the plurality of light sources is assembled into an array.

8. The device of claim **7**, wherein the light source array is linear.

9. The device of claim **1**, the prosthetic device further comprising sensors for monitoring the target cells.

10. An array comprising prosthetic devices according to claim **1**.

11. A prosthetic device for optical control of target cells, comprising:

an array of probes, each probe comprising:

a plurality of light sources;

a plurality of drive circuit connections, at least one drive circuit connection being connected to each light source; and

a housing surrounding the plurality of light sources and the drive circuit connections;

supporting hardware that holds the probes in position with respect to each other and the target cells; and

drive circuitry for driving and controlling the probes, the drive circuitry being capable of communicating with the probes through the drive circuit connections

12. The device of claim **11**, the drive circuit connections and drive circuitry further comprising circuitry for wireless communication.

13. The device of claim **11**, wherein the light sources are light-emitting diodes.

14. The device of claim **13**, wherein the light-emitting diodes are blue and yellow.

15. The device of claim **11**, wherein the light sources are lasers.

16. The device of claim **11**, wherein the housing is a glass capillary tube.

17. The device of claim **16**, wherein the plurality of light sources is assembled into an array.

18. The device of claim **17**, wherein the light source array is linear.

19. The device of claim **11**, the prosthetic device further comprising sensors for monitoring the target cells.

20. The device of claim **11**, wherein the array of probes is 3-dimensional.

* * * * *

APPENDIX 5

“Optical Cell Control Prosthetics,” U.S. Patent Application # 60/917,055.

US 20080306576A1

(19) **United States**

(12) **Patent Application Publication**

(10) **Pub. No.: US 2008/0306576 A1**

(43) **Pub. Date: Dec. 11, 2008**

Boyden et al.

(54) **OPTICAL CELL CONTROL PROSTHETICS**

(75) Inventors: **Edward S. Boyden**, Cambridge, MA (US); **Jacob G. Bernstein**, Cambridge, MA (US)

Correspondence Address:
NORMA E HENDERSON
HENDERSON PATENT LAW
13 JEFFERSON DR
LONDONDERRY, NH 03053 (US)

(73) Assignee: **Massachusetts Institute of Technology**, Cambridge, MA (US)

(21) Appl. No.: **12/118,673**

(22) Filed: **May 9, 2008**

Related U.S. Application Data

(60) Provisional application No. 60/917,055, filed on May 9, 2007.

Publication Classification

(51) **Int. Cl.**
A61N 5/06 (2006.01)

(52) **U.S. Cl.** **607/91**

(57) **ABSTRACT**

A prosthetic device for optical control of target cells comprises a set of light sources, hardware for guiding light to the target cells, supporting hardware that holds members of the set of light sources with respect to each other and the target cells, control circuitry for controlling the set of light sources, and power circuitry that provides power to the set of light sources and the control circuitry. The device may be wearable or implantable, and may be remotely powered or employ wireless communication. The supporting hardware may comprise implantable hypodermics or cannulas, or a plate or scaffold. The set of light sources may be assembled into an array.

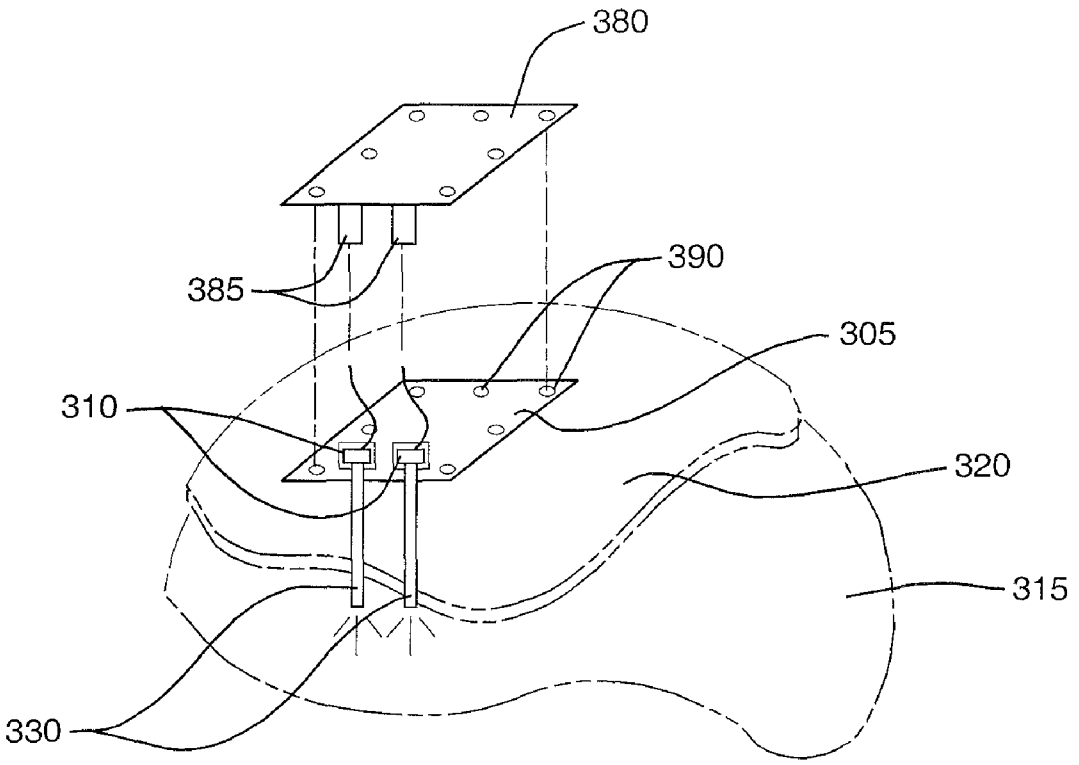

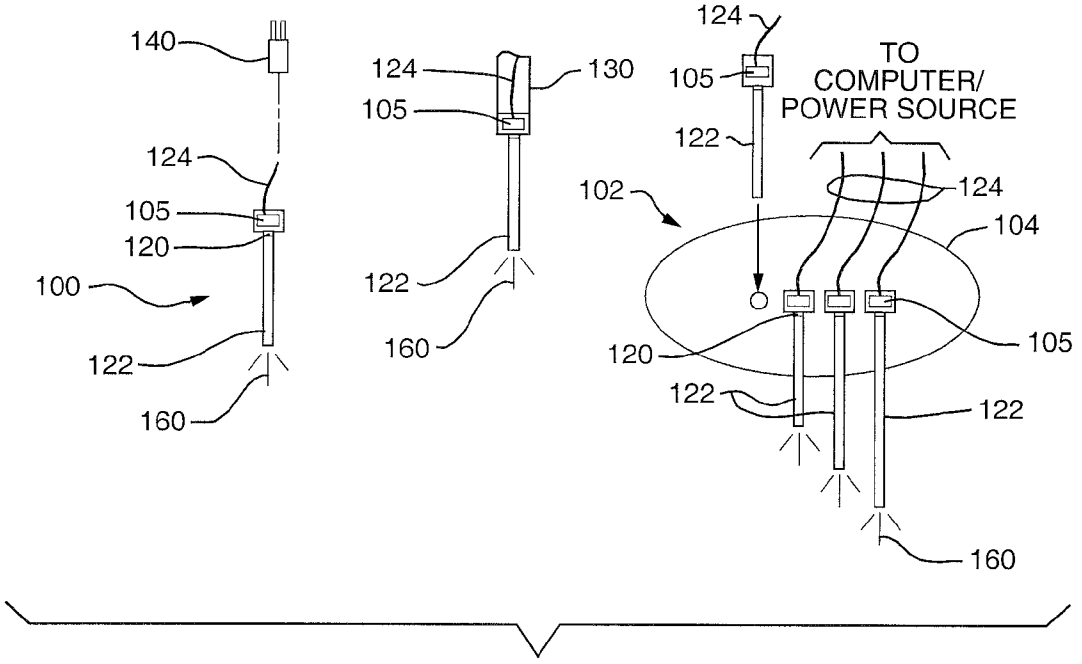
140
124
105
120
100
122
160
124
130
105
122
160
124
105
TO
COMPUTER/
POWER SOURCE
122
102
124
104
105
120
122
122
160

FIG. 1

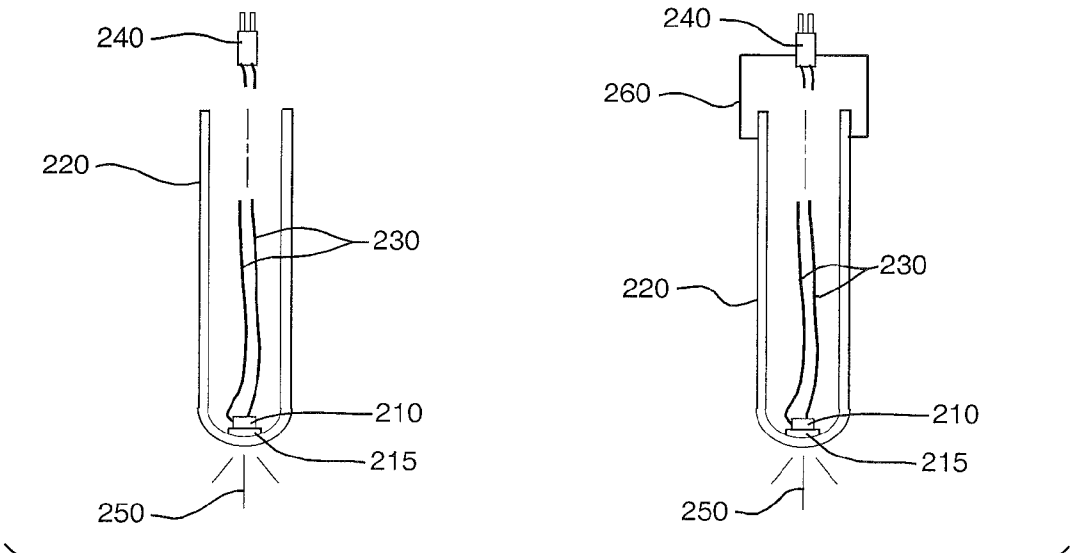
240
220
230
210
215
250
240
260
220
230
210
215
250

FIG. 2

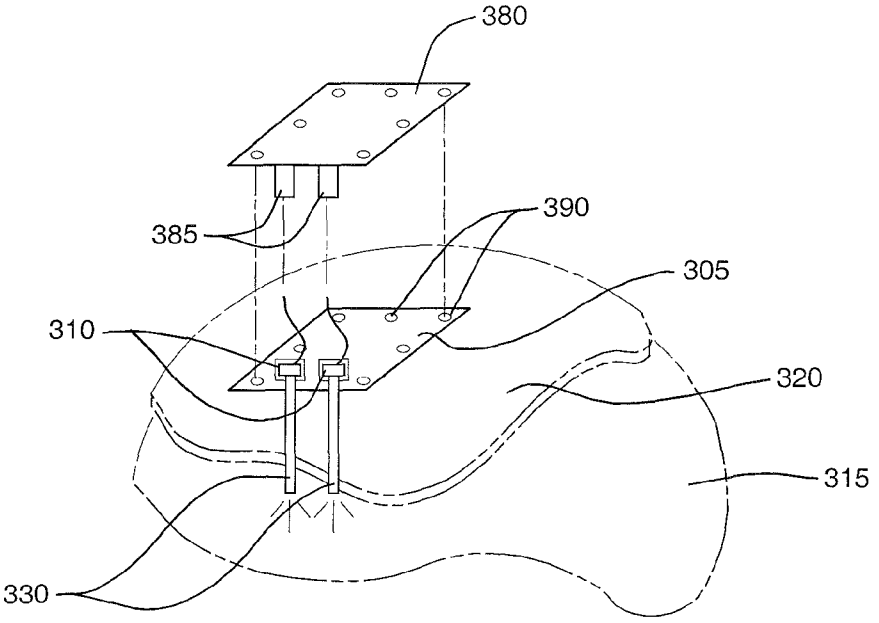

FIG. 3

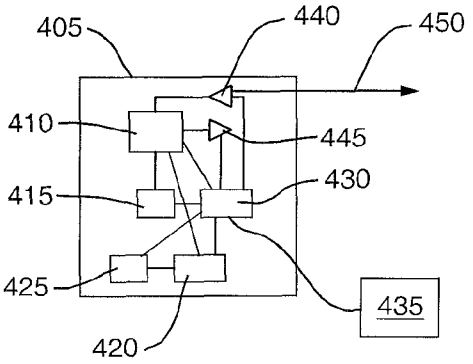

FIG. 4A

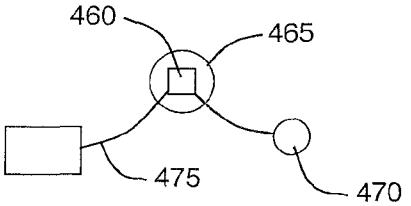

FIG. 4B

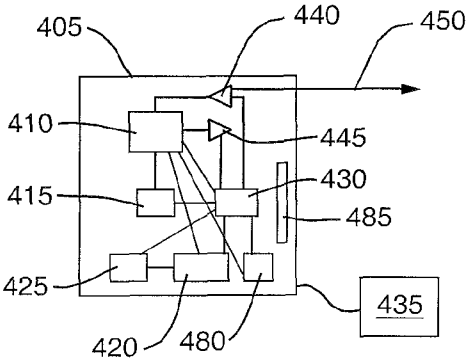

FIG. 4C

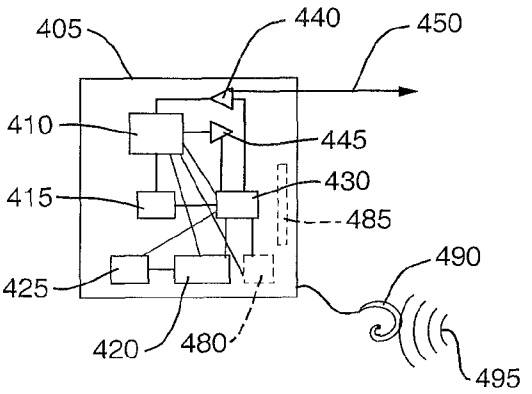

FIG. 4D

OPTICAL CELL CONTROL PROSTHETICS

RELATED APPLICATIONS

[0001] This application claims the benefit of U.S. Provisional Application Ser. No. 60/917,055, filed May 9, 2007, the entire disclosure of which is herein incorporated by reference.

FIELD OF THE TECHNOLOGY

[0002] The present invention relates to methods and devices for control of cell function and, in particular, to prosthetic devices for optical control of cells.

BACKGROUND

[0003] Many diseases of the human brain and nervous system are related to dysfunction of specific neuron types, which undergo pathological changes in number, excitability, anatomy, or synaptic connectivity. These changes lead, via altered neural circuit activity, to the perceptual, cognitive, emotional, and motor deficits associated with various neurological and psychiatric illnesses. For example, temporal lobe epilepsy is associated with increased excitability and connectivity of specific excitatory neurons [C. Bernard, A. Anderson, A. Becker et al., *Science* 305 (5683), 532 (2004); E. R. Sanabria, H. Su, and Y. Yaari, *J Physiol* 532 (Pt 1), 205 (2001); L. R. Shao and F. E. Dudek, *J Neurophysiol* 92 (3), 1366 (2004); C. R. Houser, J. E. Miyashiro, B. E. Swartz et al., *J Neurosci* 10 (1), 267 (1990)] and the loss of specific kinds of inhibitory interneurons [P. S. Buckmaster and F. E. Dudek, *J Comp Neurol* 385 (3), 385 (1997)] in the hippocampus, whereas schizophrenia is associated with atrophy of a specific kind of inhibitory neuron in the prefrontal cortex [D. A. Lewis, T. Hashimoto, and D. W. Volk, *Nat Rev Neurosci* 6 (4), 312 (2005)].

[0004] The ability to optically activate or inactivate genetically-specified excitable target cells, such as central nervous system neurons, glia, peripheral neurons, skeletal muscle, smooth muscle, cardiac muscle, pancreatic islet cells, thymus cells, immune cells, or other excitable cells, embedded in intact tissue, such as brain, peripheral nervous system, muscle, and skin, would enable radical new treatments for many disorders (e.g., neuropathic pain, Parkinson's disease, epilepsy, diabetes, and other diseases). Molecular-genetic methods for making cells such as neurons sensitive to being activated (e.g., depolarized) or inactivated (e.g., hyperpolarized) by light have been previously developed [X. Han and E. S. Boyden, "Multiple-color optical activation, silencing, and desynchronization of neural activity, with single-spike temporal resolution," *PLoS ONE* 2, e299 (2007)], but no method currently exists for delivering light to precise locations in intact tissues.

SUMMARY

[0005] The present invention is a device for delivering light to precise locations in intact tissues, in order to optically activate or inactivate specified excitable target cells. The invention comprises a set of light sources, accessory hardware for guiding light, supporting hardware to hold members of the set of light sources with respect to each other, the target cells, and external structures, and control and power electronics that monitor target cell state, provide regulated power to the light sources, and communicate data, stimulation protocols, and algorithms. The device may be wearable or implantable, and may optionally be remotely powered or employ wireless communication. The set of light sources may be assembled into an array.

[0006] In a preferred embodiment, an array of fiber-coupled LED elements are attached to a support. The LED elements are each connected to an optical fiber and a wire. Each wire can run through an optional cannula and are attached to the control circuitry. The target ends of the fibers are aimed to deliver light to specific target cells. In an alternative preferred embodiment, the LED is placed at the tip of a hypodermic or cannula and optionally coated by a biocompatible coating.

BRIEF DESCRIPTION OF THE DRAWINGS

[0007] Other aspects, advantages and novel features of the invention will become more apparent from the following detailed description of the invention when considered in conjunction with the accompanying drawings wherein:

[0008] FIG. **1** is a diagram depicting a fiber-coupled LED element and an array composed of multiple such elements, according to one aspect of the present invention;

[0009] FIG. **2** is a diagram depicting a hypodermic LED source, according to another aspect of the present invention;

[0010] FIG. **3** is a diagram depicting an embodiment of a plate for holding the circuitry and LEDs, according to another aspect of the present invention; and

[0011] FIGS. **4**A-D are diagrams depicting four alternative embodiments of an electronics board for operating the fiber array, according to a further aspect of the present invention.

DETAILED DESCRIPTION

[0012] The present invention is a device for delivering light to precise locations in intact tissues. The invention employs sets of light sources coupled to optical fibers whose ends deliver light to specified groups of target cells within tissue, sets of light sources in hypodermic cannulas that can deliver light locally to specified groups of target cells within tissue, and sets of light sources attached to nerve cuff holding devices that stably bring the light sources into close proximity to a group of target nerve cells. In support of the function of these sets of light sources, the present invention in some aspects includes control and power electronics, which enable battery-powered, wearable, fully implantable, wirelessly-operated, and/or remotely-powered versions of the electronics to drive these light sources, thus enabling the use of these devices as prosthetics. In another aspect, the present invention includes steerable light sources, ways of coupling multiple colors into the same fiber, and other uses of such fibers.

[0013] The invention comprises several parts: a set of light sources (such as, but not limited to, LEDs or lasers) with accessory hardware (e.g., fibers) for guiding light, supporting hardware to hold members of the set of light sources with respect to each other, with respect to the target cells such as, but not limited to, brain, glia, peripheral nerve, skeletal muscle, smooth muscle, cardiac muscle, pancreatic islet cells, thymus cells, or other excitable cells, embedded in the tissue (such as, but not limited to, brain, peripheral nervous system, muscle, skin, pancreas, and heart), and perhaps held firm with respect to external structures (such as, but not limited to, skull, skeleton, muscle, or skin), and control and power electronics that monitor target cell state, provide regulated power to the light sources, communicate data, stimulation protocols,

and algorithms to and from the outside world, and/or may be remotely powered by external electromagnetic fields or other kinds of wireless energy.

[0014] In the present invention, it should be understood by one of ordinary skill in the art that each of the variations on the component parts of the invention are swappable with any of the other variations. Similarly, when a use of the present invention is described with respect to a particular tissue or body part, it will be understood by one of ordinary skill in the art that the invention can be used in a similar manner for other body parts and tissues. For example, if a use is described is for the "brain," then it may similarly used in any other bodily tissue (e.g., peripheral nerve, pancreas, etc.). As another example, if it is described how to affix something to the skin, it may similarly be used in dealing with muscle and other tissues as well. The terms light source, LED, or laser are also used interchangeably, as they all have similar functionality in the context of the present invention. The light produced by the source may be visible light, infrared, spectrally complex, or any other type of light found to be suitable for the particular application.

[0015] A set of light sources is typically employed, although not absolutely required, because tissues are highly scattering, so that in many cases no one light source will be able to illuminate all the target cells in the entire desired target area [M. H. Niemz, *Laser-Tissue Interactions: Fundamentals and Applications*. (Springer-Verlag Telos, 1996); Bevilacqua, F, Marquet, P, Depeursinge, C, Haller, E B "Determination of reduced scattering and absorption coefficients by a single charge-coupled device array measurement, part II: measurements on biological tissues." Opt. Eng. 34: 2064-2069 (1995); E Okada, E, Schweiger, M, Arridge, S R, Firbank, M, Delpy, D T, "Experimental validation of Monte Carlo and finite-element methods for the estimation of the optical path length in inhomogenous tissue", Appl. Opt., 1996. 35: p. 3362-71 (1996)]. Each individual light source must receive electrical power, and deliver light locally to its target cells. In one embodiment, each light source is coupled to an optical fiber that projects deep into the tissue of interest to deliver light to the target cells. The electrical leads of the light source extend to the power/control circuitry, which provides timed pulses of electricity to the light source. The entire set of light sources may comprise many such optical elements, and in a preferred embodiment are arranged in an array on supporting hardware, with all the light sources in a plane, the fibers projecting perpendicularly into a tissue, and the ends terminating in various target regions where the target cells reside. In alternative preferred embodiments, the plane is a flexible substrate, so that fibers project inward from a curved surface into the tissue (e.g., if the target cells are in a tissue that is a naturally curved substrate like the brain), or there are multiple flat planes connected at their edges (e.g., forming part of a polyhedron).

[0016] FIG. **1** is a schematic diagram depicting fiber-coupled LED element **100** and array **102** composed of multiple such elements, attached to plate **104**, according to one aspect of the present invention. In FIG. **1**, LEDs **105** (such as, but not limited to, yellow or blue ones) are shown glued with optical adhesive **120** to optical fibers **122**, each with a wire **124** (such as, but not limited to, copper) emerging in the direction opposite to the direction of a fiber **122**. The wires can run through optional cannula **130** for protection, strain relief, and biocompatibility, and are optionally attached to electrical socket **140** at the end to provide easy attachment and disconnection. Cannula **130** may be made of any suitable material known in the art including, but not limited to, stainless steel, titanium, or glass. The target ends of the fibers are aimed to deliver light **160** to specific target cells in the target tissue, and can terminate at different depths within it. For example, in the brain, the target cells might be neurons. Array holder plate **102** may be made of any suitable material known in the art including, but not limited to, PCB board, kaptan, or steel. It may also alternatively be a hollow scaffold-type design, rather than being a solid plate.

[0017] An alternative preferred implementation of the set of light sources is to place the LED at the tip of a hypodermic or cannula, attached to the walls of the cannula with optical adhesive and optionally coated by a biocompatible coating. FIG. **2** is a diagram depicting a hypodermic LED source, according to this aspect of the present invention. LED **210** is attached by optical adhesive **215** at the aperture of implantable hypodermic **220**. In a preferred embodiment, hypodermic **220** is steel, but it may be any suitable material known in the art. Wires **230** attached to LED **210** snake up tube **220**, which is optionally attached to connector **240**. This has the advantage of delivering light **250** directly to the area of interest, while minimizing fiber-coupling losses. Optional housing **260** may also be used. The need to place a large LED at depth may require more room for the implantation, as opposed to a very small fiber, but as LEDs become smaller and smaller, this difference will become moot. Calculations indicate that tissue heating due to local light generation will be negligible for almost all clinically relevant applications of the LED. The LEDs and hypodermics can optionally be assembled into an array, as shown in FIG. **1**.

[0018] Another preferred implementation has a bare LED, potted in a biocompatible coating, with wires leading out of the coating. Yet another preferred implementation has the LED on a peripheral nerve cuff (e.g., as used in nerve cuff electrodes), which brings the LED in close apposition to a nerve that is desired to be stimulated. This enables stimulation of peripheral nerves, e.g. for sensory replacement, controlling motor outputs, or silencing pain neurons.

[0019] FIG. **3** depicts an embodiment of a plate for holding the circuitry and LEDs, according to one aspect of the present invention. Plane **305** containing all the light sources can correspond to a physical plate made of printed circuit board materials, including, but not limited to, kapton, polyimide, titanium, and stainless steel, that holds LEDs **310** firmly oriented, via adhesive or mechanical fitting into holes, towards the targets on brain **315** and skull **320**. Plate **305** may be conformal or may alternatively be of scaffold-type design. LEDs **310** may be connected to optical fibers **330**, as in FIG. **1**, or within hypodermic tubes, as in FIG. **2**. The cannulas, plates, sockets, etc. make up the supporting hardware, which is designed to connect to electronics board **380** (and FIG. **4**) via sockets **385** and holes **390** for screws, dental acrylic, or other means known in the art for docking board **305** with the upper layers of the device. The embodiment of FIG. **3** is suitable for use with many different types of implementations, including wearable, implanted, wirelessly-controlled, or remotely-powered implementations. The device of FIG. **3** is capable of being implanted under the skull, within the brain, or in within one or more parts of the body.

[0020] In all of the above scenarios, the light source typically has one or more wires emerging from the supporting hardware. These wires lead to the control and power electronics. The wires need not be physical strands; instead, multiple

circuit boards can directly dock with one another. The control and power electronics contain all of the elements needed to power the light sources when light is desired, to perform any necessary computations, to communicate with the outside world to obtain light pulse programs or to upload data, to store data locally, to acquire power from remote sources, or to detect local phenomena in the brain circuit (including, but not limited to, spikes or field potentials detected on an electrode) in order to react appropriately and deliver light of the appropriate wavelength, power, timecourse, etc. For example, a particularly appealing way to modulate LED power with a simple circuit is to pulse width modulate (PWM) the LED. A particularly simple wireless method is to simply attach an LED to an inductor, which is then remotely powerable.

[0021] Various embodiments of these circuits are battery-powered, wearable, fully implantable, wirelessly-operated, and/or remotely-powered, so different versions of the electronics may be advantageously employed to drive the LEDs. FIGS. **4**A-D are diagrams depicting four alternative electronics boards for operating the fiber array, according to this aspect of the present invention. Wearable (FIG. **4**A) implementations contain all the computational and power capacity onboard, as do implantable (FIG. **4**B) versions. As shown in FIG. **4**A, board **405** supports microcontroller **410**, preferably with D/A converters (such as, for example, but not limited to, a PIC microcontroller), RAM **415**, flash memory **420** to store the pulse program, and USB **425** for uploading programs and downloading data and/or logs. On-board DC power source **430** is supported by battery **435**, which is an Li ion battery in a preferred embodiment but could also be any other suitable battery or other power source known in the art including, but not limited to, an ultra capacitor or even a wall connection. Board **405** also supports amplifiers **440**, **445** or other circuits to drive the LEDs and electrodes or other neural sensors **450**, which provide information that can permit microcontroller **410** to trigger light pulses in a dynamic way. As shown in FIG. **4**B, LED **460** is embedded in biocompatible coating **465**, powered by battery **470**, and is connected **475** to a board that is similar to, or the same as board **405** from FIG. **4**A.

[0022] Wirelessly-operated devices, such as the one shown in FIG. **4**C, are implemented like the wearable and implantable devices of FIGS. **4**A and **4**B, but they also comprise transceiver **480** and antenna **485** in order to receive and transmit information via RF. While RF transceiving is described, it will be clear to one of ordinary skill in the art that any kind of wireless communication may be advantageously employed in the present invention, including, but not limited to, ultrasound and optical, each of which have associated specialized hardware requirements. Remotely-powered devices, such as the one shown in FIG. **4**D, require antenna **490**, specialized for the capture of magnetic or RF energy **495**, such as, but not limited to an inductor, power RF coil, or RFID chip. They can also be wireless, like the embodiment of FIG. **4**C by incorporating transceiver **480** and antenna **485**. Depending on the disorder being treated, the duration of the treatment, and the risks associated with various kinds of implant, various subsets or combinations of these specifications may be found to be desirable for a particular individual patient.

[0023] In an example implementation, specific to the brain and skull, materials used include unjacketed optical fiber—100 μm, 200 μm, or 500 μm UV-VIS transmitting (FIG. **1**), ultra-thin wall stainless steel hypodermic tubing, ultrabright blue LEDs (e.g., EZ1000 for coupling to fibers (FIG. **1**) or EZ290 used for coupling to fibers or being implanted directly in brain in hypodermic (FIG. **2**)), ultrabright yellow LEDs (Luxeon III, Luxeon Rebel, used for coupling to fibers (FIG. **1**), Lumileds P4—implanted directly in brain in hypodermic (FIG. **2**)), and optical adhesive. Tools required include UV curer, Dremel, water jet cutter, laser cutter, excimer laser, and 3-D printer. The fiber array is made up of two components—the supporting hardware (FIG. **3**), and a collection of modular light guides (FIGS. **1** and **2**). For small structures, 100 μm and 200 μm optical fiber light guides may be used (FIG. **1**), whereas for larger structures, hypodermic light guides may be used (FIG. **2**).

[0024] For assembly of this example implementation, the lowest layer of the supporting hardware is cut on an excimer laser, with holes for screws to attach the supporting hardware to the skull. The second layer of the supporting hardware screws or pops onto the first, and is a printed circuit board, containing a wireless transceiver, an embedded antenna, a programmable IC, and circuitry to drive current through the LEDs in the light guides (FIG. **3**). It interfaces with each light guide through a custom plug. Each light guide has a clearance hole in both layers, as well as docking holes for the housing in the first layer. The light guides are encased in a custom 3D printed housing. At the top of each light guide is a socket to interface with the electronics on the supporting hardware. At the bottom of each light guide is an opening for the optical fiber or LED to emerge. Steel cannulas are cut circumferentially with a Dremel to avoid collapsing or crimping the tubing. For the optical fiber light guides (FIG. **1**), the LED sits inside of the housing and is coupled directly to the fiber with optical adhesive, generating light that is sent down the optical fiber, which is implanted directly in the brain. For the hypodermic light guide (FIG. **2**), a thin walled stainless steel tube is wired with a 300 μm wide LED at the base, which shines light directly into the brain. Any exposed wire is insulated with biocompatible coating. This particular implementation can shine light about 0.5-1 mm away from atypical fiber (diameter 0.2-0.5 mm).

[0025] Currently these fiber arrays are being implemented using individual lasers or LEDs, but arrays of vertical cavity surface emitting lasers (VCSELs) or other optical sources work just as well. It is further envisioned that if, in the future, xenon bulbs, halogen lamps, incandescent bulbs, or other light sources become miniaturized enough to fit, they may also be advantageously used in the prosthetics of the present invention (likely with filters on the bulbs), although current embodiments of these devices are not as viable as LEDs and lasers due to their wasted energy, expense, danger, and limited life.

[0026] An optional enhancement is the use of a dichroic (or beamsplitter, or other equivalent optical part) attached to a fiber in a way so that it couples two different light sources (e.g., a blue LED and a yellow LED, or a blue laser and a yellow laser) into the fiber, so that the target cells at the end of the fiber can be activated and deactivated by two different colors of light (see, e.g., X. Han and E. S. Boyden, "Multiple-color optical activation, silencing, and desynchronization of neural activity, with single-spike temporal resolution", *PLoS ONE* 2, e299 (2007)). Also suitable is a series of cascaded dichroics, capable of coupling more than two colors of light into the same fiber. Another optional enhancement is a steerable element (such as, but not limited to, a galvanometer, an acousto-optic deflector, a MEMS mirror, or other steering device), on one or both ends of the fiber, in order to direct light

in a controlled way, enabling locally selective targeting of the light to specific areas of the tissue, preferably with as few moving parts as possible.

[0027] While the present invention has been described in the context of the use of light to excite and inhibit electrically excitable cells, it will be understood by one of skill in the art that the present invention may also be advantageously employed to deliver light to other realms, such as to drive the production of cAMP in deep tissue [Schröder-Lang S, Schwärzel M, Seifert R, Strünker T, Kateriya S, Looser J, Watanabe M, Kaupp U B, Hegemann P, Nagel G. "Fast manipulation of cellular cAMP level by light in vivo", *Nature methods* (2006)], to simulate the action of a G-protein coupled receptor acting drug [J. M. Kim, J. Hwa, P. Garriga et al., "Light-driven activation of beta 2-adrenergic receptor signaling by a chimeric rhodopsin containing the beta 2-adrenergic receptor cytoplasmic loops", *Biochemistry* 44 (7), 2284 (2005)], or to change the pH of a cell [G. Nagel, D. Ollig, M. Fuhrmann et al., "Channelrhodopsin-1: a light-gated proton channel in green algae", *Science* 296 (5577), 2395 (2002)]. There are many therapeutic reasons to desire these abilities.

[0028] While a preferred embodiment is disclosed, many other implementations will occur to one of ordinary skill in the art and are all within the scope of the invention. Each of the various embodiments described above may be combined with other described embodiments in order to provide multiple features. Furthermore, while the foregoing describes a number of separate embodiments of the apparatus and method of the present invention, what has been described herein is merely illustrative of the application of the principles of the present invention. Other arrangements, methods, modifications, and substitutions by one of ordinary skill in the art are therefore also considered to be within the scope of the present invention, which is not to be limited except by the claims that follow.

What is claimed is:

1. A prosthetic device for optical control of target cells, comprising:

a set of light sources;

lightguide hardware, connected to the light sources, for guiding light to the target cells;

supporting hardware that holds members of the set of light sources with respect to each other and the target cells;

control circuitry for controlling the set of light sources; and

power circuitry that provides power to the set of light sources and the control circuitry.

2. The device of claim **1**, further comprising circuitry for wireless communication.

3. The device of claim **1**, wherein the power circuitry comprises a battery.

4. The device of claim **1**, wherein the power circuitry is remotely powered.

5. The device of claim **1**, wherein the supporting hardware comprises implantable hypodermics or cannulas.

6. The device of claim **1**, wherein the supporting hardware comprises a plate or scaffold.

7. The device of claim **6**, wherein the set of light sources is assembled into an array.

8. The device of claim **1**, wherein the light sources are embedded in a biocompatible coating.

9. The device of claim **1**, further comprising sensors for monitoring the target cells.

10. An array of prosthetic devices for optical control of target cells, each prosthetic device comprising:

a light source;

lightguide hardware, connected to the light source, for guiding light to at least one target cell;

supporting hardware that holds the prosthetic device with respect to other prosthetic device and the target cells;

control circuitry for controlling the light source; and

power circuitry that provides power to the light sources and the control circuitry.

11. The array of claim **10**, further comprising circuitry for wireless communication.

12. The array of claim **10**, wherein the power circuitry is battery powered.

13. The array of claim **10**, wherein the power circuitry is remotely powered.

14. The array of claim **10**, wherein the supporting hardware comprises an implantable hypodermic or cannula.

15. The array of claim **10**, wherein the supporting hardware comprises a shared plate or scaffold.

16. The array of claim **10**, wherein the array is embedded in a biocompatible coating.

17. The array of claim **10**, further comprising sensors for monitoring the target cells.

* * * * *

APPENDIX 6

Chow, B.Y., Han, X., Qian, X., Li, M., Monahan, P.E., Chuong, A.S., Boyden, E.S. (2009) High-Performance Neural Activity Silencing by Light-Driven Proton Pumping, in press, *Nature.*

High-Performance Genetically-Targetable Optical Neural Silencing via the Class of Light-Driven Proton Pumps

Brian Y. Chow [(†)], Xue Han [(†)], Allison S. Dobry, Xiaofeng Qian, Amy S. Chuong, Mingjie Li, Michael A. Henninger, Patrick E. Monahan, and Edward S. Boyden [(*)]

The MIT Media Laboratory, Department of Biological Engineering, and Department of Brain and Cognitive Sciences, Massachusetts Institute of Technology, Cambridge, MA 02139 (†) These authors contributed equally to this work.

The ability to silence the activity of genetically specified neurons in a temporally precise fashion would open up the ability to investigate the causal role of specific cell classes in neural computations, behaviors, and pathologies. Promise has emerged from the discovery that halorhodopsins, light-driven chloride pumps, can mediate inhibitory photocurrents when expressed in neurons[1-4], but these currents are small relative to the current drive of many neurons in the brain[5-8]. Here, through a cross-kingdom functional molecular screen, we reveal a new class of neural silencer, the light-driven proton pumps, capable of mediating powerful and safe silencing of neural activity. In particular, the gene archaerhodopsin-3 from *H. sodomense* (here abbreviated Arch), a putative yellow-green light-driven proton pump, enables near-100% optical silencing of neurons in the awake brain when lentivirally expressed in mouse cortex. Arch mediates currents of several hundred picoamps at low light powers, enabling significantly greater brain volume to be inhibited than prior tools,

and additionally possesses a large dynamic range of light responsivity, supporting neural silencing currents approaching 900 pA at light powers safely achievable *in vivo*. Arch is capable of spontaneous functional recovery after illumination, unlike halorhodopsins which remain in a long-lasting inactive state. Arch function in neurons is well tolerated because pH excursions created by Arch illumination are minimized by intrinsic regulatory mechanisms to levels comparable to those mediated by channelrhodopsins or by normal activity. To highlight how proton pump diversity may yield novel neural tools, we demonstrate that the blue-green light driven proton pump from the fungus *L. maculans* can be used to sensitize neurons to being silenced by blue light, thus enabling independent silencing of distinct neural populations by blue vs. red light. These silencers will open up a wide variety of neuroscientific and biotechnological experiments and support synthetic neurobiology approaches to prototyping therapies for neurological and psychiatric disorders[9].

We launched a homology-driven functional screen of type I microbial opsins (see **Table 1** for complete list) from species representing four different kingdoms – archaebacteria, bacteria, plants, and fungi[4,10-25] – including several molecules that were previously uncharacterized as unambiguously electrogenic (Arch/aR-3, cHR-3, aHR-3, cHR-5, and SalHO). Mammalian codon-optimized opsin genes were synthesized, cloned into GFP fusion expression vectors, and then transfected into cultured neurons for whole cell voltage clamp recording under illumination with light (575 ± 25 nm at 7.8 mW/mm^2 for all but Mac/LR/Ops, gPR, bPR, and Ace/AR, which were at 535 $\pm$ 25 nm at irradiance 9.4 mW/mm^2). We measured photocurrents and cell capacitance-normalized photocurrent densities (**Fig. 1A,** black and gray bars respectively), as well as action spectra (i.e., peak photocurrent as a function of wavelength; **Supplementary Table 1**), for each opsin. Using the action spectra, we estimated the photocurrent densities for each opsin at its own spectral

peak (**Fig. 1A**, white bars; see **Methods** for details). The previously published reagent Halo/NpHR was included in the screen for comparison[1-4]. One of the genes, the gene archaerhodopsin-3 (aR-3; here abbreviated Arch in codon-optimized form; GENBANK ID ***[to be submitted after publication]***) from *Halorubrum sodomense*[26], hypothesized based on sequence to be a proton pump[10,11], generated spectral peak-adjusted photocurrent densities much greater than Halo in the screen. Two other genes that encode for proton pumps, the opsin of *L. maculans* (aka Mac, LR, Ops)[23] and the molecule cruxrhodopsin-1[24], also yielded currents larger than that of Arch (**Fig. 1A**).

Arch is a yellow-green light sensitive (λ_{max} = 566 ± 66 nm; **Fig. 1B**) opsin which expresses well on the plasma membrane of neurons (**Fig. 1C**). Arch-mediated currents exhibited rapid onset and offset, modest inactivation, and spontaneous recovery from inactivation (**Fig. 1D, 1E**). Upon illumination, Arch currents rose very quickly, with a 15%-85% onset time of 8.8 ± 1.8 ms (mean $\pm$ standard error (SE) reported throughout unless otherwise indicated; N = 16 neurons), less than half that of Halo (20.2 ± 2.3 ms, N = 13; $p < 0.001$, t-test). Despite the larger currents, after light cessation, Arch currents had an 85%-15% offset time of 19.3 ± 2.9 ms (N = 16), significantly less than that of Halo (30.8 ± 5.5 ms, N = 13; $p < 0.05$). Under continuous yellow illumination (7.8 mW/mm^2), Arch photocurrent declined over 15 seconds to 70.8 ± 4.7% (N = 11) of its initial peak, very similar to the inactivation of Halo[3]. However, unlike Halo and all other light-driven chloride pumps that we evaluated in this screen, which after illumination remain in an inactivated state for tens of minutes (and can only be restored to an optically drivable form with additional blue wavelength light, thus elaborating the hardware required for optimal usage)[13,27], Arch spontaneously recovers to a functional state over a period of several seconds in the dark – at least two orders of magnitude faster (**Fig. 1D, 1E**), with a time

constant similar to channelrhodopsin-2 (ChR2)[28,29], and without requiring a second color of light to facilitate recovery (e.g., from an unresponsive photo-intermediate).

At powers typically utilized *in vitro* and *in vivo* for optical neural control (**Fig. 1F**), Arch mediates currents up to an order of magnitude greater than the hyperpolarizing currents possible with earlier reported microbial opsin silencing reagents. At low light powers of 0.35, 1.28, and 7.8 mW/mm^2 irradiance (**Fig. 1Fi**), neural Arch currents were 120, 189 pA and 350 pA respectively, 600%, 380%, and 280% of the values that would be supported by Halo at the same powers (20, 50 pA and 125 pA, respectively). At higher light powers, Halo currents saturate (**Fig. 1Fi**), but the light responsivity of Arch possesses a much higher dynamic range, enabling responses that continue to increase in magnitude with increased light power (**Fig. 1Fii**) – for example, enabling photocurrents approaching 900 pA at effective irradiances (see **Methods** for details on how effective irradiances were calculated) of 36 mW/mm^2, well within the reach of current *in vivo* experiments. The large dynamic range of Arch may enable better utilization of bright light sources such as LEDs and lasers that are safe and effective for optical control *in vivo*[9,30].

We next characterized the functional effects of expressing and operating an apparent proton pump in mammalian neurons. First, several lines of evidence supported the idea that Arch functioned as a proton pump when expressed in neurons: removing all Cl- or K+ from both intracellular and extracellular solutions did not change the magnitude of measured photocurrents or photocurrent densities under yellow light illumination (N = 16 neurons measured in regular solutions, N = 8 in Cl- free solutions, N = 7 in K+ free solutions; $p > 0.4$ comparing either K+ free or Cl- free to regular, t-test; **Fig. 2A**). Furthermore, in solutions lacking the major charge carriers Na^+, K^+, Cl^-, and Ca^{2+}, illuminated Arch-expressing neurons still generated currents which were no different than

currents measured in normal solutions (N = 4 neurons tested without these four charge carriers; $p > 0.4$ current magnitude; $p > 0.9$ current density). Such currents followed a linear current-voltage relationship at potentials below -60 mV (**Fig. 2B**), suggesting a reversal potential less than -120 mV, a finding which is also consistent with the idea that Arch is a proton pump. We next assessed the voltage swings that would emerge in current-clamped neurons expressing Arch, under illumination. As plotted in **Fig. 1F**, as effective irradiance increased from 7.8 mW/mm^2 to 36.3 mW/mm^2, Arch exhibited peak currents that increased from 350 $\pm$ 35 pA (N = 16 neurons) to 863 ± 62 pA (N = 8 neurons), respectively – a 2.5-fold increase. Under these two irradiance conditions, however, current-clamped cultured neurons underwent strong hyperpolarizations of neural voltage by -69.6 ± 7.3 mV (N =10, mean ± SE) and -76.2 ± 10.1 mV (N = 8, mean ± SE) respectively. Surprisingly, these values were not significantly different from one another ($p > 0.7$, t-test). This finding suggests the existence of a rapidly activated transporter or exchanger (perhaps the Na^+-dependent Cl^-/HCO_3^- exchanger), or the opening of hyperpolarization-dependent channels easily capable of shunting protons, that thus self-limit the effects of Arch on accumulated proton (or other charge carrier) gradients across neural membranes. This enabling of effective, but not excessive, silencing, may make Arch safer and more reliable for long-term silencing, especially at high light powers, than pumps that accumulate ions without such self-regulatory properties.

Given that Arch was likely acting by funnelling protons out of neurons, we next assessed how Arch activation would affect intracellular pH (pH_i), using the cell-permeant ratiometric fluorescent pH indicator carboxy-SNARF-1. Within one second of illumination with green light ($\lambda = 535 \pm 25$ nm, 6.1 mW/mm^2, to allow simultaneous SNARF-1 imaging and Arch activation), pH_i rose from 7.309 ± 0.011 (N = 57 neurons) to 7.431 ± 0.020 (N = 20; **Fig. 2C**), plateauing rapidly. After 15 seconds of illumination, the pH_i increased only

slightly further, to 7.461 ± 0.024 (N = 10), despite the fact that photocurrents would have remained sizable throughout the illumination period (**Fig. 1E**). The fast stabilization of pH_i may reflect the same proton-normalizing influence that limits proton-mediated voltage swings to a safe range, as described above, and may contribute to the safe operation of Arch in neurons by preventing excessive pH_i swings. Indeed, the changes in pH_i observed here with Arch activation are comparable in magnitude to those observed during illumination of channelrhodopsin-2-expressing cells[31] (due to the strong proton currents carried by channelrhodopsins[28,32]) and are also within the magnitudes of changes observed during normal neural activity[33-36]. Passive properties of neurons expressing Arch, such as membrane capacitance (**Fig. 2D**), membrane resistance (**Fig. 2E**), and resting potential (**Fig. 2F**), measured in the dark, were not different between Arch-infected and uninfected control neurons ($p > 0.6$ for all comparisons, t-test; N = 7 each), nor was cell death as assessed by Trypan Blue staining affected by Arch expression (33 Trypan Blue positive cells/512 total = 6.4% dead uninfected cells, 40 Trypan Blue positive/669 total = 6.0% Arch-expressing cells; $\chi^2 = 0.26$; $p > 0.6$, **Fig. 2G**). Thus, lentiviral expression of Arch does not affect the health or membrane properties of neurons *in vitro*.

We assessed the efficiency of Arch in mediating neural silencing *in vivo* both by estimating the volumes of tissue that would be silenced using well-controlled *in vitro* experiments and computational modeling, and by recording in awake mice while illuminating Arch-expressing excitatory neurons in motor and sensory cortices using a laser-coupled fiber[30,37]. In neurons expressing Arch or a trafficking-improved variant of Halo, eNpHR[1,2], we simulated different levels of excitatory drive in current-clamped cultured neurons by somatically injecting different current levels (200, 350, 500 pA) for 15 ms pulse durations at 5 Hz, driving spiking. We then exposed Arch- or eNpHR-expressing neurons to periods of 575 nm yellow light (0.35, 1.28, or 6 mW/mm^2, simulating the light

approximately 1.7, 1.2, and 0.6 mm away from the tip of a 200 micron fiber emitting 200 mW/mm^2 irradiance at the fiber tip; see **Supplementary Figure 3** for Monte Carlo simulation), and measured the percentage reduction in spike rate for each condition (**Fig. 3A**). Across the board, Arch-expressing neurons were inhibited to a greater extent than eNpHR-expressing cells. For example, we found that the 350 pA-injected Arch-expressing neurons were ~95% silenced at just 1.3 mW/mm^2, whereas the eNpHR-expressing neurons were only ~45% silenced at that power. At lower powers of 0.35 mW/mm^2, Arch-expressing neurons were still ~55% silenced, whereas eNpHR-expressing neurons were barely (~5%) silenced. Based on our model, the increase in volume of brain tissue (again, using the 350 pA value, and calculating for a 200 micron fiber emitting 200 mW/mm^2 irradiance) that would be 45-55% inhibited by light would be >8x larger for Arch than for eNpHR. To directly test Arch efficacy *in vivo*, we injected lentivirus encoding for Arch into the mouse cortex, and recorded neurons in the awake headfixed animal at least 1 month later. Arch was well expressed in neurons (**Fig. 3Bi**), and appeared well localized to the plasma membrane, labeling cell bodies, processes, and dendritic spines (**Fig. 3Bii**). We recorded neurons in awake headfixed mice with glass electrodes, illuminating neurons via a 200 micron diameter optical fiber coupled to a yellow laser (593 nm; ~150 mW/mm^2 radiant flux out the fiber tip; recording electrode tip ~800 μm away from the fiber tip; power at electrode tip expected to be ~3 mW/mm^2 [9,30,37]). Upon light onset, firing rates of recorded units were immediately and strongly reduced, and remained low throughout the period of illumination, whether the pulse was brief, as might be desired during probing of the timing of neural dynamics (**Fig. 3Ci, ii, 3D)**, or long, appropriate for simulating a temporary lesion (**Fig. 3Ciii, iv**). We recorded 13 single units which showed any decrease in firing during the illumination period, objectively identified as described in the **Methods**, and analyzed the magnitude of these decreases during 5 second periods of exposure to

continuous yellow light (**Fig. 3D**). The firing rate of these units dropped by an average of 90 $\pm$ 15% (mean $\pm$ standard deviation (SD); **Fig. 3E, 3F**), restoring to levels indistinguishable from baseline values after light cessation ($p > 0.2$, paired t-test; **Fig. 3F**). However, given that not all recorded neurons were necessarily lentivirally labelled (and therefore Arch-expressing), we hypothesized that this averaged value may reflect both direct silencing of Arch-expressing neurons as well as network dependent reductions in activity of non-Arch-expressing neurons that receive input from Arch-expressing neurons. Consistent with this hypothesis of hetereogeneity, the distribution was not Gaussian: 6 of the 13 units were silenced to a level of 99.5% or greater, and the median decrease in spike rate of the 13 units was 97.1% (**Fig. 3G**). Thus it is possible that Arch-expressing cells were almost completely silenced, whereas non-infected cells reduced activity due to suppressed network activity during illumination. Optical silencing could be repeated many times without alteration of the magnitude of silencing ($p > 0.1$, paired t-test comparing, for each neuron, responses to the first 3 vs. last 3 light exposures; 20 trials were typically measured for each neuron). The kinetics of silencing were rapid: for the 6 neurons that underwent > 99.5% silencing, as described above, spike firing reduced with near-0 ms latency (that is, they almost never fired spikes after light onset), and there was also very rapid recovery after light cessation. Averaged across all cells, firing rate reductions reached the steady state level within 229 ± 310 milliseconds of light onset (mean $\pm$ SD), and after light cessation, firing rate restored to baseline level 355 ± 505 ms later. The level of post-light firing did not vary with repeated light exposure ($p > 0.7$, paired t-test comparing, for each neuron, after-light firing rates during the first 3 vs. the last 3 trials). Thus, Arch could mediate high-performance, near-digital silencing of neurons in the awake mammalian brain, safely, reliably, and efficaciously.

Arch appeared to be well localized to the plasma membrane (**Fig. 1C)** (see **Supplementary Figure 1** for method of analysis); the absolute expression level on the plasma membrane was similar to that of Halo ($p > 0.2$, N = 5 cells each). We experimented with adding targeting sequences that improve trafficking, and found that adding a signal sequence from the MHC Class I antigen ('ss')[38] as well as the Kir2.1 ER export sequence ('ER2') (which is part of the sequence that boosts Halo currents by 75%, resulting in eNpHR, ref. [1,2]), did not augment Arch currents ($p > 0.6$, N = 16 Arch cells, N = 9 ss-Arch-ER2 cells). Thus, the effect of a given trafficking-improving sequence on opsin expression is opsin-specific (and perhaps species-specific), but nonetheless deserves further attention. For example, adding the Prolactin signal sequence ('Prl')[39] to the N terminus of Arch trended towards boosting the Arch current (+32%; $p < 0.08$, N = 18 ss-Prl-Arch cells). Improving opsin targeting, however, is unlikely to alter opsin recovery kinetics or light dynamic range.

Proton pumps naturally exist with a wide diversity of action spectra, in contrast to known chloride pumps, which are primarily driven by yellow to orange light. Mutagenesis in our hands has shown that altering retinal flanking residues in halorhodopsin either eliminates pumping activity or shifts the action spectrum by less than 16 nm (see **Supplementary Table 2**); in contrast, many residues in bacteriorhodopsin are known to result in large blueshifts of action spectrum when mutated, with limited reduction of pump performance[40-44]. Furthermore, many natural examples of proton pumps that absorb strongly in the blue exist (e.g., Ace, Mac, gPR, and bPR in **Table 1**). We found that gPR and bPR did not function in neurons, Ace functioned minimally in neurons (the action spectrum was, however, measurable in HEK cells; see **Supplementary Figure 2**), and Mac mediated significant screen photocurrents of over 250 pA (**Fig. 1A**) when expressed in neurons. Given the difference in action spectra between Mac and Halo (**Fig. 4A**), we

realized that two populations of neurons – one expressing Mac, the other expressing Halo – would be able to be selectively silenced with blue light and red light respectively. Indeed, in prototype experiments using low light powers in culture, delivered via bandpass excitation filters (**Fig. 4B, 4C**), Mac-expressing neurons underwent 4.1-fold larger hyperpolarizations with blue light than with red light, and Halo-expressing neurons demonstrated 3.3-fold larger hyperpolarizations with red light than with blue light. The use of lasers that can deliver strong light in very narrow bandwidths will further reduce opsin cross-talk, and future mutagenesis to blueshift the spectrum of Mac may also be of use in improving multicolor silencing performance.

Optogenetic microbial reagents such as light-gated cation channels (e.g., ChR2) and light-driven chloride pumps (e.g., Halo/NpHR) are fast, single-protein reagents that allow genetically targeted sensitization of specific neural functions to light, without the need for exogenous chemical supplementation when used in the mammalian brain. Arch and Mac represent members of a new, diverse, and powerful class of optogenetic reagent, the light-driven proton pump. We here have reported the discovery of several surprising properties of this class of molecules that open up entirely new possibilities for cell-type specific neural silencing. First, these proton pumps are highly efficacious at driving hyperpolarizing currents in mammalian tissue across a large range of light powers – a perhaps surprising result, given that protons are fairly rare (~100 nanomolar) in mammalian tissue, a millionfold-lower in concentration than the ions carried by other optical control molecules. In part this high efficacy may be due to the fast photocycle of Arch (see also [45,46]), but it may also be due to the high efficiency of proton uptake of high-pKa residues in proton pumps[45,47]. The large current mediated by Arch, increases the typical volume addressable by a single optical fiber by manyfold, relative to even enhanced halorhodopsins. Second, we reveal the surprising discovery that proton pumps expressed in neurons possess self-

normalizing limits on light-driven swings in neural voltage and pH, preventing unsafe excursions of pH or voltage when proton pumps are used. In addition, the shuntlike effect that results may enable more naturalistic neural silencing. Third, we show that the kinetics of proton pumps allow recovery in the dark after optical activation, enabling these proton pumps to be used for a variety of purposes (e.g., repeated neural silencing during the course of a behavior), whereas halorhodopsins would have entered a long-lasting dormant state. (Halorhodopsin mutagenesis of several critical residues that govern opsin kinetics did not result in enhanced recovery in the dark; see **Supplementary Table 2**).

Proton pumps naturally exist with a wide diversity of action spectrum peaks, in contrast to chloride pumps, all of which that have been described to date are primarily yellow or orange-light driven. Thus, in our screen, proton pumps were not only more efficacious than chloride pumps, but their spectral diversity enabled multiple-color silencing of distinct neural populations. This opens up novel kinds of experiment, in which, for example, two neuron classes, or two sets of neural projections from a single site, can be independently silenced at different times during a behavioral task. Importantly, yellow-light driven Arch can be used simultaneously with the blue light driven neural activator ChR2, appropriate for creating "informational lesions" in which spike statistics can be manipulated with multi-color bidirectional neural control[3,48]. Our study highlights the importance of natural ecological diversity, combined with homology-driven screening, in discovering novel molecular reagents for biological control, as has been previously shown by the fluorescent protein community. Given that the structure and function of the light-driven proton pump *H. salinarum* bacteriorhodopsin is well known, structure-guided mutagenesis of Arch and Mac may facilitate development of novel neural silencers with altered spectrum, kinetics, or ion selectivity.

These opsins are likely to find uses across the spectrum of neuroscientific, biological, and bioengineering fields. Expression of these opsins in neurons, muscle, heart, immune cells, and other excitable cells will allow control over their membrane potential, opening up the ability to investigate the causal role of specific cells' activities in intact organisms, and opening up the ability to understand the causal contribution of such cells to disease states in animal models. Well controlled hyperpolarization may also support novel biotechnologies such as automated drug screening for molecules that affect hyperpolarization-gated channels. Finally, with the recent demonstration of the safe and efficacious use of the microbial opsin ChR2 in non-human primates[9], it is in principle possible that in the future, these opsins may subserve novel kinds of molecularly-supported cell-specific control prosthetics.

Methods

See **Supplementary Methods** for detailed methods. Constructs with Arch, Mac, and Halo are available at ***[will be posted after article acceptance];*** see **Supplementary Methods** for specific Genbank and Addgene reference numbers and URLs). In brief, codon-optimized genes were ordered to be synthesized by Genscript and fused to GFP in a lentiviral/mammalian expression vector as used previously[3,9] for transfection or infection of neurons. Primary hippocampal or cortical neurons were cultured and then transfected with expression plasmids or infected with viruses encoding for the genes of interest, as described previously[3,29]. Images were taken using a Zeiss LSM 510 confocal microscope. Patch clamp recordings were made using glass microelectrodes and a Multiclamp 700B/Digidata electrophysiology setup, using appropriate pipette and bath solutions for the experimental

goal at hand. Neural pH imaging was done using SNARF-1-AM ester (Invitrogen). Cell health was assayed using Trypan blue staining (Gibco). HEK cells were cultured and patch clamped using standard protocols. Mutagenesis was performed using the QuikChange kit (Stratagene). Computational modelling of light propagation was done with Monte Carlo simulation with MATLAB. *In vivo* recordings were made on headfixed awake mice, which were surgically injected with lentivirus, and implanted with a headplate as described before[9,49]. Glass pipettes attached to laser-coupled optical fibers were inserted into the brain, to record neural activity during laser illumination in an artifact-free way. Data analysis was performed using Clampfit, Excel, Origin, and MATLAB. Histology was performed using transcardial perfusion followed by sectioning and subsequent imaging via the Zeiss LSM 510 confocal.

REFERENCES

1 Zhao, S. *et al.* Improved expression of halorhodopsin for light-induced silencing of neuronal activity. *Brain cell biology* **36**, 141-154 (2008).

2 Gradinaru, V., Thompson, K. R. & Deisseroth, K. eNpHR: a Natronomonas halorhodopsin enhanced for optogenetic applications. *Brain cell biology* **36**, 129-139 (2008).

3 Han, X. & Boyden, E. S. Multiple-color optical activation, silencing, and desynchronization of neural activity, with single-spike temporal resolution. *PLoS ONE* **2**, e299 (2007).

4 Zhang, F. *et al.* Multimodal fast optical interrogation of neural circuitry. *Nature* **446**, 633-639 (2007).

5 Leinekugel, X. *et al.* Correlated bursts of activity in the neonatal hippocampus in vivo. *Science* **296**, 2049-2052 (2002).

6 Wehr, M. & Zador, A. M. Balanced inhibition underlies tuning and sharpens spike timing in auditory cortex. *Nature* **426**, 442-446 (2003).

7 Richter, D. W., Pierrefiche, O., Lalley, P. M. & Polder, H. R. Voltage-clamp analysis of neurons within deep layers of the brain. *J Neurosci Methods* **67**, 121-123 (1996).

8 Narikawa, K., Furue, H., Kumamoto, E. & Yoshimura, M. In vivo patch-clamp analysis of IPSCs evoked in rat substantia gelatinosa neurons by cutaneous mechanical stimulation. *J Neurophysiol* **84**, 2171-2174 (2000).

9 Han, X. *et al.* Millisecond-timescale optical control of neural dynamics in the nonhuman primate brain. *Neuron* **62**, 191-198 (2009).

10 Mukohata, Y., Ihara, K., Tamura, T. & Sugiyama, Y. Halobacterial rhodopsins. *J Biochem* **125**, 649-657 (1999).

11 Ihara, K. *et al.* Evolution of the archaeal rhodopsins: evolution rate changes by gene duplication and functional differentiation. *J Mol Biol* **285**, 163-174 (1999).

12 Klare, J. P., Chizhov, I. & Engelhard, M. Microbial rhodopsins: scaffolds for ion pumps, channels, and sensors. *Results Probl Cell Differ* **45**, 73-122 (2008).

13 Han, X. & Boyden, E. S. Multiple-color optical activation, silencing, and desynchronization of neural activity, with single-spike temporal resolution. *PLoS ONE* **2**, e299 (2007).

14 Bamberg, E., Tittor, J. & Oesterhelt, D. Light-driven proton or chloride pumping by halorhodopsin. *Proc Natl Acad Sci U S A* **90**, 639-643 (1993).

15 Soppa, J., Duschl, J. & Oesterhelt, D. Bacterioopsin, haloopsin, and sensory opsin I of the halobacterial isolate Halobacterium sp. strain SG1: three new members of a growing family. *J Bacteriol* **175**, 2720-2726 (1993).

16 Kitajima, T. *et al.* Novel bacterial rhodopsins from Haloarcula vallismortis. *Biochem Biophys Res Commun* **220**, 341-345 (1996).

17 Baliga, N. S. *et al.* Genome sequence of Haloarcula marismortui: a halophilic archaeon from the Dead Sea. *Genome Res* **14**, 2221-2234 (2004).

18 Bolhuis, H. *et al.* The genome of the square archaeon Haloquadratum walsbyi : life at the limits of water activity. *BMC Genomics* **7**, 169 (2006).

19 Antón, J. *et al.* in *Adaptation to Life in High Salt Concentrations in Archaea, Bacteria and Eukarya* eds N. Gunde-Cimerman, Plemenitas. A, & A. Oren) 257–266. (Kluwer Academic Publishers, 2005).

20 Brown, L. S. Fungal rhodopsins and opsin-related proteins: eukaryotic homologues of bacteriorhodopsin with unknown functions. *Photochem Photobiol Sci* **3**, 555-565 (2004).

21 Luecke, H., Schobert, B., Richter, H. T., Cartailler, J. P. & Lanyi, J. K. Structure of bacteriorhodopsin at 1.55 A resolution. *J Mol Biol* **291**, 899-911 (1999).

22 Beja, O., Spudich, E. N., Spudich, J. L., Leclerc, M. & DeLong, E. F. Proteorhodopsin phototrophy in the ocean. *Nature* **411**, 786-789 (2001).

23 Waschuk, S. A., Bezerra, A. G., Shi, L. & Brown, L. S. Leptosphaeria rhodopsin: Bacteriorhodopsin-like proton pump from a eukaryote. *Proceedings of the National Academy of Sciences of the United States of America* **102**, 6879-6883, doi:10.1073/pnas.0409659102 (2005).

24 Tateno, M., Ihara, K. & Mukohata, Y. The novel ion pump rhodopsins from Haloarcula form a family independent from both the bacteriorhodopsin and archaerhodopsin families/tribes. *Arch Biochem Biophys* **315**, 127-132 (1994).

25 Tsunoda, S. P. *et al.* H+ -pumping rhodopsin from the marine alga Acetabularia. *Biophys J* **91**, 1471-1479 (2006).

26 Oren, A. Halobacterium sodomense sp. nov., a Dead Sea Halobacterium with an Extremely High Magnesium Requirement. *Int J Syst Bacteriol* **33**, 381-386 (1983).

27 Hegemann, P., Oesterhelt, D. & Steiner, M. The photocycle of the chloride pump halorhodopsin. I: Azide-catalyzed deprotonation of the chromophore is a side

reaction of photocycle intermediates inactivating the pump. *Embo J* **4**, 2347-2350 (1985).

28 Nagel, G. *et al.* Channelrhodopsin-2, a directly light-gated cation-selective membrane channel. *Proc Natl Acad Sci U S A* **100**, 13940-13945 (2003).

29 Boyden, E. S., Zhang, F., Bamberg, E., Nagel, G. & Deisseroth, K. Millisecond-timescale, genetically targeted optical control of neural activity. *Nat Neurosci* **8**, 1263-1268 (2005).

30 Aravanis, A. M. *et al.* An optical neural interface: in vivo control of rodent motor cortex with integrated fiberoptic and optogenetic technology. *Journal of neural engineering* **4**, S143-156 (2007).

31 Lin, J. Y., Lin, M. Z., Steinbach, P. & Tsien, R. Y. Characterization of engineered channelrhodopsin variants with improved properties and kinetics. *Biophys J* **96**, 1803-1814 (2009).

32 Berthold, P. *et al.* Channelrhodopsin-1 Initiates Phototaxis and Photophobic Responses in Chlamydomonas by Immediate Light-Induced Depolarization. *Plant Cell* **20**, 1665-1677, doi:10.1105/tpc.108.057919 (2008).

33 Bevensee, M. O., Cummins, T. R., Haddad, G. G., Boron, W. F. & Boyarsky, G. pH regulation in single CA1 neurons acutely isolated from the hippocampi of immature and mature rats. *J Physiol* **494 (Pt 2)**, 315-328 (1996).

34 Chesler, M. Regulation and modulation of pH in the brain. *Physiological reviews* **83**, 1183-1221 (2003).

35 Meyer, T. M., Munsch, T. & Pape, H. C. Activity-related changes in intracellular pH in rat thalamic relay neurons. *Neuroreport* **11**, 33-37 (2000).

36 Trapp, S., Luckermann, M., Brooks, P. A. & Ballanyi, K. Acidosis of rat dorsal vagal neurons in situ during spontaneous and evoked activity. *J Physiol* **496 (Pt 3)**, 695-710 (1996).

37 Bernstein, J. G. *et al.* Prosthetic systems for therapeutic optical activation and silencing of genetically-targeted neurons. *Proceedings - Society of Photo-Optical Instrumentation Engineers* **6854**, 68540H (2008).

38 Munoz-Jordan, J. L. *et al.* Inhibition of alpha/beta interferon signaling by the NS4B protein of flaviviruses. *J Virol* **79**, 8004-8013 (2005).

39 Jungnickel, B. & Rapoport, T. A. A posttargeting signal sequence recognition event in the endoplasmic reticulum membrane. *Cell* **82**, 261-270 (1995).

40 Mogi, T., Marti, T. & Khorana, H. G. Structure-function studies on bacteriorhodopsin. IX. Substitutions of tryptophan residues affect protein-retinal interactions in bacteriorhodopsin. *J Biol Chem* **264**, 14197-14201 (1989).

41 Mogi, T., Stern, L. J., Chao, B. H. & Khorana, H. G. Structure-function studies on bacteriorhodopsin. VIII. Substitutions of the membrane-embedded prolines 50, 91, and 186: the effects are determined by the substituting amino acids. *J Biol Chem* **264**, 14192-14196 (1989).

42 Mogi, T., Stern, L. J., Hackett, N. R. & Khorana, H. G. Bacteriorhodopsin mutants containing single tyrosine to phenylalanine substitutions are all active in proton translocation. *Proc Natl Acad Sci U S A* **84**, 5595-5599 (1987).

43 Mogi, T., Stern, L. J., Marti, T., Chao, B. H. & Khorana, H. G. Aspartic acid substitutions affect proton translocation by bacteriorhodopsin. *Proc Natl Acad Sci U S A* **85**, 4148-4152 (1988).

44 Greenhalgh, D. A., Farrens, D. L., Subramaniam, S. & Khorana, H. G. Hydrophobic amino acids in the retinal-binding pocket of bacteriorhodopsin. *J Biol Chem* **268**, 20305-20311 (1993).

45 Ming, M. *et al.* pH dependence of light-driven proton pumping by an archaerhodopsin from Tibet: comparison with bacteriorhodopsin. *Biophys J* **90**, 3322-3332 (2006).

46 Lukashev, E. P. *et al.* pH dependence of the absorption spectra and photochemical transformations of the archaerhodopsins. *Photochem Photobiol* **60**, 69-75 (1994).

47 Lanyi, J. K. Proton transfers in the bacteriorhodopsin photocycle. *Biochimica et Biophysica Acta (BBA) - Bioenergetics* **1757**, 1012-1018 (2006).

48 Han, X., Qian, X., Stern, P., Chuong, A. S. & Boyden, E. S. Informational Lesions: Optical Perturbation of Spike Timing and Neural Synchrony Via Microbial Opsin Gene Fusions. *Front. Mol. Neurosci.* **doi:10.3389/neuro.02.012.2009** (2009).

49 Boyden, E. S. & Raymond, J. L. Active reversal of motor memories reveals rules governing memory encoding. *Neuron* **39**, 1031-1042 (2003).

50 Váró, G. Analogies between halorhodopsin and bacteriorhodopsin. *Biochimica et Biophysica Acta (BBA) - Bioenergetics* **1460**, 220-229 (2000).

51 Mongodin, E. F. *et al.* The genome of Salinibacter ruber: convergence and gene exchange among hyperhalophilic bacteria and archaea. *Proc Natl Acad Sci U S A* **102**, 18147-18152 (2005).

52 Espagne, E. *et al.* The genome sequence of the model ascomycete fungus Podospora anserina. *Genome Biology* **9**, R77 (2008).

53 Bieszke, J. A. *et al.* The nop-1 gene of Neurospora crassa encodes a seven transmembrane helix retinal-binding protein homologous to archaeal rhodopsins. *Proc Natl Acad Sci U S A* **96**, 8034-8039 (1999).

54 Beja, O. *et al.* Bacterial rhodopsin: evidence for a new type of phototrophy in the sea. *Science* **289**, 1902-1906 (2000).

55 Wang, W. W., Sineshchekov, O. A., Spudich, E. N. & Spudich, J. L. Spectroscopic and photochemical characterization of a deep ocean proteorhodopsin. *J Biol Chem* **278**, 33985-33991 (2003).

Supplementary Information accompanies the paper on www.nature.com/nature

Acknowledgments

ESB acknowledges funding by the NIH Director's New Innovator Award (DP2 OD002002-01), as well as by the NSF (0835878 and 0848804), the McGovern Institute Neurotechnology Award Program, the Department

of Defense, NARSAD, the Alfred P. Sloan Foundation, the Jerry Burnett Foundation, the SFN Research Award for Innovation in Neuroscience, the MIT Media Lab, the Benesse Foundation, and the Wallace H. Coulter Foundation. XH acknowledges the Helen Hay Whitney Foundation and NIH 1K99MH085944. The authors thank Robert Desimone for advice, Yingxi Lin and Gabi Belfort for cortical neural cultures, John Lin for technical aid on intracellular pH measurements, Kunio Ihara for discussions about archaerhodopsins, and Michael Hemann and Neil Gershenfeld and the Center for Bits and Atoms for use of their respective lab facilities.

Authors' Contributions

B.Y.C., X.H., and E.S.B. designed experiments, analyzed data, and wrote the paper. B.Y.C. and X.H. carried out experiments. A.S.D. assisted with electrophysiological recording. X.Q., M.L., and A.S.C. assisted with molecular biology, virus making, and transfections. M.A.H. performed Monte Carlo modelling. P.E.M. created hippocampal neural cultures.

Correspondence

(*) Correspondence and requests for materials should be addressed to E.S.B. (edboyden@mit.edu).

Figure Legends

Figure 1. Optical neural silencing via light-driven proton pumping, revealed by a cross-kingdom functional molecular screen. **(A)** Screen data showing outward photocurrents (left ordinate, black bars), photocurrent densities (right ordinate, gray bars), and action spectrum-normalized photocurrent densities (right ordinate, white

bars), measured via whole-cell patch clamp of cultured neurons (see **Table 1** for explanation of abbreviations here used). The N below each bar indicates the number of neurons utilized to obtain the data represented by that bar. All data in this and other figures are mean ± standard error (SE) unless otherwise indicated. **(B)** Action spectra of Arch measured in cultured neurons by scanning illumination light wavelength through the visible spectrum in 29 nm increments (N = 7 neurons). **(C)** Confocal fluorescence image of a lentivirally-infected neuron expressing Arch-GFP (scale bar, 20 µm). **(D)** Raw current trace of a neuron lentivirally-infected with Arch, illuminated by a 15 second light pulse (575 ± 25 nm, irradiance 7.8 mW/mm^2), followed by brief 1 s test pulses delivered starting 15, 45, 75, 105, and 135 seconds after the end of the light pulse. **(E)** Population data of averaged Arch photocurrents (N = 11 neurons) sampled at the times indicated by the vertical dotted lines that extend into **Fig. 1D**. **F)** Photocurrents of Arch vs. Halo measured as a function of 575 ± 25 nm light irradiance (or effective light irradiance; see **Methods** for details), in patch-clamped cultured neurons (N = 4 – 16 neurons for each point), for low (**i**) and high (**ii**) light powers. The line is a single Hill fit to the data.

Figure 2. Functional properties of the light-driven proton pump Arch in neurons. (**A**) Photocurrent of Arch measured as a function of ionic composition (575 ± 25 nm light, 7.8 mW/mm^2), showing no significant dependence of photocurrent on concentration of Cl- or K+ ions in either the external Tyrode, or the intracellular pipette solution (N = 16, 8 and 7 neurons, from left to right). **(B)** Photocurrent of Arch measured as a function of holding potential, normalized to the photocurrent at

-60 mV (N = 4 neurons). (**C**) Intracellular pH measurements obtained over a period of one minute of continuous illumination (535 ± 25 nm light, irradiance 6.1 mW/mm^2, for simultaneous SNARF-1 and Arch illumination) using SNARF-1 pH-sensitive ratiometric dye (N = 10 – 20 cells per datapoint). **(D)** Membrane capacitance, **(E)** membrane resistance, and **(F)** resting potential in neurons lentivirally-infected with Arch vs. wild-type (WT) neurons, measured at 11 days *in vitro* (N = 7 cells each). **(G)** Trypan blue staining of neurons lentivirally-infected with Arch vs. wild-type (WT) neurons, measured at 18 days *in vitro* (N = 669 Arch-expressing, 512 wild-type, neurons).

Figure 3. High-performance Arch-mediated optical neural silencing of neocortical regions in awake mice. (**A**) *In vitro* data showing, in cultured neurons expressing Arch or eNpHR and current-clamped to receive trains of somatic current injections (200, 350, 500 pA), the percent reduction of spiking under varying light powers (6.0, 1.28, and 0.35 mW/mm^2, all with 575 ± 25 nm light) as might be encountered in a typical *in vivo* experiment. *, difference between Arch and eNpHR $p < 0.05$ t-test; **, $p < 0.01$, t-test. N = 7-8 cells were recorded for each condition. (**B**) Fluorescence images showing lentivirally-transduced Arch-GFP expression in mouse cortex (**i**; scale bar, 200 μm) and in a mouse cortical excitatory neuron (**ii**; scale bar, 20 μm), >1 month after lentiviral injection. (**C**) Exemplar extracellular recordings showing neurons undergoing 5-second (**i, ii**), 15-second (**iii**), and 1-minute (**iv**) periods of yellow laser light illumination (593 nm; ~150 mW/mm^2 radiant flux out the fiber tip; recording electrode tip ~800 μm away from fiber tip; power at electrode tip expected to be on the order of 3 mW/mm^2 [9,30,37]). (**D**) Neural activity

in an exemplar neuron before, during, and after 5 seconds of yellow light illumination, shown as a spike raster plot (top) displaying each spike as a black dot (20 trials are shown in horizontal rows), and also as a histogram of instantaneous firing rate averaged across all trials (bottom; bin size, 20 ms). (**E**) Instantaneous firing rate, averaged across all single units observed to undergo any amount of activity suppression during 5 seconds of yellow light illumination (black line, mean; gray lines, mean ± SE; n = 13 units). (**F**) Average change in spike firing across single units, during 5 seconds of yellow light illumination (left) and during the 5 seconds immediately after light offset (right), for the data shown in **D**. (**G**) Histogram of percentage reductions in spike rate, for all recorded single units observed to undergo any amount of activity suppression during light illumination.

Figure 4. Multicolor silencing of two neural populations, enabled by blue- and red-light drivable ion pumps of different optogenetic classes. (**A**) Action spectra of Mac vs. Halo, along with rectangles indicating filter bandwidths used for demonstration of multi-color silencing *in vitro*. Blue light power is via a 470 $\pm$ 20 nm filter at 0.92 mW/mm^2, and red light power is via a 630 $\pm$ 15 nm filter at 2.6 mW/mm^2. (**B**) Action potentials evoked by current injection into patch clamped neurons transfected with Halo (i) were selectively silenced by the red light but not by the blue light, whereas neurons transfected with Mac (ii) were selectively silenced by the blue light but not by the red light. (**C**) Membrane hyperpolarizations elicited by the blue light versus the red light, in cells expressing Halo versus Mac.

Tables

Table 1: Molecular screening candidates.

Abbreviations	Molecule class	Species of origin	GENBANK Accession	References
Halo, NpHR, pHR	halorhodopsin	*Natronomas pharaonis*	ABQ08589	[4,13,50]
sHR, HR	halorhodopsin	*Halobacterium salinarum*	NP_279315	[10,50]
aHR-3	archaehalorhodopsin	*Halorubrum sodomense*	BAA75202	[10]
aHR-1, SGHR	archaehalorhodopsin	*Halorubrum aus-1 (sp. SG1)*	CAA49773	[10,15]
cHR-3	cruxhalorhodopsin	*Haloarcula vallismortis*	BAA06679	[12,16]
cHR-5	cruxhalorhodopsin	*Haloarcula marismortui*	AAV46572	[12,17]
SquareHOP	square halorhodopsin	*Haloquadratum walysbyi*	CAJ53165	[18]
dHR-1	deltahalorhodopsin	*Haloterrigena sp. Arg-4*	BAA75201	[10,12]
SalHO, SRU_2780	bacterial halorhodopsin	*Salinibacter ruber*	AAT76430	[19,51]
pop	fungal opsin related protein	*Podospora anserina (DSM980)*	XP_001904282	[52]
nop-1	fungal opsin related	*Neospora crassa*	XP_959421	[53]

	protein			
Arch, aR-3	archaerhodopsin	*Halorubrum sodomense*	BAA09452	[10]
Mac, LR, Ops	Fungal opsin related protein, bacteriorhodopsin	*Leptosphaeria maculans*	AAG01180	[23]
BR	Bacteriorhodopsin	*Halobacterium salinarum*	CAA23744	[10]
cR-1	Cruxrhodopsin	*Haloarcula argentinensis (sp. arg-1*	BAA06678	[24]
gPR, BAC31A8	Proteorhodopsin	*γ - proteobacterium BAC31A8*	AAG10475	[54,55]
bPR, Hot75m4	proteorhodopsin	*γ- proteobacterium Hot75m4*	Q9AFF7	[54,55]
Ace, AR	Algal bacteriorhodopsin	*Acetabularia acetabulum*	AAY82897	[25]

Summary of molecules screened, including abbreviations, molecule classification, species of origin, GenBank accession number, and references. Major molecule types are defined as “bacteriorhodopsins” or “rhodopsins” for outwardly rectifying proton pumps and “halorhodopsins” for inwardly rectifying chloride pumps. Sub-classifications of molecule type are determined by kingdom and/or genus of species of origin (e.g. archaerhodopsin = proton pump from halorubrum genus of halobacteria / haloarchaea).

Chow, Han, et al., 2009, Figure 1

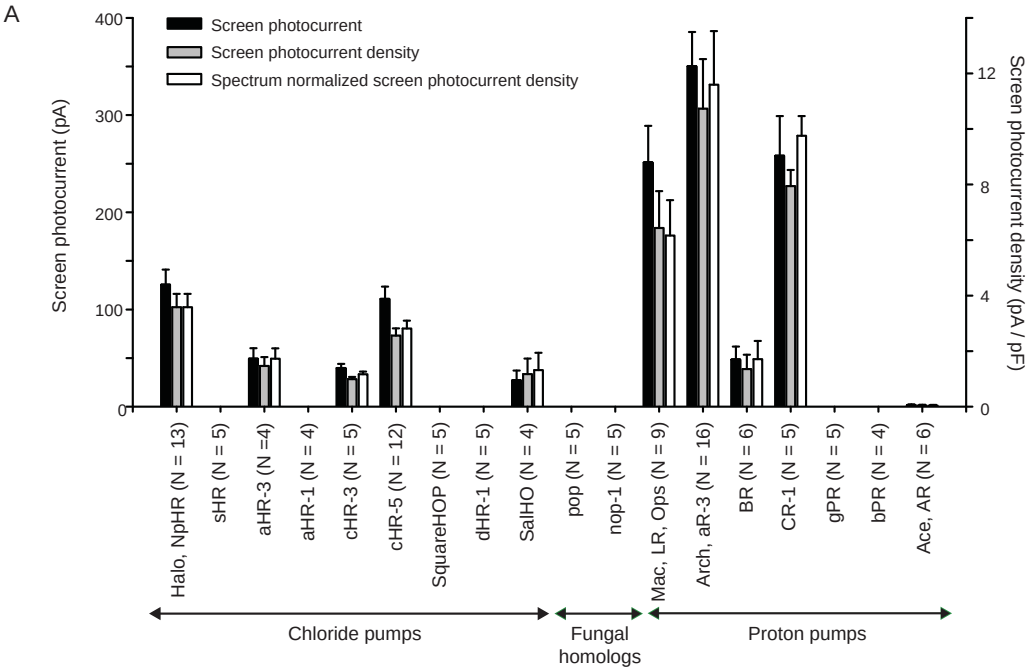

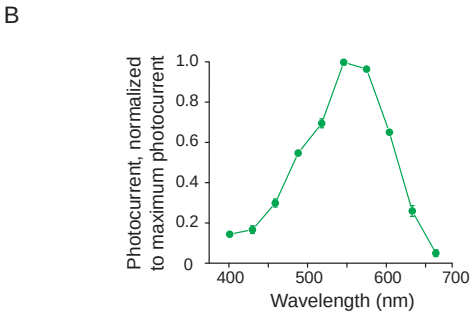

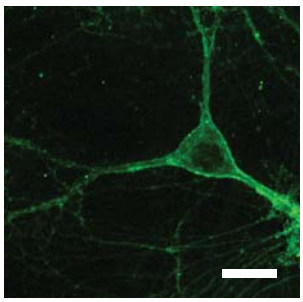

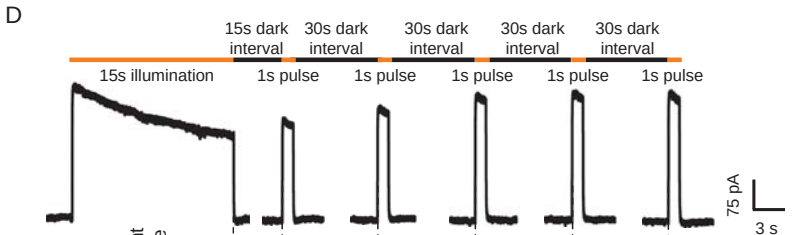

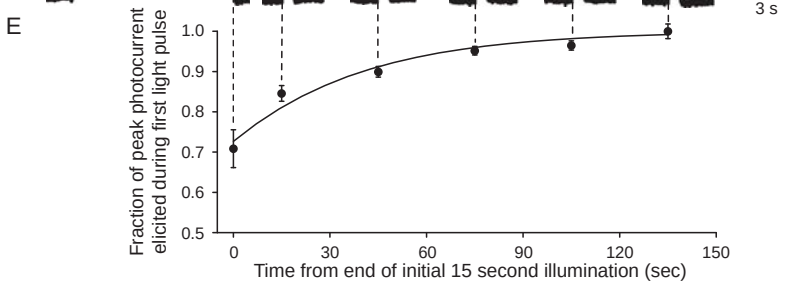

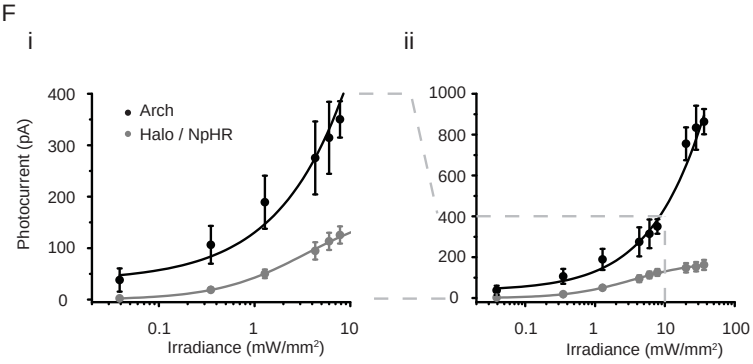

Chow, Han, et al., 2009
Figure 2

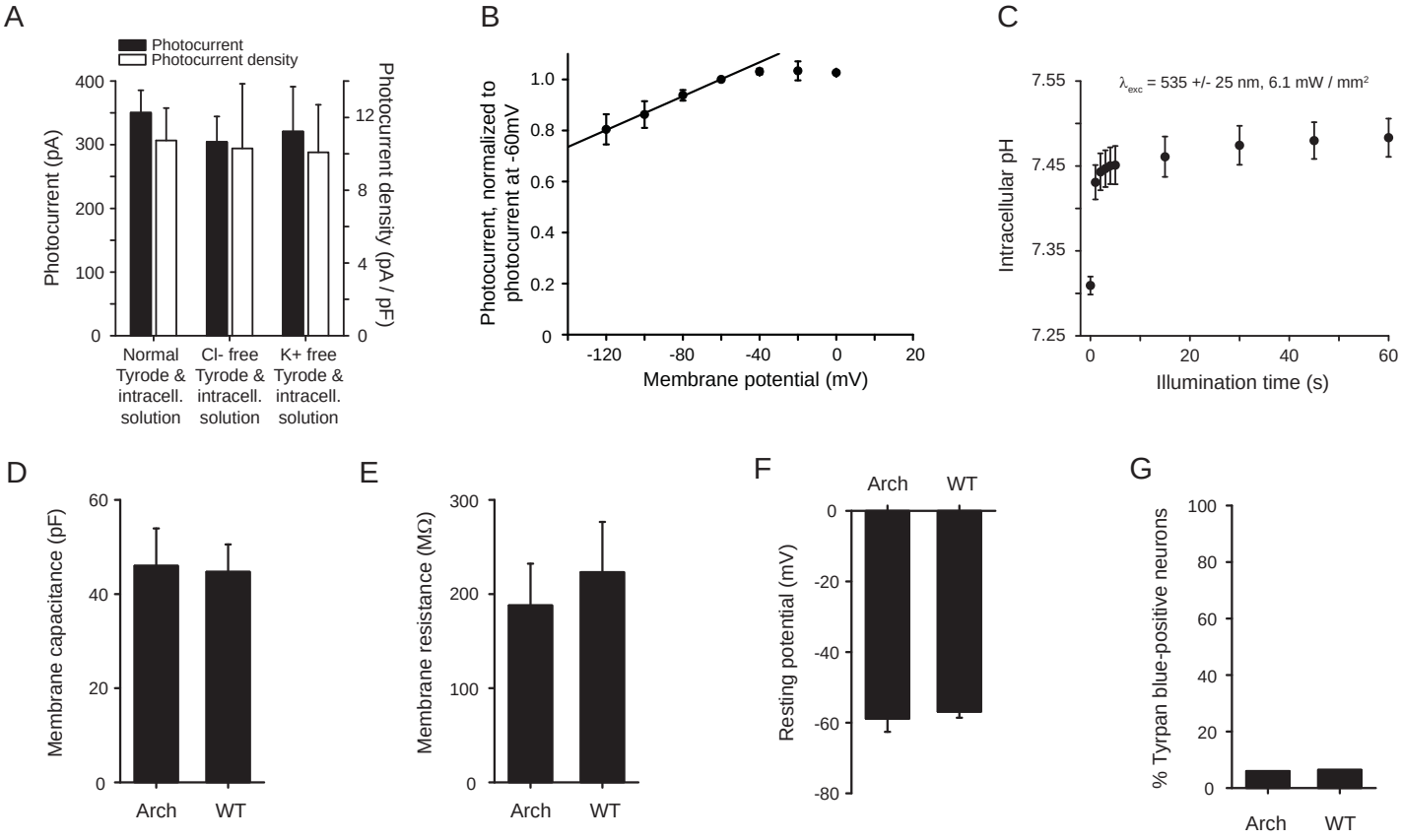

Chow, Han, et. al 2009

Figure 3

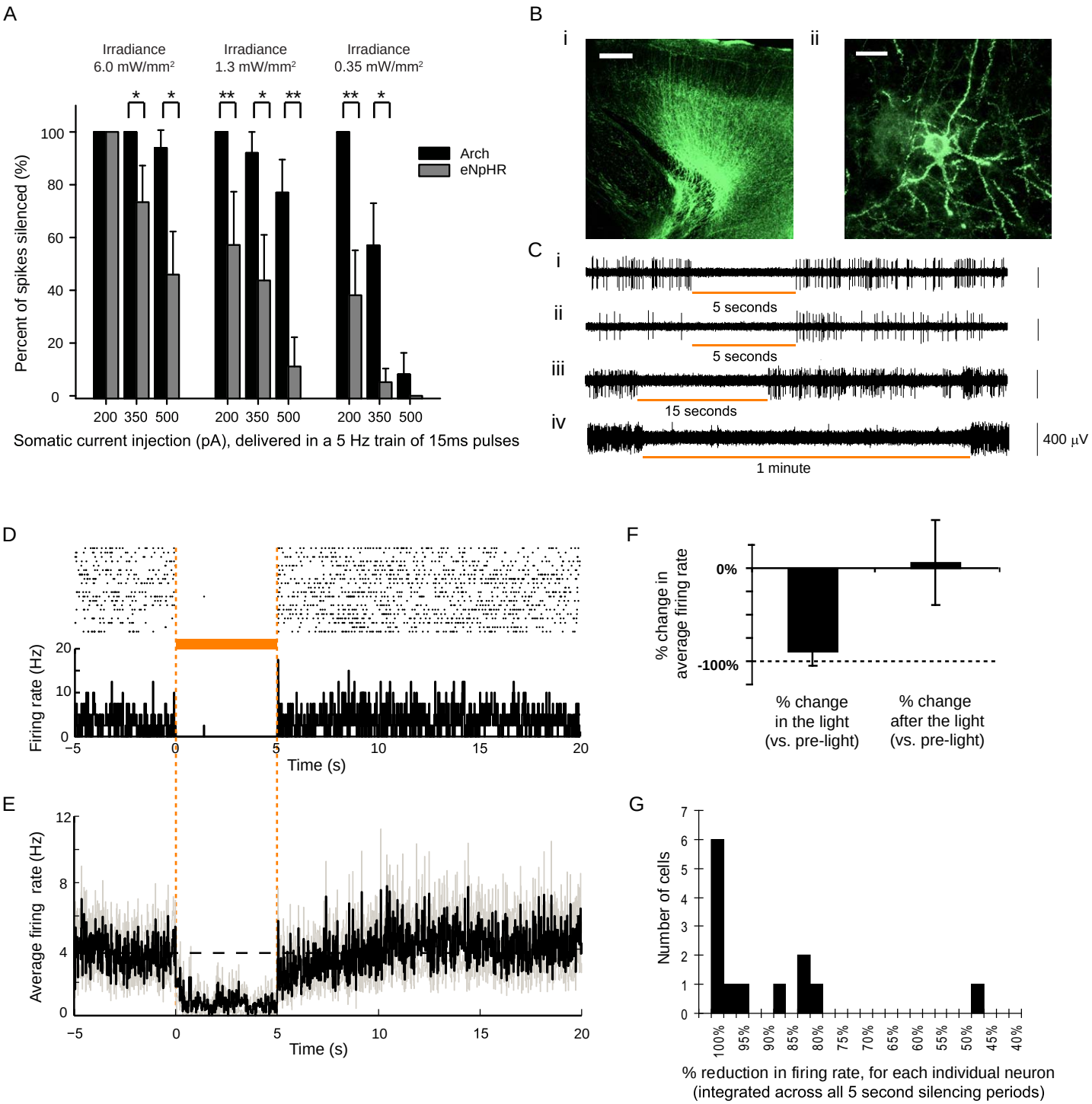

Chow, Han, et. al 2009
Figure 4

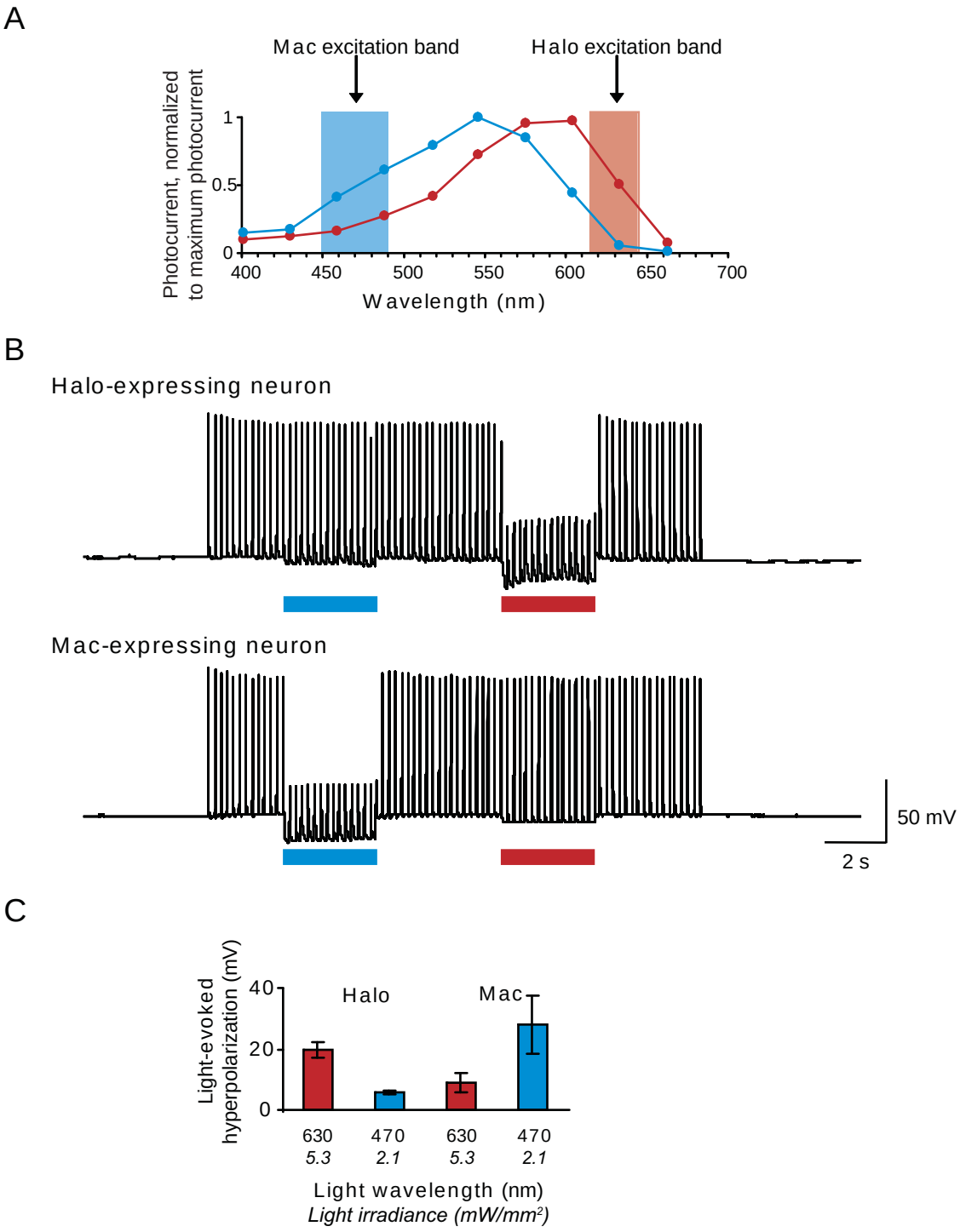

APPENDIX 7

Boyden, E. S. (2009) Optical Neural Control: Engineering Therapeutic Circuit Dynamics: Application to Post-Traumatic Stress Disorder, Talk 7-9, Poster P31-11, PTSD Treatment, Military Health Research Forum, Kansas City, MO.

P31-11

Optical Neural Control: Engineering Therapeutic Circuit Dynamics Application to Post-Traumatic Stress Disorder

J. G. BERNSTEIN, M. V. BARATTA, E. Y. KO, M. A. HENNINGER, M. LI, K. GOOSENS, E. S. BOYDEN
Massachusetts Institute of Technology

Massachusetts Institute of Technology
MIT Media Lab

Synthetic Neurobiology (Neuromedia) Group

Introduction

In recent years we have developed optogenetic molecular reagents for neuroscience, starting with channelrhodopsin-2 (ChR2) and N. pharaonis halorhodopsin (Halo/NpHR), as well as other novel and useful reagents (Arch, spHalo, and Mac), that enable neural circuits to be activated and silenced with different colors of light. At the hardware level, however, many neural circuits of interest possess complex 3-dimensional shapes. To enable sophisticated neural manipulations, including 1) perturbation of complexly-shaped brain regions such as hippocampus and amygdala, 2) bilateral manipulations of neural structures, and 3) well-timed manipulation of multiple brain regions to study synchrony and plasticity, we recently developed inexpensive, end user-fabricatable arrays of blue LED-coupled optical fibers ("fiber arrays") that enable easily-customized deployment of light to multiple sites in the brain. Each optical fiber (200 microns in diameter, with maximal radiant flux of >200 mW/mm2 at the fiber tip) can illuminate a volume within the brain up to a cubic millimeter or so in size.

Here we apply our optical fiber array system to study prefrontal regulation of fear extinction, selectively activating excitatory neurons without driving fibers of passage. Lentiviruses carrying the gene for the blue light responsive excitatory cation channel, ChR2, were bilaterally injected into mouse infralimbic cortex (IL). After two weeks to permit ChR2 expression, they received three tones (30 s duration) coterminating with a footshock (1 s duration, 0.5 mA magnitude). One day later, all subjects received 10 more tones (ITI = 60 s) without footshock (extinction phase), in a context different from the conditioning context. Data suggest that simultaneous bilateral delivery of a 500 ms train of 125 Hz blue-light pulses (4 ms in duration each) to the IL, starting 100 ms after tone onset, resulted in reliably-reduced fear responding to conditioned tones, relative to controls. We anticipate that the ability to manipulate complex 3-dimensional neural substrates with light will greatly advance the understanding of how neural circuits contribute to normal behavior as well as in animal models of neurological and psychiatric illness.

Safety and efficacy of optical neural control

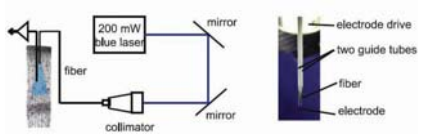

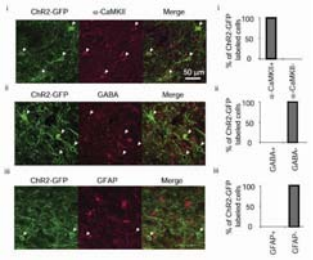

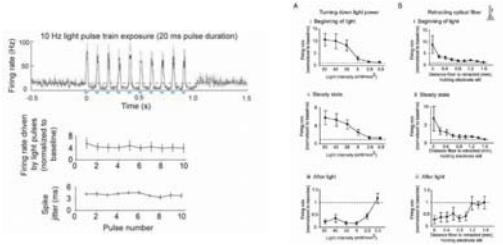

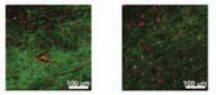

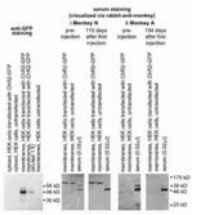

Optical prosthetics

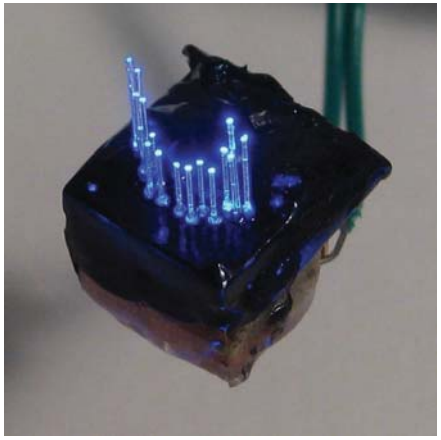

Optical neural control applied to the PTSD circuit

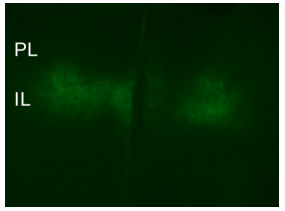

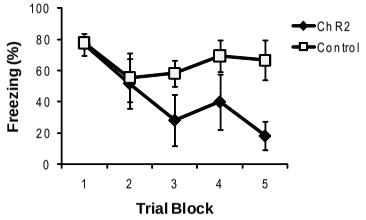

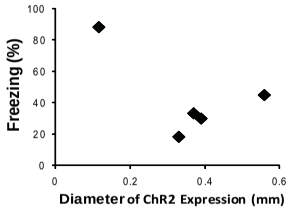

Acknowledgments

E.S.B. acknowledges support from the: NIH Director's New Innovator Award (DP2 OD002002-01), NSF (0835878 and 0848804), McGovern Institute Neurotechnology Award, Department of Defense, NARSAD, Alfred P. Sloan Foundation, Jerry Burnett Foundation, SFN Research Award for Innovation in Neuroscience, MIT Media Lab, Benesse Foundation, and Wallace H. Coulter Foundation.

APPENDIX 8

Bernstein, J. G., Baratta, M. V., Ko, E. Y., Henninger, M. A. Li, M., Goosens, K., Boyden, E. S. (2009) "Modulation of fear behavior via optical fiber arrays targeted to bilateral prefrontal cortex." ***Society for Neuroscience*****, Online.**

Print this Page for Your Records Close Window

Control/Tracking Number: 2009-S-16418-SfN
Activity: Scientific Abstract
Current Date/Time: 5/15/2009 10:29:05 AM

Modulation of fear behavior via optical fiber arrays targeted to bilateral prefrontal cortex

AUTHOR BLOCK: *J. G. BERNSTEIN[1], M. V. BARATTA[2], E. Y. KO[3], M. A. HENNINGER[4], M. LI[2], K. GOOSENS[3], E. S. BOYDEN[5];
[2]Media Lab., [3]Brain and Cognitive Sci., [4]Physics, [5]Media Lab, Biol. Engineering, Brain and Cognitive Sci., [1]MIT, Cambridge, MA

Abstract: In recent years we have developed optogenetic molecular reagents for neuroscience, starting with channelrhodopsin-2 (ChR2) and N. pharaonis halorhodopsin (Halo/NpHR), as well as other novel and useful reagents to be described at this conference (Arch, spHalo, and Mac), that enable neural circuits to be activated and silenced with different colors of light. At the hardware level, however, many neural circuits of interest possess complex 3-dimensional shapes. To enable sophisticated neural manipulations, including 1) perturbation of complexly-shaped brain regions such as hippocampus and amygdala, 2) bilateral manipulations of neural structures, and 3) well-timed manipulation of multiple brain regions to study synchrony and plasticity, we recently developed inexpensive, end user-fabricatable arrays of blue LED-coupled optical fibers (“fiber arrays”) that enable easily-customized deployment of light to multiple sites in the brain. Each optical fiber (200 microns in diameter, with maximal radiant flux of >200 mW/mm2 at the fiber tip) can illuminate a volume within the brain up to a cubic millimeter or so in size.
Here we apply our optical fiber array system to study prefrontal regulation of fear extinction, selectively activating excitatory neurons without driving fibers of passage. Lentiviruses carrying the gene for the blue-light responsive excitatory cation channel, ChR2, were bilaterally injected into mouse infralimbic cortex (IL). After two weeks to permit ChR2 expression, they received three tones (30 s

duration) coterminating with a footshock (1 s duration, 0.5 mA magnitude). One day later, all subjects received 10 more tones (ITI = 60 s) without footshock (extinction phase), in a context different from the conditioning context. Data suggest that simultaneous bilateral delivery of a 500 ms train of 125 Hz blue-light pulses (4 ms in duration each) to the IL, starting 100 ms after tone onset, resulted in reliably-reduced fear responding to conditioned tones, relative to controls. We anticipate that the ability to manipulate complex 3-dimensional neural substrates with light will greatly advance the understanding of how neural circuits contribute to normal behavior as well as in animal models of neurological and psychiatric illness.
:

Presentation Preference (Complete): Poster Only
Linking Group (Complete): CarrotCotton
Nanosymposium Information (Complete):
Theme and Topic (Complete): G.01. Molecular, Biochemical, and Genetic Techniques ; G.04. Physiological Methods
Keyword (Complete): Optogenetics ; Medial Prefrontal Cortex ; Fear
Support (Complete):
Support: Yes
Grant/Other Support: : NIH Director's New Innovator Award (DP2 OD002002-01)
Grant/Other Support: : NSF (0835878 and 0848804)
Grant/Other Support: : McGovern Institute Neurotechnology Award
Grant/Other Support: : Department of Defense, NARSAD
Grant/Other Support: : Alfred P. Sloan Foundation, Jerry Burnett Foundation
Grant/Other Support: : SFN Research Award for Innovation in Neuroscience, MIT Media Lab
Grant/Other Support: : Benesse Foundation, and Wallace H. Coulter Foundation

Special Requests (Complete):
Religious Conflict?: No Religious Conflict
Additional Conflict?: No

Status: Finalized

OASIS Helpdesk

Powered by OASIS, The Online Abstract Submission and Invitation System SM

APPENDIX 9

Chan, S. C., Bernstein, J. G., Boyden, E. S. (2009) Scalable Fluidic Injector Arrays for Viral Targeting of Intact 3-D Brain Circuits. in press, Journal of Visualized Experiments.

JoVE Article Template:

TITLE

Scalable Viral Injector Arrays for Genetic Targeting of Intact 3-D Brain Circuits

Authors:

Stephanie C. Chan, Jacob G. Bernstein, Edward S. Boyden

Authors: institution(s)/affiliation(s) for each author:

Stephanie C. Chan
MIT Media Lab, MIT McGovern Institute, MIT Dept. of Brain and Cognitive Sciences, MIT Dept. of Biological Engineering, MIT Dept. of Physics
Massachusetts Institute of Technology
schan09@mit.edu

Jacob G. Bernstein
MIT Media Lab, MIT McGovern Institute, MIT Dept. of Brain and Cognitive Sciences, MIT Dept. of Biological Engineering
Massachusetts Institute of Technology
jberns@mit.edu

Edward S. Boyden
MIT Media Lab, MIT McGovern Institute, MIT Dept. of Brain and Cognitive Sciences, MIT Dept. of Biological Engineering
Massachusetts Institute of Technology
esb@media.mit.edu

Corresponding author:

Edward S. Boyden
MIT Media Lab, MIT McGovern Institute, MIT Dept. of Brain and Cognitive Sciences, MIT Dept. of Biological Engineering
Massachusetts Institute of Technology
esb@media.mit.edu

Keywords: (minimum 4, maximum 10)

Lentivirus, adeno-associated virus, channelrhodopsin, optogenetics, neuroscience, infusion, transgenic, gene therapy, drug delivery, neurotechnology.

Short Abstract: should include a general description of the article (10 word minimum, 50 word maximum)

Controlling and analyzing neural circuits *in vivo* would be facilitated by a technology for delivery of viruses and other reagents to desired 3-dimensional sets of brain regions. We demonstrate customized fluidic injector array fabrication, and delivery of virally-encoded optical sensitizers, enabling optical manipulation of complex brain circuits.

Long Abstract: (150 word minimum, 400 word maximum)

Understanding how neural circuits mediate the computations that subserve sensation, thought, emotion, and action, and are corrupted in neurological and psychiatric disorders, would be greatly facilitated by a technology for rapidly targeting genes to complex 3-dimensional neural circuits, enabling fast creation of "circuit-level transgenics." We have recently developed methods in which viruses encoding for light-sensitive proteins can sensitize specific cell types to millisecond-timescale activation and silencing in the intact brain. We here present the design and implementation of an injector array capable of delivering viruses (or other fluids) to dozens of defined points within the 3-dimensional structure of the brain (**Figs. 1A, 1B**). The injector array comprises one or more displacement pumps that each drive a set of syringes, each of which feeds into a polyimide/fused-silica capillary via a high-pressure-tolerant connector. The capillaries are sized, and then inserted into, desired locations specified by custom-milling a stereotactic positioning board, thus allowing viruses or other reagents to be delivered to the desired set of brain regions. To use the device, the surgeon first fills the fluidic subsystem entirely with oil, backfills the capillaries with the virus, inserts the device into the brain, and infuses reagents slowly (<0.1 microliters/min). The parallel nature of the injector array facilitates rapid, accurate, and robust labeling of entire neural circuits with viral payloads such as optical sensitizers to enable light-activation and silencing of defined brain circuits. Along with other technologies, such as the optical fiber arrays for light delivery to desired sets of brain regions that we describe in a companion JoVE article, we hope to create a toolbox that enables the systematic probing of causal neural functions in the intact brain. This technology may not only open up such systematic approaches to circuit-focused neuroscience in mammals, and facilitate labeling of brain regions in large animals such as non-human primates, but may also open up a clinical translational path for cell-specific optical control prosthetics, whose precision may improve the treatment of intractable brain disorders. Finally, such devices as described here may facilitate precisely-timed fluidic delivery of other payloads, such as stem cells and pharmacological agents, to 3-dimensional structures, in an easily user-customizable fashion.

T**ext:** should include a step-by-step description of the experimental procedure *(protocol)*. Describe procedures in sufficient detail so that the work can be reproduced. Please use complete sentences, and write with a style similar to the example below, so that the protocol sounds natural when read.

Part 1) Constructing Stereotaxic Clamp

1.0 The stereotaxic clamp is used to attach the injector array to the stereotax in such a way that the injectors are parallel to the stereotaxic arm.
1.1 Each lab needs only one clamp, unless it is anticipated that more than one surgery may take place simultaneously. In this case, make the same number as the anticipated maximum number of simultaneous surgeries. It might also be advisable to make an extra, in case of damage to the first.
1.2 To make the stereotaxic clamp, firstly, a 1.5 mm outer diameter (OD) steel cannula is cut to 2 inches in length, and one of the ends is Dremeled down until flat.
1.3 Next, a small piece (approximately 0.5 x 0.5 cm) is cut out of PCB proto-board, to be used as a spacer.
1.4 Using a laser cutter to ensure that any cuts made are perpendicular to the surface of the material, two identical rectangles (1/2" x 3/8") are cut from 1/8" acrylic sheeting, each rectangle having two circular holes in opposite corners of the rectangle. The first hole has diameter 1.5mm, and is just large enough to hold the metal cannula tightly. The second hole has diameter 1/16" (**Fig. 1C**).
1.5 The metal cannula is inserted into the 1.5 mm hole of one rectangle, then through the 1.5 mm hole of the second. The bottom end of the cannula is aligned with the bottom face of the bottom rectangle, forming the shape of a hockey stick.
1.6 While keeping the spacer tightly held between the two rectangles, this structure is cemented together by using hot glue around the cannula and 1.5mm holes, being careful to avoid gluing the spacer to the rectangles. Modeling clay may be helpful to hold things together during this process.
1.7 After the glue has dried, a 1-72 hex nut can be attached to hold the clamp together as follows. Small amounts of 5-minute epoxy are dropped around the edge of the 1/16" hole. Then the hex nut is centered over the hole and placed firmly into the epoxy, without allowing the epoxy to get into the threads of the hex nut.
1.8 Once the epoxy has hardened, a 1-72 binding slotted machine screw is inserted into the 1/16" hole from the top side of the rectangles, and screwed into the nut. Any modeling clay is removed, and it is confirmed that the spacer can be held firmly in place by tightening the screw.

Part 2) Preparing the system for the customized injector array: Hamilton pump and stereotax

2.0 The injector array system can be customized to virtually any set of coordinates in the brain.
2.1 The user first locates coordinates of desired injection sites in a mouse (or other species) brain atlas, converting to the appropriate coordinates used by the stereotax (here, X-, Y-, and Z-coordinates). The number of injection sites (three in **Figs. 1A, 1B**) will hereafter be called *k*.
2.2 *k* number of 10 μl Hamilton syringes are placed in an injection/withdrawal syringe pump such as this one from Harvard apparatus.
2.3 Next, 3-foot-long pieces of polyethylene tubing are securely attached to the needle of each Hamilton syringe.
2.4 For each piece of polyethylene tubing, an F-252 tubing sleeve from Upchurch Scientific is slid over the open end and attached to a P-627 tubing adapter using the included nut and ferrule, also from Upchurch Scientific.

Part 3) Constructing the Customized Injector Array

3.0 Each injector array is customized to the set of coordinates that the user chooses. However, for sets of coordinates that differ only by a translation and/or rotation, the same injector array can be used.

3.1 Considering only the relative X and Y coordinates of the injection sites, *k* holes are drilled into a PCB proto-board of thickness 1/32", with the same relative spacings. These holes are drilled using a Modela mini mill and a .011" diameter drill bit from Mcmaster-Carr. Be sure to use a slow rate of drilling (Z-speed) to avoid breaking or wearing out the drill bit. Before removing the board from the mill, a rectangle is drilled around the small holes, using a larger drill bit of diameter 1/32", to avoid wearing out the smaller one. Code for the mini mill can be generated easily using MATLAB; sample code is provided in the following files.

i. generate.m - MATLAB code for generating Modela code from desired coordinates
ii. holes_ex.rml - Modela code for drilling ring pattern (eight holes) into Proto-board
iii. outline_ex.rml - Modela code for drilling rectangle around holes

3.2 245 μm OD/100 μm inner diameter (ID) fused silica capillary tubing, available from Polymicro Technologies, is cut into *k* number of 3 inch pieces. These comprise the individual injectors. A discardable piece of capillary tubing is poked through each of the holes, to clear away debris without clogging the actual injectors. The injectors are then inserted halfway into each hole, so that they are held tightly and parallel to one another. The injectors are epoxied to the board, forming the structure of the injector array. All that remains is to trim the injectors to the correct length.

3.3 The injector array is attached to the stereotaxic clamp by placing one corner of the proto-board between the acrylic rectangles, and then by tightening the screw of the stereotaxic clamp. Next, the metal cannula of the clamp is attached to the stereotax, using the attachment mechanism of the stereotax.

3.4 All of the following is done under a microscope. For one of the outer injectors (that is, one that can be approached from the side with a straight edge, without bumping into any of the other injectors), the tip extending beyond the bottom of the proto-board is cut with scissors. For cortical injections, it is appropriate to have the injector extending approximately 5mm beyond the surface of the proto-board. For deeper injections, this number can be increased by the corresponding increase in depth. The tip is flattened with a Dremel tool. Injector tips can also be ground at an angle as an extra precaution against clogging, if precision in depth is less important.

3.5 Next, a stable reference point is chosen within range of the stereotaxic arm, and the injector array is moved so that the flattened tip of the outer injector, is at this reference point.

3.6 A second injector is chosen, along with its corresponding coordinates. Considered is the relative difference in height (z-direction) between the first and second injector coordinates. The injector array is moved along the Z axis by this relative distance. The second injector is trimmed and Dremeled to the correct length, so that the tip of the second injector is now flat and at the height of the reference point. The injector array can be moved in the X and Y directions to facilitate comparison of the injector tip with the reference point.

3.7 This process of trimming is repeated for the remaining injectors.

Part 4) Assembling the entire system

4.0 The stereotaxic clamp and customized injector array, both already constructed, are required for this part.

4.1 The back end of each injector (the end that has not been trimmed) is inserted into a blue F-240 tubing sleeve and, using a P-235 nut and P-200 ferrule from Upchurch Scientific, is attached to the threaded adaptor already connected to the Hamilton pump by polyethylene tubing. Manufacturer's instructions can be consulted for details.

4.2 Using a 27-gauge needle, silicone oil is injected into the back of the Hamilton syringes so that the entire system is filled from the Hamilton syringe to the injector tip, with no air bubbles at all.

4.3 As the Hamilton syringes are re-placed in the Hamilton pump, the greatest possible volume of silicone oil is maintained in the syringes.

4.4 If the experiment requires more syringes than the pump is designed for (two in this case), the syringes can be spaced with small pieces of plastic (e.g., needle caps) to keep them parallel to one another, and to insure that all pieces are pushed by the pump to the same extent.

Part 5) Injections/surgery:

5.0 The process of injecting with a parallel injector is very similar to that of injecting with a single pipette.

5.1 It is essential to use slow refill/infuse rates throughout this process, because fast pumping might put stress on the joint between large and small tubing. Recommended max rate: 2 μl/min for loading virus, and 0.1 μl/min for infusing virus.

5.2 An anesthetized mouse is placed in the stereotax, and remains anesthetized throughout the experiment.

5.3 Prepare the mouse as needed. For example, with a scalpel, a single cut is made down the midline of the skin, from between the eyes to between the ears. The skin is pulled back to expose the skull, and the fascia is cleaned off. A pulled glass pipette is attached to the stereotax. The positions of the ear bars are adjusted until bregma and lambda are aligned to the same height, and so that the line connecting them is parallel to the Y-axis of the stereotax. The axes of the stereotax are oriented according to the coordinate system in which the injection coordinates have been calculated. The stereotaxic is zeroed with the tip of the glass pipette at bregma, and then the tip is positioned slightly above the skull at the X- and Y-coordinates of one of the injection sites.

5.4 Using a dental drill, the skull below the tip is carefully pared away until there remains an extremely thin layer of bone. The glass pipette can be lowered and raised to check that the hole being drilled is centered at the correct position. Using a 30-gauge needle, a tiny piece of the layer is gently picked off, at the correct X- and Y- coordinates, so that the dura mater is exposed. This hole should be just large enough to fit one of the injectors (0.25mm wide). See **Figure 1D** for diagram. In this way, small, 0.25mm wide holes are made in the skull, at the X- and Y- coordinates corresponding to each injection site.

5.5 Then screws are inserted into the skull, as required for the implantation of an LED-fiber array. The holes made previously will be used for the LED-fiber array as well, in the companion JoVE piece[1].

5.6 The glass pipette is discarded in a sharps container, and the customized injector array is attached to the stereotax using the stereotaxic clamp.

5.7 In order to correctly set the angle of the injector array, two outer injectors are chosen to be calibrated to a given reference point, as follows. After one of the injectors is matched with the reference point, consider the relative X- and Y- distances between the injection sites relative to this injector and one other. The axes of the stereotax are adjusted so that entire

injector array is moved in the X- and Y-directions by these relative distances. If the second injector is not now aligned with the reference point, the metal cannula is loosened and rotated. This process is repeated iteratively until the injector array is angled correctly.

5.8 Before filling the injectors with virus, the injectors are filled with silicone oil until the syringes are at the 2 μl point (or greater). This provides a buffer zone, so that any air bubbles or clogging in the tip can be easily removed by pushing oil forward using the Hamilton pump, without having to refill the entire system with silicone oil from the back of the syringes, as describe previously.

5.9 A clean piece of Parafilm is placed on the skull, and the injectors are gently lowered onto the Parafilm. For coordinates with greatly varying depths, a custom-milled part (e.g. a staircase-shaped object) could facilitate loading.

5.10 The following parts assume that 1 μl of virus is to be loaded at each site (the following quantities should be scaled down if smaller quantities are desired). In order to guarantee that >1 μl of virus is injected at each site, 1.5 μl of virus is pipetted onto the Parafilm or staircase at the tip of each injector.

5.11 With the refill rate of the Hamilton pump set to 1 μl/min, 1.2 μl of the virus is refilled into each injector.

5.12 The tip of the longest injector is zeroed at bregma, and then the injector array is shifted to the X- and Y- coordinates of that injector. If clogging is an issue, say if many deep targets are involved: even before inserting the injector tips into the brain, it is sometimes advisable to start the pump infusing, until virus can be seen emerging from all the injector tips. This removes any air bubbles at the injector tips, and also ensures that there is no clogging. In the case of clogging, the Hamilton pump is set to infuse a brief pulse at a higher speed of 2 μl/min, to blast out any clogging.

5.13 The injector array is then lowered, through the small holes made with the 30-gauge needles, to the correct Z-depth.

5.14 1 μl of virus is injected through each injector, at 0.1 μl /min.

5.15 The injections are left alone for 30 minutes.

5.16 After the injector array is slowly extracted from the brain, the Hamilton pump is set to infuse at the same rate of 0.1 μl /min, in order to check for clogging in each injector.

5.17 Then the injectors are cleaned by refilling and infusing 1.5 μl of ethanol at 2 μl/min.

5.18 Finally, the injectors are refilled with silicone oil to maintain the 2 μl buffer zone in each Hamilton syringe.

5.19 The LED-fiber array can now be implanted.

Part 6) Representative Results

The parallel injector array speeds up a surgery roughly by a factor equal to the number of injectors, not counting setup and recovery time, although individual times will depend on the skill of the practitioner. For a 1 microliter injection, we typically saw virus expression in a sphere of approximately diameter 1mm (**Fig. 1E**). The precision of the injection was such that the variability in tip positioning, from trial to trial, was about 45 microns (standard deviation of the distance from the tip position to the intended tip position).

Discussion: Short discussion on critical steps, possible modifications, applications, significance, etc…

In recent years, a number of genetically-encoded optical sensitizers have enabled neurons to be activated and silenced in vivo in a temporally-precise fashion, in response to brief pulses of light (e.g., [2]). A key method with which neurons have been sensitized to light in the mammalian brain, is via viruses such as lentiviruses and adeno-associated viruses (AAV), which can deliver genes encoding for opsins to brains of animals ranging from mice to monkeys, in a safe and enduring fashion (e.g., [3]). Viruses allow faster turnaround time than do transgenics, especially for organisms that are not genetic model organisms such as rats and monkeys, and for opsins may enable high expression levels that may not be possible in transgenic scenarios[4]. Here we demonstrate a parallel injector array capable of creating, in a rapid timescale, "circuit-level transgenics," enabling entire 3-dimensional brain structures to be virally targeted with a gene, in a single surgical step. The injector array comprises one or more displacement pumps that each drive a set of syringes, each of which feeds into a polyimide/fused-silica capillary via a high-pressure-tolerant connector. The capillaries are sized, and then inserted into, desired locations specified by custom-milling a stereotactic positioning board, thus allowing viruses or other reagents to be delivered to the desired set of brain regions. To use the device, the surgeon first fills the fluidic subsystem entirely with oil, backfills the capillaries with the virus, inserts the device into the brain, and infuses reagents slowly (<0.1 μL/min).

This technology will enable a wide variety of new kinds of experiments, such as millisecond-timescale shutdown of complexly-shaped structures (such as the hippocampus) at precise times during behavior, temporally-precise inactivation of bilateral structures that may act redundantly (such as the left and right amygdala), and the perturbation of multiple discrete brain regions (e.g., driving two connected regions out of phase to study how cross-region synchrony depends upon activity within each region, or stimulating inputs to a region while silencing a subset of the targets in order to understand which of the several targets are critical for mediating the effects of those inputs). For large brains like those in the primate, in which we have recently demonstrated optical cell-type specific neural activation[5], perturbing activity in a behaviorally-relevant area may require viral labeling of large, complex structures. Along with other technologies, such as the optical fiber arrays for light delivery to desired sets of brain regions that we describe in a companion JoVE article[1], we hope to create a toolbox that enables the systematic probing of causal neural functions in the intact brain. We note that parallel injector arrays may be used to inject almost any payload – drugs, neuromodulators, neurotransmitters, or even cells – in complex 3-D patterns in the brain, in a temporally-precise manner. Finally, from a translational standpoint, it is possible that rapid, patient-customized gene therapy or drug delivery devices may be rapidly custom-designed and fabricated to match individual brain geometries, supporting new treatments for a variety of pathologies, potentially through the use of optical control molecules.

The injector arrays are designed to be precise, both spatially and volumetrically. In the X- and Y-directions, this is accomplished by drilling very accurately placed holes using an inexpensive mini-mill, with the holes just large enough to fit the injectors, so that injectors are held parallel to one another, and in a precise location. In the Z-direction, the injectors are trimmed using a stereotaxic apparatus, allowing a level of precision equivalent to that of the stereotaxic surgery itself. The volumetric precision arises from the precision of the Hamilton pump, as well as the near-zero dead-volume connectors, adapted from the high-pressure liquid chromatography (HPLC) field. The injectors are made from fused silica capillary tubing, which is strong and rigid enough that it maintains precise shape and spacing under pressure, without the larger wall thickness of alternatives such as steel cannulas. Small modifications can easily be made to adapt the parallel injector array to a variety of experiments. For example, if smaller volumes of virus or finer spacings are required, smaller capillary tubing can be employed, along with a corresponding smaller drill bit. Future devices may utilize microfluidic channels and pumps, to

increase the number of parallel injectors, to minimize the size (perhaps enabling such devices to be mounted on the heads of freely-moving animals).

Acknowledgments:

S.C. and J.G.B. are supported by the MIT Media Lab, the MIT UROP program, and the Hugh Hampton Young Memorial Fund. E.S.B. acknowledges support from the: NIH Director's New Innovator Award (DP2 OD002002-01), Society for Neuroscience Research Award for Innovation in Neuroscience, NSF Emerging Frontiers in Research and Innovation, NSF SGER, Department of Defense Post-Traumatic Stress Disorder Concept Award, NARSAD, Alfred P. Sloan Foundation, Jerry Burnett Foundation, MIT Media Lab and MIT Media Lab Consortia, MIT McGovern Institute and MIT McGovern Institute Neurotechnology (MINT) program, Benesse Foundation, MIT Neurotechnology Fund, and Wallace H. Coulter Foundation.

Disclosures:

All procedures were in accordance with the NIH Guide for Laboratory Animals and approved by the MIT Animal Care and Use and Biosafety Committees.

Tools and Materials:

Tools	Company	Catalogue number	Comments (optional)
Dremel Tool	Dremel	3956-02	
Laser Cutter	Universal Laser Systems	VLS2.30	
Hot glue gun	Stanley Bostitch	GR20	
Injection/withdrawal syringe pump (Hamilton pump)	Harvard Apparatus	702001	
10 μl Hamilton syringes	Hamilton Company	701N	Need one per injection site
Mouse stereotax	Stoelting	51725D	
Modela mini-mill	Roland	MDX-15	
0.011” diameter drill bit for mini mill	Mcmaster-Carr	8915A12	
1/32” diameter drill bit For mini-mill	McMaster-Carr	8848A35	
High speed dental drill	Lynx	333	
Dental drill accessories	Pearson	F 35-08-25 F 35-07-10 P 86-02-38	

Materials	Company	Catalogue number	Comments (optional)
1.5mm outer diameter (OD) stainless steel cannula	Small-Parts	HTX-15R	
1-72 binding slotted machine screw	Small-Parts	MX-0172B	
1-72 hex nut	Small-Parts	HNX-0172	
PCB proto-board, 1/32" thick	Digi-Key	PC57-T-ND	
Acrylic Sheet, 1/8" thick	Mcmaster-Carr	8560K239	
HPLC connectors	Upchurch Scientific	F-252, P-627, P-200, P-235, F-240 (some of these can be bought in 10-packs; simply add an 'x' to the end of the part number)	Need one per injection per site, except F-252, P-627, and P-235, which can be reused
Fused silica capillary tubing, OD: 245 μm, ID: 100 μm	Polymicro Technologies	2000022-10M	
5-minute general purpose epoxy	Permatex	84101	5-minute general purpose epoxy
Polyethylene tubing .066 x .095 inch	VWR	63018-827	

Figure legends

Figure 1. Design, implementation, and use of a parallel virus injector array. **A**, schematic of the parallel injector array system, showing a triple injector configuration, for three simultaneous injections. **B,** photograph of a triple parallel injector array as diagrammed in **A**. **C**, stereotaxic clamp, shown in outline from the top. **D,** illustration of technique for efficient, damage-minimizing, opening of holes in skull for injector insertion into brain: with a dental drill, thin the skull down to ~50 microns thickness, then use the tip of a sharp needle to open a small craniotomy. **E**, fluorescence image showing ChR2-GFP-labeled cells in three mouse cortical regions, as targeted by the triple injector array shown in **B.**

Files:
generate.m
holes_ex.rml
outline_ex.rml

REFERENCES

[1] J. G. Bernstein, E. Ko, M. A. Henninger, and E. S. Boyden, *Journal of Visualized Experiments* submitted (2009).

[2] B. Chow, X. Han, X. Qian, and E. S. Boyden, *Frontiers in Systems Neuroscience. Conference Abstract: Computational and systems neuroscience.* doi: 10.3389/conf.neuro.10.2009.03.347 (2009); F. Zhang, L. P. Wang, M. Brauner, J. F. Liewald, K. Kay, N. Watzke, P. G. Wood, E. Bamberg, G. Nagel, A. Gottschalk, and K. Deisseroth, *Nature* 446 (7136), 633 (2007); E. S. Boyden, F. Zhang, E. Bamberg, G. Nagel, and K. Deisseroth, *Nat Neurosci* 8 (9), 1263 (2005); X. Han and E. S. Boyden, *PLoS ONE* 2 (3), e299 (2007); L. Luo, E. M. Callaway, and K. Svoboda, *Neuron* 57 (5), 634 (2008); S. Szobota, P. Gorostiza, F. Del Bene, C. Wyart, D. L. Fortin, K. D. Kolstad, O. Tulyathan, M. Volgraf, R. Numano, H. L. Aaron, E. K. Scott, R. H. Kramer, J. Flannery, H. Baier, D. Trauner, and E. Y. Isacoff, *Neuron* 54 (4), 535 (2007); S. Q. Lima and G. Miesenbock, *Cell* 121 (1), 141 (2005).

[3] A. Bi, J. Cui, Y. P. Ma, E. Olshevskaya, M. Pu, A. M. Dizhoor, and Z. H. Pan, *Neuron* 50 (1), 23 (2006); X. Han, X. Qian, J. G. Bernstein, H.-H. Zhou, G. Talei Franzesi, P. Stern, R. T. Bronson, A. M. Graybiel, R. Desimone, and E. S. Boyden, *Neuron* 62 (2), 191 (2009); F. Zhang, L. P. Wang, E. S. Boyden, and K. Deisseroth, *Nat Methods* 3 (10), 785 (2006); T. Ishizuka, M. Kakuda, R. Araki, and H. Yawo, *Neurosci Res* 54 (2), 85 (2006).

[4] H. Wang, J. Peca, M. Matsuzaki, K. Matsuzaki, J. Noguchi, L. Qiu, D. Wang, F. Zhang, E. Boyden, K. Deisseroth, H. Kasai, W. C. Hall, G. Feng, and G. J. Augustine, *Proc Natl Acad Sci U S A* 104 (19), 8143 (2007).

[5] X. Han, X. Qian, J. Bernstein, H.-H. Zhou, G. Talei Franzesi, Stern P., R. T. Bronson, A. Graybiel, R. Desimone, and E. S. Boyden, *in press, Neuron* (2009).